EARLY TAU PATHOLOGY IN THE POSTMORTEM DEFAULT MODE NETWORK IN ALZHEIMER'S DISEASE

By

Betul Kara

A DISSERTATION

Submitted to
Michigan State University
in partial fulfillment of the requirements
for the degree of

Cell and Molecular Biology—Doctor of Philosophy

2025

ABSTRACT

Alzheimer's disease (AD) is characterized by the accumulation of two pathological hallmarks in brain areas mediating cognitive function: 1) extracellular senile plaques consisting of aggregated amyloid-beta peptides and 2) intracellular neurofibrillary tangles (NFTs) composed of fibrillar aggregates of the protein tau. Although NFT pathology is strongly linked to neurodegeneration and cognitive decline in AD, several lines of evidence indicate that it is the soluble "pre-tangle" aggregates of tau formed prior to NFTs that are the neurotoxic species driving disease progression resulting in cognitive impairment. In this study, we aimed to quantify pre-tangle tau moieties in the cognitive brain regions that falter the earliest in AD to advance our understanding of disease mechanisms and test if pre-tangle tau pathology associates with cognitive decline. We examined postmortem tissue from three brain regions–frontal cortex (FC), posterior cingulate cortex (PCC), and precuneus (PreC)–that form functionally connected Default Mode Network (DMN), which shows altered functional connectivity in patients with subjective cognitive decline (SCD) as well as with mild cognitive impairment (MCI) who later convert to frank AD. Immunohistochemical and biochemical quantification of pre-tangle tau by epitope-specific antibodies (pS422, TOC1, TNT2, and TauC3) indicated that pathological tau was present in the low Braak stages in the DMN, and its level significantly increased between the transition from Braak stage IV to Braak stage V. The pre-tangle tau pathology also demonstrated a tight and inverse correlation with several antemortem cognitive test scores, including those related to global cognition, episodic and semantic memory, as well as with postmortem neuropathological diagnostic scores. We also found possible regional

differences in pre-tangle tau load among those three brain regions, with PCC showing higher pathology compared to its neighboring region, PreC. To further investigate the tau protein interactome that may underlie the regional difference in pre-tangle tau pathology burden, we performed a co-immunoprecipitation of pathological tau and its protein binding partners for mass spectrometric analysis. The results revealed that tau interactions within PCC and PreC were associated with different stress response to AD pathology, while PCC demonstrated abnormally elevated lipid metabolism and immune activation. Collectively, our findings contribute to the timeline of pre-tangle tau accumulation in the DMN network in AD with a potential regional difference for the pathology load between the two posterior hubs. We also found a close and inverse correlation between the pre-tangle tau and cognitive decline, emphasizing the potential of the study to develop effective disease-mitigating strategies.

Dedicated to all Alzheimer's disease patients from ancient times to the modern day. You will be remembered even if you cannot.

&

Also dedicated to my parents, Melek and Nevzat Kara, who constantly reminded me of the meaning of my work to help others. Who knows, the flap of this butterfly's wing may trigger something bigger somewhere.

ACKNOWLEDGEMENTS

First and foremost, my deepest gratitude is to The El-Alim, The All-Knower, who expanded my knowledge, gave me the strength beyond my imagination to go through this PhD journey, especially when things get tough, and taught me so much about myself and Himself along the way. As I can see now, my PhD was not only a learning process for how to do rigorous science but also an opportunity to meet amazing people and learn so much from them. My dear scientific mentor, Scott E Counts, undoubtedly deserves most of the praise. From day one, his belief in me helped me to regain my self-esteem as a young scientist. He valued my opinion and cherished my ideas. Well, with an occasional eye-rolling over my ephemeral excitement about extracurricular activities, like taking an engineering class out of pure curiosity. Okay, it may not be the greatest idea:) Thank you so very much, Scott! I also thank my dear committee, Dr. Caryl Sortwell, Dr. Irving Vega, Dr. Nicholas Kanaan, and Dr. Timothy Collier, for their support and student-centered attitude. I have learned a lot from each and every one of you.

Past and current members of the Counts lab, Erin McKay, John Beck, Mahsa Gifani, Moumita Hore, and Mona Abdelhamid, I am so grateful to know you and work with you side by side, especially Moumita Hore, for waking up my inner chatty child whenever we talk and helped me to decompress my stress in tough times. Thank you, Tessa Grabinski, Nathan Khun, Andrew Umstead, Jared Lamp, Ahmed Atwa, and Mike Ahmadi, for always being available to answer my questions.

I would not be able to finish this turned out to be a very long journey without my family’s unbreakable support. When I doubted myself, a good many times, they were

the ones who supported my education, put their trust in me, and even traveled from thousands of miles away to come to support me when needed. I could not ask for better parents! I am also grateful for those two women in my life, my grandmas. They are my biggest fans. My two brothers, sister-in-law, and the cutest nephew ever, I appreciate seeing you always by my side.

My appreciation also goes to my CMB people, especially our Alaina Burghardt and Margaret Petroff, for their meticulous work to make CMB a standout program, to my TransNeuro people, especially Jack Lipton, Caryl Sortwell, again, and Betsy Matazel not only to run the program successfully but making the trainees feel cared and supported.

Thank you to all my non-MSU friends that I befriended during my PhD. You are from vastly different backgrounds, ages, and perspectives, and your friendship has enriched my life. I was amazed by the number of you who were willing to help, especially during my thesis writing.

Finally, I want to give special thanks to the RROS and MADC study participants for their participation and donation to the study. I would not be able to do this research without you.

TABLE OF CONTENTS

LIST OF TABLES

LIST OF FIGURES

LIST OF ABBREVIATIONS

Aβ	Beta Amyloid
AD	Alzheimer's Disease
aMCI	Amnestic Mild Cognitive Impairment
APOE	Apolipoprotein
APP	Amyloid Precursor Protein
α-Syn	Alpa Synuclein
BA	Broadman Area
CAA	Cerebral Amyloid Angiopathy
CBF	Cholinergic Basal Forebrain
CDR	Clinical Dementia Rating
CERAD	Consortium to Establish a Registry for Alzheimer's Disease
CK2	Casein Kinase 2
CSF	Cerebrospinal Fluid
DLPFC	Dorsolateral Prefrontal Cortex
DMN	Default Mode Network
DTI	Diffusion Tension Imaging
FAT	Fast Axonal Transport
fc	Functional Connectivity
FC	Frontal Cortex
FDR	False Discovery Rate
fMRI	Functional Magnetic Resonance Imaging
GCS	Global Cognitive z-Score

GFAP	Glia Fibrillary Acidic Protein
GSK3β	Glycogen Synthase Kinase-3 Beta
HSP	Heat Shock Protein
IDP	Intrinsically Disordered/Unfolded Protein
IF	Immunofluorescent
IHC	Immunohistochemistry
IP	Immunoprecipitation
ISF	Interstitial Fluid
JNK3	c-Jun N-terminal Kinase 3
LC	Locus Coeruleus
LTD	Long Term Depression
LTP	Long Term Potentiation
NDH	Network Degeneration Hypothesis
MADC	Michigan Alzheimer's Disease Center
MAPT	Microtubule Binding Protein Tau
MCI	Mild Cognitive Impairment
MMSE	Mini-Mental State Examination
MRI	Magnetic Resonance Imaging
MT	Microtubule
MTBR	Microtubule Binding Region
MTL	Medial Temporal Lobe
NCI	No Cognitive Impairment
NE	Norepinephrine

NFT	Neurofibrillary Tangle
NT	Neurophil Thread
PAD	Phosphatase Activating Domain
PCCAA	Posterior Cingulate Cortex
PET	Positron Emission Tomography
PMI	Post Mortem Interval
PreC	Precuneus
PSEN	Presenilin
PTM	Post Translational Modification
ROS	Reactive Oxygen Species
RP	Ribosomal Protein
RROS	Rush Religious Orders Study
rTMS	Repetitive Transcranial Magnetic Stimulation
SCD	Subjective Cognitive Decline
SD	Standard Deviation
TDP-43	Transactive Response DNA-Binding Protein 43
UPS	Ubiquitin-Proteosome System
WB	Western Blot

CHAPTER 1: INTRODUCTION AND DISSERTATION OBJECTIVES

INTRODUCTION

Dementia during human history: Has it always been in the picture, or is it a modern-day disease?

Although the definition of “dementia” has evolved throughout history and found its recent description in the last two centuries, extreme forgetfulness and inability to learn new concepts is as old as human history. The first documented dementia case goes back to 3,000 BC in Ancient Egypt. An important figure, the chief consular of the king, Ptah-Hotep, was recorded as being unable to remember the day before and becoming more and more childish every night (Vatanabe, 2020; Garcia-Albea, 1999). The Ebers Papyrus, dated to 1,500 BC, is considered an important medical record of its time, and it briefly mentions depression and dementia (York, 2010). Later on, records show only a few references to dementia in Ancient Greece and more mentions in the medical texts from Ancient Rome (Finch, 2024; Assal, 2019). However, dementia was also considered melancholy or delirium, which makes it harder to extract more information from ancient texts.

Often under-credited, between the 8th and 13th centuries (also known as the Islamic Golden Age), several researchers and philosophers in the East (Seifaddini, 2015) contributed to the understanding of dementia. Avicenna categorized dementia into three categories, which largely overlaps with today’s definition of Alzheimer’s disease (AD), frontotemporal dementia, and dementia with Lewy bodies (Taheri-Targhi, 2019; Rahimi, 2017; Jack, 2024) in his famous Al-Qanun fi al-Tibb (The Canon of Medicine) book. Avicenna’s influence pervaded Western science until the 18th century, despite alternative opinions, such as Thomas Willis referring to dementia as “stupidity”

in the 17th century, suggesting it to be a combination of age and heritage (genetics by modern translation) (Vatanabe, 2020; Yang, 2016). From this point dementia research began to advance more rapidly, such that by the 19th century Otto Ludwig Binswanger, a Swiss psychiatrist and neurologist, recognized cerebrovascular lesions and neurosyphilis as potential causes of dementia (Yang, 2016; Mast, 1995; Roman, 1999).

Discovery of Alzheimer's disease

Another dementia scientist who worked with Binswanger at the time was Alois Alzheimer. Alzheimer was the senior assistant at the Frankfurt Psychiatric Hospital when he first met with Auguste Deter, a fifty-year-old woman who was admitted to the clinic due to progressive sleep disturbances, aggression, memory problems, and confusion. Senile dementia was already known at the time; however, Auguste was too young for her severe symptoms. (She would stay in that clinic for five years until her death in 1906). During his first year of attending to Auguste, Alzheimer kept detailed notes of her condition and the interviews he conducted with her, asking basic questions regarding time, place, and names, which she unfortunately failed to answer. Instead, she repetitively said, "I have lost myself, so to say." Even after he departed from the clinic to join Emil Kraepelin's team at the Heidelberg Hospital in 1902, Alzheimer stayed informed about some peculiar cases, including Auguste's (Yang, 2016; Hippius, 2003). When she died in 1906, some of her brain samples were sent to Alzheimer for pathological assessment. By using a Bielschowsky silver stain, Alzheimer was able to stain two distinct pathological features, "thickened miliary foci" and "peculiar fibrillary changes of the nerve cells" (which later would be known as amyloid plaques and neurofibrillary tangles [NFTs], respectively), and shared his detailed findings in the

South-West German Psychiatrists Meeting in Tubingen in 1906 (Hippius, 2003; Tagarelli, 2006). Unfortunately, the crowd did not show much interest in his case. Undeterred, Alzheimer's kept seeing patients and doing pathology research.

He met another patient in 1907 who showed similar symptoms to Auguste and died three years after his diagnosis. Interestingly, this patient had only plaques (Graeber, 1997; Moller, 1998). Later, histological sections from both cases were obtained from the archives and reexamined with modern techniques in 1998 by Möller and Graeber (Moller, 1998) to find similar results to Alzheimer's initial report and further extrapolated that the second case might indicate an earlier time point in the progression of the disease. With the support and suggestion of Kraepelin in 1910, the disease went into the literature as Alzheimer's disease (AD), ironically to be forgotten until the 1970s, with increasing appreciation into the 1980s and 90s as disease prevalence began to rise dramatically and researchers discovered that the APP and MAPT genes generated protein products comprising plaques (amyloid-β, or Aβ) and NFTs (tau), respectively (Brion, 1985 ;Grundke-Iqbal, 1986a; Grundke-Iqbal, 1986b; Glenner, 1984; Goldgaber, 1987). The biology of these protein products is discussed below.

AD: Disease Staging and Diagnostic Criteria

Postmortem diagnosis of AD

The postmortem diagnosis of AD has historically relied upon Dr. Alzheimer's first observations and, even today, a definitive diagnosis of AD requires postmortem evidence of amyloid plaques and tangles, which can be visualized using silver and thioflavin S stains. These two pathological markers are critical for determining the presence and severity of AD. More recently, antibodies recognizing plaques and tangles

have been employed (Ward, 2013; Combs, 2016; Vana, 2011; Glenner, 1984). Several widely used scoring systems provide a standardized approach to diagnosing AD based on these markers:

Consortium to Establish a Registry for Alzheimer's Disease (CERAD): This scoring system evaluates neuritic plaque density and the senile plaque score in five brain regions: medial frontal, medial temporal, inferior parietal, entorhinal cortex, and hippocampus. The assessment results in one of four possible designations ranging from 1 to 4, corresponding to the severity of plaque accumulation (Mirra, 1991).

- 1: Normal (no evidence of AD or other dementing processes)
- 2: Possible AD
- 3: Probable AD
- 4: Definite AD

Braak Stage: This system assesses the presence of NFTs in the same five brain regions as the CERAD system. The stages range from 1 to 6, with higher numbers indicating more advanced neurofibrillary pathology (Braak, 1991). Specific stage characteristics are discussed in Chapter 2.

NIA-Reagan Diagnosis: The NIA-Reagan system integrates the global load of diffuse plaques, neuritic plaques, and NFTs in the aforementioned brain regions (Newell, 1999). The scoring system is inverse, with the following categories providing a different aspect of neuropathological assessment:

- 1: High likelihood of AD
- 2: Intermediate likelihood of AD
- 3: Low likelihood of AD

- 4: No AD

ABC Scoring System: Another comprehensive scoring system that combines plaque and tangle pathology measures is called the ABC scoring system. "A" stands for amyloid pathology based on the Thal phase (Thal, 2002), "B" represents the NFT score based on the Braak stage, and "C" incorporates the neuritic plaque quantification based on the CERAD score (Robinson, 2021). The scale goes from 1-4 for each category, with 4 showing the most severe pathology.

Clinical diagnosis of AD

Cognitive deterioration brings patients to the clinic in the first place. To be able to diagnose the disease, physicians initially perform an extensive physical and neurological examination, assess global cognitive function using tools such as the Mini-Mental State Exam (MMSE), Montral Cognitive Assessment (MoCA) exam, or Clinical Disease Rating (CDR) scale, and talk to the patient's family about the patient's cognitive history. Although it is not a required practice, physicians may request brain scans (MRI, fMRI, CT, or PET) and plasma or CSF for Aβ, tau, and other neurodegeneration markers such as neurofilament light. The three-marker disease staging has been suggested based on the presence of amyloid plaques (A), tau tangles (T), and neurodegeneration (N), resulting in three biological stages of AD: A+T-N-, A+T+N-, A+T+N+. (Jack, 2024).

Fortunately, the arduous efforts of dedicated researchers in the field have started to pay off as new CSF and plasma biomarkers (Aβ42, Aβ40, p-tau217, p-tau181, and p-tau231). In addition, the development of Aβ and tau PET tracers have revolutionized the field by allowing clinicians to view the development of plaque and tangle pathology in vivo. Other diagnostic imaging modalities include volumetric MRI to study brain atrophy

and vascular lesions that might contribute to dementia (Mungas, 2002; Zhang, 2017). With the increased incorporation of CSF, plasma, and imaging biomarkers as criteria for recruitment into clinical trials, the field has advanced more rapidly in the last 20 years, which has in turn created the need to update the criteria for disease diagnosis and biomarkers as well as staging. In June 2024, multiple study groups were formed by the National Institute on Aging and Alzheimer's Association (NIAAA), and they published an update on AD diagnosis criteria and biomarkers for each clinical stage (Jack, 2024). The revisions include the biological and clinical staging of the disease, which are summarized below.

Biological: In addition to the A/T/N staging, the new guideline proposes a four-stage scheme considering the emergence of different biomarkers: Initiation stage, early stage, intermediate stage, and advanced stage.

Clinical: Based on the cognitive deterioration, seven stages were proposed from 0 to 6 to parallel the increased impairment.

Clinical symptoms of AD based on integrated biological and clinical staging

Initiation Phase

This phase includes stage 1 in the clinical staging. In the initiation phase, also known as the “pre-clinical phase”, pathological hallmarks start to accumulate in the brain up to 10-15 years before the initial symptoms start to emerge. There are no distinguishable symptoms, and patients do not realize any changes in their cognitive abilities. Pathology accumulation continues at varying speeds, reflecting the genetic/epigenetic/environmental (e.g., exposures to pollutants and toxins) differences in cases. This temporal lag between the pathology building and cognitive deterioration

might be due to cognitive reserve (ability to compensate for dysfunctional networks by activating alternative networks), brain reserve or resilience (the brain's capacity to endure the existing pathology and related biological imbalances), or existing co-pathologies (alpha-synuclein, cerebral amyloid angiopathy [CAA]) (Santiago, 2021; Shim, 2022; Greenberg, 2020).

Early Phase

This phase includes the stages 2 & 3 in the clinical staging. It starts with basic forgetfulness, such as trouble with remembering a word or misplacing items and repeating themselves during a conversation. In AD, episodic memory typically shows the earliest changes (see Chapter 3 for a more detailed discussion). Initiation of these symptoms is difficult to differentiate from age-related cognitive decline. The patients classified as subjective cognitive impairment/dementia (SCI/SCD) are considered to be in the early part of this phase before transitioning into mild cognitive impairment (MCI) (Petersen, 2004) –particularly amnestic MCI–a prodromal AD syndrome marked by poorer performance on episodic memory tests but minimal impact in activities of daily living (Lanz, 1975).

Intermediate Phase

This phase includes the stages 4 & 5 in the clinical staging as people begin to present mild/moderate dementia. Memory failure in remembering certain events, names, and information becomes more frequent, and the person can struggle at work or social gatherings. Their time span to concentrate decreases, and it starts to take longer to complete a task. They may have poor judgment and bad decisions in daily activities. This is the stage in which patients start to fail on more than memory tasks, including

language problems, inability to do basic calculations, and developing sleep disturbances. Sleep disturbances, in particular, may become a major problem since melatonin secretion and circadian rhythm are impacted (Wu, 2007; Zhang, 2025). Lack of sleep at night may contribute to agitation, aggression, and mood changes through impaired glymphatic function. The glymphatic system is known as the washing machine of the brain due to its function of clearing the waste material, including soluble amyloid and tau, from the CSF via mixing with interstitial fluid (ISF) to be drained from the subarachnoid space (Iliff, 2013). The clearance mostly happens during sleep. Multiple studies emphasized the role of the glymphatic system in AD pathology and claimed that disrupted sleep exacerbates the symptoms by preventing the brain from clearing the waste material (Hablitz, 2020; Hablitz, 2021). As this stage progresses, the patient withdraws from social activities, loses track of time and place, and may wander mindlessly and get lost. Apathy, depression, and hallucinations may follow the previous symptoms. The patient becomes more and more dependent on a caregiver.

Advanced Phase

This phase includes stage 6 in the clinical staging. All cognitive abilities fail to some degree at this stage. Meaningful communication becomes very hard. The patient may not recognize their loved ones. Severe personality changes may occur, usually towards aggression and anxiety. Behavioral changes are not universal, so they may or may not be seen in every patient. Weight loss and loss of bowel control may happen. Increased hallucinations, delusions, and paranoia may be seen. Advanced patients need help with personal care, walking, sitting, and even swallowing. Thus, aspiration

pneumonia is the major cause of death among AD patients due to difficulty in swallowing.

Challenges of staging AD in the clinic

Compared to postmortem assessments, it is a lot more challenging to accurately diagnose AD in living patients due to multiple reasons. First, interpersonal differences in brain reserve and cognitive reserve create variability in disease trajectory for each patient. The temporal gap between the pathology accumulation and initial clinical symptoms of the disease may be up to 10-15 years (Figure 1.1).

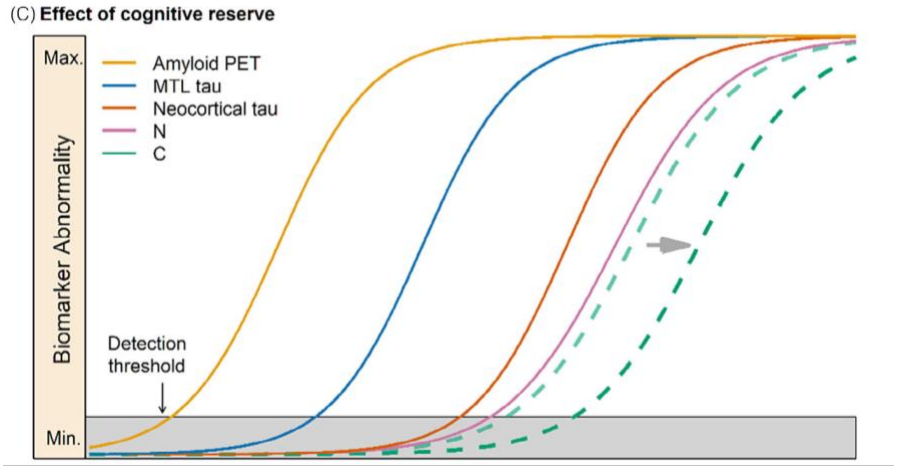

Figure 1. 1 The effect of cognitive reserve on the transition from pre-clinical to clinical stage (Jack et al., 2024)

Exceptional cognitive reserve (dashed dark green line) may delay the clinical onset of the disease (dashed light green line) showed by the horizontal gray arrow.

This temporal lag may be due to cognitive reserve (the ability to compensate for dysfunctional networks by activating alternative networks) and/or brain reserve or resilience (the brain's capacity to endure the existing pathology and related biological imbalances). Second, it is very common to see plaque and tangle pathology in AD

patients accompanied by other pathologies such as TDP-43 in frontotemporal dementia, alpha-synuclein (α -syn) in Lewy body disease, small or large vascular infarcts, and CAA. Those cases are often called mixed dementia rather than AD. Co-pathologies exacerbate the plaque and tangle pathology and speed up the clinical manifestation of AD (Robinson, 2021). Additionally, biomarkers and imaging techniques for TDP-43 and α-syn are less developed compared to pathological Aβ and tau markers and detection techniques, which makes the information about those co-pathologies less available; therefore, an unequivocal differential clinical diagnosis of AD is more challenging.

Finally, there is technical difficulty in detecting or monitoring the building blocks of plaques and tangles in living patients, particularly small diffusible aggregates such as tau oligomers, whose toxicity will be discussed in detail in the upcoming chapters. The current PET tracers cannot differentiate between oligomers vs. filamentous plaques or tangles. The “unmasking” of disease trajectory by the development of more sensitive and specific fluid AD biomarkers (Islam, 2025) and next-gen PET tracers will eventually allow scientists to integrate pathological and clinical staging of AD progression improved clinical trial enrollment and earlier therapeutic interventions.

AD Pathological Proteins: Biology and Function

Amyloid beta (Aβ)

Aβ is a 37-49 amino acid residue peptide that gets cleaved from the larger Amyloid Precursor Protein (APP), which is a transmembrane protein with a single-membrane spanning domain with a long flanging extracellular N-terminal domain and shorter intracellular C-terminus. APP is synthesized in the endoplasmic reticulum and transferred to the Golgi for maturation and eventually to the cell membrane to play

multiple roles in cellular processes, including but not limited to nervous system development, synaptogenesis, axonal growth and guidance, dendritic arborization, and synaptic plasticity (Muller, 2017; Chen, 2017). APP is expressed by the excitatory neurons as well as the GABAergic interneurons in the neocortex and the hippocampus, and it interacts with extracellular matrix players (collagen and heparin), lipoprotein receptor proteins, and several mediators and adaptor proteins that regulate multiple molecular pathways (Muller, 2017). APP can be processed in two alternative pathways: nonamyloidogenic and amyloidogenic. Cleavage of APP via alpha-secretase creates the APPα peptide, which has been shown to inhibit caspase-dependent apoptosis and upregulate neuroprotective molecules (Muller, 2017) and is therefore neuroprotective. The further cleavage of the remaining APP transmembrane fraction with gamma-secretase results in a small peptide (P3) with a 3kDa molecular weight. There is no known function of P3. However, no indicator of P3-related toxicity was found. Neuronal activity and the activation of muscarinic acetylcholine receptors are shown to increase alpha-secretase activity (Muller, 1997). Another sequential cleavage of APP, on the other hand, via beta-secretase and gamma-secretase, which eventually creates a 40-42 amino acid-long Aβ peptide that has shown to be toxic, especially when it forms oligomers. One of the pathways through which Aβ promotes cell death is binding p75NTR receptors to initiate the intracellular apoptotic signaling cascade (Sotthibundhu, 2008). Aβ also activates caspase 3 and caspase 8, causing the creation of the reactive oxygen species (ROS), which disrupts a variety of mechanisms in the cell (Kumar, 2023; Stadelmann, 1999).

The relation of Aβ to AD was not known until a 1984 study in which the researchers extracted Aβ from the senile plaques in AD brains and sequenced it (Glenner, 2012). With more groups working on it, Aβ became known as a 37-49 amino acid peptide with a 4kDa molecular weight and was associated with many functions in the cell, such as regulating synaptic plasticity via regulating synaptic transmission (Rice, 2019; Hampel, 2021) and vesicle trafficking (Wilhelm, 2014), helping to protect the integrity of the blood-brain barrier (BBB), and suppressing microbial activity (Jeong, 2022). Both Aβ40 and Aβ42 peptides are present in the AD plaques. However, the ratio is more skewed towards the Aβ42 form. Nuclear magnetic resonance (NMR) spectroscopy studies showed that Aβ42 has different biophysical properties and conformational states compared to Aβ40, making the 42 forms more prone to self-aggregate (Hampel, 2021). Although an extensive review of the Aβ pathology in AD is beyond the scope of this thesis, a possible explanation for the increased ratio of Aβ42/ Aβ40 in familial AD patients might be due to mutations in the presenilin-1 and -2 genes (PSEN1, PSEN2) that were discovered in genomic linkage analysis studies in familial AD pedigrees (Bertram, 2009; Gerrish, 2012). Presenilins, along with the presenilin enhancer, nicastrin, and Aph-1 Homolog A, form the gamma-secretase enzyme (De Strooper, 2003). Some of the known presenilin mutations were shown to result in decreased efficacy of the enzyme and contribute to the increased Aβ42/ Aβ40 ratio (Chen, 2017).

According to the still-followed amyloid cascade hypothesis (ACH) of AD, Aβ monomers start to self-aggregate due to an unknown etiology, which causes ionic imbalances and increased ROS formation that eventually disrupts tau homeostasis and

causes tau to self-aggregate as well (Hardy, 1992). Together, this results in synaptic and, eventually, cellular loss. Despite the ongoing debate on the matter, there are gaps that the hypothesis falls short to explain:

-Non-overlapping tau and Aβ trajectories in the brain

The ACH suggests that Aβ directly or indirectly initiates tau pathology by interacting with tau itself (Stancu, 2014; Blurton-Jones, 2006) or activating the tau phosphorylating kinases or by triggering an immune response by activated glial cells or inhibiting tau degradation by proteosomes, collectively resulting in aberrant posttranslational modifications (PTMs) that yield detachment of monomeric tau from the microtubules and making self-aggregates (Blurton-Jones, 2006) (see below for a discussion of tau biology and function). However, the trajectory of Aβ and tau pathology in the brain does not fully overlap. While Aβ forms fibrils and subsequent cross-beta pleated structures (Sunde, 1998) starting from the neocortex and spreading to all cortical regions and midbrain and later on to the cerebellum and brainstem (Hampel, 2021), tau follows a different route. Tau starts to accumulate into NFTs in subcortical regions such as the locus coeruleus and limbic regions (e.g., the transentorhinal cortex) and spreads to to other limbic regions such as hippocampus, subsequently appearing in the neocortical regions (Braak, 1991). Therefore, although regional plaque load was found to be a strong predictor of the regional NFT pathology accumulation by multiple studies and computer models, the overall trajectory of plaque and tangles do not align until the later stages of the disease.

-Cognitive decline that does not parallel Aβ pathology

Aβ might start to silently accumulate in the brain 20-30 years prior to the initial cognitive deterioration without any symptoms. According to Aβ-PET studies, Aβ plaques already reach their peak abundance before the clinical stage and remain fairly stable. Conversely, plaque removal by immunotherapy has only very modest effects on cognitive improvement in clinical trials (see below). By contrast, tau-bearing NFT-PET levels continue to rise as the cognitive decline deepens. The dissonance may suggest reconsidering the ACH as an accurate disease model.

-Failed clinical trials to improve cognition by removing Aβ plaques

AD clinical trials have been focused on removing Aβ plaques by expecting this would reverse the cognitive deterioration. Even the two FDA-approved amyloid-targeting drugs (Aducanumab and Lecanemab), which have been administered despite their serious side effects, could not improve cognition or mood (Hunter, 2024). Therefore, unfortunately, amyloid-attacking drugs are far from showing a real impact on patient's lives, which mitigates the credibility of the ACH hypothesis.

Tau Tangles: From physiological monomers to NFT pathology

The second hallmark of AD, and the focus of this dissertation, is the pathological form of a physiological protein called tau. In 1974, NFTs were isolated from an AD brain, and the following year, tau, as a newly defined protein, was extracted from a porcine brain without knowing it was the building block of the previously isolated NFTs (Kirschner, 2024). About a decade later, in 1986, Inge Grundke-Iqbal, under the supervision of Lester (Skip) Binder, showed the presence of abnormally hyperphosphorylated tau in the paired helical filaments isolated from an AD brain, also

paving the road for the discovery of other tauopathies (Grundke-Iqbal, 1986a, Iqbal, 2006).

Tau is a monomeric, intrinsically unfolded protein that is coded by the MAPT gene located on chromosome 17. Due to the alternative splicing of exons 2 & 3 (on the N terminal) and exon 10 (on the microtubule-binding domain), there are six isoforms of tau (0N3R, 1N3R, 2N3R, ON4R, 1N4R, 2N4R), which all are expressed in humans (Guo, 2017). The sequence of those isoforms varies between the 352-441 amino acid residues. Functionally, tau has four domains: the N-terminus (1-165), the proline-rich region (166-242), the microtubule-binding region (MTBR, 243-367), and the C-terminus (368-441) (Barbier, 2019) with different electrostatic properties. At physiological pH, proline-rich and MTBR regions are positively charged due to their predominant positively charged amino acids, while the N-terminus consists of mostly negatively charged amino acids, altogether contributing to tau's interaction with several ions and molecules, including microtubules (MTs) (Castro, 2019; Mietelska-Porowska, 2014).

Tau is considered a hydrophilic molecule due to these charged regions and low abundance of the hydrophobic amino acids (i.e., alanine, valine, and methionine) (Avila, 2016). As previously stated, the primary structure of tau is unfolded, however, the intramolecular structures may cause both N- and C-terminus fold over the MTBR domain creating a "paperclip" structure (Jeganathan, 2008) that is suggested to be protective against self-aggregation due to blocking the interaction of the folded terminals with other molecules (Avila, 2016; Oakley, 2020). It is also suggested that for tau to form the paperclip folding, it has to be bound to MTs, and once it detaches, the paperclip

unfolds (Di Primio, 2017). In this regard, the formation of paperclip structures might be impacted by MAPT mutations, e.g., P301L (Di Primio, 2017).

Tau protein expression is primarily detected in the brain; however, it is also present in the peripheral nervous system as well as in the periphery, such as the submandibular gland, colon, and abdominal skin (Dugger, 2016). In the brain, tau is expressed by neurons, oligodendrocytes, and astrocytes across all the regions. Research has shown that tau can also be localized in synapses and dendrites, involving synaptic transmission, and can interact with the cell membrane regulating neurite development, or be transferred into the nucleus to play various roles (Grundke-Iqbal, 1986a, Guo, 2017; Younas, 2023; Litman, 1993).

Physiological Tau Has Multiple Functions

Microtubule Binding and Cellular Trafficking

Tau is most known for its role in binding to MTs for dynamic stabilization. MTs are composed of globular alpha- and beta-tubulin units bound to either GDP or GTP. MTs have two ends, plus and minus, both growing; however, the plus grows faster and includes a GTP-cap, which prevents a rapid shrinking through depolymerization of the units. Tau binds to both ends (Breuzard, 2013; Qiang, 2018), with a primary role in stabilizing the minus end by binding to GDP-bound tubulin while facilitating stable elongation at the plus end by interacting with GTP-bound tubulin. Thus, tau both stabilizes and promotes the elongation of MTs (Barbier, 2019).

In addition to its structural role, tau regulates axonal transport, which is essential for the movement of cytoskeletal proteins, organelles, and vesicles within neurons, through slow and fast transport that differ in their movement pattern. The anterograde

transport occurs from the cell body to the synapses via kinesin molecules that can move along the MTs, whereas retrograde transport occurs from synapses to the cell body via dyneins. Tau can interact directly with kinesin and dynein or alter MT dynamics, thus influencing the efficiency and direction of axonal trafficking (Mietelska-Porowska, 2014; Dixit, 2008; Lacovich, 2017). PTMs or mutations of tau may change its electrostatic feature as well as the conformation, thus impacting axonal transport. Several animal and human studies demonstrated that axonal transport is disrupted in AD due to disassociations of cargos, reduced MT binding, or changing the direction of dynein (Morfini, 2002; Morfini, 2009; Dixit, 2008) due to the activities of multiple kinases, such as glycogen synthase kinase-3 beta (GSK3β), presenilin-1 (PS1), c-Jun N-terminal kinase 3 (JNK3), and Casein kinase 2 (CK2) that was altered by the accumulation of pathological Aβ and tau (Kanaan, 2013).

Synaptic Function

Tau may play a role in regulating synaptic vesicular release from the presynaptic compartment by activating kinases and phosphatases (i.e., GSK3β and PP1, respectively) (Mietelska-Porowska, 2014). It also acts as a postsynaptic scaffolding protein and modulates the activity of c-Src and Fyn kinases (Mietelska-Porowska, 2014). Additionally, tau facilitates the formation of the Fyn & PSD95/ NMDA complex, and in the absence of physiological tau, Fyn cannot be trafficked to the postsynaptic dendrites (Ittner, 2010). Therefore, physiological tau is considered essential for LTP (Kimura, 2014). Tau gets released to the synaptic compartment in an activity-dependent manner (Frandemiche, 2014). Although the exact mechanism(s) is yet to be explored, numerous animal model studies, as well as data from AD patients, indicate that several

tau PTMs, mutations, and oligomers may impair LTP (Lasagna-Reeves, 2012; Robbins, 2021; Fa, 2016) through reversal of LTP toward LDP or reducing synaptic transmission through reducing the vesicular activity (Zhou, 2017).

Nuclear Function

Data have shown that tau can be present in the nucleus, primarily around the dense fibrillar component (DFC), which is localized in the nucleolus (Brady, 1995; Loomis, 1990), specifically where pre-ribosomal RNA is processed (Bukar Maina, 2016), modulating gene expression (Siano, 2019). Studies have also shown that tau binds to DNA and increases its stability by increasing its melting temperature (Guo, 2017) and protecting it from free reactive oxygen species (ROS) acting like a heat shock protein (HSP) (Guo, 2017). Tau is also involved in DNA repair mechanisms (Violet, 2014). Interestingly, similar to MT binding, the DNA binding ability of tau gets reduced upon phosphorylation (Guo, 2017). Therefore, phosphorylation also impacts the behavior of nuclear tau.

Regulating Glucose Metabolism

Another function of tau is regulating brain glucose metabolism through its bidirectional interaction with insulin. Insulin is known to influence hippocampal plasticity and memory function, though the precise mechanisms have remained unclear (Fernandez, 2012; Grillo, 2015; Jo, 2025). Multiple studies have highlighted glucose insensitivity and insulin resistance in AD patients, with some researchers even proposing AD as a potential Type III diabetes mellitus (Sotiropoulos, 2017; Talbot, 2012; Gonzalez, 2022). Marciniak and Leboucher demonstrated that deleting tau in mice impaired hippocampal responses to insulin and caused insulin resistance, which

resulted in increased food intake independent of leptin and metabolic disturbance. Additionally, tau knockout mice showed lower long-term depression (LTD) on hippocampal slides, indicating disrupted memory and learning (Marciniak, 2017).

Intriguingly, human studies have revealed that insulin influences the activity of GSK3β, a key enzyme involved in tau phosphorylation (Hobday, 2021). Interestingly, antidiabetic drugs, such as metformin, can slow down cognitive decline in AD (Tran, 2024). Furthermore, elevated insulin levels have been observed in hippocampal neurons with hyperphosphorylated tau (Rodriguez-Rodriguez, 2017). A recent study also suggests that tau may directly suppress insulin secretion in the pancreatic B-islet cells by regulating MT assembly (Mangiafico, 2023). Our own research further supports a correlation between impaired insulin mechanism and clinical diagnosis of AD (Beck, 2022).

Oligodendrocyte Function

Finally, due to its presence in glial cells such as astrocytes, tau may have similar regulatory mechanisms as in neurons. However, with respect to oligodendrocytes, tau plays a unique role in the complex maturation and myelination process of these cells by regulating Fyn kinases (Guo, 2017; Mueller, 2021). A study found that knocking down tau in oligodendrocytes in vitro impaired the outgrowth and differentiation mechanisms, therefore resulting in reduced neuron-glia contact formation when the oligodendrocytes were cocultured with the dorsal root ganglion neurons (Seiberlich, 2015). Another study found that silencing the Fyn expression in mouse oligodendrocytes in vitro reduces their ability to apoptosis (Luo, 2020). Therefore, Fyn is a key kinase in oligodendritic function, and so is tau as a direct regulator of Fyn.

Post Translational Mutations (PTMs) That May Contribute to Tau Aggregation

Despite the disease history that goes back more than a century, the etiology of AD is still not fully understood. The presence of pathological Aβ folded into beta-sheet structures and pathological tau self-aggregated in the NFTs are well established. However, what triggers the self-aggregation of these two molecules, which both have important physiological functions in the brain as monomers, is yet to be elucidated. Some pathogenic mechanisms are suggested for making normal Aβ and tau monomers more prone to aggregation, such as free radicals, which attack proteins, lipids, and DNA, or PTMs that may change the charge distribution, physiological function, as well as the physiological properties of Aβ and tau, or maybe both collectively making them pathological entities. Some of the known PTMs that tau receives are listed below:

Phosphorylation

The central focus of tau PTMs has long been phosphorylation. Phosphorylation is adding a phosphate group to serine (Ser), threonine (Thr), or tyrosine (Tyr) residues of a protein via kinases. The longest tau isoform has around 85 phosphorylation sites (Basheer, 2023), and the number of phosphorylated sites is increased in AD brains several fold compared to the controls (Grundke-Iqbal, 1986a, Alonso, 1994; Kopke, 1993). There are some phosphorylation sites unique to pathological tau (Thr69, Ser210, Ser214, Thr403, Ser409, Ser422) and some sites that are observed both in normal tau as well as the pathological tau (Ser202, Ser205, Tyr217, Thr231, Ser396, Ser404, Ser412) (Basheer, 2023). The major identified kinases that phosphorylate tau are GSK3β, cyclin-dependent kinase-5 (Cdk5), mitogen-activated protein kinases (MAPKs),

and Src family kinases (Fyn, Src, and c-Abl) (Guo, 2017; Basheer, 2023; Hernandez, 2013; Kimura, 2014; Lebouvier, 2009).

Abnormal phosphorylation has been associated with the self-aggregation process of tau by reducing its affinity to bind MTs (Mandelkow, 1995). Detached tau starts to form dimers and oligomers and the subsequent higher-order paired-helical filaments (PHFs) and NFTs. Phosphorylation also impacts tau binding to its binding partners, such as Fyn, resulting in diminishing its aforementioned nuclear and synaptic functions. Another facet of the increased phosphorylation tau is due to the reduced phosphatase activity, which is the removal of a phosphate group. PP1, PP2A, PP5, and PTEN are some of the major phosphatases that remove phosphate groups from tau molecules. In tauopathies, including AD, their activity was shown to often decrease yielding hyperphosphorylation (Basheer, 2023; Martin, 2013; Kerr, 2006), therefore contributing to tau pathology.

S199/Ser202/Thr205 phosphorylation is detected by the AT8 antibody (Biernat, 1992; Goedert, 1995) and used for the Braak staging to label NFTs in AD pathological diagnosis (Kelley, 2022). Another commonly used tau antibody (PHF-1) binds to pS396/pS404 tau residues and is used to label extracellular NFTs (Otvos, 1994). pT153, pS262, pS422, and TG3 antibodies, on the other hand, detect various abnormal phosphorylation, which are suggested to detect earlier forms of pathological tau (Augustinack, 2002).

Acetylation

This process is defined by adding an acetyl group to the N terminus or lysine residues of a protein by acetyltransferases (histone acetyltransferase (HAT) or lysine

acetyltransferase) cAMP-response element binding protein (CREB)-binding protein (CBP); and can be reversed by deacetylases (histone deacetylase (HDAC) or lysine deacetylase; mostly sirtuin 1 (SIRT1) and HDAC6), therefore is considered as a reversible modification, similar to phosphorylation. Acetylation is related to both the physiological and pathological state of tau. Acetylation on 259, 290, 321, and 353 lysine residues has been detected in the control cases (Cook, 2014), whereas acetylation on lysine 174, 274, 280, and 281 has been shown in several tauopathies (Guo, 2017; Tracy, 2016; Trzeciakiewicz, 2017).

Acetylation and phosphorylation both change the electrical charge of tau, conferring a greater negative charge (Castro, 2023). In physiological conditions, the negatively charged C terminus of microtubules greatly interacts with positively charged molecules, including the MTBR and C-terminal domain of tau. However, both acetylation and phosphorylation lead to a relatively negative charge in these domains and thus decrease tau's affinity to bind MTs (Trzeciakiewicz, 2017). In an in-silico study, the researchers modeled tau's behavior under several phosphorylation and acetylation PTMs and concluded that, compared to the structural changes, electrostatic changes impact tau binding to MTs more (Castro, 2023). Another study also found that acetylation exacerbates tau pathology by decreasing its degradation (Min, 2010).

Truncation

Physiologic tau has a fixed life span in cells due to its regulated turnover. However, due to its presence in non-dividing neurons and providing structural support to other large cell assemblies for months to years, it is considered a long-lived protein (LLP). Truncation by proteolysis is a natural process for LLPs to maintain normal protein

function, which may be compromised due to the accumulated PTMs over time. Studies have shown that physiological tau gets proteolytically cleaved by caspases and calpains in neurologically normal human brains (Friedrich, 2021; Yang, 1995). Additional pathology-associated truncation sites were found in AD brains (Chu, 2024) and non-AD tauopathies (Guillozet-Bongaarts, 2007). An in vitro study looked at the impact of the truncation of tau from different domains on site-specific phosphorylation and self-aggregation of tau. They found that the truncation of the first 150 and the last 50 amino acids greatly enhanced tau hyperphosphorylation, aggregation, and binding to human brain-derived oligomer seeds, while truncation of the last 20 amino acids did not have a similar impact (Gu, 2020). They also found that the Tau151–391 truncated fragment showed the highest pathological activities.

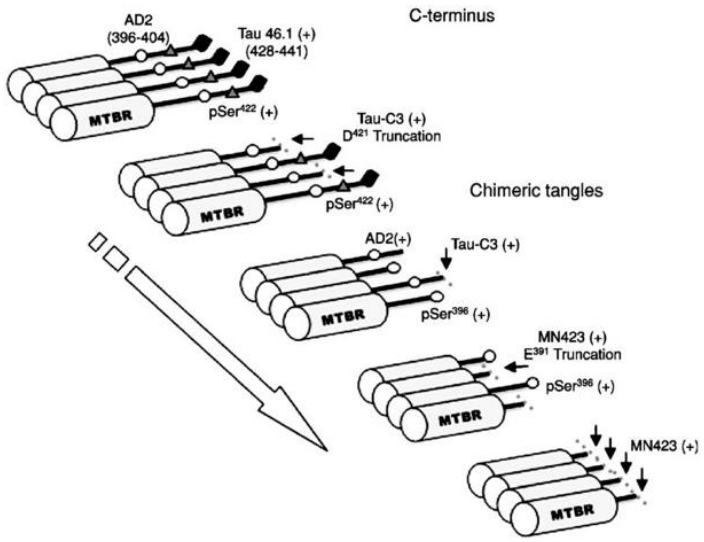

Figure 1. 2 The sequential cleavage of tau suggested by Basurto-Islas et al., 2008

The most studied truncation sites are Glu391 and Asp421, shown to be present in vitro (Gamblin, 2003) as well as in the PHFs and late-stage NFTs in AD brains (Zhou, 2018; Arezoumandan, 2022; Basurto-Islas, 2008). Basurto-Islas and colleagues found that the tau labeling with Mn423 and Tauc3 antibodies (detects Glu391 and Asp421

truncated tau, respectively) correlates with the Cambridge Examination for Mental Disorder of the Elderly (CAMDEX) and Braak staging (Basurto-Islas, 2008). They also found that tau sequentially gets cleaved from the C terminus towards the MTBR (their suggested model is shown in Figure 1.2) throughout NFT maturation, and that Glu391 and Asp42 truncations are mutually exclusive; therefore, co-labeling with Mn423 and Tauc3 did not overlap (Basurto-Islas, 2008). Another study found that caspase-cleaved Asp-421 tau was associated with increased calcium-dependent phosphatase calcineurin activity and subsequent mitochondrial fragmentation and dysfunction (Quintanilla, 2009).

Ubiquitination

Ubiquitination is the first step of a major protein degradation system that works in the cytoplasm and nucleus by attaching ubiquitin tags to damaged, malfunctional or mutant proteins via various ligases to initiate the recognition and degradation of them by proteosomes (Hallengren, 2013). The turnover of full-length monomeric tau is thought to be through the ubiquitin-proteosome system (UPS). However, the conformation and aggregation state of tau was suggested to determine whether it would go through the ubiquitin-dependent or independent clearance systems (Lee, 2013). Truncated tau, oligomeric tau, and PHFs are inaccessible to proteosomes. Therefore, they need to be degraded by autophagosomes (Lee, 2013). Interestingly, highly ubiquitinylated tau in the PHFs and CSF from AD patients was reported (Iqbal, 1991; Iqbal, 1998). Additionally, several detected lysosomal abnormalities in AD may contribute to the failure of the UPS in pathologic tau clearance (Ihara, 2012).

Glycosylation and Glycation

Tau also can receive a carbohydrate molecule to a lysine residue enzymatically (glycosylation) or to asparagine or serine/threonine residues non-enzymatically (glycation). Glycosylation is well-controlled and contributes to various cellular functions (Ohtsubo, 2006; Uceda, 2024). O-glycosylation, in particular, may decrease tau phosphorylation by GSK3β (Liu, 2004). Contrarily, glycation is observed in disease and aging, preventing protein degradation or release from the cell, therefore greatly promoting aggregation (Martin, 2011). Glycation also makes proteins more sensitive to oxidation, promotes ROS production, and blocks tau degradation (Uceda, 2024; Martin, 2011).

Besides the aforementioned PTMs, tau can get methylated, SUMOylated, nitrated, polyaminated, and oligomerized (Alhadidy, 2024). All of these modifications play a role either in the direction of pathology development or against self-aggregation. However, none of them, including phosphorylation as the most suspected modification for aggregation, by itself has been proven to initiate tau aggregation in AD (Wegmann, 2021; Necula, 2004).

PTMs may also compete with each other; for instance, acetylation may compete with phosphorylation, and ubiquitination may compete with acetylation. Or they bidirectionally impact each other. Oligomerization has been shown to be associated with the dysfunctional UPS (Tai, 2012). Impaired glucose metabolism causes overactivation of GSK3β, which then suppresses O-glycosylation on the Ser/Thr residues (Liu, 2009). To summarize, all the PTMs that a tau molecule receives play a collective and possibly synergistic role in determining its biophysical and chemical state, which eventually

defines its fate on either to stay attached to MTs and maintain its numerous functions or to detach from MTs, self-aggregate, and trigger so many molecular and metabolic abnormalities in the cell.

Are We Targeting the Wrong Target: Tangles vs oligomers and pre-tangle tau

The discovery of tau in NFTs in AD in 1974 opened up new possibilities to establish functional associations with cognitive decline, which did not correlate with Aβ and plaque load. The advent of large cohort clinical pathological studies revealed that NFT pathology, on the other hand, was tightly correlated with MMSE scores and other global cognitive measures (Nelson, 2012). This discovery put the NFTs in the spotlight. They were considered as the source of toxicity that entails dysfunction of various cellular mechanisms as well as the subsequent inevitable neuronal death as the disease progresses. However, as time progresses, more research on the matter has been conducted only to find that NFTs might not be as toxic as originally thought. Tau PET studies revealed that NFTs can start building up in the brain for a decade prior to the symptomatic stage (Bateman, 2012). Not only can NFT-bearing neurons stay alive, but they also remain functional. An animal study found that, despite the presence of NFTs, neurons can remain integrated in the neuronal circuits (Kuchibhotla, 2014). Another recent study went a little further and said NFTs are dynamic structures, not just tombstones, contributing to the equilibrium for soluble tau (Croft, 2021). In animal studies, NFTs, along with monomers, were shown to be incapable of seeding pathology in mice, while oligomers succeeded (Ghag, 2018). Another study showed that intraneuronal NFTs in P301L mutation-carrying mice did not halt the integration of

synaptic inputs (Rudinskiy, 2014). Altogether, these accumulating data increasingly suggest that NFTs are not the real culprit in neurodegeneration in AD.

Oligomers: Without a consensus in terminology, oligomeric tau can be defined as small tau clusters that are made of two (i.e., dimers) or more monomeric tau proteins. Electron microscopy and atomic force microscopy studies demonstrated that recombinant oligomeric tau has a spherical form with around 12-14nm diameter (Flach, 2012; Cehlar, 2024). As a typical amyloidogenic protein, tau oligomers are enriched with beta sheets but not necessarily cross-beta structures, which are seen more in NFTs. Intriguingly, a recent cryo-EM study showed that the folding of tau filaments may vary from disease to disease (Shi, 2021) increasing the complexity of the disease etiology and providing evidence that different oligomeric tau moieties might exist in different tauopathies with different dynamics in the synapses, or even among patients with the same disease, depending on the PTM profiles and the genetic background of the patient.

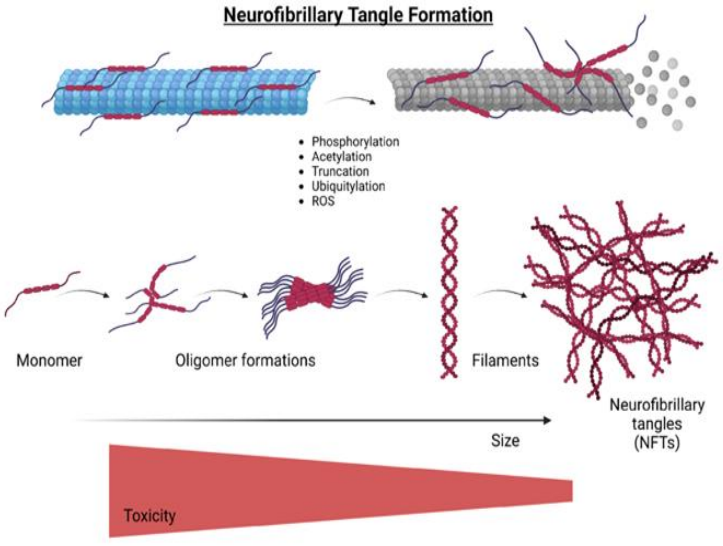

Figure 1. 3 Illustration of tau detachment and oligomer formation

Oligomers are considered intermediate pre-tangle species between the physiological monomers and NFTs (Shafiei, 2017) and have remarkable toxicity (Figure 1.3). Recombinant tau oligomers were shown to impair membrane integrity by causing phospholipid vesicle leakage and reduce cell viability (Flach, 2012), inhibit fast axonal transport (FAT) (Ward, 2012), induce mitochondrial dysfunction and fission (Shafiei, 2017), and cause memory impairment and synaptic dysfunction (Lasagna-Reeves, 2011).

More intriguingly, research indicates that AD brain-derived oligomers are even more toxic than recombinant oligomers and have the ability to propagate pathology with endogenous murine tau once they are injected in mice (Lasagna-Reeves, 2012). Collectively, findings indicate that tau oligomers are a lot more toxic than fibrillar tau and NFTs. It might be speculated that it is due to the spherical structure of the oligomers, which leaves the pathologic epitopes exposed, or the organization of the β -sheet structures in the oligomers, which are not stacked into the cross-beta sheet forms as they are in NFTs. An alternative explanation might be the ability of oligomeric tau to be taken up by neuronal and non-neuronal cells via phagocytosis and pinocytosis for degradation. The fate of internalized oligomeric tau is relatively a new research question. Although there are studies that demonstrated the internalization of full-length monomeric human tau and oligomeric tau and the degradation of the monomers in cell models, how effective the degradation of the oligomers remains elusive. It is possible that impaired endosomal-lysosomal pathway in diseases might cause an ineffective digestion, which entails the release of the still toxic oligomers into the synaptic cleft further in the brain only to be taken up by another cell and spread the pathology. There

are also additional “pre-tangle tau” PTMs and formations that confer toxicity such as pS422 and TNT2 (Combs, 2016; Tiernan, 2016; Sayas, 2021) and likely contribute to oligomer formation. These species will be discussed in Chapter 2.

Tau Pathology Spread in the Brain

There are multiple hypotheses for pathological tau propagation in the brain. Tau can spread trans-synaptically due to its activity-dependent release in the presynaptic terminal (Frandemiche, 2014; Colom-Cadena, 2023). Post-mortem immunolabeling of pathological tau indicated the presence of tau in both pre-and post-synaptic terminals (Puangmalai, 2020). Therefore, pathological tau might propagate long distances in the brain via a series of reuptakes and releases between anatomically connected brain regions,. Supporting this idea, tau-PET images confirm the presence of tau NFTs in anatomically and functionally connected brain regions (Franzmeier, 2022; Colom-Cadena, 2023).

Another hypothesis supports a prion-like propagation of tau. Once tau starts to accumulate in the locus coeruleus and the transentorhinal cortex, it might spread in a prion-like manner, seeding pathology in normal tau wherever it encounters. “Seeding” terminology comes from the prion field and is used for the process of a normal protein becoming a pathological disease-causing form due to conformational changes once it interacts with another disease-causing form (Telling, 1996).

A third hypothesis is based on a potential regional deposition of tau pathology based on a possible regional or cell-type specific susceptibility. The brain regions with high metabolic rates and energy demand, e.g., limbic areas and neocortex, are found to be hubs for tau accumulation (Adams, 2019). It might be due to both a possible

selective vulnerability or to the spread between the functionally connected regions, e.g., resting state large-scale brain networks. These theories are not mutually exclusive; they might happen in different regions simultaneously, collectively spreading the tau pathology in the brain.

Default Mode Network (DMN) as a model connectome for tau pathological spread

Neuronal cells communicate through their trillions of synaptic connections between each other as well as the non-neuronal cells in the brain. Hence, the brain can be considered a huge communication center comprised of countless connectomes. Communication via electrical or chemical signals is essential for neurons not only to function properly but also simply to survive. This communication is not limited to the proximity between neurons. Centuries of neuroanatomical studies have shown that long synaptic projections enable neurons to communicate with their partners even from a long distance in the brain through white matter tracks and thinly myelinated fiber bundles that facilitate coupled neuronal activity between non-neighboring regions.

Aside from postmortem neuroanatomical studies, in vivo visualization of the structural connectivity of these communication networks is mostly achieved by structural magnetic resonance imaging (sMRI) or diffusion tension imaging (DTI) (Babaeeghazvini, 2021). By contrast, visualizing the functional connectivity (fc) of these communication networks is based more on their statistical connectivity, or the probability of coactivation between the regions during functionally demanding tasks. Functional magnetic resonance imaging (fMRI) provides measures for fc, and once it is combined with structural measures, it provides highly accurate models to assess the precise

connectomes in the brain mediating cognitive function (Babaeeghazvini, 2021; Litwinczuk, 2022).

With the increased research on the brain's glucose metabolism via PET imaging in the late 90's, an interesting discovery happened. Several groups were trying to measure brain glucose levels, which would increase due to neuronal activity-dependent oxygen consumption. Their approach was subtracting the basal brain activation from the task-related activation. To their surprise, while most tasks resulted in oxygen consumption in discrete anatomically connected regions suggesting that activation of those networks mediated those tasks, oxygen levels of other discrete brain areas were decreased during the tasks. The same phenomenon was repeatedly detected in multiple studies and was further tested with the incorporation of fMRI, which also assesses the visualization of blood oxygenation and flow to these regions. The brain regions involved in this phenomenon were collectively named the Default Mode Network (DMN) (Raichle, 2015), the brain network that is active by default.

DMN regions: The widely accepted DMN regions, also referred to as hubs, minimally include the medial prefrontal/frontal cortex (FC, e.g., Brodmann areas 9/10), posterior cingulate cortex (PCC, Brodmann areas 23/31), and precuneus (PreC, Brodmann area 7) (Hafkemeijer, 2012; Utevsky, 2014). Other regions are suggested to be involved, such as the angular gyrus, hippocampus, and inferior temporal cortex, but in the context of this dissertation, FC, PCC, and PreC are referred to as the main DMN hubs.

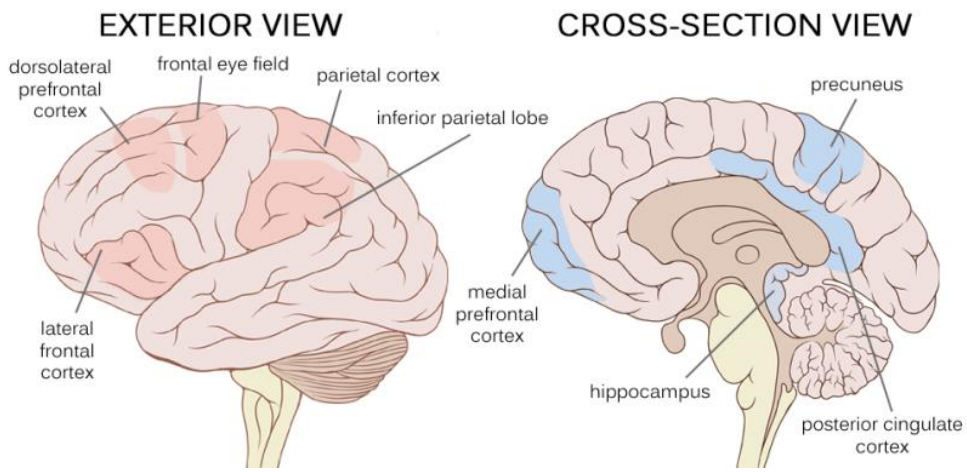

Figure 1. 4 Illustration of the main default mode network (DMN) hubs, adopted from Sultan Tarlaci, Journal of Neurophilosophy (2023)

Medial Prefrontal Cortex

This region, referred to as FC in this thesis, is located in the front of the frontal lobe, bordering the frontopolar cortex, sensory-motor areas, and the anterior cingulate cortex. Based on the cytoarchitectural differences, it has four subregions with distinct roles in cognitive function. FC is the association cortex of the frontal lobe that receives motor and sensory input from associated cortical areas as well as higher-order information from the hippocampus, subiculum, posterior cingulate cortex, amygdala, and thalamus (Xu, 2019) to perform complex cognitive functions such as decision-making, inhibitory control, emotions and perception, and language processing (Euston, 2012). FC is also involved in learning and memory consolidation (Euston, 2012; Jobson, 2021).

Abnormal FC activity is associated with several psychiatric disorders, such as bipolar disorder, schizophrenia, depression, and anxiety, as well as neuropathological diseases, such as Alzheimer's and Parkinson's diseases (Jobson, 2021). Although

without a consensus, in Aβ -positive but cognitively intact prodromal AD patients, abnormal fc changes between the FC and hippocampus were reported (Hedden, 2009; Sheline, 2010). The discrepancy might be due to the difference in the analysis methods or possible subregional differences in the FC and hippocampus used for those studies. In amnestic MCI patients (aMCI), a more consistent trend starts to emerge, which is a decrease in fc between FC and hippocampus (Cai, 2017; Yue, 2015).

In the context of DMN, however, an increased fc of FC from the posterior DMN hubs (PCC/PreC) was found in aMCI patients (Gardini, 2015; Jin, 2012), which is often interpreted as a maladaptive response (Penalba-Sanchez, 2022). Once the disease advances, the trend becomes clearer, and FC becomes more functionally detached from PCC/PreC in AD cases (Scherr, 2021; Vipin, 2018). This might be partially due to the vascular dysfunction and atrophy that often accompany primary AD pathology. The decrease in fc of the FC was also found to correlate with episodic memory decline (Ranasinghe, 2014; Vipin, 2018).

Posterior Cingulate Cortex

PCC is a region that is part of the posteromedial cortex and is cytoarchitectonically characterized as the paralimbic cortex. PCC has many connections with other brain regions, including the retrosplenial cortex, PreC, hippocampus, and medial temporal lobes. The area itself is big and can be considered as two distinct dorsal and ventral parts, which might be involved in different tasks in different directions (Leech, 2011). Ventral PCC (Brodmann area 23) has been thought to be largely involved in the internal deep focus requiring tasks such as episodic and semantic memory retrieval, autobiographical thoughts, future planning, etc. The dorsal part of the

PCC (Brodmann area 31) involves broader communication in the brain, controlling the internal and external attention shifts and the co-activation/deactivations in synchrony with other brain networks, including the dorsal attention network and fronto-parietal cortical network (Leech, 2014). The activity of the dorsal PCC might increase during 'external attention demanding' tasks (Leech, 2011).

Possibly due to its high metabolism (~40% greater than the adjacent PreC) (Raichle, 2001; Pfefferbaum, 2011; Leech, 2014), this a susceptible region to metabolism changes in aging and diseases such as AD, ADHD, schizophrenia, focal lesions, autism, and depression (Leech, 2014). Although the level of the functional connectivity changes might be heterogeneous between the dorsal and ventral parts, in early AD patients, PCC activation decreases (Bai, 2009). The rapid activation/deactivation between the DMN and task-positive tasks is also impacted, possibly due to the diminished interconnectivity between the PCC and other related regions. Therefore, to make an accurate conclusion on the activity changes of PCC in different diseases as well as healthy aging, we need to better understand the complex activation pattern of the region during different tasks, which are seemingly external but require unexpected reasoning and rapid attention switch.

Precuneus

Another DMN hub is PreC, which is located in the posteromedial cortex, right above the PCC. This rectangular-shaped region is also neighbor to the cuneus and the somatosensory cortex. Cytoarchitecturally, the PreC has three subregions: dorsal anterior, dorsal posterior, and ventral (Cunningham, 2017). Those subregions are selectively involved in episodic memory, self-awareness, visuospatial control, and

consciousness (Yamaguchi, 2024). Possibly due to its connections to the sensorimotor cortex and the supplementary motor area (SMA), the dorsal anterior and posterior precuneus show activation during spatially guided behavior (Zhang, 2012). Anterior and posterior precuneus are also shown to be involved in motor imagery, such as a finger-tapping task (Zhang, 2012). Ventral precuneus, on the other hand, shows strong connections with PCC and is involved in episodic memory retrieval, recalling past experiences, interoception, and daydreaming (Stillesjo, 2019), which highly overlaps the activation pattern of the DMN on a larger scale.

Similar to the previously mentioned DMN regions, PreC shows aberrant fc in AD patients. Importantly, those changes occur starting from the early course of the disease. One study looked at the precuneus fc in a risk group that had a family member with AD and found an increased fc of precuneus without structural changes (Green, 2023). Interestingly, this connectivity was diminished in aMCI and AD patients. Another study showed parallel results that in AD patients, the fc between the hippocampus and precuneus, as well as the fc between the precuneus and post-central gyrus, was reduced, claiming the aberrant fc might proceed the effect size of the structural atrophy (Kim, 2013).

Notably, there is a growing interest in transcranial magnetic stimulation (rTMS) in various regions of the brain, including PreC, to halt AD progression. Although the sample sizes are modest and most studies primarily targeted early AD cases, overall results demonstrate a promising pattern, such as a positive effect on cognitive function and a delay in cognitive decline (Millet, 2023). There was even a Phase 2 clinical trial that targeted precuneus with rTMS in AD patients, which reported a stable CDR and

MMSE score in the rTMS-received AD group compared to the sham AD controls (Koch, 2022). Additionally, they observed local gamma oscillations in the rTMS-received AD group, which normally shows an irregular pattern in AD patients (Moussavi, 2022).

Besides their individual roles in autobiographical memory and interoception, episodic and semantic memory formation and storage, decision-making making, and executive function, in the context of DMN, the activity of FC, PCC, and PreC synchronizes when an attention-demanding external task is absent. This functional connectivity may change due to race, sex, normal aging, or diseases, including AD (Hafkemeijer, 2012; Misiura, 2020; Ficek-Tani, 2023). The intriguing point is that fc changes start to take place very early in the disease without any structural atrophy. Although those changes might be bidirectional depending on the disease stage, detecting DMN fc changes in people who are at risk of developing AD, or even for people with sporadic AD, may provide an incredibly useful platform to accurately predict the disease timeline and determine the patient group who might be better candidates for clinical trials.

AD plaques and tangles coincide in the DMN

Antemortem amyloid and tau PET imaging results reveal the presence of amyloid plaques and NFTs within the DMN hubs (Hojjati, 2021; Li, 2019; Yokoi, 2018). However, there are some contradictions in the literature regarding the relationship between these pathologies and functional connectivity (fc) changes, especially during the early stages of the disease, which will be discussed later. One of the most intriguing aspects is the overlapping trajectories of amyloid and tau in the DMN.

In typical AD, the origin and propagation patterns of amyloid plaques and NFTs differ. Amyloid plaques initially accumulate in the neocortex, particularly in association areas, and then gradually spread to other regions. In contrast, NFTs begin in the entorhinal cortex and hippocampus, extending to the limbic system and, eventually, to the neocortex. Although, in advanced stages of the disease, both amyloid plaques and NFTs spread throughout the brain, individuals with MCI may show positivity for both Aβ and tau within the DMN. When combined with fc data from fMRI, these findings help bridge the gap in understanding how these pathologies contribute to cognitive changes. As discussed in more detail in subsequent chapters, Aβ-carrying patients have been shown to demonstrate hyperaction and hyperconnectivity. However, the first study to combined tau and amyloid PET found that the fc changed direction and turned into hypoconnectivity once NFTs appeared (Schultz, 2017). Hence, the field is still trying to decode the fc changes due to amyloid and tau pathology. Yet, a more important question remains unanswered: Where is the more toxic pre-tangle tau in this picture?

DISSERTATION OBJECTIVES

Oligomeric tau toxicity has now been widely reported and shown to spread in the brain via multiple possible mechanisms. However, oligomeric tau in the context of AD is still an underexplored area, with more and more details continuing to emerge regarding the mechanisms underlying oligomer activity and behavior, as well as the binding partners and molecular pathways through which it causes dysfunction. Another largely unexplored facet of oligomeric tau is how it impacts cognition. Animal studies demonstrated that tau oligomers at the synapses disrupt LTP and impair learning and memory (Robbins, 2021; Fa, 2016). Since NFTs were shown to correlate inversely with

cognitive function and reflect its decline throughout the AD progression in living patients, oligomeric tau is expected to be highly detrimental to cognitive health. However, the absence of oligomeric tau-specific PET tracers prevents us from assessing the phenomenon in living patients. Therefore, the question of when tau pathology meets with cognitive decline remains unanswered. Hence, the goal of this dissertation project is to quantify early pathological tau within the DMN and to determine the extent to which this tau pathology is associated with cognitive decline. Due to all its previously mentioned features, the DMN should provide an excellent model connectome to study tau pathology-related cognitive changes throughout the AD progression.

We hypothesized that pre-tangle pathological tau accumulates early in the DMN in correlation to cognitive decline and with a possible regional difference among the DMN hubs. This overarching hypothesis was tested through three aims:

Aim1: Investigate pre-tangle tau pathology in the DMN hubs during the progression of AD. *We hypothesize that pathological pre-tangle tau epitopes accumulate in the DMN in early NFT pathological stages.*

Aim2: Determine the relationship between pre-tangle tau in DMN and related antemortem cognitive scores. *We hypothesize that pathological pre-tangle tau load correlates with antemortem cognitive performance (e.g., episodic memory, working memory, perceptual speed) and neuropathological scores (e.g., NIA-Reagan, Braak, CERAD).*

Aim3: Proteomics investigation of differential tau protein binding partners between PreC and PCC. *We hypothesize that tau pathology preferentially accumulates in PCC*

compared to PreC and that this is due to the presence of novel tau protein binding partners in PCC that mechanistically drive pre-tangle and NFT formation.

Impact Of The Proposed Work

Identifying the earliest pathological factors driving functional brain changes in AD will be crucial for modifying disease progression. In the absence of pre-tangle Tau-PET tracers, our study will pioneer efforts to investigate the accumulation and distribution of pre-tangle tau within DMN hubs during AD. If successful, this project may also identify novel tau-regulating targets for precision AD therapy.

REFERENCES

Adams, J. N., Lockhart, S. N., Li, L., & Jagust, W. J. (2019). Relationships Between Tau and Glucose Metabolism Reflect Alzheimer's Disease Pathology in Cognitively Normal Older Adults. *Cereb Cortex, 29*(5), 1997-2009. doi:10.1093/cercor/bhy078

Alhadidy, M. M., & Kanaan, N. M. (2024). Biochemical approaches to assess the impact of post-translational modifications on pathogenic tau conformations using recombinant protein. *Biochem Soc Trans, 52*(1), 301-318. doi:10.1042/BST20230596

Alonso, A. C., Zaidi, T., Grundke-Iqbal, I., & Iqbal, K. (1994). Role of abnormally phosphorylated tau in the breakdown of microtubules in Alzheimer disease. *Proc Natl Acad Sci U S A, 91*(12), 5562-5566. doi:10.1073/pnas.91.12.5562

Arezoumandan, S., Xie, S. X., Cousins, K. A. Q., Mechanic-Hamilton, D. J., Peterson, C. S., Huang, C. Y., . . . Irwin, D. J. (2022). Regional distribution and maturation of tau pathology among phenotypic variants of Alzheimer's disease. *Acta Neuropathol, 144*(6), 1103-1116. doi:10.1007/s00401-022-02472-x

Assal, F. (2019). History of Dementia. *Front Neurol Neurosci, 44*, 118-126. doi:10.1159/000494959

Augustinack, J. C., Schneider, A., Mandelkow, E. M., & Hyman, B. T. (2002). Specific tau phosphorylation sites correlate with severity of neuronal cytopathology in Alzheimer's disease. *Acta Neuropathol, 103*(1), 26-35. doi:10.1007/s004010100423

Avila, J., Jimenez, J. S., Sayas, C. L., Bolos, M., Zabala, J. C., Rivas, G., & Hernandez, F. (2016). Tau Structures. *Front Aging Neurosci, 8*, 262. doi:10.3389/fnagi.2016.00262

Babaeeghazvini, P., Rueda-Delgado, L. M., Gooijers, J., Swinnen, S. P., & Daffertshofer, A. (2021). Brain Structural and Functional Connectivity: A Review of Combined Works of Diffusion Magnetic Resonance Imaging and Electro-Encephalography. *Front Hum Neurosci, 15*, 721206. doi:10.3389/fnhum.2021.721206

Bai, F., Watson, D. R., Yu, H., Shi, Y., Yuan, Y., & Zhang, Z. (2009). Abnormal resting-state functional connectivity of posterior cingulate cortex in amnestic type mild cognitive impairment. *Brain Res, 1302*, 167-174. doi:10.1016/j.brainres.2009.09.028

Barbier, P., Zejneli, O., Martinho, M., Lasorsa, A., Belle, V., Smet-Nocca, C., . . . Landrieu, I. (2019). Role of Tau as a Microtubule-Associated Protein: Structural and Functional Aspects. *Front Aging Neurosci, 11*, 204. doi:10.3389/fnagi.2019.00204

Basheer, N., Smolek, T., Hassan, I., Liu, F., Iqbal, K., Zilka, N., & Novak, P. (2023). Does modulation of tau hyperphosphorylation represent a reasonable therapeutic strategy for Alzheimer's disease? From preclinical studies to the clinical trials. *Mol Psychiatry, 28*(6), 2197-2214. doi:10.1038/s41380-023-02113-z

Basurto-Islas, G., Luna-Munoz, J., Guillozet-Bongaarts, A. L., Binder, L. I., Mena, R., & Garcia-Sierra, F. (2008). Accumulation of aspartic acid421- and glutamic acid391-cleaved tau in neurofibrillary tangles correlates with progression in Alzheimer disease. *J Neuropathol Exp Neurol, 67*(5), 470-483. doi:10.1097/NEN.0b013e31817275c7

Bateman, R. J., Xiong, C., Benzinger, T. L., Fagan, A. M., Goate, A., Fox, N. C., . . . Dominantly Inherited Alzheimer, N. (2012). Clinical and biomarker changes in dominantly inherited Alzheimer's disease. *N Engl J Med, 367*(9), 795-804. doi:10.1056/NEJMoa1202753

Beck, J. S., Madaj, Z., Cheema, C. T., Kara, B., Bennett, D. A., Schneider, J. A., . . . Counts, S. E. (2022). Co-expression network analysis of frontal cortex during the progression of Alzheimer's disease. *Cereb Cortex, 32*(22), 5108-5120. doi:10.1093/cercor/bhac001

Bertram, L., & Tanzi, R. E. (2009). Genome-wide association studies in Alzheimer's disease. *Hum Mol Genet, 18*(R2), R137-145. doi:10.1093/hmg/ddp406

Biernat, J., Mandelkow, E. M., Schroter, C., Lichtenberg-Kraag, B., Steiner, B., Berling, B., . . . Mandelkow, E. (1992). The switch of tau protein to an Alzheimer-like state includes the phosphorylation of two serine-proline motifs upstream of the microtubule binding region. Embo j, 11(4), 1593-1597. doi:10.1002/j.1460-2075.1992.tb05204.x

Blurton-Jones, M., & Laferla, F. M. (2006). Pathways by which Abeta facilitates tau pathology. *Curr Alzheimer Res, 3*(5), 437-448. doi:10.2174/156720506779025242

Braak, H., & Braak, E. (1991). Neuropathological stageing of Alzheimer-related changes. *Acta Neuropathol, 82*(4), 239-259. doi:10.1007/bf00308809

Braak, H., & Braak, E. (1991). Neuropathological stageing of Alzheimer-related changes. *Acta Neuropathol, 82*(4), 239-259. doi:10.1007/bf00308809

Brady, R. M., Zinkowski, R. P., & Binder, L. I. (1995). Presence of tau in isolated nuclei from human brain. Neurobiol Aging, 16(3), 479-486. doi:10.1016/0197-4580(95)00023-8

Breuzard, G., Hubert, P., Nouar, R., De Bessa, T., Devred, F., Barbier, P., . . . Peyrot, V. (2013). Molecular mechanisms of Tau binding to microtubules and its role in

microtubule dynamics in live cells. *J Cell Sci, 126*(Pt 13), 2810-2819. doi:10.1242/jcs.120832

Brion, J. P., Couck, A. M., Passareiro, E., & Flament-Durand, J. (1985). Neurofibrillary tangles of Alzheimer's disease: an immunohistochemical study. *J Submicrosc Cytol, 17*(1), 89-96. Retrieved from https://www.ncbi.nlm.nih.gov/pubmed/3973960

Bukar Maina, M., Al-Hilaly, Y. K., & Serpell, L. C. (2016). Nuclear Tau and Its Potential Role in Alzheimer's Disease. *Biomolecules, 6*(1), 9. doi:10.3390/biom6010009

Cai, S., Chong, T., Peng, Y., Shen, W., Li, J., von Deneen, K. M., . . . Alzheimer's Disease Neuroimaging, I. (2017). Altered functional brain networks in amnestic mild cognitive impairment: a resting-state fMRI study. *Brain Imaging Behav, 11*(3), 619-631. doi:10.1007/s11682-016-9539-0

Castro, T. G., Ferreira, T., Matama, T., Munteanu, F. D., & Cavaco-Paulo, A. (2023). Acetylation and phosphorylation processes modulate Tau's binding to microtubules: A molecular dynamics study. *Biochim Biophys Acta Gen Subj, 1867*(2), 130276. doi:10.1016/j.bbagen.2022.130276

Castro, T. G., Munteanu, F. D., & Cavaco-Paulo, A. (2019). Electrostatics of Tau Protein by Molecular Dynamics. *Biomolecules, 9*(3). doi:10.3390/biom9030116

Cehlar, O., Njemoga, S., Horvath, M., Cizmazia, E., Bednarikova, Z., & Barrera, E. E. (2024). Structures of Oligomeric States of Tau Protein, Amyloid-beta, alpha-Synuclein and Prion Protein Implicated in Alzheimer's Disease, Parkinson's Disease and Prionopathies. *Int J Mol Sci, 25*(23). doi:10.3390/ijms252313049

Chen, G. F., Xu, T. H., Yan, Y., Zhou, Y. R., Jiang, Y., Melcher, K., & Xu, H. E. (2017). Amyloid beta: structure, biology and structure-based therapeutic development. *Acta Pharmacol Sin, 38*(9), 1205-1235. doi:10.1038/aps.2017.28

Chu, D., Yang, X., Wang, J., Zhou, Y., Gu, J. H., Miao, J., . . . Liu, F. (2024). Tau truncation in the pathogenesis of Alzheimer's disease: a narrative review. *Neural Regen Res, 19*(6), 1221-1232. doi:10.4103/1673-5374.385853

Colom-Cadena, M., Davies, C., Sirisi, S., Lee, J. E., Simzer, E. M., Tzioras, M., . . . Spires-Jones, T. L. (2023). Synaptic oligomeric tau in Alzheimer's disease - A potential culprit in the spread of tau pathology through the brain. *Neuron, 111*(14), 2170-2183 e2176. doi:10.1016/j.neuron.2023.04.020

Combs, B., Hamel, C., & Kanaan, N. M. (2016). Pathological conformations involving the amino terminus of tau occur early in Alzheimer's disease and are differentially detected by monoclonal antibodies. *Neurobiol Dis, 94*, 18-31. doi:10.1016/j.nbd.2016.05.016

Combs, B., Hamel, C., & Kanaan, N. M. (2016). Pathological conformations involving the amino terminus of tau occur early in Alzheimer's disease and are differentially detected by monoclonal antibodies. *Neurobiol Dis, 94*, 18-31. doi:10.1016/j.nbd.2016.05.016

Cook, C., Carlomagno, Y., Gendron, T. F., Dunmore, J., Scheffel, K., Stetler, C., . . . Petrucelli, L. (2014). Acetylation of the KXGS motifs in tau is a critical determinant in modulation of tau aggregation and clearance. *Hum Mol Genet, 23*(1), 104-116. doi:10.1093/hmg/ddt402

Croft, C. L., Goodwin, M. S., Ryu, D. H., Lessard, C. B., Tejeda, G., Marrero, M., . . . Golde, T. E. (2021). Photodynamic studies reveal rapid formation and appreciable turnover of tau inclusions. *Acta Neuropathol, 141*(3), 359-381. doi:10.1007/s00401-021-02264-9

Cunningham, S. I., Tomasi, D., & Volkow, N. D. (2017). Structural and functional connectivity of the precuneus and thalamus to the default mode network. *Hum Brain Mapp, 38*(2), 938-956. doi:10.1002/hbm.23429

De Strooper, B. (2003). Aph-1, Pen-2, and Nicastrin with Presenilin generate an active gamma-Secretase complex. *Neuron, 38*(1), 9-12. doi:10.1016/s0896-6273(03)00205-8

Di Primio, C., Quercioli, V., Siano, G., Rovere, M., Kovacech, B., Novak, M., & Cattaneo, A. (2017). The Distance between N and C Termini of Tau and of FTDP-17 Mutants Is Modulated by Microtubule Interactions in Living Cells. *Front Mol Neurosci, 10*, 210. doi:10.3389/fnmol.2017.00210

Dixit, R., Ross, J. L., Goldman, Y. E., & Holzbaur, E. L. (2008). Differential regulation of dynein and kinesin motor proteins by tau. *Science, 319*(5866), 1086-1089. doi:10.1126/science.1152993

Dixit, R., Ross, J. L., Goldman, Y. E., & Holzbaur, E. L. (2008). Differential regulation of dynein and kinesin motor proteins by tau. *Science, 319*(5866), 1086-1089. doi:10.1126/science.1152993

Dugger, B. N., Whiteside, C. M., Maarouf, C. L., Walker, D. G., Beach, T. G., Sue, L. I., . . . Roher, A. E. (2016). The Presence of Select Tau Species in Human Peripheral Tissues and Their Relation to Alzheimer's Disease. *J Alzheimers Dis, 51*(2), 345-356. doi:10.3233/JAD-150859

Euston, D. R., Gruber, A. J., & McNaughton, B. L. (2012). The role of medial prefrontal cortex in memory and decision making. *Neuron, 76*(6), 1057-1070. doi:10.1016/j.neuron.2012.12.002

Fa, M., Puzzo, D., Piacentini, R., Staniszewski, A., Zhang, H., Baltrons, M. A., . . . Arancio, O. (2016). Extracellular Tau Oligomers Produce An Immediate Impairment of LTP and Memory. *Sci Rep, 6*, 19393. doi:10.1038/srep19393

Fernandez, A. M., & Torres-Aleman, I. (2012). The many faces of insulin-like peptide signalling in the brain. *Nat Rev Neurosci, 13*(4), 225-239. doi:10.1038/nrn3209

Ficek-Tani, B., Horien, C., Ju, S., Xu, W., Li, N., Lacadie, C., . . . Fredericks, C. (2023). Sex differences in default mode network connectivity in healthy aging adults. *Cereb Cortex, 33*(10), 6139-6151. doi:10.1093/cercor/bhac491

Finch, C. E., & Burstein, S. M. (2024). Dementia in the Ancient Greco-Roman World Was Minimally Mentioned. *J Alzheimers Dis, 97*(4), 1581-1588. doi:10.3233/JAD-230993

Flach, K., Hilbrich, I., Schiffmann, A., Gartner, U., Kruger, M., Leonhardt, M., . . . Holzer, M. (2012). Tau oligomers impair artificial membrane integrity and cellular viability. *J Biol Chem, 287*(52), 43223-43233. doi:10.1074/jbc.M112.396176

Frandemiche, M. L., De Seranno, S., Rush, T., Borel, E., Elie, A., Arnal, I., . . . Buisson, A. (2014). Activity-dependent tau protein translocation to excitatory synapse is disrupted by exposure to amyloid-beta oligomers. *J Neurosci, 34*(17), 6084-6097. doi:10.1523/JNEUROSCI.4261-13.2014

Franzmeier, N., Brendel, M., Beyer, L., Slemann, L., Kovacs, G. G., Arzberger, T., . . . Ewers, M. (2022). Tau deposition patterns are associated with functional connectivity in primary tauopathies. *Nat Commun, 13*(1), 1362. doi:10.1038/s41467-022-28896-3

Friedrich, M. G., Skora, A., Hancock, S. E., Mitchell, T. W., Else, P. L., & Truscott, R. J. W. (2021). Tau Is Truncated in Five Regions of the Normal Adult Human Brain. *Int J Mol Sci, 22*(7). doi:10.3390/ijms22073521

Gamblin, T. C., Chen, F., Zambrano, A., Abraha, A., Lagalwar, S., Guillozet, A. L., . . . Cryns, V. L. (2003). Caspase cleavage of tau: linking amyloid and neurofibrillary tangles in Alzheimer's disease. *Proc Natl Acad Sci U S A, 100*(17), 10032-10037. doi:10.1073/pnas.1630428100

Garcia-Albea, E. (1999). [Neurology in the medical papyruses of the pharaohs]. *Rev Neurol, 28*(4), 430-433. Retrieved from https://www.ncbi.nlm.nih.gov/pubmed/10714329

Gardini, S., Venneri, A., Sambataro, F., Cuetos, F., Fasano, F., Marchi, M., . . . Caffarra, P. (2015). Increased functional connectivity in the default mode network in mild cognitive impairment: a maladaptive compensatory mechanism associated with

poor semantic memory performance. *J Alzheimers Dis, 45*(2), 457-470. doi:10.3233/JAD-142547

Gerrish, A., Russo, G., Richards, A., Moskvina, V., Ivanov, D., Harold, D., . . . Williams, J. (2012). The role of variation at AbetaPP, PSEN1, PSEN2, and MAPT in late onset Alzheimer's disease. *J Alzheimers Dis, 28*(2), 377-387. doi:10.3233/JAD-2011-110824

Ghag, G., Bhatt, N., Cantu, D. V., Guerrero-Munoz, M. J., Ellsworth, A., Sengupta, U., & Kayed, R. (2018). Soluble tau aggregates, not large fibrils, are the toxic species that display seeding and cross-seeding behavior. *Protein Sci, 27*(11), 1901-1909. doi:10.1002/pro.3499

Glenner, G. G., & Wong, C. W. (1984). Alzheimer's disease: initial report of the purification and characterization of a novel cerebrovascular amyloid protein. *Biochem Biophys Res Commun, 120*(3), 885-890. doi:10.1016/s0006-291x(84)80190-4

Glenner, G. G., & Wong, C. W. (2012). Alzheimer's disease: initial report of the purification and characterization of a novel cerebrovascular amyloid protein. 1984. *Biochem Biophys Res Commun, 425*(3), 534-539. doi:10.1016/j.bbrc.2012.08.020

Goedert, M., Jakes, R., & Vanmechelen, E. (1995). Monoclonal antibody AT8 recognises tau protein phosphorylated at both serine 202 and threonine 205. Neurosci Lett, 189(3), 167-169. doi:10.1016/0304-3940(95)11484-e

Goldgaber, D., Lerman, M. I., McBride, O. W., Saffiotti, U., & Gajdusek, D. C. (1987). Characterization and chromosomal localization of a cDNA encoding brain amyloid of Alzheimer's disease. *Science, 235*(4791), 877-880. doi:10.1126/science.3810169

Gonzalez, A., Calfio, C., Churruca, M., & Maccioni, R. B. (2022). Glucose metabolism and AD: evidence for a potential diabetes type 3. *Alzheimers Res Ther, 14*(1), 56. doi:10.1186/s13195-022-00996-8

Graeber, M. B., Kosel, S., Egensperger, R., Banati, R. B., Muller, U., Bise, K., . . . Mehraein, P. (1997). Rediscovery of the case described by Alois Alzheimer in 1911: historical, histological and molecular genetic analysis. *Neurogenetics, 1*(1), 73-80. doi:10.1007/s100480050011

Green, Z. D., Vidoni, E. D., Swerdlow, R. H., Burns, J. M., Morris, J. K., & Honea, R. A. (2023). Increased Functional Connectivity of the Precuneus in Individuals with a Family History of Alzheimer's Disease. *J Alzheimers Dis, 91*(2), 559-571. doi:10.3233/JAD-210326

Greenberg, S. M., Bacskai, B. J., Hernandez-Guillamon, M., Pruzin, J., Sperling, R., & van Veluw, S. J. (2020). Cerebral amyloid angiopathy and Alzheimer disease - one peptide, two pathways. *Nat Rev Neurol, 16*(1), 30-42. doi:10.1038/s41582-019-0281-2

Grillo, C. A., Piroli, G. G., Lawrence, R. C., Wrighten, S. A., Green, A. J., Wilson, S. P., . . . Reagan, L. P. (2015). Hippocampal Insulin Resistance Impairs Spatial Learning and Synaptic Plasticity. *Diabetes, 64*(11), 3927-3936. doi:10.2337/db15-0596

Grundke-Iqbal, I., Iqbal, K., Quinlan, M., Tung, Y. C., Zaidi, M. S., & Wisniewski, H. M. (1986b). Microtubule-associated protein tau. A component of Alzheimer paired helical filaments. *J Biol Chem, 261*(13), 6084-6089. Retrieved from https://www.ncbi.nlm.nih.gov/pubmed/3084478

Grundke-Iqbal, I., Iqbal, K., Tung, Y. C., Quinlan, M., Wisniewski, H. M., & Binder, L. I. (1986a). Abnormal phosphorylation of the microtubule-associated protein tau (tau) in Alzheimer cytoskeletal pathology. *Proc Natl Acad Sci U S A, 83*(13), 4913-4917. doi:10.1073/pnas.83.13.4913

Gu, J., Xu, W., Jin, N., Li, L., Zhou, Y., Chu, D., . . . Liu, F. (2020). Truncation of Tau selectively facilitates its pathological activities. *J Biol Chem, 295*(40), 13812-13828. doi:10.1074/jbc.RA120.012587

Guillozet-Bongaarts, A. L., Glajch, K. E., Libson, E. G., Cahill, M. E., Bigio, E., Berry, R. W., & Binder, L. I. (2007). Phosphorylation and cleavage of tau in non-AD tauopathies. *Acta Neuropathol, 113*(5), 513-520. doi:10.1007/s00401-007-0209-6

Guo, T., Noble, W., & Hanger, D. P. (2017). Roles of tau protein in health and disease. *Acta Neuropathol, 133*(5), 665-704. doi:10.1007/s00401-017-1707-9

Hablitz, L. M., & Nedergaard, M. (2021). The Glymphatic System: A Novel Component of Fundamental Neurobiology. *J Neurosci, 41*(37), 7698-7711. doi:10.1523/JNEUROSCI.0619-21.2021

Hablitz, L. M., Pla, V., Giannetto, M., Vinitsky, H. S., Staeger, F. F., Metcalfe, T., . . . Nedergaard, M. (2020). Circadian control of brain glymphatic and lymphatic fluid flow. *Nat Commun, 11*(1), 4411. doi:10.1038/s41467-020-18115-2

Hafkemeijer, A., van der Grond, J., & Rombouts, S. A. (2012). Imaging the default mode network in aging and dementia. *Biochim Biophys Acta, 1822*(3), 431-441. doi:10.1016/j.bbadis.2011.07.008

Hallengren, J., Chen, P. C., & Wilson, S. M. (2013). Neuronal ubiquitin homeostasis. *Cell Biochem Biophys, 67*(1), 67-73. doi:10.1007/s12013-013-9634-4

Hampel, H., Hardy, J., Blennow, K., Chen, C., Perry, G., Kim, S. H., . . . Vergallo, A. (2021). The Amyloid-beta Pathway in Alzheimer's Disease. *Mol Psychiatry, 26*(10), 5481-5503. doi:10.1038/s41380-021-01249-0

Hardy, J. A., & Higgins, G. A. (1992). Alzheimer's disease: the amyloid cascade hypothesis. *Science, 256*(5054), 184-185. doi:10.1126/science.1566067

Hedden, T., Van Dijk, K. R., Becker, J. A., Mehta, A., Sperling, R. A., Johnson, K. A., & Buckner, R. L. (2009). Disruption of functional connectivity in clinically normal older adults harboring amyloid burden. *J Neurosci, 29*(40), 12686-12694. doi:10.1523/JNEUROSCI.3189-09.2009

Hernandez, F., Lucas, J. J., & Avila, J. (2013). GSK3 and tau: two convergence points in Alzheimer's disease. *J Alzheimers Dis, 33 Suppl 1*, S141-144. doi:10.3233/JAD-2012-129025

Hippius, H., & Neundorfer, G. (2003). The discovery of Alzheimer's disease. *Dialogues Clin Neurosci, 5*(1), 101-108. doi:10.31887/DCNS.2003.5.1/hhippius

Hobday, A. L., & Parmar, M. S. (2021). The Link Between Diabetes Mellitus and Tau Hyperphosphorylation: Implications for Risk of Alzheimer's Disease. *Cureus, 13*(9), e18362. doi:10.7759/cureus.18362

Hojjati, S. H., Feiz, F., Ozoria, S., Razlighi, Q. R., & Alzheimer's Disease Neuroimaging, I. (2021). Topographical Overlapping of the Amyloid-beta and Tau Pathologies in the Default Mode Network Predicts Alzheimer's Disease with Higher Specificity. *J Alzheimers Dis, 83*(1), 407-421. doi:10.3233/JAD-210419

Hunter, P. (2024). The controversy around anti-amyloid antibodies for treating Alzheimer's disease : The European Medical Agency's ruling against the latest anti-amyloid drugs highlights the ongoing debate about their safety and efficacy. *EMBO Rep, 25*(12), 5227-5231. doi:10.1038/s44319-024-00294-4

Ihara, Y., Morishima-Kawashima, M., & Nixon, R. (2012). The ubiquitin-proteasome system and the autophagic-lysosomal system in Alzheimer disease. *Cold Spring Harb Perspect Med, 2*(8). doi:10.1101/cshperspect.a006361

Iliff, J. J., & Nedergaard, M. (2013). Is there a cerebral lymphatic system? *Stroke, 44*(6 Suppl 1), S93-95. doi:10.1161/STROKEAHA.112.678698

Iqbal, K., & Grundke-Iqbal, I. (1991). Ubiquitination and abnormal phosphorylation of paired helical filaments in Alzheimer's disease. *Mol Neurobiol, 5*(2-4), 399-410. doi:10.1007/BF02935561

Iqbal, K., & Grundke-Iqbal, I. (2006). Discoveries of tau, abnormally hyperphosphorylated tau and others of neurofibrillary degeneration: a personal

historical perspective. *J Alzheimers Dis, 9*(3 Suppl), 219-242. doi:10.3233/jad-2006-9s325

Iqbal, K., Alonso, A. C., Gong, C. X., Khatoon, S., Pei, J. J., Wang, J. Z., & Grundke-Iqbal, I. (1998). Mechanisms of neurofibrillary degeneration and the formation of neurofibrillary tangles. *J Neural Transm Suppl, 53*, 169-180. doi:10.1007/978-3-7091-6467-9_15

Islam, T., Hill, E., Abrahamson, E. E., Servaes, S., Smirnov, D. S., Zeng, X., . . . Karikari, T. K. (2025). Phospho-tau serine-262 and serine-356 as biomarkers of pre-tangle soluble tau assemblies in Alzheimer's disease. *Nat Med, 31*(2), 574-588. doi:10.1038/s41591-024-03400-0

Ittner, L. M., Ke, Y. D., Delerue, F., Bi, M., Gladbach, A., van Eersel, J., . . . Gotz, J. (2010). Dendritic function of tau mediates amyloid-beta toxicity in Alzheimer's disease mouse models. *Cell, 142*(3), 387-397. doi:10.1016/j.cell.2010.06.036

Jack, C. R., Jr., Andrews, J. S., Beach, T. G., Buracchio, T., Dunn, B., Graf, A., . . . Carrillo, M. C. (2024). Revised criteria for diagnosis and staging of Alzheimer's disease: Alzheimer's Association Workgroup. *Alzheimers Dement, 20*(8), 5143-5169. doi:10.1002/alz.13859

Jack, C. R., Jr., Andrews, J. S., Beach, T. G., Buracchio, T., Dunn, B., Graf, A., . . . Carrillo, M. C. (2024). Revised criteria for diagnosis and staging of Alzheimer's disease: Alzheimer's Association Workgroup. *Alzheimers Dement, 20*(8), 5143-5169. doi:10.1002/alz.13859

Jeganathan, S., Hascher, A., Chinnathambi, S., Biernat, J., Mandelkow, E. M., & Mandelkow, E. (2008). Proline-directed pseudo-phosphorylation at AT8 and PHF1 epitopes induces a compaction of the paperclip folding of Tau and generates a pathological (MC-1) conformation. *J Biol Chem, 283*(46), 32066-32076. doi:10.1074/jbc.M805300200

Jeong, H., Shin, H., Hong, S., & Kim, Y. (2022). Physiological Roles of Monomeric Amyloid-beta and Implications for Alzheimer's Disease Therapeutics. *Exp Neurobiol, 31*(2), 65-88. doi:10.5607/en22004

Jin, M., Pelak, V. S., & Cordes, D. (2012). Aberrant default mode network in subjects with amnestic mild cognitive impairment using resting-state functional MRI. *Magn Reson Imaging, 30*(1), 48-61. doi:10.1016/j.mri.2011.07.007

Jo, D., Choi, S. Y., Ahn, S. Y., & Song, J. (2025). IGF1 enhances memory function in obese mice and stabilizes the neural structure under insulin resistance via AKT-GSK3beta-BDNF signaling. *Biomed Pharmacother, 183*, 117846. doi:10.1016/j.biopha.2025.117846

Jobson, D. D., Hase, Y., Clarkson, A. N., & Kalaria, R. N. (2021). The role of the medial prefrontal cortex in cognition, ageing and dementia. *Brain Commun, 3*(3), fcab125. doi:10.1093/braincomms/fcab125

Kanaan, N. M., Pigino, G. F., Brady, S. T., Lazarov, O., Binder, L. I., & Morfini, G. A. (2013). Axonal degeneration in Alzheimer's disease: when signaling abnormalities meet the axonal transport system. *Exp Neurol, 246*, 44-53. doi:10.1016/j.expneurol.2012.06.003

Kelley, C. M., Ginsberg, S. D., Liang, W. S., Counts, S. E., & Mufson, E. J. (2022). Posterior cingulate cortex reveals an expression profile of resilience in cognitively intact elders. *Brain Commun, 4*(4), fcac162. doi:10.1093/braincomms/fcac162

Kerr, F., Rickle, A., Nayeem, N., Brandner, S., Cowburn, R. F., & Lovestone, S. (2006). PTEN, a negative regulator of PI3 kinase signalling, alters tau phosphorylation in cells by mechanisms independent of GSK-3. *FEBS Lett, 580*(13), 3121-3128. doi:10.1016/j.febslet.2006.04.064

Kim, J., Kim, Y. H., & Lee, J. H. (2013). Hippocampus-precuneus functional connectivity as an early sign of Alzheimer's disease: a preliminary study using structural and functional magnetic resonance imaging data. *Brain Res, 1495*, 18-29. doi:10.1016/j.brainres.2012.12.011

Kimura, T., Ishiguro, K., & Hisanaga, S. (2014). Physiological and pathological phosphorylation of tau by Cdk5. *Front Mol Neurosci, 7*, 65. doi:10.3389/fnmol.2014.00065

Kimura, T., Whitcomb, D. J., Jo, J., Regan, P., Piers, T., Heo, S., . . . Cho, K. (2014). Microtubule-associated protein tau is essential for long-term depression in the hippocampus. *Philos Trans R Soc Lond B Biol Sci, 369*(1633), 20130144. doi:10.1098/rstb.2013.0144

Kirschner, M. (2024). The discovery of tau protein. *Cytoskeleton (Hoboken), 81*(1), 78-82. doi:10.1002/cm.21796

Koch, G., Casula, E. P., Bonni, S., Borghi, I., Assogna, M., Minei, M., . . . Martorana, A. (2022). Precuneus magnetic stimulation for Alzheimer's disease: a randomized, sham-controlled trial. *Brain, 145*(11), 3776-3786. doi:10.1093/brain/awac285

Kopke, E., Tung, Y. C., Shaikh, S., Alonso, A. C., Iqbal, K., & Grundke-Iqbal, I. (1993). Microtubule-associated protein tau. Abnormal phosphorylation of a non-paired helical filament pool in Alzheimer disease. *J Biol Chem, 268*(32), 24374-24384. Retrieved from https://www.ncbi.nlm.nih.gov/pubmed/8226987

Kuchibhotla, K. V., Wegmann, S., Kopeikina, K. J., Hawkes, J., Rudinskiy, N., Andermann, M. L., . . . Hyman, B. T. (2014). Neurofibrillary tangle-bearing neurons

are functionally integrated in cortical circuits in vivo. *Proc Natl Acad Sci U S A, 111*(1), 510-514. doi:10.1073/pnas.1318807111

Kumar, S., Budhathoki, S., Oliveira, C. B., Kahle, A. D., Calhan, O. Y., Lukens, J. R., & Deppmann, C. D. (2023). Role of the caspase-8/RIPK3 axis in Alzheimer's disease pathogenesis and Abeta-induced NLRP3 inflammasome activation. *JCI Insight, 8*(3). doi:10.1172/jci.insight.157433

Lacovich, V., Espindola, S. L., Alloatti, M., Pozo Devoto, V., Cromberg, L. E., Carna, M. E., . . . Falzone, T. L. (2017). Tau Isoforms Imbalance Impairs the Axonal Transport of the Amyloid Precursor Protein in Human Neurons. *J Neurosci, 37*(1), 58-69. doi:10.1523/JNEUROSCI.2305-16.2016

Lanz, U. (1975). [Variations of the median nerve at the carpal tunnel]. *Handchirurgie, 7*(4), 163-164. Retrieved from https://www.ncbi.nlm.nih.gov/pubmed/1213605

Lasagna-Reeves, C. A., Castillo-Carranza, D. L., Sengupta, U., Clos, A. L., Jackson, G. R., & Kayed, R. (2011). Tau oligomers impair memory and induce synaptic and mitochondrial dysfunction in wild-type mice. *Mol Neurodegener, 6*, 39. doi:10.1186/1750-1326-6-39

Lasagna-Reeves, C. A., Castillo-Carranza, D. L., Sengupta, U., Guerrero-Munoz, M. J., Kiritoshi, T., Neugebauer, V., . . . Kayed, R. (2012). Alzheimer brain-derived tau oligomers propagate pathology from endogenous tau. *Sci Rep, 2*, 700. doi:10.1038/srep00700

Lebouvier, T., Scales, T. M., Williamson, R., Noble, W., Duyckaerts, C., Hanger, D. P., . . . Derkinderen, P. (2009). The microtubule-associated protein tau is also phosphorylated on tyrosine. *J Alzheimers Dis, 18*(1), 1-9. doi:10.3233/JAD-2009-1116

Lee, M. J., Lee, J. H., & Rubinsztein, D. C. (2013). Tau degradation: the ubiquitin-proteasome system versus the autophagy-lysosome system. *Prog Neurobiol, 105*, 49-59. doi:10.1016/j.pneurobio.2013.03.001

Leech, R., & Sharp, D. J. (2014). The role of the posterior cingulate cortex in cognition and disease. *Brain, 137*(Pt 1), 12-32. doi:10.1093/brain/awt162

Leech, R., Kamourieh, S., Beckmann, C. F., & Sharp, D. J. (2011). Fractionating the default mode network: distinct contributions of the ventral and dorsal posterior cingulate cortex to cognitive control. *J Neurosci, 31*(9), 3217-3224. doi:10.1523/JNEUROSCI.5626-10.2011

Li, Y., Yao, Z., Yu, Y., Zou, Y., Fu, Y., Hu, B., & Alzheimer's Disease Neuroimaging, I. (2019). Brain network alterations in individuals with and without mild cognitive

impairment: parallel independent component analysis of AV1451 and AV45 positron emission tomography. *BMC Psychiatry, 19*(1), 165. doi:10.1186/s12888-019-2149-9

Litman, P., Barg, J., Rindzoonski, L., & Ginzburg, I. (1993). Subcellular localization of tau mRNA in differentiating neuronal cell culture: implications for neuronal polarity. *Neuron, 10*(4), 627-638. doi:10.1016/0896-6273(93)90165-n

Litwinczuk, M. C., Muhlert, N., Cloutman, L., Trujillo-Barreto, N., & Woollams, A. (2022). Combination of structural and functional connectivity explains unique variation in specific domains of cognitive function. *Neuroimage, 262*, 119531. doi:10.1016/j.neuroimage.2022.119531

Liu, F., Iqbal, K., Grundke-Iqbal, I., Hart, G. W., & Gong, C. X. (2004). O-GlcNAcylation regulates phosphorylation of tau: a mechanism involved in Alzheimer's disease. *Proc Natl Acad Sci U S A, 101*(29), 10804-10809. doi:10.1073/pnas.0400348101

Liu, F., Shi, J., Tanimukai, H., Gu, J., Gu, J., Grundke-Iqbal, I., . . . Gong, C. X. (2009). Reduced O-GlcNAcylation links lower brain glucose metabolism and tau pathology in Alzheimer's disease. *Brain, 132*(Pt 7), 1820-1832. doi:10.1093/brain/awp099

Loomis, P. A., Howard, T. H., Castleberry, R. P., & Binder, L. I. (1990). Identification of nuclear tau isoforms in human neuroblastoma cells. Proc Natl Acad Sci U S A, 87(21), 8422-8426. doi:10.1073/pnas.87.21.8422

Luo, X., Li, Z., Zhao, J., Deng, Y., Zhong, Y., & Zhang, M. (2020). Fyn gene silencing reduces oligodendrocytes apoptosis through inhibiting ERK1/2 phosphorylation in epilepsy. *Artif Cells Nanomed Biotechnol, 48*(1), 298-304. doi:10.1080/21691401.2019.1671428

Mandelkow, E. M., Biernat, J., Drewes, G., Gustke, N., Trinczek, B., & Mandelkow, E. (1995). Tau domains, phosphorylation, and interactions with microtubules. *Neurobiol Aging, 16*(3), 355-362; discussion 362-353. doi:10.1016/0197-4580(95)00025-a

Mangiafico, S. P., Tuo, Q. Z., Li, X. L., Liu, Y., Haralambous, C., Ding, X. L., . . . Lei, P. (2023). Tau suppresses microtubule-regulated pancreatic insulin secretion. *Mol Psychiatry, 28*(9), 3982-3993. doi:10.1038/s41380-023-02267-w

Marciniak, E., Leboucher, A., Caron, E., Ahmed, T., Tailleux, A., Dumont, J., . . . Blum, D. (2017). Tau deletion promotes brain insulin resistance. *J Exp Med, 214*(8), 2257-2269. doi:10.1084/jem.20161731

Martin, L., Latypova, X., & Terro, F. (2011). Post-translational modifications of tau protein: implications for Alzheimer's disease. *Neurochem Int, 58*(4), 458-471. doi:10.1016/j.neuint.2010.12.023

Martin, L., Latypova, X., Wilson, C. M., Magnaudeix, A., Perrin, M. L., & Terro, F. (2013). Tau protein phosphatases in Alzheimer's disease: the leading role of PP2A. *Ageing Res Rev, 12*(1), 39-49. doi:10.1016/j.arr.2012.06.008

Mast, H., Tatemichi, T. K., & Mohr, J. P. (1995). Chronic brain ischemia: the contributions of Otto Binswanger and Alois Alzheimer to the mechanisms of vascular dementia. *J Neurol Sci, 132*(1), 4-10. doi:10.1016/0022-510x(95)00116-j

Mietelska-Porowska, A., Wasik, U., Goras, M., Filipek, A., & Niewiadomska, G. (2014). Tau protein modifications and interactions: their role in function and dysfunction. *Int J Mol Sci, 15*(3), 4671-4713. doi:10.3390/ijms15034671

Millet, B., Mouchabac, S., Robert, G., Maatoug, R., Dondaine, T., Ferreri, F., & Bourla, A. (2023). Transcranial Magnetic Stimulation (rTMS) on the Precuneus in Alzheimer's Disease: A Literature Review. *Brain Sci, 13*(9). doi:10.3390/brainsci13091332

Min, S. W., Cho, S. H., Zhou, Y., Schroeder, S., Haroutunian, V., Seeley, W. W., . . . Gan, L. (2010). Acetylation of tau inhibits its degradation and contributes to tauopathy. *Neuron, 67*(6), 953-966. doi:10.1016/j.neuron.2010.08.044

Mirra, S. S., Heyman, A., McKeel, D., Sumi, S. M., Crain, B. J., Brownlee, L. M., . . . Berg, L. (1991). The Consortium to Establish a Registry for Alzheimer's Disease (CERAD). Part II. Standardization of the neuropathologic assessment of Alzheimer's disease. *Neurology, 41*(4), 479-486. doi:10.1212/wnl.41.4.479

Misiura, M. B., Howell, J. C., Wu, J., Qiu, D., Parker, M. W., Turner, J. A., & Hu, W. T. (2020). Race modifies default mode connectivity in Alzheimer's disease. *Transl Neurodegener, 9*, 8. doi:10.1186/s40035-020-0186-4

Moller, H. J., & Graeber, M. B. (1998). The case described by Alois Alzheimer in 1911. Historical and conceptual perspectives based on the clinical record and neurohistological sections. *Eur Arch Psychiatry Clin Neurosci, 248*(3), 111-122. doi:10.1007/s004060050027

Morfini, G. A., You, Y. M., Pollema, S. L., Kaminska, A., Liu, K., Yoshioka, K., . . . Brady, S. T. (2009). Pathogenic huntingtin inhibits fast axonal transport by activating JNK3 and phosphorylating kinesin. *Nat Neurosci, 12*(7), 864-871. doi:10.1038/nn.2346

Morfini, G., Szebenyi, G., Elluru, R., Ratner, N., & Brady, S. T. (2002). Glycogen synthase kinase 3 phosphorylates kinesin light chains and negatively regulates kinesin-based motility. *Embo j, 21*(3), 281-293. doi:10.1093/emboj/21.3.281

Moussavi, Z. (2022). Repetitive TMS applied to the precuneus stabilizes cognitive status in Alzheimer's disease. *Brain, 145*(11), 3730-3732. doi:10.1093/brain/awac322

Mueller, R. L., Combs, B., Alhadidy, M. M., Brady, S. T., Morfini, G. A., & Kanaan, N. M. (2021). Tau: A Signaling Hub Protein. *Front Mol Neurosci, 14*, 647054. doi:10.3389/fnmol.2021.647054

Muller, D. M., Mendla, K., Farber, S. A., & Nitsch, R. M. (1997). Muscarinic M1 receptor agonists increase the secretion of the amyloid precursor protein ectodomain. *Life Sci, 60*(13-14), 985-991. doi:10.1016/s0024-3205(97)00038-6

Muller, U. C., Deller, T., & Korte, M. (2017). Not just amyloid: physiological functions of the amyloid precursor protein family. *Nat Rev Neurosci, 18*(5), 281-298. doi:10.1038/nrn.2017.29

Mungas, D., Reed, B. R., Jagust, W. J., DeCarli, C., Mack, W. J., Kramer, J. H., . . . Chui, H. C. (2002). Volumetric MRI predicts rate of cognitive decline related to AD and cerebrovascular disease. *Neurology, 59*(6), 867-873. doi:10.1212/wnl.59.6.867

Necula, M., & Kuret, J. (2004). Pseudophosphorylation and glycation of tau protein enhance but do not trigger fibrillization in vitro. *J Biol Chem, 279*(48), 49694-49703. doi:10.1074/jbc.M405527200

Nelson, P. T., Alafuzoff, I., Bigio, E. H., Bouras, C., Braak, H., Cairns, N. J., . . . Beach, T. G. (2012). Correlation of Alzheimer disease neuropathologic changes with cognitive status: a review of the literature. *J Neuropathol Exp Neurol, 71*(5), 362-381. doi:10.1097/NEN.0b013e31825018f7

Newell, K. L., Hyman, B. T., Growdon, J. H., & Hedley-Whyte, E. T. (1999). Application of the National Institute on Aging (NIA)-Reagan Institute criteria for the neuropathological diagnosis of Alzheimer disease. *J Neuropathol Exp Neurol, 58*(11), 1147-1155. doi:10.1097/00005072-199911000-00004

Oakley, S. S., Maina, M. B., Marshall, K. E., Al-Hilaly, Y. K., Harrington, C. R., Wischik, C. M., & Serpell, L. C. (2020). Tau Filament Self-Assembly and Structure: Tau as a Therapeutic Target. *Front Neurol, 11*, 590754. doi:10.3389/fneur.2020.590754

Ohtsubo, K., & Marth, J. D. (2006). Glycosylation in cellular mechanisms of health and disease. *Cell, 126*(5), 855-867. doi:10.1016/j.cell.2006.08.019

Otvos, L., Jr., Feiner, L., Lang, E., Szendrei, G. I., Goedert, M., & Lee, V. M. (1994). Monoclonal antibody PHF-1 recognizes tau protein phosphorylated at serine residues 396 and 404. *J Neurosci Res, 39*(6), 669-673. doi:10.1002/jnr.490390607

Penalba-Sanchez, L., Oliveira-Silva, P., Sumich, A. L., & Cifre, I. (2022). Increased functional connectivity patterns in mild Alzheimer's disease: A rsfMRI study. *Front Aging Neurosci, 14*, 1037347. doi:10.3389/fnagi.2022.1037347

Petersen, R. C. (2004). Mild cognitive impairment as a diagnostic entity. *J Intern Med, 256*(3), 183-194. doi:10.1111/j.1365-2796.2004.01388.x

Pfefferbaum, A., Chanraud, S., Pitel, A. L., Muller-Oehring, E., Shankaranarayanan, A., Alsop, D. C., . . . Sullivan, E. V. (2011). Cerebral blood flow in posterior cortical nodes of the default mode network decreases with task engagement but remains higher than in most brain regions. *Cereb Cortex, 21*(1), 233-244. doi:10.1093/cercor/bhq090

Puangmalai, N., Bhatt, N., Montalbano, M., Sengupta, U., Gaikwad, S., Ventura, F., . . . Kayed, R. (2020). Internalization mechanisms of brain-derived tau oligomers from patients with Alzheimer's disease, progressive supranuclear palsy and dementia with Lewy bodies. *Cell Death Dis, 11*(5), 314. doi:10.1038/s41419-020-2503-3

Qiang, L., Sun, X., Austin, T. O., Muralidharan, H., Jean, D. C., Liu, M., . . . Baas, P. W. (2018). Tau Does Not Stabilize Axonal Microtubules but Rather Enables Them to Have Long Labile Domains. *Curr Biol, 28*(13), 2181-2189 e2184. doi:10.1016/j.cub.2018.05.045

Quintanilla, R. A., Matthews-Roberson, T. A., Dolan, P. J., & Johnson, G. V. (2009). Caspase-cleaved tau expression induces mitochondrial dysfunction in immortalized cortical neurons: implications for the pathogenesis of Alzheimer disease. *J Biol Chem, 284*(28), 18754-18766. doi:10.1074/jbc.M808908200

Rahimi, R., Irannejad, S., & Noroozian, M. (2017). Avicenna's pharmacological approach to memory enhancement. *Neurol Sci, 38*(7), 1147-1157. doi:10.1007/s10072-017-2835-7

Raichle, M. E. (2015). The brain's default mode network. *Annu Rev Neurosci, 38*, 433-447. doi:10.1146/annurev-neuro-071013-014030

Raichle, M. E., MacLeod, A. M., Snyder, A. Z., Powers, W. J., Gusnard, D. A., & Shulman, G. L. (2001). A default mode of brain function. *Proc Natl Acad Sci U S A, 98*(2), 676-682. doi:10.1073/pnas.98.2.676

Ranasinghe, K. G., Hinkley, L. B., Beagle, A. J., Mizuiri, D., Dowling, A. F., Honma, S. M., . . . Vossel, K. A. (2014). Regional functional connectivity predicts distinct cognitive impairments in Alzheimer's disease spectrum. *Neuroimage Clin, 5*, 385-395. doi:10.1016/j.nicl.2014.07.006

Rice, H. C., de Malmazet, D., Schreurs, A., Frere, S., Van Molle, I., Volkov, A. N., . . . de Wit, J. (2019). Secreted amyloid-beta precursor protein functions as a GABA(B)R1a ligand to modulate synaptic transmission. *Science, 363*(6423). doi:10.1126/science.aao4827

Robbins, M., Clayton, E., & Kaminski Schierle, G. S. (2021). Synaptic tau: A pathological or physiological phenomenon? *Acta Neuropathol Commun, 9*(1), 149. doi:10.1186/s40478-021-01246-y

Robinson, J. L., Richardson, H., Xie, S. X., Suh, E., Van Deerlin, V. M., Alfaro, B., . . . Trojanowski, J. Q. (2021). The development and convergence of co-pathologies in Alzheimer's disease. *Brain, 144*(3), 953-962. doi:10.1093/brain/awaa438

Rodriguez-Rodriguez, P., Sandebring-Matton, A., Merino-Serrais, P., Parrado-Fernandez, C., Rabano, A., Winblad, B., . . . Cedazo-Minguez, A. (2017). Tau hyperphosphorylation induces oligomeric insulin accumulation and insulin resistance in neurons. *Brain, 140*(12), 3269-3285. doi:10.1093/brain/awx256

Roman, G. C. (1999). A historical review of the concept of vascular dementia: lessons from the past for the future. *Alzheimer Dis Assoc Disord, 13 Suppl 3*, S4-8. doi:10.1097/00002093-199912001-00002

Rudinskiy, N., Hawkes, J. M., Wegmann, S., Kuchibhotla, K. V., Muzikansky, A., Betensky, R. A., . . . Hyman, B. T. (2014). Tau pathology does not affect experience-driven single-neuron and network-wide Arc/Arg3.1 responses. *Acta Neuropathol Commun, 2*, 63. doi:10.1186/2051-5960-2-63

Santiago, J. A., & Potashkin, J. A. (2021). The Impact of Disease Comorbidities in Alzheimer's Disease. *Front Aging Neurosci, 13*, 631770. doi:10.3389/fnagi.2021.631770

Sayas, C. L., & Avila, J. (2021). GSK-3 and Tau: A Key Duet in Alzheimer's Disease. *Cells, 10*(4). doi:10.3390/cells10040721

Scherr, M., Utz, L., Tahmasian, M., Pasquini, L., Grothe, M. J., Rauschecker, J. P., . . . Riedl, V. (2021). Effective connectivity in the default mode network is distinctively disrupted in Alzheimer's disease-A simultaneous resting-state FDG-PET/fMRI study. *Hum Brain Mapp, 42*(13), 4134-4143. doi:10.1002/hbm.24517

Schultz, A. P., Chhatwal, J. P., Hedden, T., Mormino, E. C., Hanseeuw, B. J., Sepulcre, J., . . . Sperling, R. A. (2017). Phases of Hyperconnectivity and Hypoconnectivity in the Default Mode and Salience Networks Track with Amyloid and Tau in Clinically Normal Individuals. *J Neurosci, 37*(16), 4323-4331. doi:10.1523/JNEUROSCI.3263-16.2017

Seiberlich, V., Bauer, N. G., Schwarz, L., Ffrench-Constant, C., Goldbaum, O., & Richter-Landsberg, C. (2015). Downregulation of the microtubule associated protein tau impairs process outgrowth and myelin basic protein mRNA transport in oligodendrocytes. *Glia, 63*(9), 1621-1635. doi:10.1002/glia.22832

Seifaddini, R., Tajadini, H., & Choopani, R. (2015). Physiopathology of dementia from the perspective of traditional Persian medicine. *J Evid Based Complementary Altern Med, 20*(3), 224-227. doi:10.1177/2156587214566275

Shafiei, S. S., Guerrero-Munoz, M. J., & Castillo-Carranza, D. L. (2017). Tau Oligomers: Cytotoxicity, Propagation, and Mitochondrial Damage. *Front Aging Neurosci, 9*, 83. doi:10.3389/fnagi.2017.00083

Sheline, Y. I., Raichle, M. E., Snyder, A. Z., Morris, J. C., Head, D., Wang, S., & Mintun, M. A. (2010). Amyloid plaques disrupt resting state default mode network connectivity in cognitively normal elderly. *Biol Psychiatry, 67*(6), 584-587. doi:10.1016/j.biopsych.2009.08.024

Shi, Y., Zhang, W., Yang, Y., Murzin, A. G., Falcon, B., Kotecha, A., . . . Scheres, S. H. W. (2021). Structure-based classification of tauopathies. *Nature, 598*(7880), 359-363. doi:10.1038/s41586-021-03911-7

Shim, K. H., Kang, M. J., Youn, Y. C., An, S. S. A., & Kim, S. (2022). Alpha-synuclein: a pathological factor with Abeta and tau and biomarker in Alzheimer's disease. *Alzheimers Res Ther, 14*(1), 201. doi:10.1186/s13195-022-01150-0

Siano, G., Caiazza, M. C., Varisco, M., Calvello, M., Quercioli, V., Cattaneo, A., & Di Primio, C. (2019). Modulation of Tau Subcellular Localization as a Tool to Investigate the Expression of Disease-related Genes. *J Vis Exp*(154). doi:10.3791/59988

Sotiropoulos, I., Galas, M. C., Silva, J. M., Skoulakis, E., Wegmann, S., Maina, M. B., . . . Buee, L. (2017). Atypical, non-standard functions of the microtubule associated Tau protein. *Acta Neuropathol Commun, 5*(1), 91. doi:10.1186/s40478-017-0489-6

Sotthibundhu, A., Sykes, A. M., Fox, B., Underwood, C. K., Thangnipon, W., & Coulson, E. J. (2008). Beta-amyloid(1-42) induces neuronal death through the p75 neurotrophin receptor. *J Neurosci, 28*(15), 3941-3946. doi:10.1523/JNEUROSCI.0350-08.2008

Stadelmann, C., Deckwerth, T. L., Srinivasan, A., Bancher, C., Bruck, W., Jellinger, K., & Lassmann, H. (1999). Activation of caspase-3 in single neurons and autophagic granules of granulovacuolar degeneration in Alzheimer's disease. Evidence for apoptotic cell death. *Am J Pathol, 155*(5), 1459-1466. doi:10.1016/S0002-9440(10)65460-0

Stancu, I. C., Vasconcelos, B., Terwel, D., & Dewachter, I. (2014). Models of beta-amyloid induced Tau-pathology: the long and "folded" road to understand the mechanism. *Mol Neurodegener, 9*, 51. doi:10.1186/1750-1326-9-51

Stillesjo, S., Nyberg, L., & Wirebring, L. K. (2019). Building Memory Representations for Exemplar-Based Judgment: A Role for Ventral Precuneus. *Front Hum Neurosci, 13*, 228. doi:10.3389/fnhum.2019.00228

Sunde, M., & Blake, C. C. (1998). From the globular to the fibrous state: protein structure and structural conversion in amyloid formation. *Q Rev Biophys, 31*(1), 1-39. doi:10.1017/s0033583598003400

Tagarelli, A., Piro, A., Tagarelli, G., Lagonia, P., & Quattrone, A. (2006). Alois Alzheimer: a hundred years after the discovery of the eponymous disorder. *Int J Biomed Sci, 2*(2), 196-204. Retrieved from https://www.ncbi.nlm.nih.gov/pubmed/23674983

Taheri-Targhi, S., Gjedde, A., Araj-Khodaei, M., Rikhtegar, R., Parsian, Z., Zarrintan, S., . . . Vafaee, M. S. (2019). Avicenna (980-1037 CE) and his Early Description and Classification of Dementia. *J Alzheimers Dis, 71*(4), 1093-1098. doi:10.3233/JAD-190345

Tai, H. C., Serrano-Pozo, A., Hashimoto, T., Frosch, M. P., Spires-Jones, T. L., & Hyman, B. T. (2012). The synaptic accumulation of hyperphosphorylated tau oligomers in Alzheimer disease is associated with dysfunction of the ubiquitin-proteasome system. *Am J Pathol, 181*(4), 1426-1435. doi:10.1016/j.ajpath.2012.06.033

Talbot, K., Wang, H. Y., Kazi, H., Han, L. Y., Bakshi, K. P., Stucky, A., . . . Arnold, S. E. (2012). Demonstrated brain insulin resistance in Alzheimer's disease patients is associated with IGF-1 resistance, IRS-1 dysregulation, and cognitive decline. *J Clin Invest, 122*(4), 1316-1338. doi:10.1172/JCI59903

Telling, G. C., Parchi, P., DeArmond, S. J., Cortelli, P., Montagna, P., Gabizon, R., . . . Prusiner, S. B. (1996). Evidence for the conformation of the pathologic isoform of the prion protein enciphering and propagating prion diversity. *Science, 274*(5295), 2079-2082. doi:10.1126/science.274.5295.2079

Thal, D. R., Rub, U., Orantes, M., & Braak, H. (2002). Phases of A beta-deposition in the human brain and its relevance for the development of AD. *Neurology, 58*(12), 1791-1800. doi:10.1212/wnl.58.12.1791

Tiernan, C. T., Ginsberg, S. D., Guillozet-Bongaarts, A. L., Ward, S. M., He, B., Kanaan, N. M., . . . Counts, S. E. (2016). Protein homeostasis gene dysregulation in pretangle-bearing nucleus basalis neurons during the progression of Alzheimer's disease. *Neurobiol Aging, 42*, 80-90. doi:10.1016/j.neurobiolaging.2016.02.031

Tracy, T. E., Sohn, P. D., Minami, S. S., Wang, C., Min, S. W., Li, Y., . . . Gan, L. (2016). Acetylated Tau Obstructs KIBRA-Mediated Signaling in Synaptic Plasticity

and Promotes Tauopathy-Related Memory Loss. *Neuron, 90*(2), 245-260. doi:10.1016/j.neuron.2016.03.005

Tran, J., Parekh, S., Rockcole, J., Wilson, D., & Parmar, M. S. (2024). Repurposing antidiabetic drugs for Alzheimer's disease: A review of preclinical and clinical evidence and overcoming challenges. *Life Sci, 355*, 123001. doi:10.1016/j.lfs.2024.123001

Trzeciakiewicz, H., Tseng, J. H., Wander, C. M., Madden, V., Tripathy, A., Yuan, C. X., & Cohen, T. J. (2017). A Dual Pathogenic Mechanism Links Tau Acetylation to Sporadic Tauopathy. *Sci Rep, 7*, 44102. doi:10.1038/srep44102

Uceda, A. B., Marino, L., Casasnovas, R., & Adrover, M. (2024). An overview on glycation: molecular mechanisms, impact on proteins, pathogenesis, and inhibition. *Biophys Rev, 16*(2), 189-218. doi:10.1007/s12551-024-01188-4

Utevsky, A. V., Smith, D. V., & Huettel, S. A. (2014). Precuneus is a functional core of the default-mode network. *J Neurosci, 34*(3), 932-940. doi:10.1523/JNEUROSCI.4227-13.2014

Vana, L., Kanaan, N. M., Ugwu, I. C., Wuu, J., Mufson, E. J., & Binder, L. I. (2011). Progression of tau pathology in cholinergic Basal forebrain neurons in mild cognitive impairment and Alzheimer's disease. *Am J Pathol, 179*(5), 2533-2550. doi:10.1016/j.ajpath.2011.07.044

Vatanabe, I. P., Manzine, P. R., & Cominetti, M. R. (2020). Historic concepts of dementia and Alzheimer's disease: From ancient times to the present. *Rev Neurol (Paris), 176*(3), 140-147. doi:10.1016/j.neurol.2019.03.004

Violet, M., Delattre, L., Tardivel, M., Sultan, A., Chauderlier, A., Caillierez, R., . . . Galas, M. C. (2014). A major role for Tau in neuronal DNA and RNA protection in vivo under physiological and hyperthermic conditions. *Front Cell Neurosci, 8*, 84. doi:10.3389/fncel.2014.00084

Vipin, A., Loke, Y. M., Liu, S., Hilal, S., Shim, H. Y., Xu, X., . . . Zhou, J. (2018). Cerebrovascular disease influences functional and structural network connectivity in patients with amnestic mild cognitive impairment and Alzheimer's disease. *Alzheimers Res Ther, 10*(1), 82. doi:10.1186/s13195-018-0413-8

Ward, S. M., Himmelstein, D. S., Lancia, J. K., & Binder, L. I. (2012). Tau oligomers and tau toxicity in neurodegenerative disease. *Biochem Soc Trans, 40*(4), 667-671. doi:10.1042/BST20120134

Ward, S. M., Himmelstein, D. S., Lancia, J. K., Fu, Y., Patterson, K. R., & Binder, L. I. (2013). TOC1: characterization of a selective oligomeric tau antibody. *J Alzheimers Dis, 37*(3), 593-602. doi:10.3233/JAD-131235

Wegmann, S., Biernat, J., & Mandelkow, E. (2021). A current view on Tau protein phosphorylation in Alzheimer's disease. *Curr Opin Neurobiol, 69*, 131-138. doi:10.1016/j.conb.2021.03.003

Wilhelm, B. G., Mandad, S., Truckenbrodt, S., Krohnert, K., Schafer, C., Rammner, B., . . . Rizzoli, S. O. (2014). Composition of isolated synaptic boutons reveals the amounts of vesicle trafficking proteins. *Science, 344*(6187), 1023-1028. doi:10.1126/science.1252884

Wu, Y. H., & Swaab, D. F. (2007). Disturbance and strategies for reactivation of the circadian rhythm system in aging and Alzheimer's disease. *Sleep Med, 8*(6), 623-636. doi:10.1016/j.sleep.2006.11.010

Xu, P., Chen, A., Li, Y., Xing, X., & Lu, H. (2019). Medial prefrontal cortex in neurological diseases. *Physiol Genomics, 51*(9), 432-442. doi:10.1152/physiolgenomics.00006.2019

Yamaguchi, A., & Jitsuishi, T. (2024). Structural connectivity of the precuneus and its relation to resting-state networks. *Neurosci Res, 209*, 9-17. doi:10.1016/j.neures.2023.12.004

Yang, H. D., Kim, D. H., Lee, S. B., & Young, L. D. (2016). History of Alzheimer's Disease. *Dement Neurocogn Disord, 15*(4), 115-121. doi:10.12779/dnd.2016.15.4.115

Yang, L. S., & Ksiezak-Reding, H. (1995). Calpain-induced proteolysis of normal human tau and tau associated with paired helical filaments. *Eur J Biochem, 233*(1), 9-17. doi:10.1111/j.1432-1033.1995.009_1.x

Yokoi, T., Watanabe, H., Yamaguchi, H., Bagarinao, E., Masuda, M., Imai, K., . . . Sobue, G. (2018). Involvement of the Precuneus/Posterior Cingulate Cortex Is Significant for the Development of Alzheimer's Disease: A PET (THK5351, PiB) and Resting fMRI Study. *Front Aging Neurosci, 10*, 304. doi:10.3389/fnagi.2018.00304

York, G. K., 3rd, & Steinberg, D. A. (2010). Chapter 3: neurology in ancient Egypt. *Handb Clin Neurol, 95*, 29-36. doi:10.1016/S0072-9752(08)02103-9

Younas, N., Saleem, T., Younas, A., & Zerr, I. (2023). Nuclear face of Tau: an inside player in neurodegeneration. *Acta Neuropathol Commun, 11*(1), 196. doi:10.1186/s40478-023-01702-x

Yue, C., Wu, D., Bai, F., Shi, Y., Yu, H., Xie, C., & Zhang, Z. (2015). State-based functional connectivity changes associate with cognitive decline in amnestic mild cognitive impairment subjects. *Behav Brain Res, 288*, 94-102. doi:10.1016/j.bbr.2015.04.013

Zhang, S., & Li, C. S. (2012). Functional connectivity mapping of the human precuneus by resting state fMRI. *Neuroimage, 59*(4), 3548-3562. doi:10.1016/j.neuroimage.2011.11.023

Zhang, X. Y., Yang, Z. L., Lu, G. M., Yang, G. F., & Zhang, L. J. (2017). PET/MR Imaging: New Frontier in Alzheimer's Disease and Other Dementias. *Front Mol Neurosci, 10*, 343. doi:10.3389/fnmol.2017.00343

Zhang, Z., Xue, P., Bendlin, B. B., Zetterberg, H., De Felice, F., Tan, X., & Benedict, C. (2025). Melatonin: A potential nighttime guardian against Alzheimer's. *Mol Psychiatry, 30*(1), 237-250. doi:10.1038/s41380-024-02691-6

Zhou, L., McInnes, J., Wierda, K., Holt, M., Herrmann, A. G., Jackson, R. J., . . . Verstreken, P. (2017). Tau association with synaptic vesicles causes presynaptic dysfunction. *Nat Commun, 8*, 15295. doi:10.1038/ncomms15295

Zhou, Y., Shi, J., Chu, D., Hu, W., Guan, Z., Gong, C. X., . . . Liu, F. (2018). Relevance of Phosphorylation and Truncation of Tau to the Etiopathogenesis of Alzheimer's Disease. *Front Aging Neurosci, 10*, 27. doi:10.3389/fnagi.2018.00027

CHAPTER 2: QUANTIFICATION OF PRE-TANGLE TAU IN THE POSTMORTEM DMN HUBS

INTRODUCTION

Alzheimer’s disease (AD) is a progressive neurodegenerative dementing disorder and the fifth leading cause of death among those 65 and older (Alzheimer's disease facts and figures, 2024). Pathological diagnosis of AD depends on the postmortem presence of amyloid beta (Aβ) peptide-containing amyloid plaques and neurofibrillary tangles (NFTs) composed of hyperphosphorylated and misfolded tau protein. Tau plays various roles in cellular function when in its physiological state. Although the exact mechanism (s) are still unknown, as aberrant post-translational modifications accumulate, tau begins to self-aggregate and fibrillize, ultimately coalescing as NFTs in AD and other tauopathies. NFTs first accumulate in the transentorhinal cortex and hippocampus before spreading to limbic cortical regions and the neocortex, as detailed in the Braak staging system (Braak, 1991). Historically, research on tau pathology in AD has focused on NFTs as the primary source of toxicity and neuronal death. However, recent studies have demonstrated that injections of NFTs or monomeric tau do not seed tau pathology (Lasagna-Reeves, 2011; Ghag, 2018). Additionally, neurons containing NFTs have been shown to remain responsive to sensory inputs and remain integrated within local circuits in mice, suggesting NFTs might not hinder neuronal function (Kuchibhotla, 2014). Notably, a transgenic tau mouse study revealed that turning off tau expression could rescue memory and prevent neuronal loss, even as NFTs continued to form (Santacruz, 2005). As a result, research has increasingly shifted towards investigating “pre-tangle” tau, particularly events such as protein misfolding that promote oligomer formation.

In contrast to NFTs, soluble pre-tangle tau species such as tau oligomers have been shown to disrupt mitochondrial homeostasis through impaired energy metabolism, increased reactive oxygen species, and calcium imbalances (Lasagna-Reeves, 2011; Fisar, 2022; Reddy, 2011; Zheng, 2020; Kravenska, 2024; Crossley, 2024), interfere with bidirectional axonal trafficking and microtubule assembly (Tiernan, 2016; Niewiadomska, 2021; Reddy, 2011; Mueller, 2023), and diminish synaptic vesicular signaling and long-term potentiation (LTP) (Fa, 2016; Niewiadomska, 2021; Reddy, 2011; Scaduto, 2024); presumably, these insults culminate in a toxic cellular environment promoting neurodegeneration, synaptic loss, and cognitive impairment.

Clinically, a decline in episodic and semantic memory performance is an early phenomenon in AD progression (Baudic, 2006; Desgranges, 2002; Sugarman, 2012). However, the relationship between pathological tau accrual and memory dysfunction is not fully understood and, in some cases, might not be linear due to individual differences in cognitive reserve (Bocancea, 2023). The advent of tau-PET imaging to visualize NFT accumulation in living patients, combined with structural and functional MRI (fMRI), has shown that NFTs correlate with reduced resting-state network functional connectivity, which in turn correlates with cognitive deterioration (Biel, 2022; Jann, 2023; Hoenig, 2018; Green, 2019; Berron, 2021; Luan, 2024; Nabizadeh, 2024; Roemer, 2024; Ziontz, 2024). In this regard, although most tau pathology studies have focused on the medial temporal lobe due to its crucial role in episodic memory coding and retrieval (Spens, 2024; Migliaccio, 2022; Kitamura, 2017), the cortical Default Mode Network (DMN), a resting-state network that is active by default in the absence of an attention-demanding task, may represent an additional key substrate for understanding

the role of tau pathological propagation in mediating the earliest cognitive changes in mild cognitive impairment (MCI) and AD (Flanagin, 2023).

The DMN consists minimally of three main hubs: medial frontal cortex (FC), posterior cingulate cortex (PCC), and precuneus (PreC) (Raichle, 2015; Raichle, 2001). Research suggests that AD pathology disrupts the excitation-inhibition balance within these hubs, leading to hyperexcitability (Giorgio, 2024) and hyperconnectivity when patients are positive for Aβ (Schultz, 2017; Hahn, 2019; Guzman-Velez, 2022). By contrast, as tau pathology becomes detectable by PET imaging, the DMN's functional connectivity shifts towards hypoconnectivity (Schultz, 2017). For instance, high Clinical Dementia Rating (CDR $\geq$ 1) MCI patients and mild AD patients displayed delayed disengagement during transitional tasks that deactivate the DMN while activating other networks, compared to the low CDR MCI patients and controls (Daly, 2000; Celone, 2006). Notably, these reductions in DMN connectivity were also observed in individuals experiencing subjective cognitive decline (SCD) (Hahn, 2019) or newly diagnosed with MCI*,* highlighting the need to understand the extent to which toxic pretangle tau moieties (e.g., oligomers) accumulate within the DMN and their potential mechanistic role in the progression of AD. However, a key challenge is the inability to track toxic, prefibrillar tau accumulation in living patients due to the absence of pre-tangle-specific PET ligands. This study aimed to quantify pre-tangle tau in postmortem DMN regions (FC, PCC, and PreC) obtained from subjects who died with a clinical diagnosis of no cognitive impairment (NCI), MCI, or AD, using epitope-specific tau antibodies that recognize early post-translational modifications related to soluble tau aggregation and toxicity. These antibodies allowed us to quantify the accrual of pre-tangle pathology by

immunohistochemistry and morphological analysis, as well as by custom ELISA analysis of soluble brain fractions.

MATERIALS AND METHODS

Subjects and Clinical Pathologic Assessments

Case-matched fixed and frozen FC, PCC, and PreC tissue samples were obtained from the Rush Religious Orders Study (RROS), a longitudinal clinical pathological study of aging and dementia in elderly Catholic clergy (Table 2.1) (Kelley, 2022). Subjects were classified antemortem as no cognitive impairment (NCI, n = 47), mild cognitive impairment (MCI, n = 36), or mild/moderate AD (n = 36). Details of RROS clinical and neuropathologic evaluations and diagnostic criteria have been published extensively (Counts, 2006 ; Bennett, 2002; Kelley, 2022; Schneider, 2009). Briefly, RROS participants undergo an annual neurological examination and cognitive performance testing using the Mini-Mental State Exam (MMSE) and 19 additional neuropsychological tests referable to five cognitive domains: orientation, attention, memory, language, and perception (Bennett, 2002). Composite scores of episodic memories, semantic memory, working memory, perceptual speed, and visuospatial ability, as well as a composite global cognitive z-score (GCS), were derived from this test battery for each subject; NCI subjects did not reveal impairment in any of these domains within a year of death (Bennett, 2002; Bennett, 2018). Exclusion criteria included a history of major depressive disorder, chronic alcoholism, and/or neuropathological evidence of Parkinson’s disease, Lewy body disease, TDP-43 proteinopathy, hippocampal sclerosis, or large strokes. Apolipoprotein E (APOE) genotyping was performed as reported (Kelley, 2022).

For neuropathological diagnostic analysis, brain slabs were immersion fixed in 4% paraformaldehyde, cryoprotected, cut at 40 μm and sections were immunostained with antibodies against Aβ (6E10, 1:400 dilution) and phosphorylated tau (AT8, 1:250 dilution) (Kelley, 2022). A board-certified neuropathologist evaluated all cases while blinded to clinical diagnosis (Schneider, 2009). Designations of “normal” (with respect to AD or other dementing processes), “possible AD”, “probable AD”, or “definite AD” were based on semi-quantitative estimation of neuritic plaque density, an age-related senile plaque score, and the presence or absence of dementia as established by the Consortium to Establish a Registry for Alzheimer’s Disease (CERAD) (Mirra, 1991). Braak scores based on the staging of NFT pathology were established for each case (Braak, 1991). Cases also received an NIA-Reagan Likelihood-of-AD diagnosis based on neuritic plaque and tangle pathology (Hyman, 1997). The “ABC” algorithm for the diagnosis of AD (Montine, 2012) is currently being applied to all RROS cases.

For validation studies, frozen FC, PCC, and PreC tissue blocks from low-Braak/controls (Braak stages I-II), mid-Braak (Braak stages III-IV), and hig-Braak (Braak stages V-VI) subjects (n = 12/group, n=36 total) were obtained postmortem from Michigan AD Center (MADC) clinical cohort subjects (Table 2.2) (McKay, 2019). These subjects underwent routine neuropathological diagnostic analysis (McKay, 2019). MMSE scores were utilized to calculate correlations between pre-tangle tau pathology and global cognition.

Immunohistochemistry

Forty micron-thick free-floating fixed tissue sections from the DMN regions were washed in 0.1%Triton X-100 in TBS (TBS-T) buffer, quenched with peroxidase (3% in

methanol), blocked using 10% normal goat serum /2% bovine serum albumin in 1xTBS-T, and incubated with the following primary antibodies, alone (for brightfield microscopy) or in combination (for confocal microscopy): 1) pS422 rabbit monoclonal antibody (Millipore AB79415, 1:2,500), which recognizes soluble tau phosphorylation at the serine 422 residue, an early event in NFT evolution (Guillozet-Bongaarts, 2006; Vana, 2011) that facilitates stable tau dimerization by delaying filament formation (Tiernan, 2016a); 2) TOC1 mouse monoclonal IgM antibody (1:20,000), which recognizes tau oligomers by binding to a continuous epitope within the proline-rich region (amino acids 209-224) formed by tau dimer antigen (Patterson, 2011; Ward, 2013); or 3) TNT2 mouse monoclonal IgG antibody (1:200,000), which recognizes the exposed phosphatase-activating domain (PAD) in the N-terminus as an early conformational change during tangle maturation (Combs, 2016). Neither TOC1 nor TNT2 epitopes colocalize with thiazine red (Combs, 2016; Patterson, 2011). In addition, sections were also immunostained using TauC3 mouse monoclonal antibody (1:6,000), which recognizes a truncation neoepitope at D421 in the C-terminus and serves as a marker for mid-stage NFT development (Guillozet-Bongaarts, 2005). Finally, the PHF-1 mouse monoclonal antibody (1:20,000), which detects phosphorylated serine residues at positions 396 and 404, was used to detect filamentous tau and NFTs (Greenberg, 1992). In parallel experiments, we also used the MOAB-2 mouse monoclonal antibody (1:5,000), which detects oligomeric Aβ and plaque pathology via binding residues 1-4 within the N terminus, formed by an Aβ dimer antigen (Youmans, 2012). TOC1, TNT2, TauC3, MOAB-2, and PHF-1 antibodies were kindly provided by Dr. Nicholas Kanaan

(Michigan State University) and their experimental applications are summarized in Table 2.1.

Abs	Working concentrations	Isotype	Epitopes
pS422	IHC (1:2500) IF (1:500) ELISA (1:500)	Rabbit polyclonal	pS422
TOC1	IHC (1:20,000) IF (1:2,000) ELISA (1:500)	Mouse IgM	Amino acids 209–224
TNT2	IHC (1:200,000) IF (1:20,000) ELISA (1:500)	Mouse IgG1	Phosphatase-activating domain (PAD), amino acids 2–18
TauC3	IHC (1:6,000) IF (1:500) ELISA (1:500)	Mouse IgG1	C-terminus truncated tau at aspartic acid 421
PHF-1	IHC (1:20,000)	Mouse IgG1	pS396/ pS404
Tau5	ELISA (1:1000)	Mouse IgG1	Amino acids 218-225
MOAB-2	IHC (1:5,000) IF (1:500) ELISA (1:500)	Mouse IgG2b	Amino acids 1-4

Table 2. 1 Selected pre-tangle tau markers and working concentrations

For brightfield microscopy, sections underwent three 10-minute TBS-T washes before the secondary incubation with either mouse or rabbit biotinylated secondary antibodies (1:500) for one hour at room temperature. After applying the ABC kit (Vector Laboratories PK-6100) for one hour and three more 10-minute TBS-T washes, DAB (Vector Laboratories SK-4105) was used to develop brown reaction products. The sections were then washed again, mounted on slides, Nissl-counterstained, and coverslipped for digital scanning.

For confocal microscopy, sections were first exposed to LED light for 16 hours to quench autofluorescence. On Day 1, the sections were blocked and incubated overnight with the TNT2 primary antibody (1:20,000). The following day, sections were washed,

protein blocked and incubated with Alexa568 anti-mouse IgG secondary antibody (1:500, Invitrogen A21124) for one hour. Before adding the other two primary antibodies (TOC1 (1:20,000) and pS422 (1:2,500)), the sections were treated with mouse Fab fragments (1:20, Jackson Laboratories, AB-2338476) for one hour to prevent non-specific binding between the two mouse antibodies. On Day 3, sections were washed again and incubated with Alexa-488 anti-mouse IgM (Invitrogen, A21042) and Alexa-405 anti-rabbit IgG (Invitrogen, A31556) secondaries for one hour before mounting and coverslipping. Sections were imaged using a Nikon A1 laser scanning confocal microscope with a 40x oil immersion objective.

Whole Slide Digital Imaging and Quantitative Analysis

Tissue sections were digitally scanned using a Zeiss AxioScan7 with a TL LED lamp and a 20x/0.8 M27 plan-apochromatic objective. The images were then stitched into a single composite using Zen Blue software (version 3.7.97.07000) with a pixel resolution of 0.173 µm x 0.173 µm. Five sections per case per region and per antibody were used for quantification. The entire gray matter was analyzed as the region of interest. After annotations were drawn, thresholds were adjusted for each antibody, and HALO (Area Quantification v2.1.11, Indica Labs) machine learning software was used to quantify the signal intensity and tissue area associated with the signal. For normalization purposes, % tissue area was used as the outcome measure.

Soluble Tau Extraction

For both the RROS and MADC frozen DMN tissue blocks, 150 mg tissue was cut and placed in a 10X volume of brain homogenization buffer (50mM Tris, 275mM NaCl, 5mM KCl) supplemented with protease inhibitors (10ug/ml of Pepstatin A, Leupeptin,

Bestatin, Aprotinin, and 1mM PMSF). The tissue was homogenized on ice using a Tissue Tearor rotor-stator probe (Biospec) and then centrifuged at 27,000 x g for 20 minutes at 4 °C to obtain the soluble pre-tangle tau-enriched S1 fraction for ELISAs. The pellet was resuspended in 5 volumes of brain pellet homogenization buffer (10mMTris, 0.8M NaCl, 10% sucrose,1mM EGTA, 1mM PMSF), and the homogenization and centrifugation steps were repeated. The resulting S2 supernatant was incubated with 1% Sarkozy for 1-hour at 37C and then centrifuged at 200,000 x g for 1 hour at 4°C. The supernatant was saved as S3, and the pellet was resuspended (P3) in 50ul of 1X Brain Pellet Homogenization Buffer for future analyses. S1 protein concentrations were determined using the BCA method (Thermo Fisher Scientific, A53226), and all samples were stored at -80 °C.

Custom Sandwich ELISAs

Custom sandwich ELISAs were prepared using TOC1 (2 µg/ml), TNT2 (1 µg/ml), TauC3 (2 µg/ml), and Tau5 (total tau, 1 µg/ml) antibodies as capture antibodies, combined with R1(1:10,000), a pan-tau antibody, for detection. The Tau5 and R1 antibodies were kindly provided by Dr. Nicholas Kanaan. Briefly, 96-well plates were coated with the capture antibodies in borate buffer (100 mM borate acid, 25 mM sodium borate, 75 mM NaCl, 0.25 mM thimerosal) and incubated for one hour at room temperature on a shaker. After two quick washes with wash buffer (100 mM borate acid, 25 mM sodium borate, 75 mM NaCl, 0.25 mM thimerosal, 0.4% (w/v) bovine serum albumin, 0.05% (v/v) Tween-20), the wells were blocked with 5% non-fat dry milk for one hour. Samples and monomeric or aggregated recombinant hTau40 standards (provided by Dr. Kanaan) were then added to the wells and incubated on the shaker for

90 minutes using predetermined concentrations from previous titration experiments. Following four additional washes, the R1 detection antibody was added for a 90-minute incubation, followed by a one-hour incubation with anti-rabbit horseradish peroxidase (HRP)-conjugated secondary antibody (1:5,000). TMB solution (Sigma, T0440) was then added for color development, allowing the reaction to proceed for 4-8 minutes before terminating with the stop buffer (3.5% sulfuric acid). Finally, the plates were read with a plate reader at 450 nm. The readout was transformed into the % light absorbed with the Y=100-(100*10^(-Y)) formula, Y showing optical density.

Statistical Analysis

All datasets were subjected to the Shapiro-Wilk test for normality. Demographic, clinical, and pathological variables were compared by either one-way ANOVA or the Kruskal-Wallis test with *post hoc* corrections for multiple comparisons. Chi-square testing was used to compare sex and *APOE* ε4 allele distribution across the groups. As a non-parametric alternative to paired one-way ANOVA, Friedman test combined with Dunn multiple corrections were applied for interregional comparisons. Significance levels were indicated as follows: *p < 0.05, **p < 0.01, ***p < 0.001, and ****p < 0.0001.

RESULTS

RROS Cohort Demographics and Clinical Neuropathologic Characteristics

Detailed demographic, clinical, and neuropathological data for the RROS participants (*n*=119) are listed in Table 2.2. No significant differences were observed in sex, years of education, or postmortem interval (PMI) among the NCI, MCI, and AD clinical groups. Although the APOE ε4 allele was present in 21.8% of the subjects, its prevalence did not differ across the groups. Age was significantly lower in the NCI

subjects compared to the MCI and AD subjects ($p=0.0002$). However, age was not correlated with select tau marker levels across the DMN regions in the diagnostic groups, with two exceptions in the ELISA analyses (Supplementary Table 2.1).

Global cognitive performance on both the MMSE and GCS was significantly lower in the MCI group compared to NCI ($p<0.0001$); these scores were also significantly lower in the AD group compared to MCI ($p<0.0001$). Braak, CERAD, and NIA-Reagan neuropathological diagnostic scores were significantly more severe in the MCI and AD groups compared to NCI subjects (Table 2.2).

	Clinical diagnosis				Comparison by diagnosis group
	NCI (n=47)	MCI (n=36)	AD (n=36)	Total (n=119)	(*P* value)
Age at death (years)					
Mean ± SD	88.1± 5.1	92.2±5.9	92.3±4.5	90.6± 5.5	0.0003[a***]
(Range)	(70.5 , 98.1)	(80.7 ,103.7)	(80.7 , 102.1)	(70.5 , 103.7)	
No. (%) Males	18 (37.5%)	13 (36.1%)	7 (19.4%)	38 (31.7%)	0.1535‡
Years of Education					
Mean ± SD	18.6±3.3	18.0±2.8	17.6±3.3	18.1±3.2	0.2943
(Range)	(10 , 27)	(12 , 24)	(8 , 27)	(8 , 27)	
Postmortem Interval (hours)					
Mean ± SD	11.5 ± 6.5	9.8± 6.7	9.2 ± 7.1	10.3 ± 6.8	0.1062
(Range)	(3.2 , 27.3)	(0.9 , 24.0)	(2.7 , 34.3)	(0.9 , 34.3)	
No. (%) Apoε4 (≥1 allele)	11 (23.4%)	7 (19.4%)	8 (22.2%)	26 (21.8%)	0.9023‡
MMSE					
Mean ± SD	28.0±1.8	24.2±3.2	16.3±6.6	23.4±6.4	<0.0001[b****]
(Range)	(21 , 30)	(19 , 30)	(0 , 26)	(0, 30)	
Global Cognitive Score					
Mean ± SD	0.2 ± 0.4	-0.6± 0.4	-2.1 ± 0.9	-0.7 ± 1.1	<0.0001[d****]
(Range)	(-0.7 , 1.1)	(-1.6 , 0.2)	(-4.1 , -0.4)	(-4.1 , 1.1)	
Braak Scores					
I-II	14	5	2	21	<0.0001[c****]
III-IV	31	25	11	67	
V-VI	2	6	23	31	
NIA Reagan Diagnosis (likelihood of AD)					
No AD	0	0	0	0	<0.0001[c****]
Low	30	16	5	51	
Intermediate	16	15	15	46	
High	1	5	16	22	
CERAD Diagnosis					
No AD	18	11	3	32	0.0003[c***]
Low	4	3	1	8	
Intermediate	18	12	14	44	
High	7	10	18	35	

Table 2. 2 Demographic, clinical, and pathological profile of the RROS cohort

Table 2. 2 (cont'd)

‡ Chi-Square test, a Pairwise comparisons with Kruskal-Wallis and Dunn's correction showed age in NCI was lower than MCI and AD. b Pairwise comparisons with Kruskal-Wallis and Dunn's correction showed a significant decrease from NCI to MCI to AD, or c no difference between NCI & MCI but a decrease in AD. d Pairwise comparisons with One-way ANOVA and Tukey's correction showed a significant decrease from NCI to MCI to AD. AD: Alzheimer's disease, MCI: Mild cognitive impairment, MMSE: Mini-Mental State Examination, NCI: No cognitive impairment; SD: Standard deviation

p<0.05. p<0,01**, p<0,001***, p<0.0001*****

Early Appearance of Pathological Tau in the DMN In the RROS Cohort

Fixed free-floating FC, PCC, and PreC tissue sections (NCI=19, MCI=16, AD=16, n=51 total) were labeled separately with the select site-specific tau antibodies (pS422, TOC1, TNT2, and TauC3) for IHC quantification. PHF-1 was used in the PCC samples for comparisons between the accrual of these markers and that of a canonical NFT marker (Supplementary Figure 2.1). As shown in Figure 2.1, tau pathology was observed only sparsely as neuropil threads (NTs) in Braak stages III/IV, with an appreciable accumulation of NTs and the appearance of NFTs within cortical layers 2/3 and 5/6 by Braak stage V. Qualitatively, pS422+ NTs appeared to accumulate prior to the TOC1+ and TNT2+ NTs, whereas TauC3 appeared more confined to NFTs in later Braak stages (Figure 2.1).

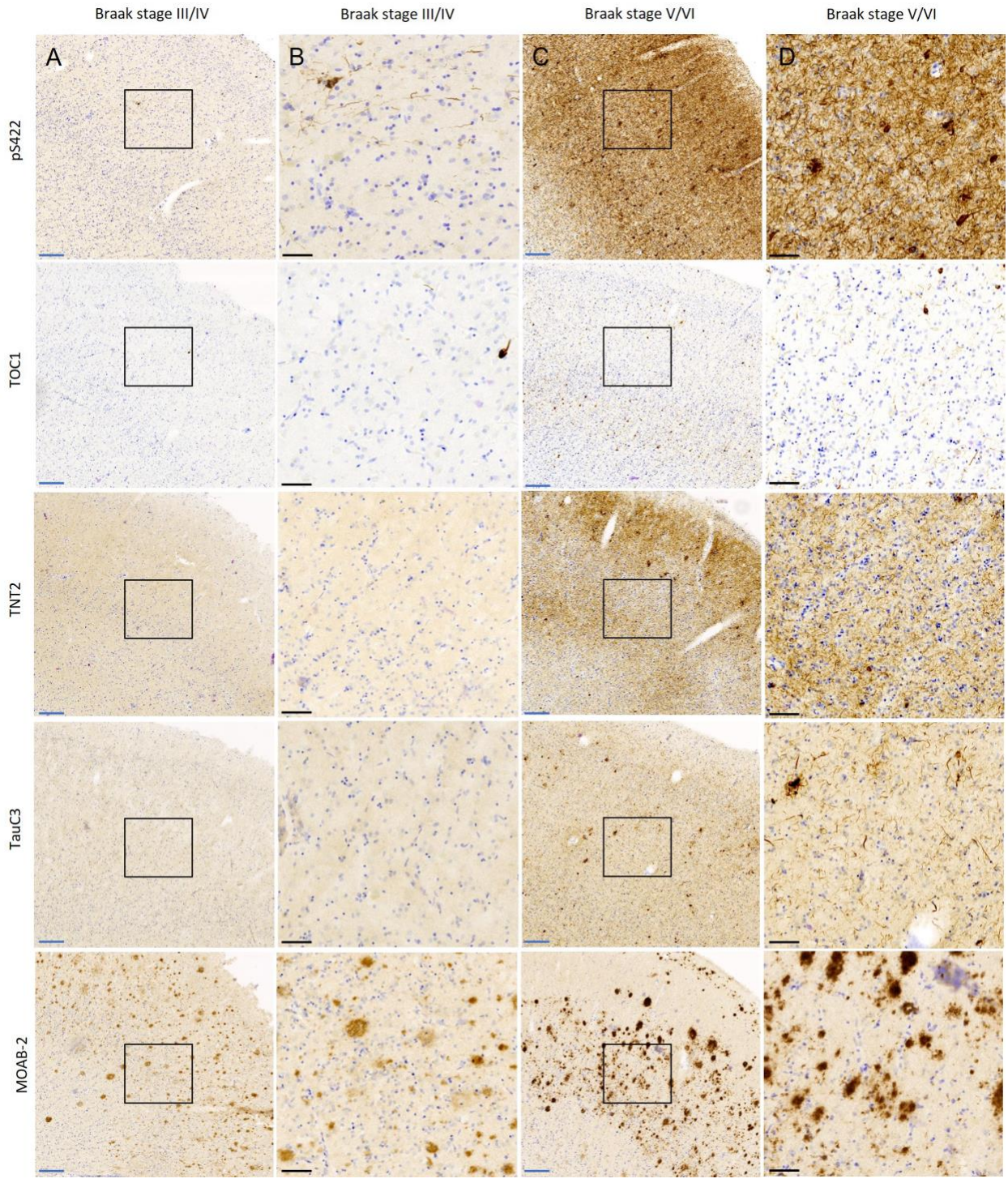

Figure 2. 1 Immunolabeling of early pathological tau in the PCC

Representative photomicrographs showing pS422, TOC1, TNT2, TauC3, and MOAB-2-immunoreactive profiles in layer V from a (Column A) Braak stage III/IV and (Column C)

Figure 2. 1 (cont'd)

Braak stage V/VI case. (Columns B and D) High magnification micrographs showing labeling for each marker within the square boxes outlined in (Columns A and C). Similar qualitative immunolabeling patterns were observed in FC and PreC. Scale bars: Blue= 200 µm, Black = 50 µm.

Multiplexed fluorescence microscopy of the pS422, TOC1, and TNT2 pre-tangle markers in higher Braak cases revealed co-labeling in the cell bodies of both pre-tangle and NFT-bearing neurons, as well as within NTs (Figure 2.2) and neuritic plaques (Figure 2.3A). However, there were also prominent differential spatial patterns of these markers within the NTs (Figure 2.2, Figure 2.3A). Compared to these earlier pre-tangle markers, the mid-stage NFT marker TauC3 (Vana, 2011; Kanaan, 2016) did not overlap appreciably with the pre-tangle markers within cell bodies and typically displayed overlap with the pre-tangle markers in limited NTs (Figure 2.3B).

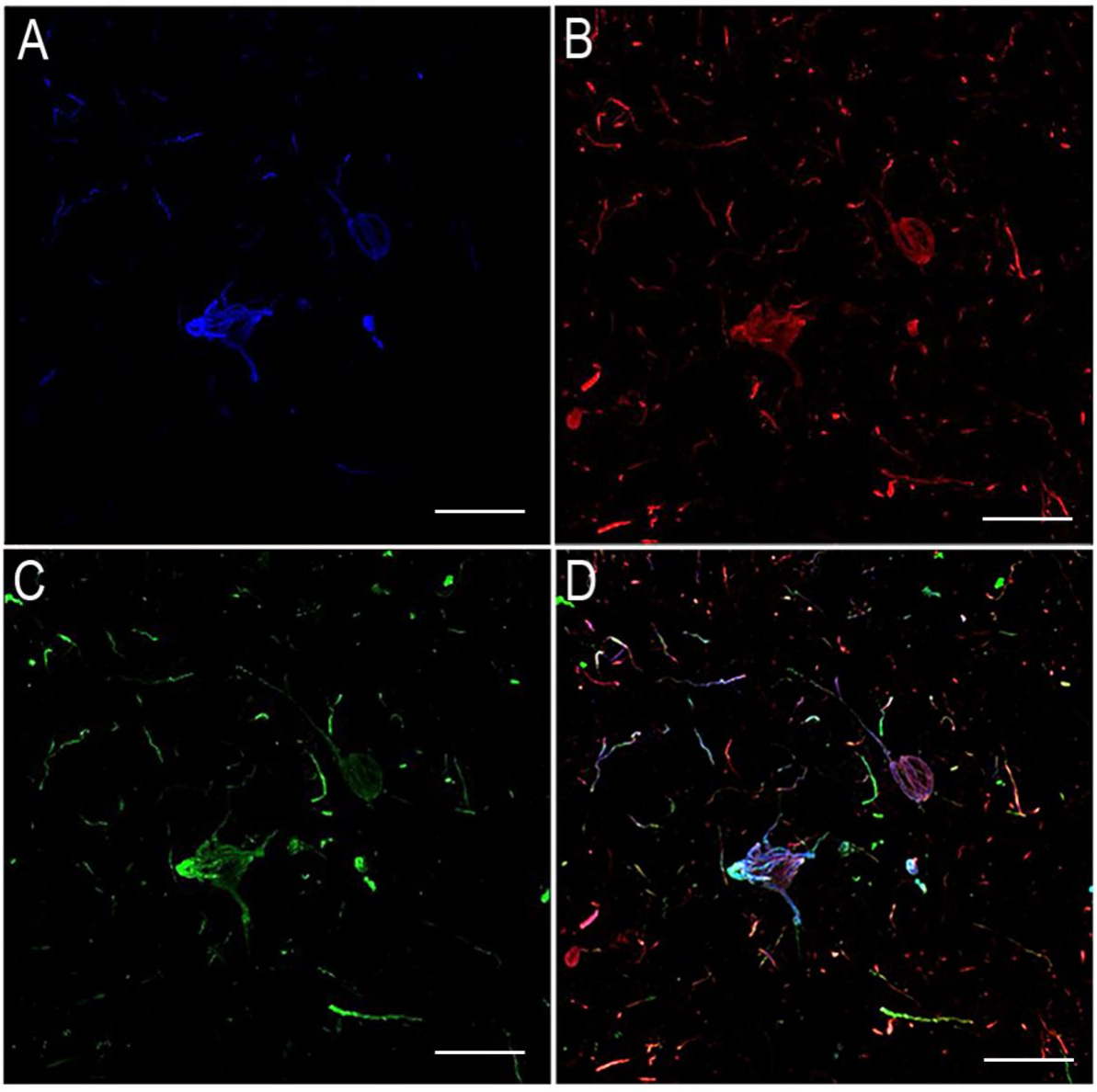

Figure 2. 2 Representative fluorescence micrograph of tau pre-tangle marker-immunoreactive profiles in the PCC layer III of an AD case (Braak stage V) pS422 signal was collected from the blue (405 nm) channel, TOC1 from the green (488 nm) channel, and TNT2 from the red (568 nm) channel. The image was captured using a confocal microscope with a 40X oil objective. Scale bar: 25 µm. Note the differential spatial resolution among the markers within neuropil threads, whereas marker overlap was more prominent in the neuronal soma.

A B

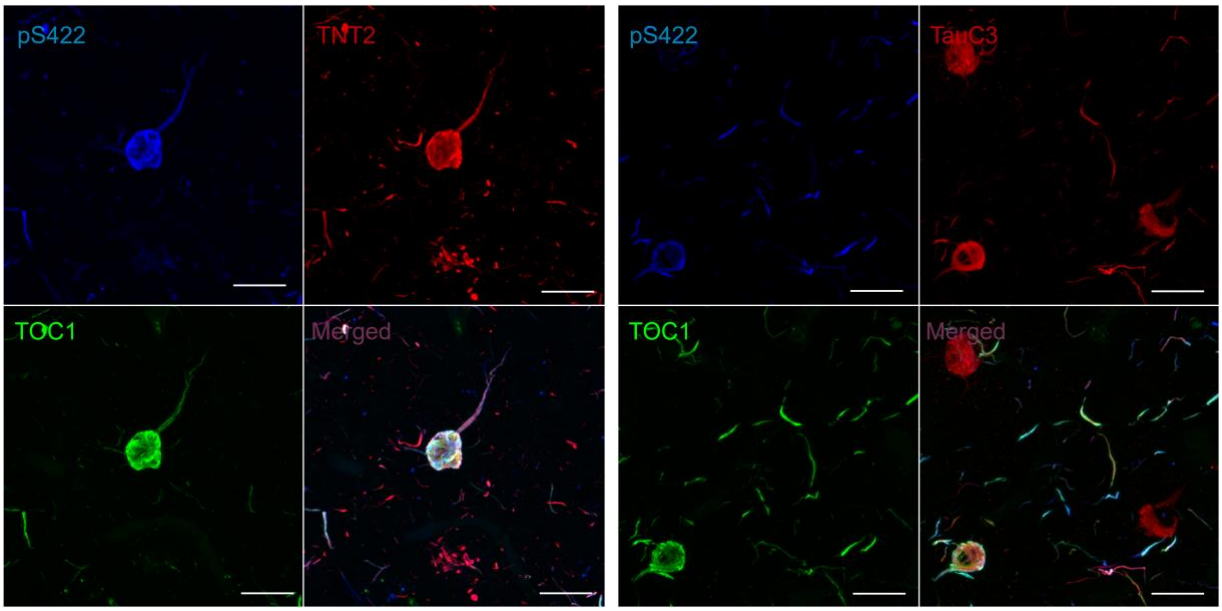

Figure 2. 3 Co-labeling with pS422, TOC1, and TNT2/TauC3 in an AD case

A: Immunofluorescence co-labeling in a late-stage AD case, with pS422 signal collected from the blue (405 nm) channel, TOC1 from the green (488 nm) channel, and TNT2 from the red (568 nm) channel. B: Co-labeling with the same markers but substituting TNT2 with TauC3. While pS422, TOC1, and TNT2 displayed significant overlap, particularly in the cell body, TauC3 showed minimal overlap with the other markers. The image was captured using a confocal microscope with a 40X oil objective. Scale bar: 25 μm.

Quantitative morphological analysis revealed that pS422+ profile levels were significantly elevated from Braak stage III/IV to V in all three regions (FC, $p = 0.0245$; PCC, $p = 0.0214$; PreC, $p = 0.0111$), and this elevation persisted in Braak stage VI (Figure 2.4A, B, C). The TOC1 levels also began to rise between Braak stages IV and V in all three DMN regions but reached statistical significance only at Braak stage VI. The TNT2 marker exhibited a similar pattern of a significant increase by Braak stage V in FC

and PCC (p=0,0351, p=0.0003, respectively) (Figure 2.4A). The TauC3 marker, which typically displayed a lower abundance than the other pre-tangle markers, was significantly increased in Braak V in the FC and Braak VI in PCC (p=0.0176, p=0.0477, respectively). By contrast, MOAB-2 immunoreactivity revealed increases in amyloid pathology as early as Braak stages II-III, although none of the measured changes was significant across the DMN hubs except the increase in PreC by Braak stage 6 (p= 0.0144).

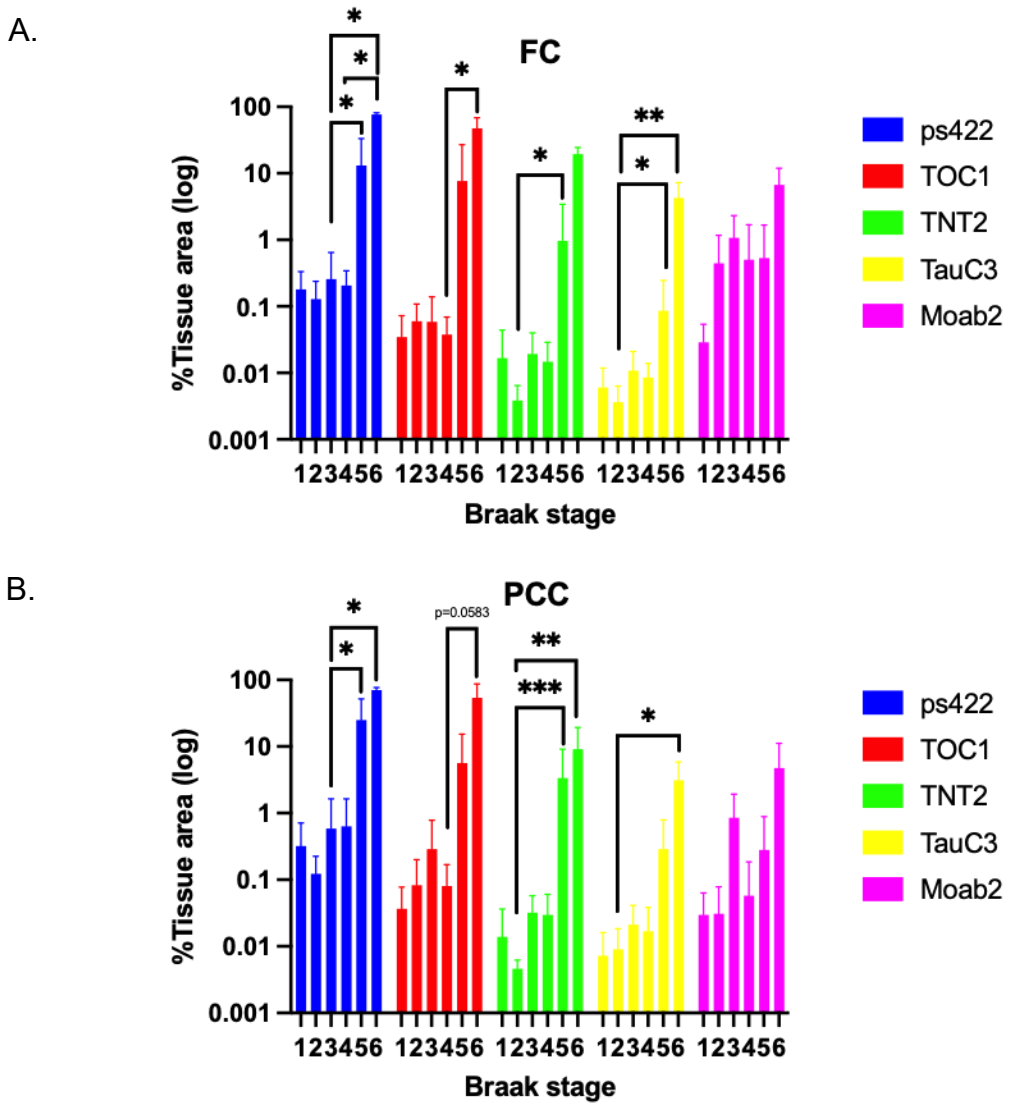

Figure 2. 4 Early pathological tau accumulations in the fixed DMN samples

Figure 2. 4 (cont'd)

C.

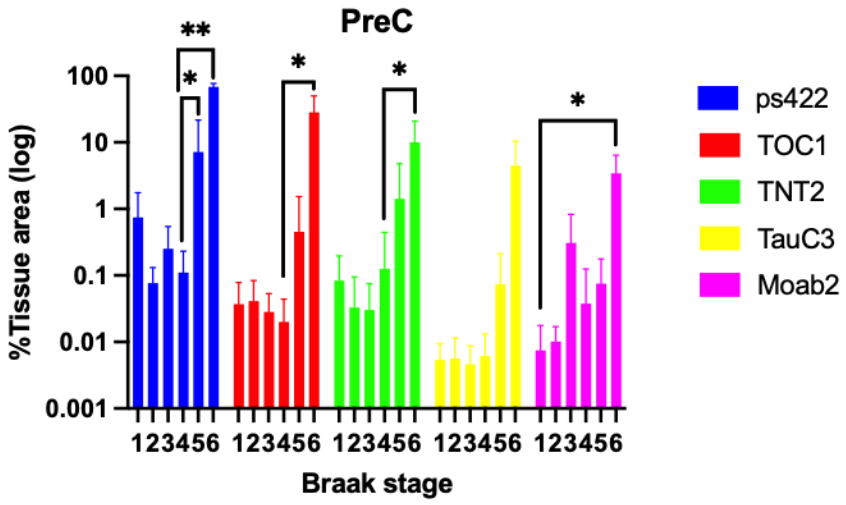

Quantitative analysis of selected pre-tangle markers was performed on fixed samples from the frontal cortex (FC), posterior cingulate cortex (PCC), and precuneus (PreC) The data represent % area of tissue region of interest for normalized comparisons for each marker according to the Braak stages. Data were log-transformed to reduce skewness. Bar graphs were used to display the mean values and the percentage coefficient of variation (%CV) for each marker. Statistical analyses were conducted using the Kruskal-Wallis test, followed by Dunn's multiple comparisons for pairwise analysis.

When compared among the clinical diagnostic groups, all four markers were significantly increased in the AD cases in all the regions, except TOC1 in the PreC (p=0.1311). There was also a significant increase in the levels of pS422 and TOC1 in the FC (p=0.0386, p=0.0186, respectively) and PCC (p=0.0245, p=0.0357, respectively) from MCI to AD. In only FC, TNT2 level significantly increased in the MCI group compared to the controls (0.0025). Interestingly, in PreC, the MOAB-2 signal was lower

in the NCI and MCI groups and significantly increased in the AD cases (p=0.0412) (Figure 2.5).

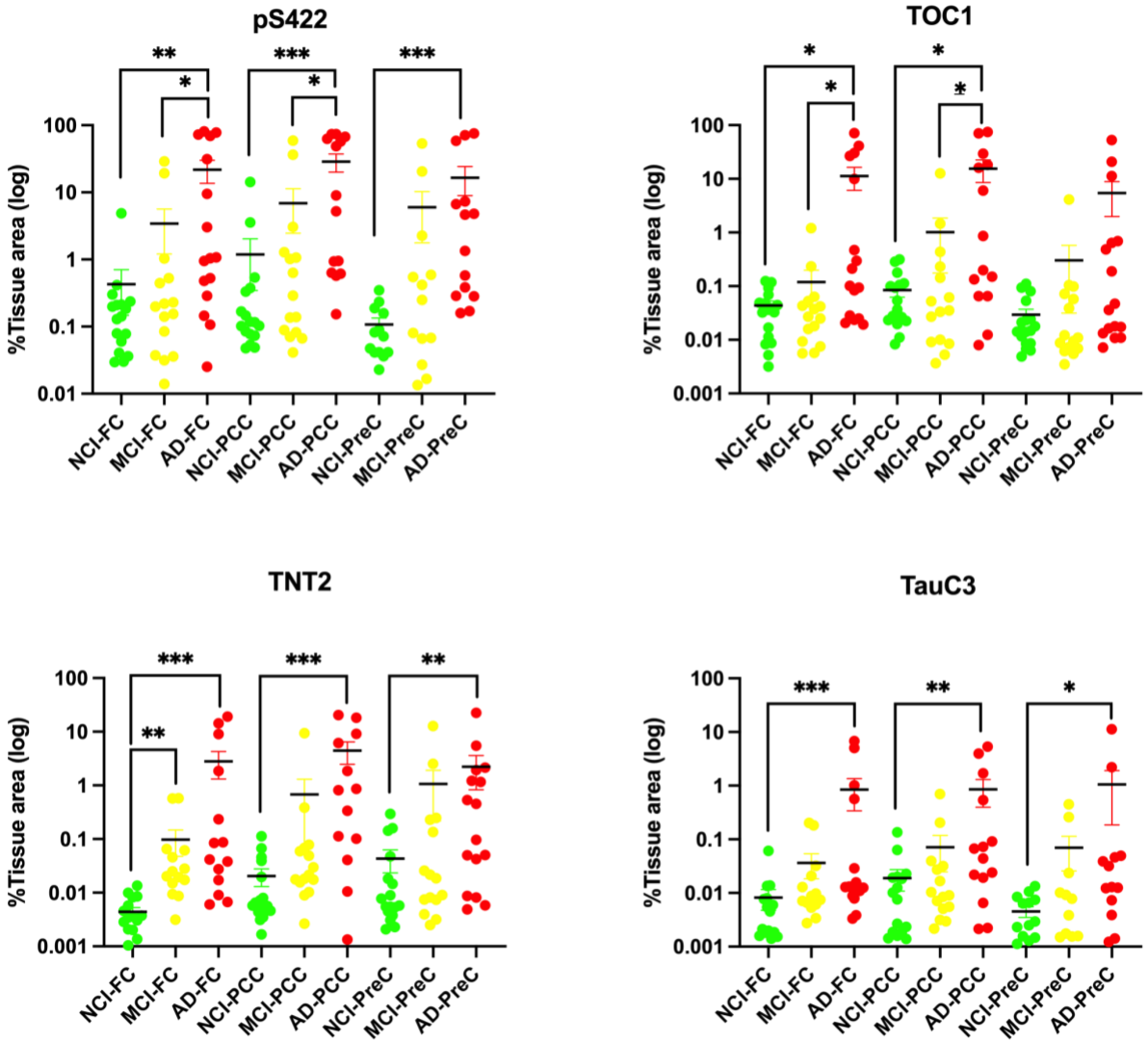

Figure 2. 5 Early pathological tau accumulations in the fixed DMN samples based on the clinical groups

Figure 2. 5 (cont'd)

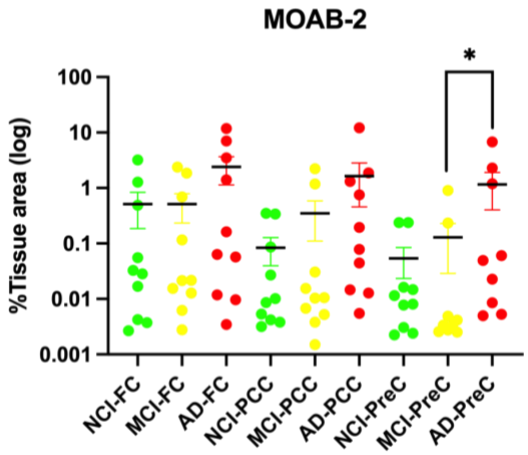

Quantitative analysis of selected pre-tangle markers was performed on fixed samples based on the clinical groups. The data represent % area of tissue region of interest for normalized comparisons for each marker according to the Braak stages. Data were log-transformed to reduce skewness. Bar graphs were used to display the mean values and the percentage coefficient of variation (%CV) for each marker. Statistical analyses were conducted using the Kruskal-Wallis test, followed by Dunn's multiple comparisons for pairwise analysis.

Soluble Pre-Tangle Tau Markers in DMN Hubs

To complement the quantitative immunohistochemistry studies, which detected the presence of the tau epitopes regardless of their pre-fibrillar or fibrillar status, we used custom ELISAs to measure TOC1, TNT2, and TauC3 in soluble fractions to isolate diffusible, presumably toxic tau moieties. We could not achieve reliable measurements using the pS422 antibody (data not shown), so this pre-tangle marker was not analyzed. We found that TOC1 oligomeric tau levels were significantly increased during the transition from Braak stage IV to V in all three regions (FC, p=0.0139; PCC, p=0.003;

PreC, p=0.0006). Likewise, TNT2 levels were elevated significantly in Braak V cases in FC (p=0.0223) and PCC (p=0.0001) and in Braak VI cases in the PreC (p=0.0462). TauC3 levels were also increased in DMN hubs in Braak stage V in the FC and PCC (p= 0.0545, p=0.0128, respectively) and in Braak stage VI in PreC (p=0.0138). By contrast, Tau 5 total tau levels were only elevated in the Braak VI cases (Figure 2.6).

A.

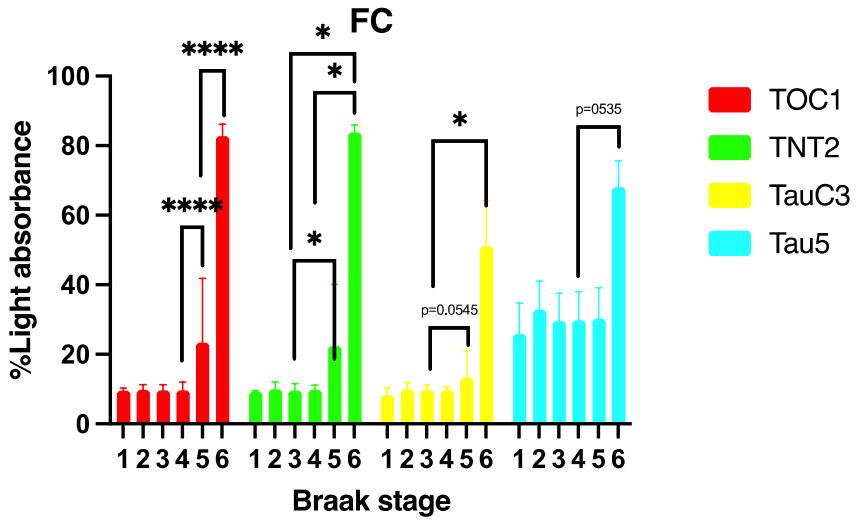

B.

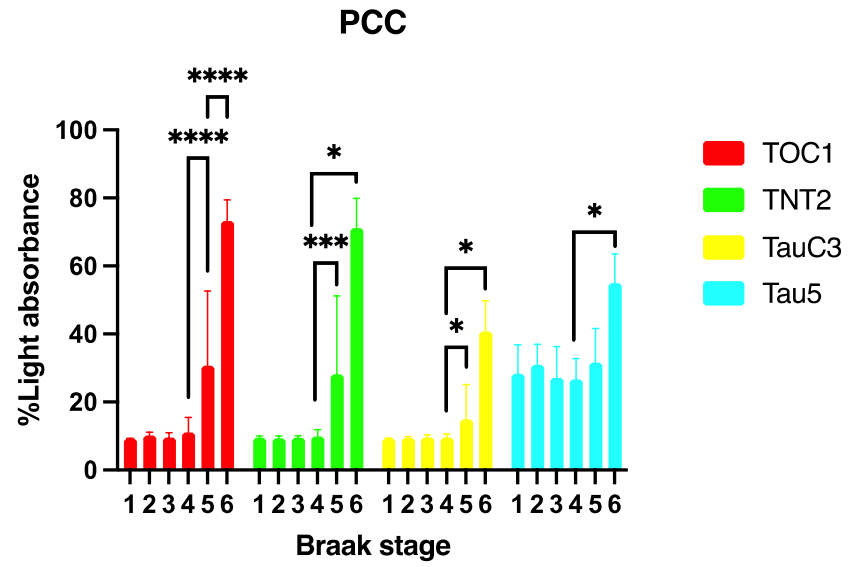

Figure 2. 6 Sandwich ELISA quantification of the pathological tau in the soluble fraction of the case-matched frozen DMN samples

Figure 2. 6 (cont'd)

C.

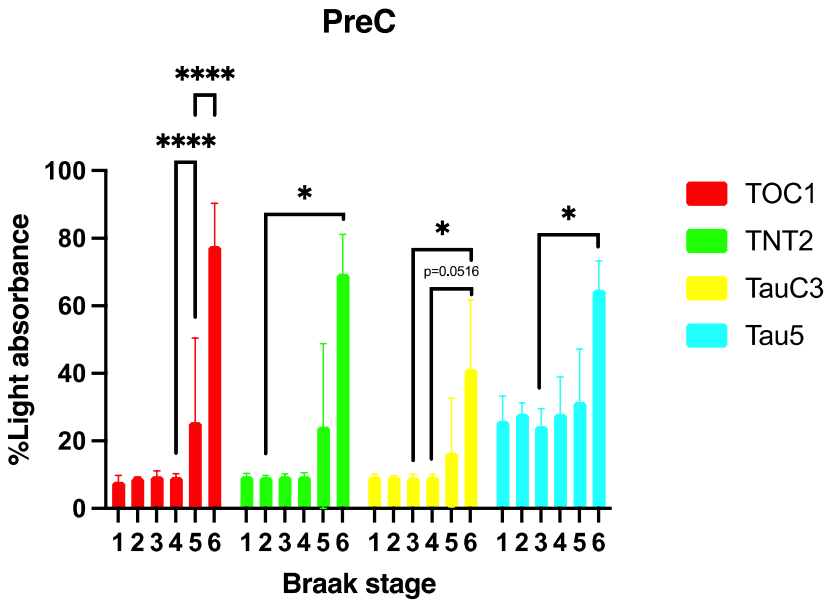

The same selected pre-tangle markers were used as capture antibodies combined with the R1 total tau antibody measure tau levels. The data for each marker were categorized according to the Braak stages. Bar graphs were used to display the mean values and the percentage coefficient of variation (%CV) for each marker. Statistical analyses were conducted using the Kruskal-Wallis test, followed by Dunn's multiple comparisons for pairwise analysis.

When comparing these markers across the clinical groups, TOC1 level increased in all three regions from MCI to AD (FC, p=0.0223, PCC, p=0.0228, PreC, p=0.0280), and TNT2 level increased in the FC (p=0.0293) and PCC (p=0.0146), did not reach statistical significance in PreC. Similarly, TauC3 showed a significant increase only in the PCC samples of the AD group compared to the controls (p=0.0096). Total tau levels, as indicated by Tau5, did not differ significantly between clinical groups (Figure 2.7).

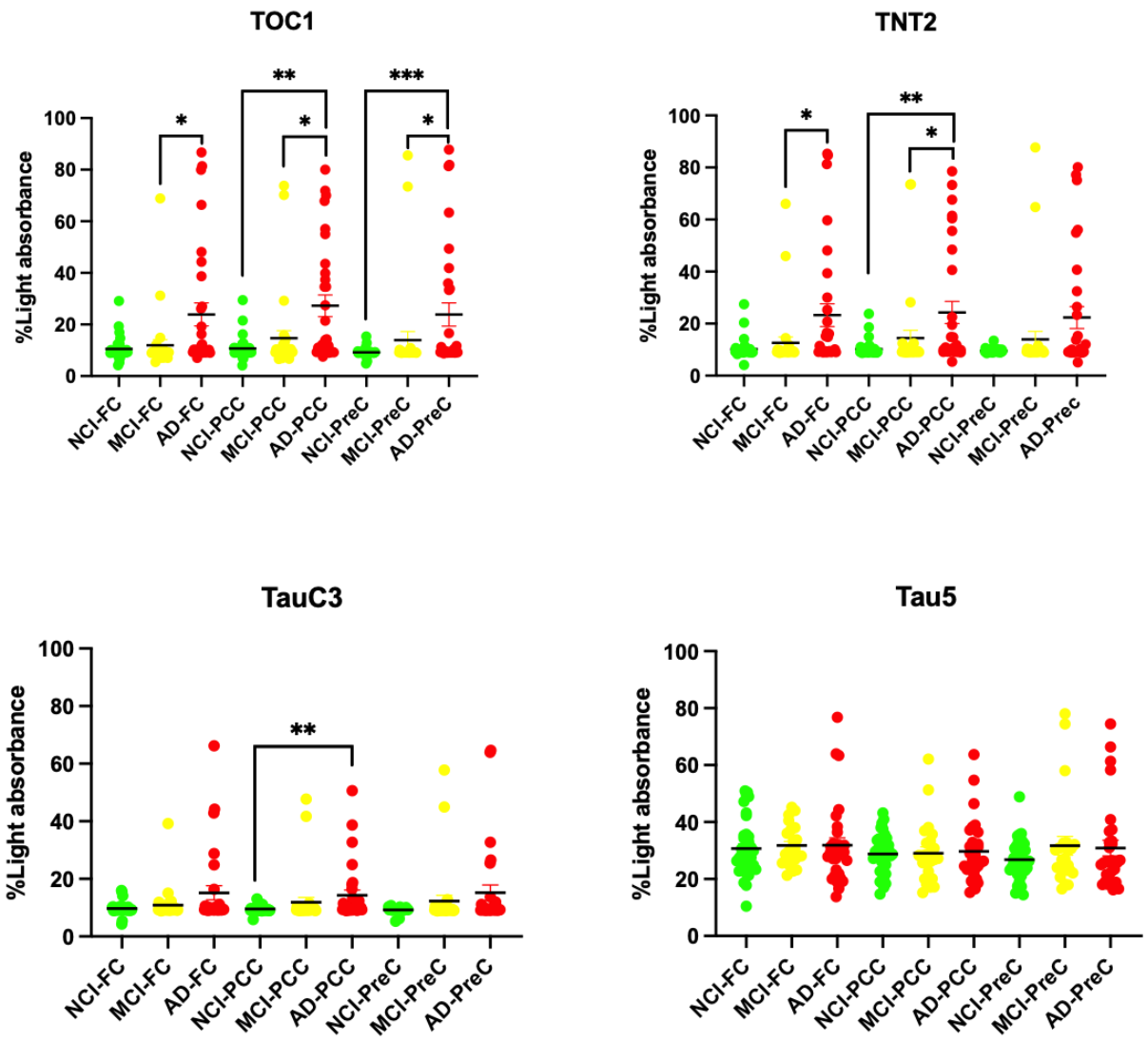

Figure 2. 7 Soluble pathological tau quantification in the frozen DMN samples based on the clinical groups

Quantification of selected pre-tangle markers was performed using sandwich ELISA on the soluble fraction of frozen, case-matched DMN samples, grouped according to clinical classification. Statistical analyses were conducted using the Kruskal-Wallis test, followed by Dunn's multiple comparisons for pairwise analysis.

Regional Differences for the Pathology Distribution

Interestingly, when the results from both total and soluble pre-tangle tau comparisons were paired across three regions for each case, regardless of their Braak status, and compared the ranks within each group, some of the markers showed regional differences in their abundance, favoring either PCC or FC. The most abundant marker in the study, pS422, was significantly higher in the PCC ($p=0.0029$ compared to FC and $p<0.0001$ compared to the PreC). Similarly, both total TOC1 and soluble TOC1 were higher in the PCC. Total TNT2 was also higher in the PCC, but the significance was only reached when compared to the FC. Soluble TauC3 was slightly higher in the FC compared to the PreC. Although there was no difference in the total tau between the posterior hubs, intriguingly, the total tau was higher in the FC. Finally, MOAB-2 was significantly higher in the PCC and FC compared to PreC. The overall pattern indicates divergence in the posterior DMN, with a higher pre-tangle tau load in the PCC possible resistance to tau pathology in neighboring PreC. This potential mechanisms for this differential pattern of tau pathology is ripe for future exploration and explored further in Specific Aim 3 experiments (Chapter 4).

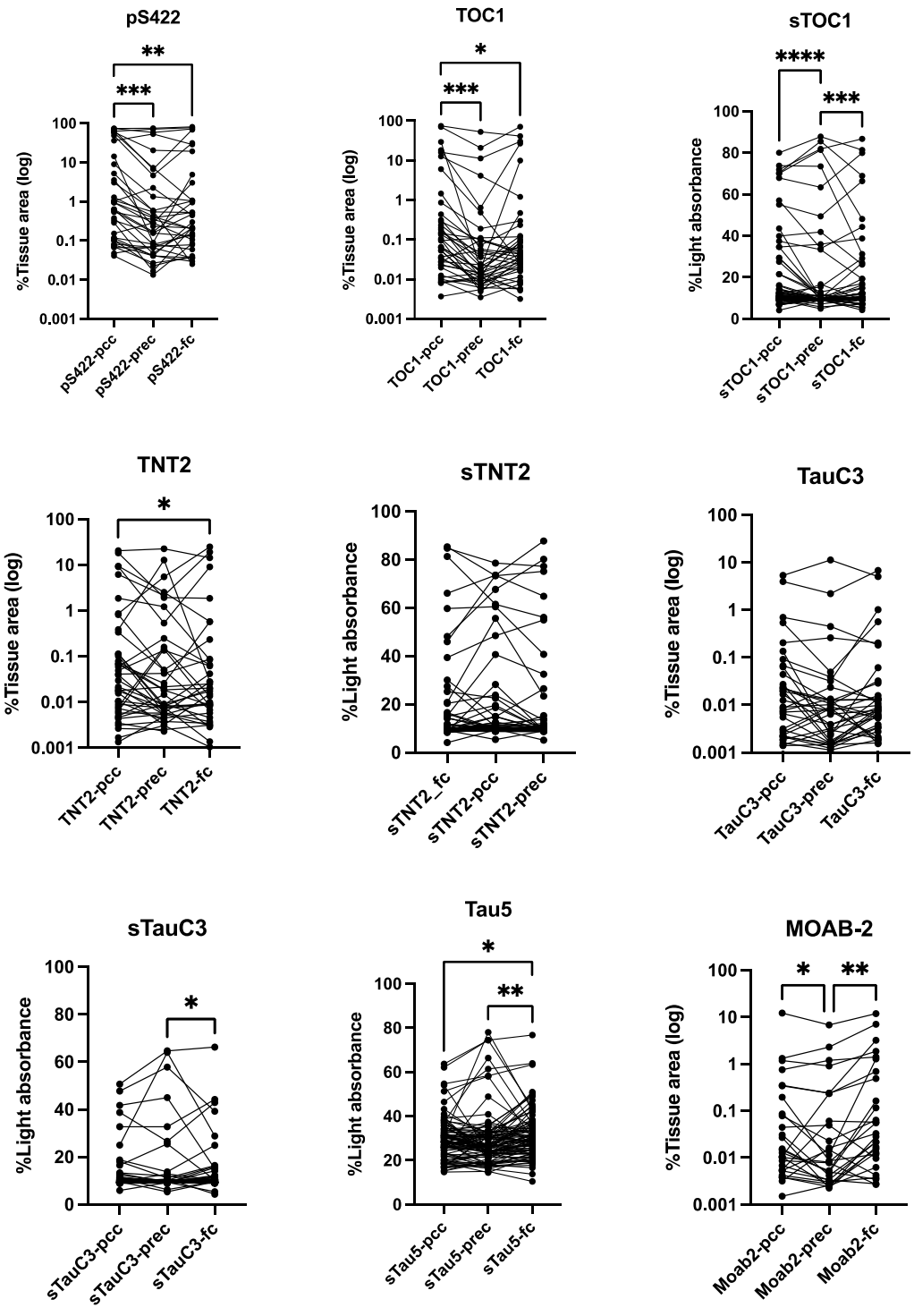

Figure 2. 8 Regional comparisons of soluble and total tau markers

Nonparametric Friedman test with a Dunn's multiple comparisons were used to analyze regional differences for each case. s = soluble

Validation Studies

DMN samples from MADC clinical cohort subjects were used to validate the findings from our soluble tau ELISA studies using the RROS cohort (Table 2.3). The subjects did not differ in age, sex, education, or PMI across the low-Braak/control, mid-Braak, and high-Braak groups (Table 2.3). However, MMSE scores were significantly lower in the high-Braak group (Table 2.3). Interestingly, the tau pathological load was notably higher for all markers in successive Braak stages in this cohort (Figure 2.9 A, B, C) compared to the RROS (Figure 2.6) and elevated by Braak stage IV. However, the increase reached statistical significance in Braak stage V and onwards with the exception of TOC1, was significantly increased in Braak stage IV in PCC ($p=0.0404$), followed by even more significant elevation by Braak stages V ($p=0.0130$) and VI ($p=0.0060$). TNT2 mimicked the TOC1 pattern in Braak stage IV and showing a significant increase in Braak stage V (PCC, $p=0.0127$, PreC, $p=0.0368$) and VI (FC, $p=0.0172$). TauC3 load was relatively minimal and showed significance in Braak stage VI. (FC, $p=0.0107$, PCC, $p=0.0456$) (Fig. 2.9A, B). There were no differences in Tau5 levels across the Braak stages, with a slight drop in Braak stage V in the PreC. The comparisons of the markers among the low-, mid-, and high-Braak groups showed a significant increase only in the high-Braak group (Supplementary Figure 2.2).

	Clinical diagnosis				Comparison by diagnosis group
	low-Braak (n=12)	mid-Brak (n=12)	high-Braak (n=12)	Total (n=36)	(*P* value)
Age at death (years)					
Mean ± SD	67.8 ± 14.9	80.3 ±10.8	74.3 ± 10.5	74.1 ± 7.6	0.056
(Range)	(39-87)	(60-95)	(57-92)	(39-95)	
No. (%) Males	6 (50%)	6 (50%)	6 (50%)	18 (50%)	>0.9999
Education					
Mean ± SD	15.25± 2.2	15.92± 2.4	15.33± 2.8	15.6± 2.5	0.8376
(Range)	13-18	12-20	12-20	12-20	
Postmortem Interval (hours)					
Mean ± SD	12.7 ± 7.6	8.6 ± 5.3	9.6 ± 5.5	10.2 ± 6.3	0.298
(Range)	(4-26)	(3-18)	(4-21)	(3-26)	
MMSE					
Mean ± SD	27 ± 2	15.3 ±11.9	8.1 ± 6.9	14.4 ± 10.9	0.0143 *
(Range)	(24-28)	(1-29)	(0-18)	(0-29)	
Braak Scores					
I-II	12	0	0	12	<0.0001*
III-IV	0	12	0	12	
V-VI	0	0	12	12	

Table 2. 3 Demographic, clinical, and pathological profile of the MADC cohort

‡ Chi-Square test, a Pairwise comparisons with One-way ANOVA showed no difference between the groups; Tukey's correction found the age in mid-Braak was slightly higher than low-Braak. b Pairwise comparisons with Kruskal-Wallis and Dunn's correction showed a significant difference between low- and high-Braak, and c significant decrease from low- to mid- to high. MMSE: Mini-Mental State Examination SD: Standard deviation p<0.05. p<0,01**, p<0,001***, p<0.0001****

A.

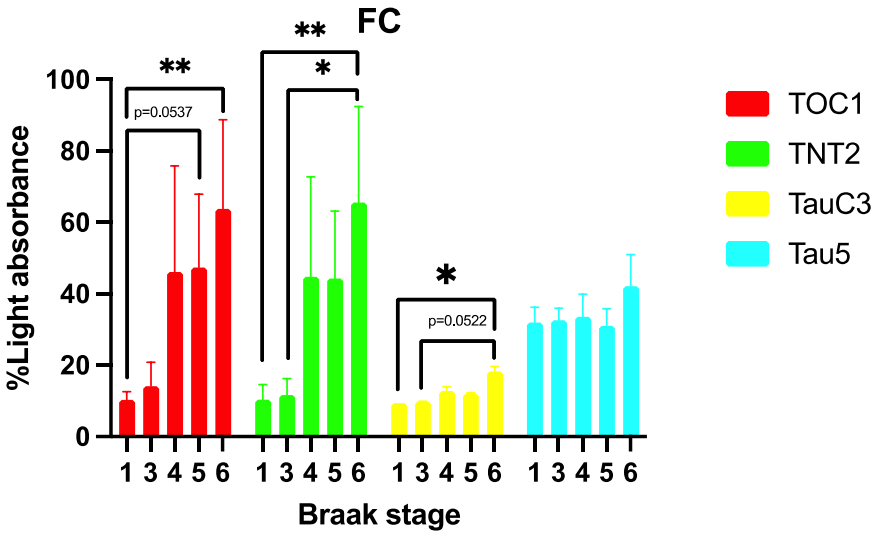

B.

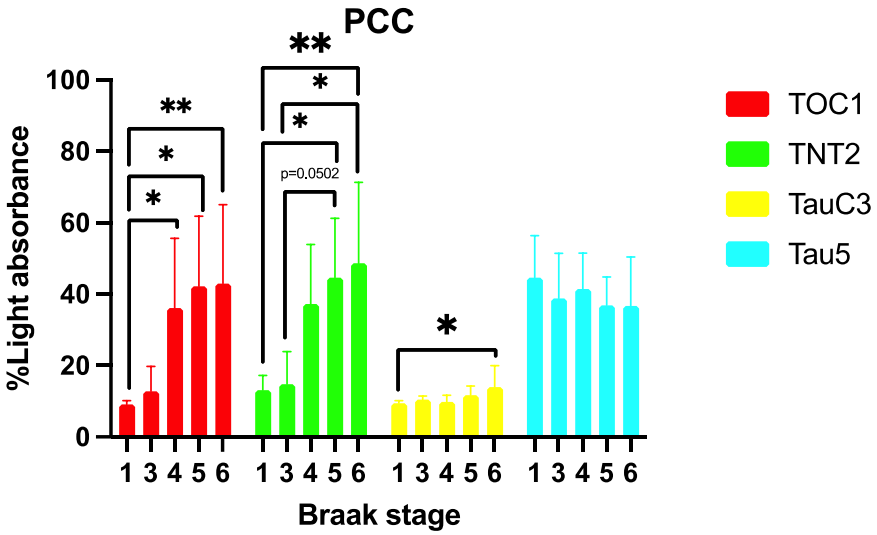

Figure 2. 9 Soluble pathological tau quantification in the MADC validation cohort

Figure 2 .9 (cont'd)

C.

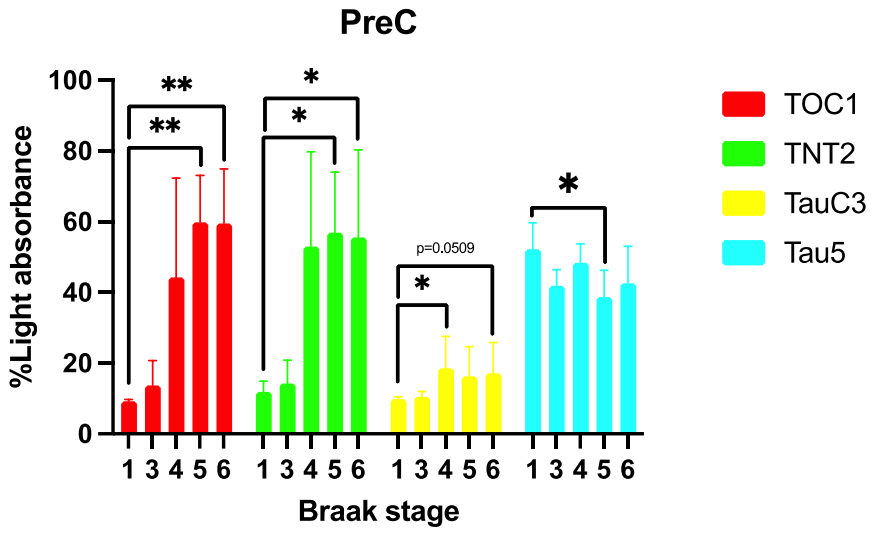

Tau extraction from the MADC validation cohort was similarly performed and S1 fractions were used to the perform sandwich ELISAs. The same selected pre-tangle markers were used as capture antibodies combined with the R1 total tau antibody measure tau levels in the MADC cohort. The data for each marker were categorized according to the Braak stages. Bar graphs were used to display the mean values and the percentage coefficient of variation (%CV) for each marker. Statistical analyses were conducted using the Kruskal-Wallis test, followed by Dunn's multiple comparisons for pairwise analysis for each tau marker in each DMN region.

DISCUSSION

Pre-tangle tau impairs cellular trafficking, causes ionic imbalances by disrupting ion-gated calcium channels, and negatively impacts mitochondrial and lysosomal functions; physiologically, these and likely other cellular disturbances result in synaptic impairments, such as disrupted LTP, and may ultimately result in neuronal cell death, synaptic disconnection, and cognitive dysfunction in AD and related tauopathies (Fa,

2016; Princen, 2024; Reiss, 2024; Niewiadomska, 2021). However, broader questions remain regarding the extent to which these toxic tau species accumulate during AD progression and the threshold of toxic pre-tangle pathology accumulation needed in higher-order brain regions to precipitate cognitive deterioration. In this dissertation project, we aimed to address this question by focusing specifically on the FC, PCC, and PreC hubs of the DMN, a vulnerable higher-order association cortical connectome that mediates memory and attentional function and falters early in the preclinical and prodromal stages of AD (He, 2007; Wu, 2011; Grieder, 2018). In this chapter, we focused on our results quantifying the accrual of several tau pathological pre-tangle species (pS422, TOC1, TNT2, and TauC3) within the DMN hubs and demonstrate that, in general, the abundance of pre-tangle tau bearing profiles significantly increased during the transition from Braak stage IV to V. When analyzed based on antemortem clinical diagnosis, we showed significant increases in the tau markers in mild/moderate AD cases compared to NCI, with intermediate levels in MCI cases. We also detected a higher pathology load in the PCC compared to the other two hubs, and evidence for possible resistance in PreC, which may represent important differential mechanisms of tau biology underlying a regional vulnerability within the DMN. Significantly, tau marker levels were not appreciably associated with subject variables such as age, education, and APOE4 genotype status, or with postmortem interval (Supplementary Table 2.1). The extent to which pre-tangle tau marker expression correlated with antemortem neuropsychological test scores and global cognitive status, as well as postmortem neuropathologic diagnostic variables, will be the focus of Chapter 3.

Early Pathological Tau Quantification in the Postmortem DMN

Research on the role of tau in AD has predominantly focused on the medial temporal lobe due to the initiation of NFT deposition in the trans/entorhinal cortex and hippocampus; hence, the limbic and neocortical hubs of the DMN, especially posterior PCC and PreC, have remained relatively underexplored. When quantifying early pathological pre-tangle tau phosphorylation and conformational epitopes in fixed DMN tissue samples, pS422 (Serine 422 phosphorylation) was the earliest and the most abundant marker among the four selected, emerging primarily as NTs and then gradually as somal deposits (Figure 2.1). Early pS422 positive tau accrual has been noted in cholinergic nucleus basalis neurons (Vana, 2011; Mufson, 2014), as well as pyramidal neurons within the entorhinal cortex (Patterson, 2011) and frontal cortex (Tiernan, 2016a), in addition to synaptosomes isolated from the angular gyrus (Henkins, 2012). Additionally, pS422 positive tau colocalized with TOC1 in the temporal cortex of chronic traumatic encephalopathy patients (Kanaan, 2016). Phosphorylation at the tau S422 residue is associated with several kinases, including GSK3β, JNK3, and p38 (Guillozet-Bongaarts, 2006; Tiernan, 2016; Tiernan, 2016b; Yoshida, 2004), all of which have been found associated with tau toxicity through various molecular mechanisms (Sayas, 2021; Rankin, 2007; Solas, 2023; Ardanaz, 2023). S422 phosphorylation inhibits anterograde and retrograde fast axonal transport (Tiernan, 2016a), disrupts protein homeostasis (Tiernan, 2016b), and is linked to neurotransmitter abnormalities (Tiernan, 2018a). Recently, Stefanoska and colleagues systematically explored the Serine/Threonine phosphorylation sites of tau in vitro, identifying S422 phosphorylation as a master site in the proline-rich region and C-terminus of tau, where its

phosphorylation modulates the phosphorylation of the other epitopes interdependently (Stefanoska, 2022).

The other two pre-tangle markers used in this study were conformation-specific TOC1 (tau oligomers) (Ward, 2013) and TNT2 (N-terminal misfolding) (Combs, 2017). Both are present in the entorhinal cortex and medial temporal lobe (Combs, 2016; Mahady, 2023; Koss, 2018; Sarkar, 2020) as well as the frontal cortex in several tauopathies (Kanaan, 2016; Combs, 2017), and are associated with cellular toxicity (Fa, 2016; Niewiadomska, 2021; Mufson, 2014; Combs, 2017). Previously, TOC1-positive tau levels were found to be increased in synaptosome-enriched fractions from layer II of the visual cortex in the Braak stage III/IV cases (Taddei, 2023). Also, increased TOC1 levels in the temporal cortex correlated with the Braak stage in an AD cohort (Braak IV-VI) (Koss, 2016). Similar to pS422, we detected TOC1+ and TNT2+ profiles in early Braak stages, largely confined to NTs coursing throughout the DMN cortical laminae (Figures 2.1, 2.2 & 2.3), with the gradual appearance of neuronal labeling enriched in layers II/III and V/VI by Braak stage V (Figure 2.1). In terms of abundance, TOC1 and TNT2 followed a similar pattern; however, their localization differed slightly.
While TNT2 staining was more pronounced in neurites, TOC1+ neurites were less abundant and concentrated early in the cell soma, where it overlapped with TNT2 (Figures 2.1 & 2.3).

With respect to the appearance of pre-tangle markers in neurons, their emergence during Braak stage V aligns with canonical Braak staging for the initial appearance of frank NFT deposition in neocortical regions (Braak, 1991). However, pre-tangle+ NTs were the predominant pathology observed in the DMN hubs in earlier Braak

stages. The origin of these neurites remains unclear, but it is tempting to speculate that reciprocal DMN hub efferents/afferents comprise a distinct population, particularly in more superficial layers (Felleman, 1991). Moreover, the DMN hubs receive prominent innervation from subcortical structures modulating memory and attention, such as the cholinergic nucleus basalis (Mesulam, 1983). As discussed above, we have shown that TOC1 and pS422 colocalize in these cholinergic neurons very early during AD progression and that their abundance correlates with decreased MMSE and GCS (Tiernan, 2018b). We observed a similar colocalization in threads and neurons in this study (Figures 2.2 & 2.3) as well.

The final marker used, TauC3, detects truncation of aspartic acid at residue 421 and labels more advanced tau pathology and has recently been referred to as a gain of function post-translational modification due to the role in inhibiting axonal transport (Conze, 2022; Guillozet-Bongaarts, 2005). We have previously shown that TauC3 pathology is associated with cholinergic nucleus basalis neuronal dysfunction, including differential regulation of various subunits of nicotinic acetylcholine receptors (Tiernan, 2018a). In the current study, the appearance of TauC3-labeled profiles was more similar to TOC1, with relatively less prominent immunopositive NTs and more neuronal enrichment within the DMN hubs (Figure 2.1). TauC3 pathology was also relatively less abundant compared to the other markers in the early Braak stages.

Regarding regional differences observed among the DMN hubs, our findings go parallel with the previous reports that PCC is susceptible to amyloid and tau pathology, possibly due to increased high base metabolism, which starts to decline early in AD (Putcha, 2022). Insel et al. examined the Aβ initiation and accumulation rate in multiple

brain regions and found PCC showing the highest initial rates of Aβ uptake while precunus being one of the slowest regions (Insel, 2020). They also found slow tau uptake in the precuneus compared to the MTL regions. The proposed resilience of precuneus might be due to different factors, such as preserved neurotrophic signaling pathways despite the present Aβ pathology (Perez, 2015) or molecular signatures of cortical neurons (Dharshini, 2024).

Oligomeric Amyloid Pathology in the DMN

The bidirectional interaction between amyloid beta and tau has long been recognized, with each exacerbating the other's pathology and dysfunction (Castillo-Carranza, 2015; Oddo, 2003; Zhang, 2021). In the DMN, amyloid beta plaques and tau tangles coalesce despite their separate propagation trajectories in the brain. Previous PET and fMRI studies have shown that amyloid plaque positivity in the DMN is associated with hyperconnectivity (Schultz, 2017). However, once NFTs are detectable by PET, the functional connectivity shifts toward a state of hypoconnectivity. More recently, combined PET/fMRI studies in two separate cohorts showed that Aβ-associated hyperconnectivity mediates tau pathological spread across connected brain regions, providing a potential key link between Aβ deposition and NFT-associated resting state network failure (Roemer-Cassiano, 2025). Although amyloid pathology was not the primary focus of this study, we immunolabeled oligomeric Aβ using the MOAB-2 antibody and examined the correlation between oligomeric Aβ and tau pathology, as well as cognitive scores. Interestingly, MOAB-2 levels were strongly associated with pS422, TOC1, and TNT2 in all three DMN regions but amyloid oligomer burden generally did not associate with cognitive deterioration except in PCC. Together, these

findings support the prevailing concept that tau pathology more strongly impacts cognitive decline than amyloid pathology, with new insights from a key resting state network. Further studies are needed to validate these results and explore the complex interplay between these co-pathologies.

Soluble Tau Pathology within the DMN

To complement the quantitative histological assessments, ELISA assessments of S1 fractions provided additional insights into pre-tangle tau accumulation in the DMN. For instance, whereas tau molecules bearing pre-tangle pathological epitopes are associated with NFTs, soluble tau bearing TOC1, TNT2, and TauC3 epitopes may represent an enriched pool of toxic tau associated with the cellular perturbations described above. Although the distribution of tau pathology across Braak stages in the S1 fractions was similar to histologically defined pathology in the RROS cohort, with a significant increase from Braak IV to V, statistical significance for these changes was greater using the S1 fractions, particularly for the oligomeric marker TOC1, in line with a previous study showing that soluble TOC1 in the temporal cortex correlated with Braak stage, MMSE, and clinical dementia rating (CDR) scores (Koss, 2016).

Interestingly, our validation cohort using postmortem DMN S1 fractions from MADC subjects revealed a similar abrupt increase in pre-tangle tau pathology with increasing Braak stage, but this increase occurred between Braak stages IV and V instead of V and VI, as seen in the RROS sample. A possible explanation for this may relate to differences between the cohort subjects and lifestyle factors. The RROS cohort, consisting of retired Catholic clergy, benefited from more years of formal education (Tables 2.2 & 2.3) and a relatively healthy lifestyle, including a more regulated

diet, structured sleep patterns, and religious activities that may provide cognitive benefits, such as stress reduction (Bennett, 2018). Additionally, the strong sense of community and continuing education fostered by cloistered living both promotes the beneficial effects of lifelong learning and prevents the influence of social isolation as modifiable risk factors for dementia (Clarke, 2025; Guarnera, 2023). In contrast, the Michigan cohort represents a community-dwelling population more reflective of typical human experience, with average educational attainment and more potential exposures to metabolic, vascular, and related insults affecting epigenetic modulation and transciptional regulation of the genome (Agapitova, 1989; Lahiri, 2024; Counts, 2025). Moreover, this earlier accrual of tau pathology occurred despite the MADC subjects having a younger average age (74.1 ± 7.6) at death. Hence, it is tempting to speculate that the RROS cohort was enriched for pathologically resistant and cognitively resilient subjects (2365). Alternatively, another potential factor contributing to the observed differences could have been due to minor differences in Braak staging upon neuropathological examination between the two autopsy cohorts.

Study Limitations

The present study has several limitations. First, the outcome measures used to quantify the immunolabeled images were based on the percentage of labeled tissue, which allowed us to normalize the signal relative to the area of the region of interest. Hence, despite the advanced utility of leveraging machine-learning software for quantitative measurements, this may have resulted in an underestimation of total tau pre-tangle marker pathology. For instance, the predominance of NTs observed to appear first in the DMN hubs, while striking on a microscopic scale, did not necessarily

generate a high densitometric signal per region of interest. Hence, it is possible that the extent of NT pathology could be more accurately measured using stereological techniques in future studies (Kneynsberg, 2016). Secondly, PET and fMRI sequences are not typically collected during MRI sessions during annual clinical evaluations of RROS cohort participants, thus precluding a comparison between the presence of tau pathology within the DMN hubs early during disease progression and DMN tau-PET and functional analysis antemortem. On the other hand, detailed records of NFT and plaque pathology were available, including plaque density, plaque number, and NFT counts in key regions like the entorhinal cortex and hippocampus. These data were incorporated into the correlation matrices, providing valuable insights into the relationship between these pathologies (see Chapter 3).

CONCLUSION

The DMN, which displays hallmark AD pathology early in the progression of AD, is a promising candidate for studying the pathology-cognition paradigm in AD. PET-detected NFTs show strong correlations with inter- and intra-functional connectivity across DMN hubs. However, pre-tangle tau propagation within the DMN remains largely overlooked. The lack of pre-tangle tau-specific PET tracers limits the ability to monitor early-stage pathology in the brain. In this postmortem study, we observed that pre-tangle tau was present at low Braak stages and elevated as early as Braak stages IV to V in MADC and RROS cohorts, respectively. These findings might help to set the stage for further studies to understand the spatiotemporal distribution of the pre-tangle pathology in the DMN and its relation to changes in the cognitive domains that are regulated by the DMN function. Chapter 3 begins to explore these relationships.

REFERENCES

Alzheimer's disease facts and figures. (2024). *Alzheimers Dement, 20*(5), 3708-3821. doi:10.1002/alz.13809

Agapitova, I. V. (1989). [Penetration of cefazolin and methicillin into tissues of rats with aseptic inflammation]. *Antibiot Khimioter, 34*(2), 120-123. Retrieved from https://www.ncbi.nlm.nih.gov/pubmed/2730224

Ardanaz, C. G., Ezkurdia, A., Bejarano, A., Echarte, B., Smerdou, C., Martisova, E., . . . Solas, M. (2023). JNK3 Overexpression in the Entorhinal Cortex Impacts on the Hippocampus and Induces Cognitive Deficiencies and Tau Misfolding. *ACS Chem Neurosci, 14*(11), 2074-2088. doi:10.1021/acschemneuro.3c00092

Baudic, S., Barba, G. D., Thibaudet, M. C., Smagghe, A., Remy, P., & Traykov, L. (2006). Executive function deficits in early Alzheimer's disease and their relations with episodic memory. *Arch Clin Neuropsychol, 21*(1), 15-21. doi:10.1016/j.acn.2005.07.002

Bennett, D. A., Buchman, A. S., Boyle, P. A., Barnes, L. L., Wilson, R. S., & Schneider, J. A. (2018). Religious Orders Study and Rush Memory and Aging Project. *J Alzheimers Dis, 64*(s1), S161-S189. doi:10.3233/JAD-179939

Bennett, D. A., Buchman, A. S., Boyle, P. A., Barnes, L. L., Wilson, R. S., & Schneider, J. A. (2018). Religious Orders Study and Rush Memory and Aging Project. *J Alzheimers Dis, 64*(s1), S161-S189. doi:10.3233/JAD-179939

Bennett, D. A., Wilson, R. S., Schneider, J. A., Evans, D. A., Beckett, L. A., Aggarwal, N. T., . . . Bach, J. (2002). Natural history of mild cognitive impairment in older persons. *Neurology, 59*(2), 198-205. doi:10.1212/wnl.59.2.198

Berron, D., Vogel, J. W., Insel, P. S., Pereira, J. B., Xie, L., Wisse, L. E. M., . . . Hansson, O. (2021). Early stages of tau pathology and its associations with functional connectivity, atrophy and memory. *Brain, 144*(9), 2771-2783. doi:10.1093/brain/awab114

Biel, D., Luan, Y., Brendel, M., Hager, P., Dewenter, A., Moscoso, A., . . . Alzheimer's Disease Neuroimaging, I. (2022). Combining tau-PET and fMRI meta-analyses for patient-centered prediction of cognitive decline in Alzheimer's disease. *Alzheimers Res Ther, 14*(1), 166. doi:10.1186/s13195-022-01105-5

Bocancea, D. I., Svenningsson, A. L., van Loenhoud, A. C., Groot, C., Barkhof, F., Strandberg, O., . . . Ossenkoppele, R. (2023). Determinants of cognitive and brain resilience to tau pathology: a longitudinal analysis. *Brain, 146*(9), 3719-3734. doi:10.1093/brain/awad100

Braak, H., & Braak, E. (1991). Neuropathological stageing of Alzheimer-related changes. *Acta Neuropathol, 82*(4), 239-259. doi:10.1007/bf00308809

Castillo-Carranza, D. L., Guerrero-Munoz, M. J., Sengupta, U., Hernandez, C., Barrett, A. D., Dineley, K., & Kayed, R. (2015). Tau immunotherapy modulates both pathological tau and upstream amyloid pathology in an Alzheimer's disease mouse model. *J Neurosci, 35*(12), 4857-4868. doi:10.1523/JNEUROSCI.4989-14.2015

Celone, K. A., Calhoun, V. D., Dickerson, B. C., Atri, A., Chua, E. F., Miller, S. L., . . . Sperling, R. A. (2006). Alterations in memory networks in mild cognitive impairment and Alzheimer's disease: an independent component analysis. *J Neurosci, 26*(40), 10222-10231. doi:10.1523/JNEUROSCI.2250-06.2006

Clarke, K. M., Etemadmoghadam, S., Danner, B., Corbett, C., Ghaseminejad-Bandpey, A., Dopler, M., . . . Flanagan, M. E. (2025). The Nun Study: Insights from 30 years of aging and dementia research. *Alzheimers Dement, 21*(2), e14626. doi:10.1002/alz.14626

Combs, B., & Kanaan, N. M. (2017). Exposure of the Amino Terminus of Tau Is a Pathological Event in Multiple Tauopathies. *Am J Pathol, 187*(6), 1222-1229. doi:10.1016/j.ajpath.2017.01.019

Combs, B., Hamel, C., & Kanaan, N. M. (2016). Pathological conformations involving the amino terminus of tau occur early in Alzheimer's disease and are differentially detected by monoclonal antibodies. *Neurobiol Dis, 94*, 18-31. doi:10.1016/j.nbd.2016.05.016

Conze, C., Rierola, M., Trushina, N. I., Peters, M., Janning, D., Holzer, M., . . . Brandt, R. (2022). Caspase-cleaved tau is senescence-associated and induces a toxic gain of function by putting a brake on axonal transport. *Mol Psychiatry, 27*(7), 3010-3023. doi:10.1038/s41380-022-01538-2

Counts, S. E., Beck, J. S., Maloney, B., Malek-Ahmadi, M., Ginsberg, S. D., Mufson, E. J., & Lahiri, D. K. (2025). Posterior cingulate cortex microRNA dysregulation differentiates cognitive resilience, mild cognitive impairment, and Alzheimer's disease. *Alzheimers Dement, 21*(2), e70019. doi:10.1002/alz.70019

Counts, S. E., Nadeem, M., Lad, S. P., Wuu, J., & Mufson, E. J. (2006). Differential expression of synaptic proteins in the frontal and temporal cortex of elderly subjects with mild cognitive impairment. *J Neuropathol Exp Neurol, 65*(6), 592-601. doi:10.1097/00005072-200606000-00007

Crossley, C. A., Omoluabi, T., Torraville, S. E., Duraid, S., Maziar, A., Hasan, Z., . . . Yuan, Q. (2024). Hippocampal hyperphosphorylated tau-induced deficiency is rescued by L-type calcium channel blockade. *Brain Commun, 6*(2), fcae096. doi:10.1093/braincomms/fcae096

Daly, E., Zaitchik, D., Copeland, M., Schmahmann, J., Gunther, J., & Albert, M. (2000). Predicting conversion to Alzheimer disease using standardized clinical information. *Arch Neurol, 57*(5), 675-680. doi:10.1001/archneur.57.5.675

Desgranges, B., Baron, J. C., Lalevee, C., Giffard, B., Viader, F., de La Sayette, V., & Eustache, F. (2002). The neural substrates of episodic memory impairment in Alzheimer's disease as revealed by FDG-PET: relationship to degree of deterioration. *Brain, 125*(Pt 5), 1116-1124. doi:10.1093/brain/awf097

Dharshini, S. A. P., Sanz-Ros, J., Pan, J., Tang, W., Vallejo, K., Otero-Garcia, M., & Cobos, I. (2024). Molecular Signatures of Resilience to Alzheimer's Disease in Neocortical Layer 4 Neurons. *bioRxiv*. doi:10.1101/2024.11.03.621787

Fa, M., Puzzo, D., Piacentini, R., Staniszewski, A., Zhang, H., Baltrons, M. A., . . . Arancio, O. (2016). Extracellular Tau Oligomers Produce An Immediate Impairment of LTP and Memory. *Sci Rep, 6*, 19393. doi:10.1038/srep19393

Felleman, D. J., & Van Essen, D. C. (1991). Distributed hierarchical processing in the primate cerebral cortex. *Cereb Cortex, 1*(1), 1-47. doi:10.1093/cercor/1.1.1-a

Fisar, Z. (2022). Linking the Amyloid, Tau, and Mitochondrial Hypotheses of Alzheimer's Disease and Identifying Promising Drug Targets. *Biomolecules, 12*(11). doi:10.3390/biom12111676

Flanagin, V. L., Klinkowski, S., Brodt, S., Graetsch, M., Roselli, C., Glasauer, S., & Gais, S. (2023). The precuneus as a central node in declarative memory retrieval. *Cereb Cortex, 33*(10), 5981-5990. doi:10.1093/cercor/bhac476

Ghag, G., Bhatt, N., Cantu, D. V., Guerrero-Munoz, M. J., Ellsworth, A., Sengupta, U., & Kayed, R. (2018). Soluble tau aggregates, not large fibrils, are the toxic species that display seeding and cross-seeding behavior. *Protein Sci, 27*(11), 1901-1909. doi:10.1002/pro.3499

Giorgio, J., Adams, J. N., Maass, A., Jagust, W. J., & Breakspear, M. (2024). Amyloid induced hyperexcitability in default mode network drives medial temporal hyperactivity and early tau accumulation. *Neuron, 112*(4), 676-686 e674. doi:10.1016/j.neuron.2023.11.014

Green, C., Sydow, A., Vogel, S., Anglada-Huguet, M., Wiedermann, D., Mandelkow, E., . . . Hoehn, M. (2019). Functional networks are impaired by elevated tau-protein but reversible in a regulatable Alzheimer's disease mouse model. *Mol Neurodegener, 14*(1), 13. doi:10.1186/s13024-019-0316-6

Greenberg, S. G., Davies, P., Schein, J. D., & Binder, L. I. (1992). Hydrofluoric acid-treated tau PHF proteins display the same biochemical properties as normal tau. *J Biol Chem, 267*(1), 564-569

Grieder, M., Wang, D. J. J., Dierks, T., Wahlund, L. O., & Jann, K. (2018). Default Mode Network Complexity and Cognitive Decline in Mild Alzheimer's Disease. *Front Neurosci, 12*, 770. doi:10.3389/fnins.2018.00770

Guarnera, J., Yuen, E., & Macpherson, H. (2023). The Impact of Loneliness and Social Isolation on Cognitive Aging: A Narrative Review. *J Alzheimers Dis Rep, 7*(1), 699-714. doi:10.3233/ADR-230011

Guillozet-Bongaarts, A. L., Cahill, M. E., Cryns, V. L., Reynolds, M. R., Berry, R. W., & Binder, L. I. (2006). Pseudophosphorylation of tau at serine 422 inhibits caspase cleavage: in vitro evidence and implications for tangle formation in vivo. *J Neurochem, 97*(4), 1005-1014. doi:10.1111/j.1471-4159.2006.03784.x

Guillozet-Bongaarts, A. L., Garcia-Sierra, F., Reynolds, M. R., Horowitz, P. M., Fu, Y., Wang, T., . . . Binder, L. I. (2005). Tau truncation during neurofibrillary tangle evolution in Alzheimer's disease. *Neurobiol Aging, 26*(7), 1015-1022. doi:10.1016/j.neurobiolaging.2004.09.019

Guzman-Velez, E., Diez, I., Schoemaker, D., Pardilla-Delgado, E., Vila-Castelar, C., Fox-Fuller, J. T., . . . Quiroz, Y. T. (2022). Amyloid-beta and tau pathologies relate to distinctive brain dysconnectomics in preclinical autosomal-dominant Alzheimer's disease. *Proc Natl Acad Sci U S A, 119*(15), e2113641119. doi:10.1073/pnas.2113641119

Hahn, A., Strandberg, T. O., Stomrud, E., Nilsson, M., van Westen, D., Palmqvist, S., . . . Hansson, O. (2019). Association Between Earliest Amyloid Uptake and Functional Connectivity in Cognitively Unimpaired Elderly. *Cereb Cortex, 29*(5), 2173-2182. doi:10.1093/cercor/bhz020

He, Y., Wang, L., Zang, Y., Tian, L., Zhang, X., Li, K., & Jiang, T. (2007). Regional coherence changes in the early stages of Alzheimer's disease: a combined structural and resting-state functional MRI study. *Neuroimage, 35*(2), 488-500. doi:10.1016/j.neuroimage.2006.11.042

Henkins, K. M., Sokolow, S., Miller, C. A., Vinters, H. V., Poon, W. W., Cornwell, L. B., . . . Gylys, K. H. (2012). Extensive p-tau pathology and SDS-stable p-tau oligomers in Alzheimer's cortical synapses. *Brain Pathol, 22*(6), 826-833. doi:10.1111/j.1750-3639.2012.00598.x

Hoenig, M. C., Bischof, G. N., Seemiller, J., Hammes, J., Kukolja, J., Onur, O. A., . . . Drzezga, A. (2018). Networks of tau distribution in Alzheimer's disease. *Brain, 141*(2), 568-581. doi:10.1093/brain/awx353

Hyman, B. T., & Trojanowski, J. Q. (1997). Consensus recommendations for the postmortem diagnosis of Alzheimer disease from the National Institute on Aging and the Reagan Institute Working Group on diagnostic criteria for the

neuropathological assessment of Alzheimer disease. *J Neuropathol Exp Neurol, 56*(10), 1095-1097. doi:10.1097/00005072-199710000-00002

Hyman, B. T., Phelps, C. H., Beach, T. G., Bigio, E. H., Cairns, N. J., Carrillo, M. C., . . . Montine, T. J. (2012). National Institute on Aging-Alzheimer's Association guidelines for the neuropathologic assessment of Alzheimer's disease. *Alzheimers Dement, 8*(1), 1-13. doi:10.1016/j.jalz.2011.10.007

Insel, P. S., Mormino, E. C., Aisen, P. S., Thompson, W. K., & Donohue, M. C. (2020). Neuroanatomical spread of amyloid beta and tau in Alzheimer's disease: implications for primary prevention. *Brain Commun, 2*(1), fcaa007. doi:10.1093/braincomms/fcaa007

Jann, K., Boudreau, J., Albrecht, D., Cen, S. Y., Cabeen, R. P., Ringman, J. M., . . . Alzheimer's Disease Neuroimaging, I. (2023). FMRI Complexity Correlates with Tau-PET and Cognitive Decline in Late-Onset and Autosomal Dominant Alzheimer's Disease. *J Alzheimers Dis, 95*(2), 437-451. doi:10.3233/JAD-220851

Kanaan, N. M., Cox, K., Alvarez, V. E., Stein, T. D., Poncil, S., & McKee, A. C. (2016). Characterization of Early Pathological Tau Conformations and Phosphorylation in Chronic Traumatic Encephalopathy. *J Neuropathol Exp Neurol, 75*(1), 19-34. doi:10.1093/jnen/nlv001

Kelley, C. M., Ginsberg, S. D., Liang, W. S., Counts, S. E., & Mufson, E. J. (2022). Posterior cingulate cortex reveals an expression profile of resilience in cognitively intact elders. *Brain Commun, 4*(4), fcac162. doi:10.1093/braincomms/fcac162

Kitamura, T., Ogawa, S. K., Roy, D. S., Okuyama, T., Morrissey, M. D., Smith, L. M., . . . Tonegawa, S. (2017). Engrams and circuits crucial for systems consolidation of a memory. *Science, 356*(6333), 73-78. doi:10.1126/science.aam6808

Kneynsberg, A., Collier, T. J., Manfredsson, F. P., & Kanaan, N. M. (2016). Quantitative and semi-quantitative measurements of axonal degeneration in tissue and primary neuron cultures. *J Neurosci Methods, 266*, 32-41. doi:10.1016/j.jneumeth.2016.03.004

Koss, D. J., Dubini, M., Buchanan, H., Hull, C., & Platt, B. (2018). Distinctive temporal profiles of detergent-soluble and -insoluble tau and Abeta species in human Alzheimer's disease. *Brain Res, 1699*, 121-134. doi:10.1016/j.brainres.2018.08.014

Koss, D. J., Jones, G., Cranston, A., Gardner, H., Kanaan, N. M., & Platt, B. (2016). Soluble pre-fibrillar tau and beta-amyloid species emerge in early human Alzheimer's disease and track disease progression and cognitive decline. *Acta Neuropathol, 132*(6), 875-895. doi:10.1007/s00401-016-1632-3

Kravenska, Y., Koprowski, P., Nieznanska, H., & Nieznanski, K. (2024). Prion protein prevents the inhibition of large-conductance calcium-activated potassium channel by Tau peptide K18 oligomers. *Biochem Biophys Res Commun, 734*, 150793. doi:10.1016/j.bbrc.2024.150793

Kuchibhotla, K. V., Wegmann, S., Kopeikina, K. J., Hawkes, J., Rudinskiy, N., Andermann, M. L., . . . Hyman, B. T. (2014). Neurofibrillary tangle-bearing neurons are functionally integrated in cortical circuits in vivo. *Proc Natl Acad Sci U S A, 111*(1), 510-514. doi:10.1073/pnas.1318807111

Lahiri, D. K., Maloney, B., Wang, R., White, F. A., Sambamurti, K., Greig, N. H., & Counts, S. E. (2024). The seeds of its regulation: Natural antisense transcripts as single-gene control switches in neurodegenerative disorders. *Ageing Res Rev, 99*, 102336. doi:10.1016/j.arr.2024.102336

Lasagna-Reeves, C. A., Castillo-Carranza, D. L., Sengupta, U., Clos, A. L., Jackson, G. R., & Kayed, R. (2011). Tau oligomers impair memory and induce synaptic and mitochondrial dysfunction in wild-type mice. *Mol Neurodegener, 6*, 39. doi:10.1186/1750-1326-6-39

Luan, Y., Rubinski, A., Biel, D., Otero Svaldi, D., Alonzo Higgins, I., Shcherbinin, S., . . . Alzheimer's Disease Neuroimaging Initiative, A. (2024). Tau-network mapping of domain-specific cognitive impairment in Alzheimer's disease. *Neuroimage Clin, 44*, 103699. doi:10.1016/j.nicl.2024.103699

Mahady, L. J., Perez, S. E., Malek-Ahmadi, M., & Mufson, E. J. (2023). Oligomeric, phosphorylated, and truncated tau and spliceosome pathology within the entorhinal-hippocampal connectome across stages of Alzheimer's disease. *J Comp Neurol, 531*(18), 2080-2108. doi:10.1002/cne.25466

McKay, E. C., Beck, J. S., Khoo, S. K., Dykema, K. J., Cottingham, S. L., Winn, M. E., . . . Counts, S. E. (2019). Peri-Infarct Upregulation of the Oxytocin Receptor in Vascular Dementia. *J Neuropathol Exp Neurol, 78*(5), 436-452. doi:10.1093/jnen/nlz023

Mesulam, M. M., Mufson, E. J., Levey, A. I., & Wainer, B. H. (1983). Cholinergic innervation of cortex by the basal forebrain: cytochemistry and cortical connections of the septal area, diagonal band nuclei, nucleus basalis (substantia innominata), and hypothalamus in the rhesus monkey. *J Comp Neurol, 214*(2), 170-197. doi:10.1002/cne.902140206

Migliaccio, R., & Cacciamani, F. (2022). The temporal lobe in typical and atypical Alzheimer disease. *Handb Clin Neurol, 187*, 449-466. doi:10.1016/B978-0-12-823493-8.00004-3

Mirra, S. S., Heyman, A., McKeel, D., Sumi, S. M., Crain, B. J., Brownlee, L. M., . . . Berg, L. (1991). The Consortium to Establish a Registry for Alzheimer's Disease (CERAD). Part II. Standardization of the neuropathologic assessment of Alzheimer's disease. *Neurology, 41*(4), 479-486. doi:10.1212/wnl.41.4.479

Montine, T. J., Cholerton, B. A., Corrada, M. M., Edland, S. D., Flanagan, M. E., Hemmy, L. S., . . . White, L. R. (2019). Concepts for brain aging: resistance, resilience, reserve, and compensation. *Alzheimers Res Ther, 11*(1), 22. doi:10.1186/s13195-019-0479-y

Montine, T. J., Phelps, C. H., Beach, T. G., Bigio, E. H., Cairns, N. J., Dickson, D. W., . . . Alzheimer's, A. (2012). National Institute on Aging-Alzheimer's Association guidelines for the neuropathologic assessment of Alzheimer's disease: a practical approach. *Acta Neuropathol, 123*(1), 1-11. doi:10.1007/s00401-011-0910-3

Mueller, R. L., Kanaan, N. M., & Combs, B. (2023). Using Live-Cell Imaging to Measure the Effects of Pathological Proteins on Axonal Transport in Primary Hippocampal Neurons. *J Vis Exp*(202). doi:10.3791/66156

Mufson, E. J., Ward, S., & Binder, L. (2014). Prefibrillar tau oligomers in mild cognitive impairment and Alzheimer's disease. *Neurodegener Dis, 13*(2-3), 151-153. doi:10.1159/000353687

Nabizadeh, F., & Alzheimer's disease Neuroimaging, I. (2024). Local molecular and connectomic contributions of tau-related neurodegeneration. *Geroscience*. doi:10.1007/s11357-024-01339-1

Niewiadomska, G., Niewiadomski, W., Steczkowska, M., & Gasiorowska, A. (2021). Tau Oligomers Neurotoxicity. *Life (Basel), 11*(1). doi:10.3390/life11010028

Oddo, S., Caccamo, A., Shepherd, J. D., Murphy, M. P., Golde, T. E., Kayed, R., . . . LaFerla, F. M. (2003). Triple-transgenic model of Alzheimer's disease with plaques and tangles: intracellular Abeta and synaptic dysfunction. *Neuron, 39*(3), 409-421. doi:10.1016/s0896-6273(03)00434-3

Patterson, K. R., Remmers, C., Fu, Y., Brooker, S., Kanaan, N. M., Vana, L., . . . Binder, L. I. (2011). Characterization of prefibrillar Tau oligomers in vitro and in Alzheimer disease. *J Biol Chem, 286*(26), 23063-23076. doi:10.1074/jbc.M111.237974

Perez, S. E., He, B., Nadeem, M., Wuu, J., Scheff, S. W., Abrahamson, E. E., . . . Mufson, E. J. (2015). Resilience of precuneus neurotrophic signaling pathways despite amyloid pathology in prodromal Alzheimer's disease. *Biol Psychiatry, 77*(8), 693-703. doi:10.1016/j.biopsych.2013.12.016

Princen, K., Van Dooren, T., van Gorsel, M., Louros, N., Yang, X., Dumbacher, M., . . . Griffioen, G. (2024). Pharmacological modulation of septins restores calcium

homeostasis and is neuroprotective in models of Alzheimer's disease. *Science, 384*(6699), eadd6260. doi:10.1126/science.add6260

Putcha, D., Eckbo, R., Katsumi, Y., Dickerson, B. C., Touroutoglou, A., & Collins, J. A. (2022). Tau and the fractionated default mode network in atypical Alzheimer's disease. *Brain Commun, 4*(2), fcac055. doi:10.1093/braincomms/fcac055

Raichle, M. E. (2015). The brain's default mode network. *Annu Rev Neurosci, 38*, 433-447. doi:10.1146/annurev-neuro-071013-014030

Raichle, M. E., MacLeod, A. M., Snyder, A. Z., Powers, W. J., Gusnard, D. A., & Shulman, G. L. (2001). A default mode of brain function. *Proc Natl Acad Sci U S A, 98*(2), 676-682. doi:10.1073/pnas.98.2.676

Rankin, C. A., Sun, Q., & Gamblin, T. C. (2007). Tau phosphorylation by GSK-3beta promotes tangle-like filament morphology. *Mol Neurodegener, 2*, 12. doi:10.1186/1750-1326-2-12

Reddy, P. H. (2011). Abnormal tau, mitochondrial dysfunction, impaired axonal transport of mitochondria, and synaptic deprivation in Alzheimer's disease. *Brain Res, 1415*, 136-148. doi:10.1016/j.brainres.2011.07.052

Reiss, A. B., Gulkarov, S., Jacob, B., Srivastava, A., Pinkhasov, A., Gomolin, I. H., . . . De Leon, J. (2024). Mitochondria in Alzheimer's Disease Pathogenesis. *Life (Basel), 14*(2). doi:10.3390/life14020196

Roemer-Cassiano, S. N., Wagner, F., Evangelista, L., Rauchmann, B. S., Dehsarvi, A., Steward, A., . . . Franzmeier, N. (2025). Amyloid-associated hyperconnectivity drives tau spread across connected brain regions in Alzheimer's disease. *Sci Transl Med, 17*(782), eadp2564. doi:10.1126/scitranslmed.adp2564

Roemer, S. N., Brendel, M., Gnorich, J., Malpetti, M., Zaganjori, M., Quattrone, A., . . . Franzmeier, N. (2024). Subcortical tau is linked to hypoperfusion in connected cortical regions in 4-repeat tauopathies. *Brain, 147*(7), 2428-2439. doi:10.1093/brain/awae174

Santacruz, K., Lewis, J., Spires, T., Paulson, J., Kotilinek, L., Ingelsson, M., . . . Ashe, K. H. (2005). Tau suppression in a neurodegenerative mouse model improves memory function. *Science, 309*(5733), 476-481. doi:10.1126/science.1113694

Sarkar, S., Raymick, J., Cuevas, E., Rosas-Hernandez, H., & Hanig, J. (2020). Modification of methods to use Congo-red stain to simultaneously visualize amyloid plaques and tangles in human and rodent brain tissue sections. *Metab Brain Dis, 35*(8), 1371-1383. doi:10.1007/s11011-020-00608-0

Sayas, C. L., & Avila, J. (2021). GSK-3 and Tau: A Key Duet in Alzheimer's Disease. *Cells, 10*(4). doi:10.3390/cells10040721

Scaduto, P., Marcatti, M., Bhatt, N., Kayed, R., & Taglialatela, G. (2024). Calcineurin inhibition prevents synaptic plasticity deficit induced by brain-derived tau oligomers. *Brain Commun, 6*(5), fcae277. doi:10.1093/braincomms/fcae277

Schneider, J. A., Arvanitakis, Z., Leurgans, S. E., & Bennett, D. A. (2009). The neuropathology of probable Alzheimer disease and mild cognitive impairment. *Ann Neurol, 66*(2), 200-208. doi:10.1002/ana.21706

Schultz, A. P., Chhatwal, J. P., Hedden, T., Mormino, E. C., Hanseeuw, B. J., Sepulcre, J., . . . Sperling, R. A. (2017). Phases of Hyperconnectivity and Hypoconnectivity in the Default Mode and Salience Networks Track with Amyloid and Tau in Clinically Normal Individuals. *J Neurosci, 37*(16), 4323-4331. doi:10.1523/JNEUROSCI.3263-16.2017

Solas, M., Vela, S., Smerdou, C., Martisova, E., Martinez-Valbuena, I., Luquin, M. R., & Ramirez, M. J. (2023). JNK Activation in Alzheimer's Disease Is Driven by Amyloid beta and Is Associated with Tau Pathology. *ACS Chem Neurosci, 14*(8), 1524-1534. doi:10.1021/acschemneuro.3c00093

Spens, E., & Burgess, N. (2024). A generative model of memory construction and consolidation. *Nat Hum Behav, 8*(3), 526-543. doi:10.1038/s41562-023-01799-z

Stefanoska, K., Gajwani, M., Tan, A. R. P., Ahel, H. I., Asih, P. R., Volkerling, A., . . . Ittner, A. (2022). Alzheimer's disease: Ablating single master site abolishes tau hyperphosphorylation. *Sci Adv, 8*(27), eabl8809. doi:10.1126/sciadv.abl8809

Sugarman, M. A., Woodard, J. L., Nielson, K. A., Seidenberg, M., Smith, J. C., Durgerian, S., & Rao, S. M. (2012). Functional magnetic resonance imaging of semantic memory as a presymptomatic biomarker of Alzheimer's disease risk. *Biochim Biophys Acta, 1822*(3), 442-456. doi:10.1016/j.bbadis.2011.09.016

Taddei, R. N., Perbet, R., Mate de Gerando, A., Wiedmer, A. E., Sanchez-Mico, M., Connors Stewart, T., . . . Gomez-Isla, T. (2023). Tau Oligomer-Containing Synapse Elimination by Microglia and Astrocytes in Alzheimer Disease. *JAMA Neurol, 80*(11), 1209-1221. doi:10.1001/jamaneurol.2023.3530

Tiernan, C. T., Combs, B., Cox, K., Morfini, G., Brady, S. T., Counts, S. E., & Kanaan, N. M. (2016a). Pseudophosphorylation of tau at S422 enhances SDS-stable dimer formation and impairs both anterograde and retrograde fast axonal transport. *Exp Neurol, 283*(Pt A), 318-329. doi:10.1016/j.expneurol.2016.06.030

Tiernan, C. T., Ginsberg, S. D., Guillozet-Bongaarts, A. L., Ward, S. M., He, B., Kanaan, N. M., . . . Counts, S. E. (2016b). Protein homeostasis gene dysregulation in

pretangle-bearing nucleus basalis neurons during the progression of Alzheimer's disease. *Neurobiol Aging, 42*, 80-90. doi:10.1016/j.neurobiolaging.2016.02.031

Tiernan, C. T., Ginsberg, S. D., He, B., Ward, S. M., Guillozet-Bongaarts, A. L., Kanaan, N. M., . . . Counts, S. E. (2018a). Pretangle pathology within cholinergic nucleus basalis neurons coincides with neurotrophic and neurotransmitter receptor gene dysregulation during the progression of Alzheimer's disease. *Neurobiol Dis, 117*, 125-136. doi:10.1016/j.nbd.2018.05.021

Tiernan, C. T., Mufson, E. J., Kanaan, N. M., & Counts, S. E. (2018b). Tau Oligomer Pathology in Nucleus Basalis Neurons During the Progression of Alzheimer Disease. *J Neuropathol Exp Neurol, 77*(3), 246-259. doi:10.1093/jnen/nlx120

Vana, L., Kanaan, N. M., Ugwu, I. C., Wuu, J., Mufson, E. J., & Binder, L. I. (2011). Progression of tau pathology in cholinergic Basal forebrain neurons in mild cognitive impairment and Alzheimer's disease. *Am J Pathol, 179*(5), 2533-2550. doi:10.1016/j.ajpath.2011.07.044

Ward, S. M., Himmelstein, D. S., Lancia, J. K., Fu, Y., Patterson, K. R., & Binder, L. I. (2013). TOC1: characterization of a selective oligomeric tau antibody. *J Alzheimers Dis, 37*(3), 593-602. doi:10.3233/JAD-131235

Wu, X., Li, R., Fleisher, A. S., Reiman, E. M., Guan, X., Zhang, Y., . . . Yao, L. (2011). Altered default mode network connectivity in Alzheimer's disease--a resting functional MRI and Bayesian network study. *Hum Brain Mapp, 32*(11), 1868-1881. doi:10.1002/hbm.21153

Yoshida, H., Hastie, C. J., McLauchlan, H., Cohen, P., & Goedert, M. (2004). Phosphorylation of microtubule-associated protein tau by isoforms of c-Jun N-terminal kinase (JNK). *J Neurochem, 90*(2), 352-358. doi:10.1111/j.1471-4159.2004.02479.x

Youmans, K. L., Tai, L. M., Kanekiyo, T., Stine, W. B., Jr., Michon, S. C., Nwabuisi-Heath, E., . . . LaDu, M. J. (2012). Intraneuronal Abeta detection in 5xFAD mice by a new Abeta-specific antibody. *Mol Neurodegener, 7*, 8. doi:10.1186/1750-1326-7-8

Zhang, H., Wei, W., Zhao, M., Ma, L., Jiang, X., Pei, H., . . . Li, H. (2021). Interaction between Abeta and Tau in the Pathogenesis of Alzheimer's Disease. *Int J Biol Sci, 17*(9), 2181-2192. doi:10.7150/ijbs.57078

Zheng, J., Akbari, M., Schirmer, C., Reynaert, M. L., Loyens, A., Lefebvre, B., . . . Bohr, V. A. (2020). Hippocampal tau oligomerization early in tau pathology coincides with a transient alteration of mitochondrial homeostasis and DNA repair in a mouse model of tauopathy. *Acta Neuropathol Commun, 8*(1), 25. doi:10.1186/s40478-020-00896-8

Ziontz, J., Harrison, T. M., Fonseca, C., Giorgio, J., Han, F., Lee, J., . . . Alzheimer's Disease Neuroimaging, I. (2024). Connectivity, Pathology, and ApoE4 Interactions Predict Longitudinal Tau Spatial Progression and Memory. *Hum Brain Mapp, 45*(17), e70083. doi:10.1002/hbm.70083

n=51 (Fixed)	FC					
	pS422	TOC1	TNT2	TauC3	Moab2	
Age	0.955619	0.405783	0.088574	0.483902	0.450787	
Education	0.764769	0.386129	0.228674	0.652373	0.283839	
PMI	0.928517	0.279275	0.917175	0.054719	0.939538	
APOE4	0.831483	0.382653	0.918538	0.618332	0.120827	
	PCC					
	pS422	TOC1	TNT2	TauC3	Moab2	PHF-1
Age	0.123134	0.120477	0.476169	0.70105	0.124441	0.842183
Education	0.46049	0.673953	0.618838	0.709984	0.227631	0.728747
PMI	0.171827	0.516474	0.855802	0.034544	0.657741	0.713772
APOE4	0.687042	0.767758	0.43009	0.872078	0.120827	0.226034
	PreC					
	pS422	TOC1	TNT2	TauC3	Moab2	
Age	0.908519	0.14199	0.506023	0.643356	0.202283	
Education	0.976585	0.41677	0.240158	0.919871	0.676173	
PMI	0.795002	0.09386	0.045877	0.005446	0.397348	
APOE4	0.589818	0.396424	0.89421	0.955873	1	

n=98 (Frozen)	FC			
	TOC1	TNT2	TauC3	Tau5
Age	0.014383	0.994729	0.9118	0.774224
Education	0.571064	0.289705	0.216564	0.440481
PMI	0.120123	0.058075	0.169792	0.000672
APOE4	0.038004	0.698746	0.855112	0.07096
	PCC			
	TOC1	TNT2	TauC3	Tau5
Age	0.865105	0.788364	0.236629	0.644436
Education	0.150107	0.172019	0.076112	0.136712
PMI	0.101374	0.172701	0.128705	0.004093
APOE4	0.102584	0.031417	0.144345	0.078209
	PreC			
	TOC1	TNT2	TauC3	Tau5
Age	0.794712	0.022953	0.188164	0.774224
Education	0.73938	0.364305	0.104025	0.440481
PMI	0.500547	0.475541	0.171512	0.000672
APOE4	0.10141	0.01462	0.052229	0.07096

Supplementary Table 2. 1 Pre-tangle tau pathology and demographics correlation p-values

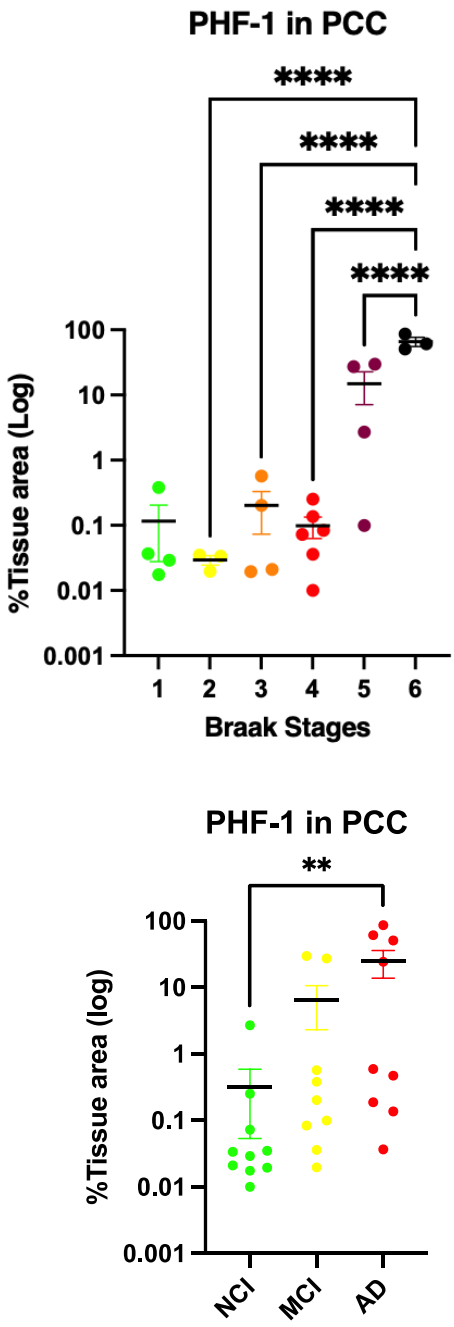

Supplementary Figure 2. 1 PHF-1 quantification in the PCC based on the Braak stage and clinical groups

For Braak stage-based group comparisons, One-Way ANOVA with Tukey test and for clinical group-based caparisons, Kruskal-Wallis with Dunn's multiple comparisons were applied for pairwise analysis.

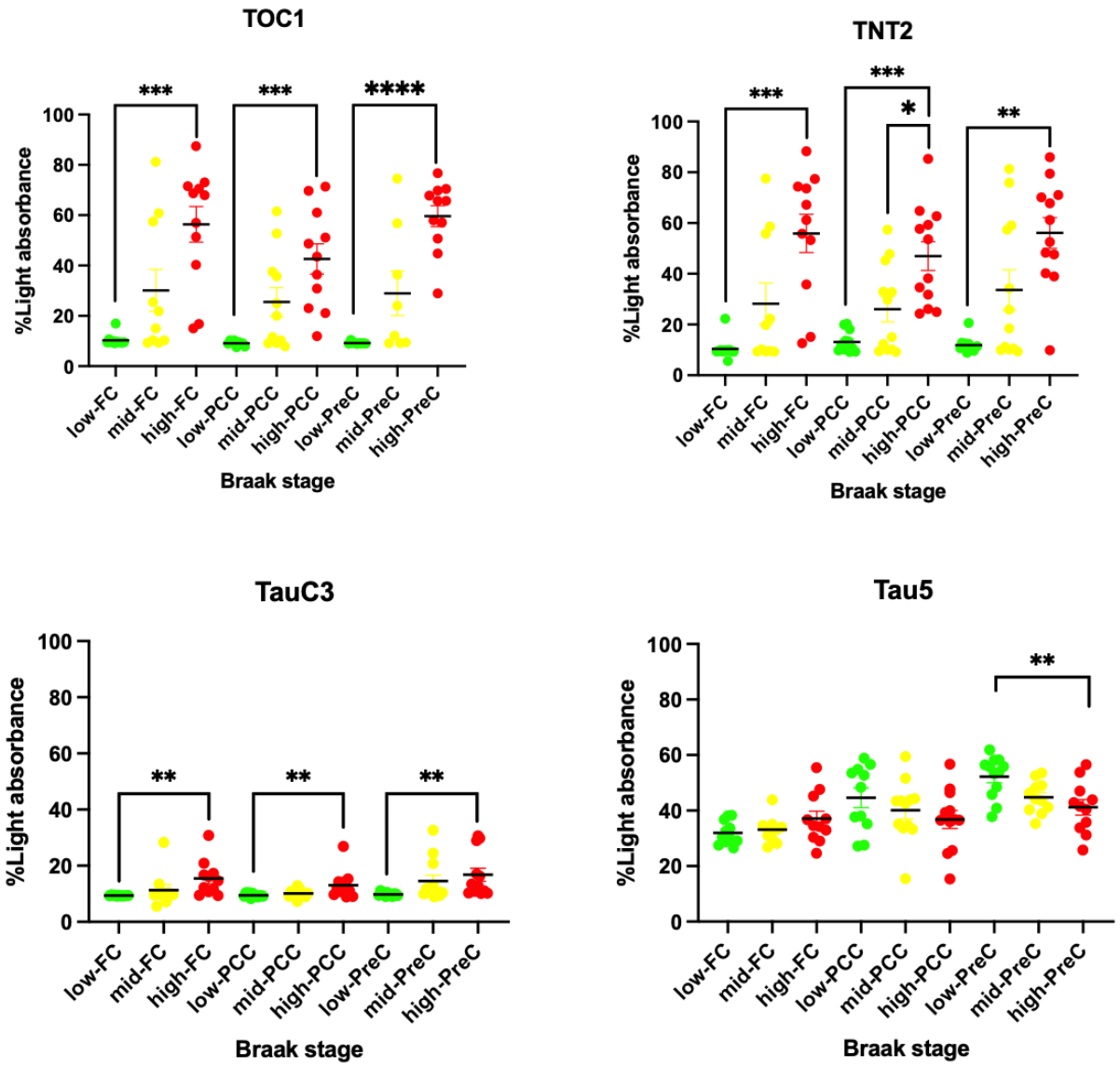

Supplementary Figure 2. 2 Soluble Pathological Tau Quantification in the MADC cases Quantification of selected pre-tangle markers was performed using sandwich ELISA on the soluble fraction of frozen MADC samples. The results were grouped according to Braak stage groupings of the cohort. Statistical analyses were conducted using the Kruskal-Wallis test, followed by Dunn's multiple comparisons for pairwise analysis.

CHAPTER 3: DMN PRE-TANGLE PATHOLOGY IN RELATION TO THE ANTEMORTEM COGNITIVE TEST SCORES AND POSTMORTEM PATHOLOGY ASSESSMENTS

INTRODUCTION

Cognitive Domains Impacted in Alzheimer's Disease

The clinical representation of Alzheimer's disease (AD) is often presented as severe memory decline. However, multiple different subdomains of memory function are affected during disease progression. Centuries-long psychological research, fortunately, offers a deeper understanding of memory classification and which subdomains are affected the most in AD patients. With the aid of functional neuroanatomical studies and the advent of advanced imaging techniques (Cassel, 2013), current memory classification has evolved since the 19th century into three broad domains, as shown below (Cowan, 2008).

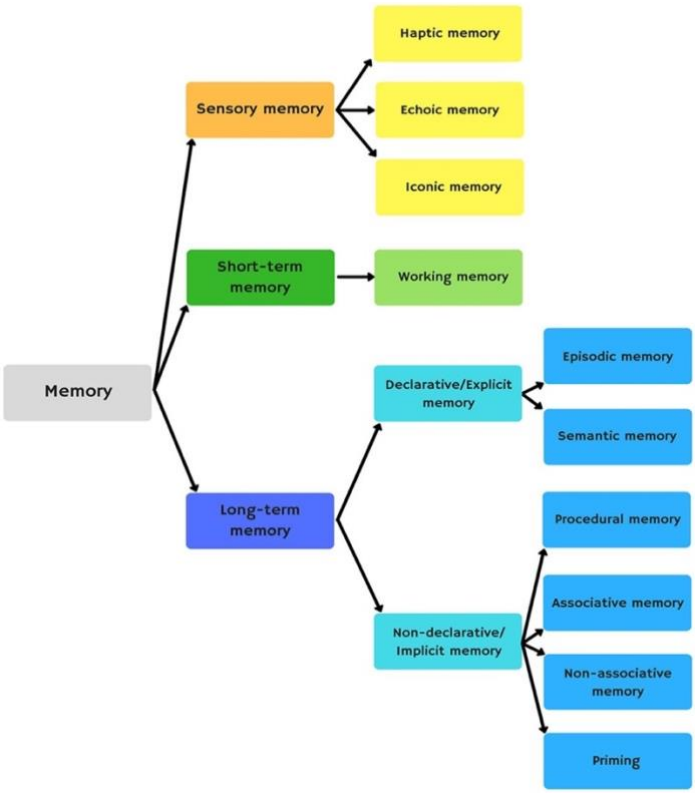

Figure 3. 1 A modern model of memory classification (Camina et al., 2017) based on the duration, capacity, and source of information

As a part of explicit long-term memory, episodic memory is the ability to remember past events in detail regarding time, place, and people, and is often the earliest to decline as a clinical hallmark of AD patients (Ahn, 2021). The entorhinal cortex, hippocampus, and the other regions in the medial temporal lobe, highly overlapping with the tau pathology trajectory in the brain, are shown to be involved in episodic memory coding, storage, and retrieval (Moscovitch, 2016). Other studies also found additional regions that are involved in episodic memory retrieval. Krause et al. observed an increased cerebral blood flow in the precuneus (PreC) during episodic memory retrieval, concluding that PreC as a multimodal association area has a specific role in episodic memory retrieval (Krause, 1999). In parallel, a more recent study found PreC activation in remembering the contextually rich memory (Foudil, 2024). As mentioned in the introductory chapter, transcranial magnetic stimulation therapies in the PreC may help slow down the cognitive decline in AD (Moussavi, 2022).

Another key region of episodic memory consolidation is the posterior cingulate cortex (PCC) (Bird, 2015). PCC synchronizes with the hippocampus during episodic memory formation by integrating contextualized information and modulating internally mediated attention (Lega, 2017). There are, however, some contradictory studies that found a strong deactivation of PCC during episodic memory retrieval (Daselaar, 2009; Natu, 2019), making it more complicated to interpret the activation/deactivation pattern in PCC. Regardless, these data indicate that the DMN PreC and PCC are actively involved in episodic memory consolidation and retrieval.

In the context of AD, episodic memory has been considered a clinical marker due to its decline in SCD and MCI patients (Backman, 2001; Tromp, 2015). A study that

evaluated the visual and verbal aspects of episodic memory found that the test performance was discernable between the early amnestic MCI (aMCI), late aMCI, and mild AD groups (Chatzikostopoulos, 2022). A longitudinal population-based study compared episodic memory performance 3 years and 6 years prior to AD converters versus non-converters and found that episodic memory was present in both 3- and 6-year assessments in the converters without an accelerated decline by the time of the diagnosis, suggesting that episodic memory starts to decline long before the clinical diagnosis (Backman, 2001). This once again underlines the temporal gap between pathology accumulation and diagnosable cognitive deterioration.

To understand this temporal gap, PET imaging studies might be useful to monitor the type of pathology and their spatiotemporal distribution in the brain. In a recent study, Bucci et al. collected tau- and Aβ-PET images and CSF pTau markers from an Alzheimer's Disease Neuroimaging Initiative (ADNI) cohort to find tau PET retention in the entorhinal cortex, amygdala, well as inferior and middle temporal cortices were better predictors of episodic memory performance of the AD group compared to the PET Aβ or CSF pTau results (Bucci, 2021). In another elegant ADNI study, researchers first determined the cognitive-domain-specific brain activation with fMRI, including episodic memory, and used those regions as the region of interest to measure tau-PET signal to test whether cognitive-domain-specific tau-PET would better predict the cognitive function compared to the conventional tau-PET (i.e., global/temporal-lobe tau-PET). The results favored the cognitive-domain-specific tau-PET and also improved patient-centered prediction of AD in Aβ positive participants (Biel, 2022).

Despite the diagnostic potential of episodic memory, there is one caveat in referring to episodic memory as a hallmark of AD. Although it is moderate, episodic memory declines with normal aging, which makes it harder to dissociate the initial decline in pre-clinical cases from normal agers (Scholl, 2016; Nyberg, 2017). Semantic memory, on the other hand, as another explicit long-term memory type, not only does not decline with age but accumulates over time as the person gets older (Kave, 2009; Haitas, 2021). It is also important to consider that episodic memory tests are often harder, and patients either with a predisposition to AD or prodromal AD may make an extra effort to conduct the test, which may translate into a greater blood-oxygen-level-dependent (BOLD) signal in fMRI studies that may skew the results. Therefore, a greater BOLD signal might be associated with a greater risk of the disease. Contrarily, because the semantic memory tests are easier in general, they may provide a sensitive measure to aid in the diagnosis of AD (Hantke, 2013).

Semantic memory refers to general knowledge about facts, concepts, objects, abstract words, and numbers (Noroozian, 2016). It is not stored in a single region in the brain, but rather, the storage is spread across the limbic and neocortex including the medial temporal areas and posterior parietal cortex (Noroozian, 2016; Krieger-Redwood, 2016). Most DMN regions, especially posterior hubs (i.e., PCC and PreC), have been shown to be involved in semantic memory function (Krieger-Redwood, 2016; Vatansever, 2021; Binder, 2011).

Decline in semantic memory may be present long before the AD diagnosis (Hodges, 1995; Tchakoute, 2017; Rogers, 2008). A large longitudinal study with 3,777 initial subjects demonstrated that semantic memory deficits may predict the conversion

to AD, and they may be present 12 years prior to the diagnosis, highlighting the prolonged preclinical stage of the disease (Amieva, 2008). Parallel results were shown in an earlier study that found semantic memory decline accompanied episodic memory failure in mild/moderate AD groups (Hodges, 1995). Additionally, semantic memory score was shown to be correlated with global cognitive scores in a women's cohort with mild/moderate AD (Tchakoute, 2017). One final note is that there are contradicting studies emerging on the distinct functions of episodic versus semantic memory. Due to sharing the same anatomical brain regions (i.e., medial temporal areas) as well as contextualized information, these two memory functions may often crosstalk, and hence their function might be intertwined (Lalla, 2022; Renoult, 2019), which is worth considering while interpreting the episodic and semantic battery scores.

Another memory type that shows impairment in AD is working memory. In contrast to the previous two, working memory is short-term memory and is described as the ability to hold a small amount of information for a short time during a task (Eriksson, 2015), such as dialing a newly-learned phone number. The prefrontal cortex (PFC) and parietal cortex are strongly involved in working memory. Noninvasive therapies such as repetitive transcranial magnetic stimulation (rTMS) on the dorsal prefrontal cortex (DPFC) were shown to improve working memory (Brunoni, 2014). The basal ganglia, specifically the striatum, is also involved in working memory. Due to the reduced dopamine levels in the striatum in Parkinson’s patients, PFC dysfunction and related working memory impairment have been reported (McNab, 2008; Ekman, 2012). Similarly, in AD patients, working memory impairment is a common feature, possibly due to frontal lobe degeneration (Kirova, 2015) or possibly involvement of posterior

hemispheres as well (Stopford, 2012). Working memory is suggested to be used as a predictor of the MCI to AD transition (Saunders, 2011; Brandt, 2009; Carretti, 2013). It is important to acknowledge that working memory may vary from person to person greatly because it is a complex function and requires multiple cognitive domains to be engaged, such as visual reasoning, language comprehension, and problem-solving (Kirova, 2015).

Although memory impairments are the most focused, and possibly the most detrimental aspects of cognitive changes, other cognitive domains are impacted in AD patients, such as visuospatial abilities and perceptual speed, which can be assessed by specific neuropsychological tests (Bennett, 2002). Both domains decline early in AD and several clinical studies show that they may improve AD diagnostic accuracy (Borkowski, 2021; Salimi, 2019; Salimi, 2018).

Temporal Discordance Between Pathology Accumulation and Clinical Presentation

The brain is an extremely fragile yet fascinating organ with extremely high adaptability and compensation ability, referred to as plasticity (Burke, 2006; Walker, 2006). In case of an insult, which might be chemical (environmental toxins), biological (viruses, pathogens), or physical (concussion, leakage of blood-brain barrier), the brain heals in part by reorganizing into compensatory functional pathways. In the case of the amyloid and NFT proteinopathy insults that define AD, it has been thought that once plaques and NFTs reach a threshold of abundance, these compensatory mechanisms succumb to the cumulative neuronal damage associated with these pathologies, thus resulting in initial changes in cognitive function. In this regard, the discovery of plaques and tangles in the brain with the development of PET tracers demonstrated that

pathology accumulation might last decades before clinical symptoms (Bateman, 2012). With the emergence of more research on the soluble oligomeric forms of plaques and tangles, showing that oligomers are associated with severe cellular toxicity and high potential in pathology propagation, AD pathogenic processes likely occur even earlier than that suggested by PET imaging (and fluid biomarker studies), insidiously disrupting cellular homeostasis, causing axonal degradation, and interfering the energy metabolism. Unfortunately, we cannot track or detect these toxic species in patients due to the lack of a PET ligand that can differentially bind the early pathological forms of amyloid and tau. For example, while NFTs correlate with cognitive decline, understanding how pre-tangle tau relates to cognitive changes is a potentially very promising yet underexplored area, and we posit that the DMN is an ideal brain network in which to explore these phenomena.

There are several reasons why the DMN is a suitable substrate to study pathology & cognitive dynamics in the context of AD, including: 1) Functional connectivity (fc) of DMN hubs bidirectionally changes depending on the disease stage and those changes may start as early as the SCD pre-clinical phase, and 2) pathological Aβ and tau trajectories in the brain do not fully overlap until later stages of the disease. However, they both spread to the DMN regions and coexist in the majority of aMCI patients (Li, 2019; Hojjati, 2021). These concepts were supported by our studies described in Chapter 2, which showed a significant increase in pre-tangle tau markers, pS422 and TNT2, by Braak stage V in fixed DMN samples and TOC1 and TNT2 in frozen DMN samples, which further increased in Braak VI. Therefore, for the present study, we aimed to investigate the relationship between the expression levels of

these soluble pre-tangle tau forms, as well as oligomeric amyloid, in the DMN with measures of antemortem cognitive function taken within a year of death in the subjects comprising our clinical neuropathologic cohort. To complement this analysis, we also tested for correlations between these markers and postmortem neuropathological diagnostic variables. We hope to contribute to the effort to understand the dynamics of the aforementioned temporal gap between pathology and cognition and how to leverage it by developing preventive therapies in the future.

MATERIALS AND METHODS

Subjects and clinical pathologic assessments

Subjects, clinical pathological assessments, and tau marker quantitative methodologies are described in detail in Chapter 2. With respect to antemortem cognitive assessments, RROS participants undergo an annual neurological examination and cognitive performance testing using the Mini-Mental State Exam (MMSE) and 19 additional neuropsychological tests referable to five cognitive domains: orientation, attention, memory, language, and perception (see Chapter 2) (Bennett, 2002). Specifically, these tests were referable to episodic memory (e.g., Word List Memory, Recall and Recognition), semantic memory (e.g., Verbal Fluency and Boston Naming), working memory (e.g., Digit Span Forward and Backward), perceptual speed (e.g., Symbol Digit Modalities Test), and visuospatial ability (e.g., Standard Progressive Matrices) (Counts, 2006) (Supplemental Table 3.1). Composite scores of episodic memory, semantic memory, working memory, perceptual speed, and visuospatial ability, as well as a composite global cognitive z-score (GCS), were derived from this test battery for each subject; NCI subjects did not reveal impairment in any of these domains within a year of

death, when adjusted for age and education, whereas MCI subjects scored ≥ 2 standard deviations worse on one or more domains when compared to NCI (Bennett, 2002; Bennett, 2018). MADC donors only received an MMSE score, which was utilized to calculate correlations between pathology and global cognition in this study. Neuropathological assessments in addition to CERAD, Braak, and NIA-Reagan staging described in Chapter 2 included: 1) diffuse and neuritic plaque and NFTs counts using silver-stained sections from midfrontal cortex, midtemporal cortex, inferior parietal cortex, entorhinal cortex, and hippocampus, where the count of each region is scaled by dividing by the corresponding standard deviation and then averaged across the 5 regions to obtain a summary measure; and 2) amyloid and NFT density, which is the mean of the square root transformation diffuse + neuritic plaque counts and NFT counts in angular gyrus, anterior cingulate cortex, calcarine cortex, entorhinal cortex, hippocampus, inferior temporal cortex, midfrontal gyrus, and superior frontal cortex (Bennett, 2018).

Statistical Analyses

Statistical analysis of demographic, clinical, and pathological variables including tau and amyloid measurements in the DMN hubs are described in detail in Chapter 2. Spearman rank correlations were used to test for associations between tau and amyloid marker levels, antemortem cognitive test scores, and postmortem neuropathological variables due to the nonnormal distribution of the pre-tangle tau markers in both fixed and frozen tissue samples (GraphPad Prism v10.4.0) (527). The statistical software also generated correlation matrices for data visualization. The Cocor analysis, an R

package, was used to compare correlation coefficients (2192). Significance levels were indicated as follows: *p < 0.05, **p < 0.01, ***p < 0.001, and ****p < 0.0001.

RESULTS

Correlations between DMN pre-tangle tau markers and antemortem cognitive test scores

With respect to pre-tangle tau pathological epitopes measured by quantitative immunohistochemistry, increasing pS422 and TNT2 levels in each DMN cortical hub correlated the most strongly with poorer performance on episodic and semantic memory, as well as perceptual speed and visuospatial ability (Figure 3.2, Table 3.1). Levels of these two pre-tangle markers also displayed the strongest inverse correlations with global cognitive performance, as measured by the MMSE and GCS, in all regions examined. By contrast, increasing TOC1+ oligomer levels were significantly but more weakly associated with poorer episodic and semantic memory scores and global cognitive scores across the regions and associated with perceptual speed and visuospatial ability only in the FC. Levels of TauC3, representing more advanced stages of tangle evolution, were significantly correlated with these cognitive measures, most strongly in the FC. By contrast, none of the tau markers were correlated with antemortem working memory performance. Finally, MOAB2+ amyloid pathology correlated tightly with pS422, TOC1, and TNT2 in all regions and also correlated with semantic and episodic memory, as well as the global cognitive score in the PCC (Figure 3.2).

PHF-1 quantification in the PCC was included as a canonical NFT marker to provide a refence point for possible NFT load. Although it was correlated with all the

markers, its strongest correlation was with pS422 (r=0.96, p<0.0001), followed by TNT2 (r=0.90, p<0.0001). Sharing the pattern with pS422, it tightly correlated with all the cognitive measures except for working memory.

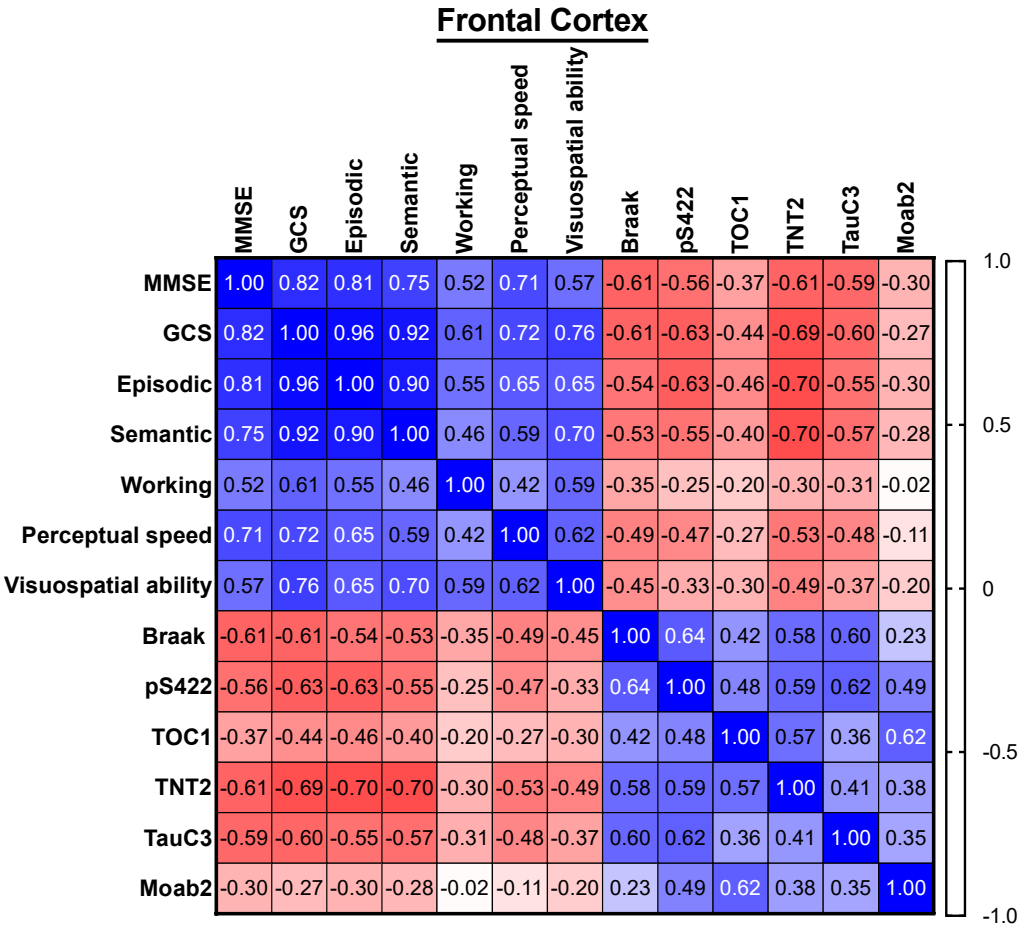

Figure 3. 2 Correlation matrices for IHC-measured pre-tangle DMN tau levels and cognitive scores in the RROS cohort

Figure 3. 2 (cont'd)

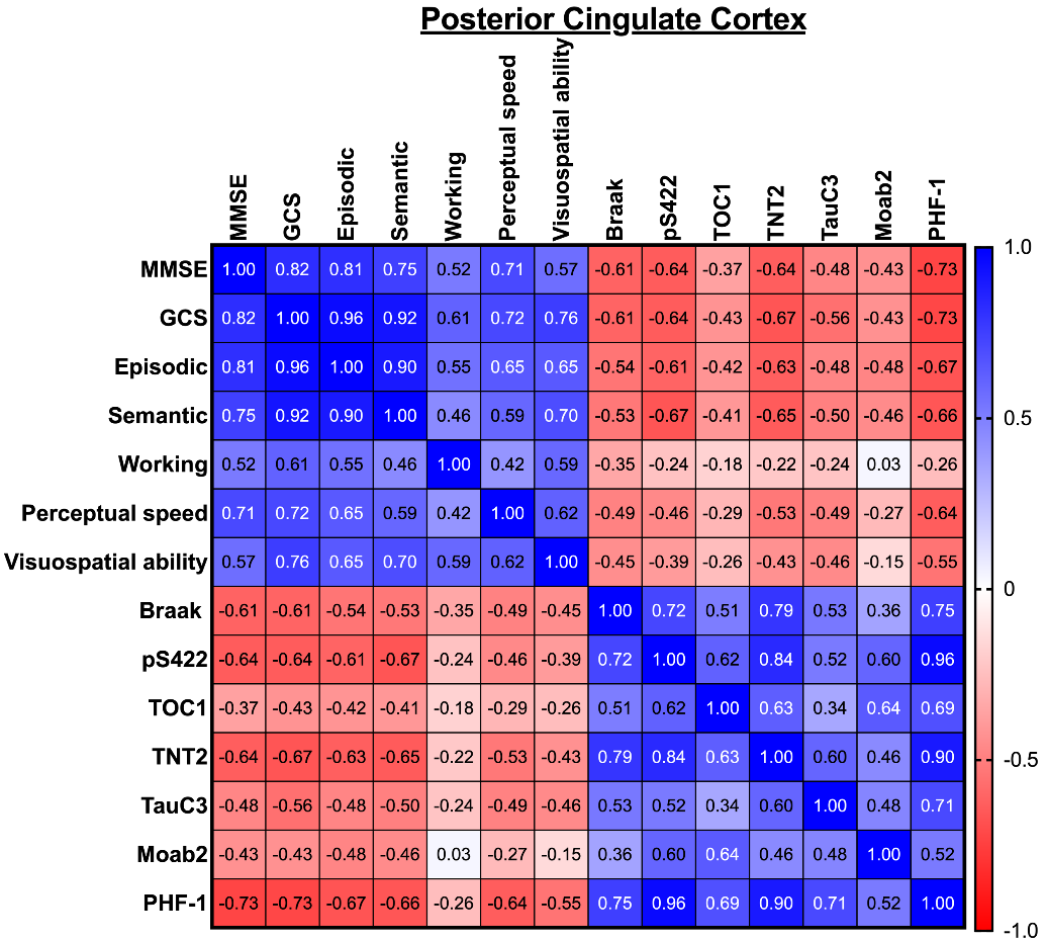

Figure 3. 2 (cont'd)

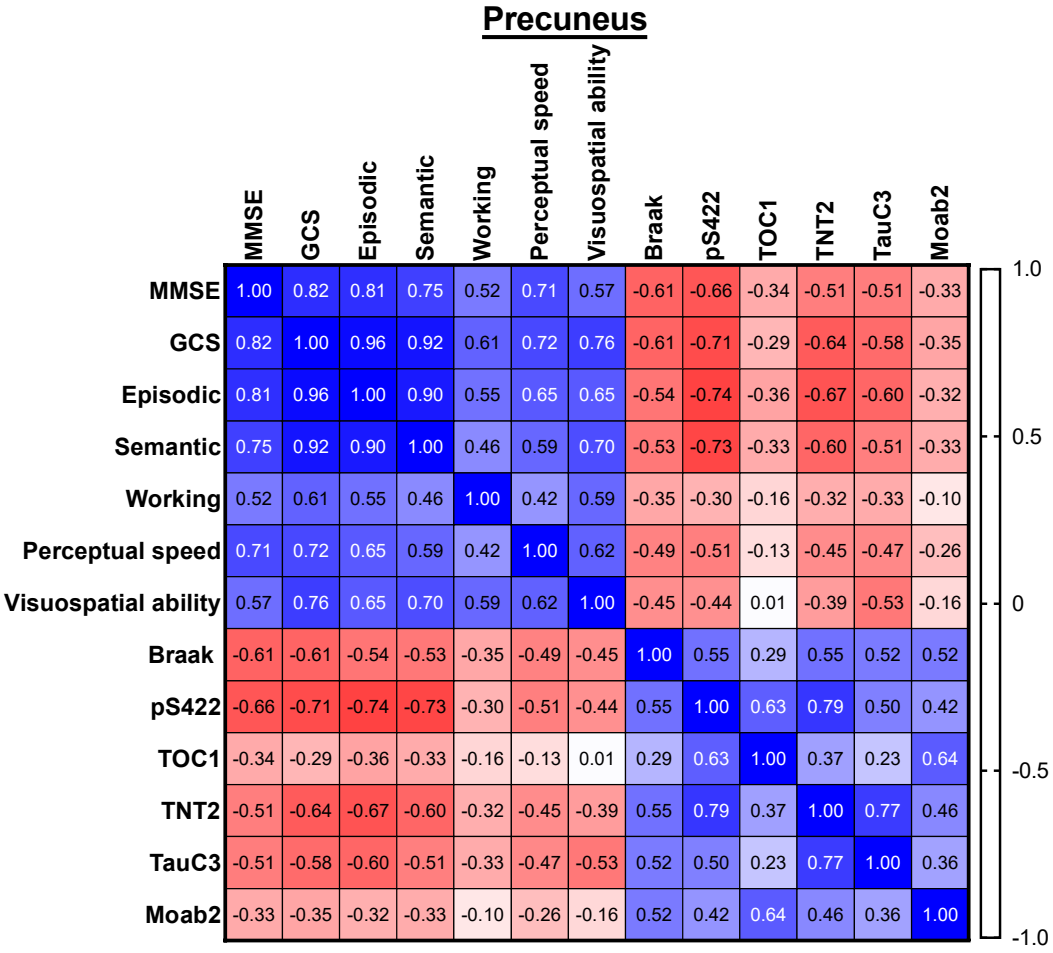

Spearman coefficients between the pre-tangle tau levels and cognitive variables in the fontal cortex, posterior cingulate cortex, and precuneus are shown. Heat map reflects the strength of correlation.

FC														
	MMSE	**GCS**	**Episodic**	**Semanti**	**Working**	**Percept**	**Visuosp**	**Braak**	**pS422**	**TOC1**	**TNT2**	**TauC3**	**Moab2**	
MMSE		1E-13	4E-13	3E-10	9E-05	5E-09	1E-05	2E-06	3E-05	0.0096	4E-06	1E-05	0.1101	
GCS	**1E-13**		2E-28	1E-21	2E-06	3E-09	9E-11	2E-06	1E-06	0.0016	5E-08	8E-06	0.1493	
Episodic	**4E-13**	**2E-28**		3E-19	2E-05	3E-07	3E-07	4E-05	1E-06	0.001	3E-08	5E-05	0.1082	
Semantic	**3E-10**	**1E-21**	**3E-19**		0.0007	4E-06	1E-08	6E-05	5E-05	0.005	3E-08	3E-05	0.1297	
Working	**9E-05**	**2E-06**	**2E-05**	**0.0007**		0.0024	5E-06	0.0123	0.088	0.1632	0.0358	0.0312	0.934	
Perceptual speed	**5E-09**	**3E-09**	**3E-07**	**4E-06**	**0.0024**		1E-06	0.0002	0.0008	0.0662	1E-04	0.0007	0.5497	
Visuospatial ability	**1E-05**	**9E-11**	**3E-07**	**1E-08**	**5E-06**	**1E-06**		0.001	0.0233	0.0382	0.0004	0.011	0.2974	
Braak	**2E-06**	**2E-06**	**4E-05**	**6E-05**	**0.0123**	**0.0002**	**0.001**		8E-07	0.0031	2E-05	1E-05	0.2195	
pS422	**3E-05**	**1E-06**	**1E-06**	**5E-05**	0.088	**0.0008**	**0.0233**	**8E-07**		0.0006	1E-05	4E-06	0.0063	
TOC1	**0.0096**	**0.0016**	**0.001**	**0.005**	0.1632	0.0662	**0.0382**	**0.0031**	**0.0006**		3E-05	0.0121	0.0002	
TNT2	**4E-06**	**5E-08**	**3E-08**	**3E-08**	**0.0358**	**1E-04**	**0.0004**	**2E-05**	**1E-05**	**3E-05**		0.0043	0.039	
TauC3	**1E-05**	**8E-06**	**5E-05**	**3E-05**	**0.0312**	**0.0007**	**0.011**	**1E-05**	**4E-06**	**0.0121**	**0.0043**		0.0621	
Moab2	0.1101	0.1493	0.1082	0.1297	0.934	0.5497	0.2974	0.2195	**0.0063**	**0.0002**	**0.039**	0.0621		

PCC														
	MMSE	**GCS**	**Episodic**	**Semanti**	**Working**	**Percept**	**Visuosp**	**Reagan**	**pS422**	**TOC1**	**TNT2**	**TauC3**	**Moab2**	**PHF-1**
MMSE		1E-13	4E-13	3E-10	9E-05	5E-09	1E-05	4E-06	1E-06	0.0113	3E-06	0.0008	0.0163	9E-06
GCS	**1E-13**		2E-28	1E-21	2E-06	3E-09	9E-11	2E-07	2E-06	0.0031	5E-07	5E-05	0.0166	1E-05
Episodic	**4E-13**	**2E-28**		3E-19	2E-05	3E-07	3E-07	4E-06	7E-06	0.0035	3E-06	0.0007	0.0073	9E-05
Semantic	**3E-10**	**1E-21**	**3E-19**		0.0007	4E-06	1E-08	2E-06	4E-07	0.0047	2E-06	0.0004	0.0112	0.0001
Working	**9E-05**	**2E-06**	**2E-05**	**0.0007**		0.0024	5E-06	0.0314	0.1065	0.2365	0.1499	0.1158	0.8638	0.1772
Perceptual speed	**5E-09**	**3E-09**	**3E-07**	**4E-06**	**0.0024**		1E-06	0.0001	0.0012	0.0516	0.0002	0.0005	0.1424	0.0003
Visuospatial ability	**1E-05**	**9E-11**	**3E-07**	**1E-08**	**5E-06**	**1E-06**		0.001	0.0067	0.0801	0.0031	0.0013	0.4393	0.0027
Reagan	**4E-06**	**2E-07**	**4E-06**	**2E-06**	**0.0314**	**0.0001**	**0.001**		2E-13	0.0002	6E-13	5E-05	0.0073	7E-09
pS422	**1E-06**	**2E-06**	**7E-06**	**4E-07**	0.1065	**0.0012**	**0.0067**	**2E-13**		5E-06	7E-13	0.0002	0.0004	3E-16
TOC1	**0.0113**	**0.0031**	**0.0035**	**0.0047**	0.2365	0.0516	0.0801	**0.0002**	**5E-06**		4E-06	0.0198	0.0001	6E-05
TNT2	**3E-06**	**5E-07**	**3E-06**	**2E-06**	0.1499	**0.0002**	**0.0031**	**6E-13**	**7E-13**	**4E-06**		1E-05	0.0111	7E-11
TauC3	**0.0008**	**5E-05**	**0.0007**	**0.0004**	0.1158	**0.0005**	**0.0013**	**5E-05**	**0.0002**	**0.0198**	**1E-05**		0.0075	2E-05
Moab2	**0.0163**	**0.0166**	**0.0073**	**0.0112**	0.8638	0.1424	0.4393	**0.0073**	**0.0004**	**0.0001**	**0.0111**	**0.0075**		0.0047
PHF-1	**9E-06**	**1E-05**	**9E-05**	**0.0001**	0.1772	**0.0003**	**0.0027**	**7E-09**	**3E-16**	**6E-05**	**7E-11**	**2E-05**	**0.0047**	

PreC													
	MMSE	**GCS**	**Episodic**	**Semanti**	**Working**	**Percept**	**Visuosp**	**Braak**	**pS422**	**TOC1**	**TNT2**	**TauC3**	**Moab2**	
MMSE		1E-13	4E-13	3E-10	9E-05	5E-09	1E-05	2E-06	3E-06	0.0183	0.0002	0.0009	0.0821	
GCS	**1E-13**		2E-28	1E-21	2E-06	3E-09	9E-11	2E-06	4E-07	0.0432	8E-07	1E-04	0.064	
Episodic	**4E-13**	**2E-28**		3E-19	2E-05	3E-07	3E-07	4E-05	4E-08	0.0106	1E-07	5E-05	0.1022	
Semantic	**3E-10**	**1E-21**	**3E-19**		0.0007	4E-06	1E-08	6E-05	1E-07	0.0207	6E-06	0.001	0.089	
Working	**9E-05**	**2E-06**	**2E-05**	**0.0007**		0.0024	5E-06	0.0123	0.0587	0.2593	0.0267	0.0387	0.6228	
Perceptual speed	**5E-09**	**3E-09**	**3E-07**	**4E-06**	**0.0024**		1E-06	0.0002	0.0009	0.3561	0.0012	0.0027	0.1873	
Visuospatial ability	**1E-05**	**9E-11**	**3E-07**	**1E-08**	**5E-06**	**1E-06**		0.001	0.0048	0.9573	0.0059	0.0005	0.4286	
Braak	**2E-06**	**2E-06**	**4E-05**	**6E-05**	**0.0123**	**0.0002**	**0.001**		0.0002	0.0442	4E-05	0.0008	0.0047	
pS422	**3E-06**	**4E-07**	**4E-08**	**1E-07**	0.0587	**0.0009**	**0.0048**	**0.0002**		1E-05	2E-09	0.002	0.0266	
TOC1	**0.0183**	**0.0432**	**0.0106**	**0.0207**	0.2593	0.3561	0.9573	**0.0442**	**1E-05**		0.0097	0.1661	0.0002	
TNT2	**0.0002**	**8E-07**	**1E-07**	**6E-06**	**0.0267**	**0.0012**	**0.0059**	**4E-05**	**2E-09**	**0.0097**		1E-08	0.0127	
TauC3	**0.0009**	**1E-04**	**5E-05**	**0.001**	**0.0387**	**0.0027**	**0.0005**	**0.0008**	**0.002**	0.1661	**1E-08**		0.0616	
Moab2	0.0821	0.064	0.1022	0.089	0.6228	0.1873	0.4286	**0.0047**	**0.0266**	**0.0002**	**0.0127**	0.0616		

Table 3. 1 p-values for Spearman rank correlations with cognitive variables in the fixed tissue samples

Significant p-values are bolded.

The correlations between pre-tangle tau in the soluble fraction of frozen DMN tissue blocks and cognitive measures were similar to those observed with immunohistochemistry (IHC), though not as strong. TOC1 was the most significantly

correlated patholarker with semantic memory scores across all regions, with the strongest associations seen in the posterior DMN hubs (Figure 3.3, Table 3.2). Showing its strongest correlations in the PCC, TNT2 also tightly correlated with the cognitive scores, especially with the MMSE and semantic memory. Notably, neither pre-tangle marker (TOC1 nor TNT2) showed any correlation with antemortem working memory performance. These findings are particularly insightful because they focus on soluble, tau species by utilizing ultracentrifugation during tissue fractionation. Total tau measured by Tau5 did not reveal any correlations, suggesting that total tau itself is probably not the primary driver of pathology or cognitive decline.

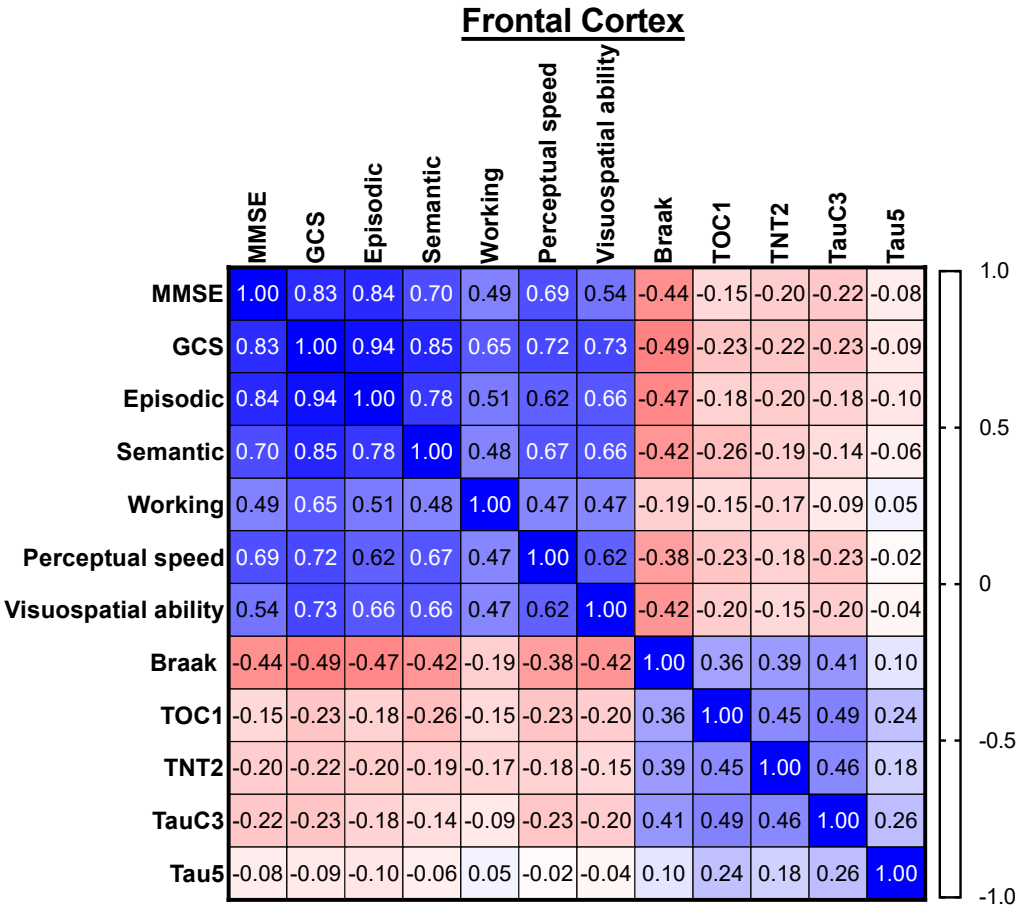

Figure 3. 3 Correlation matrices for the ELISA-measured soluble pre-tangle DMN tau levels and cognitive scores in the RROS cohort

Figure 3. 3 (cont'd)

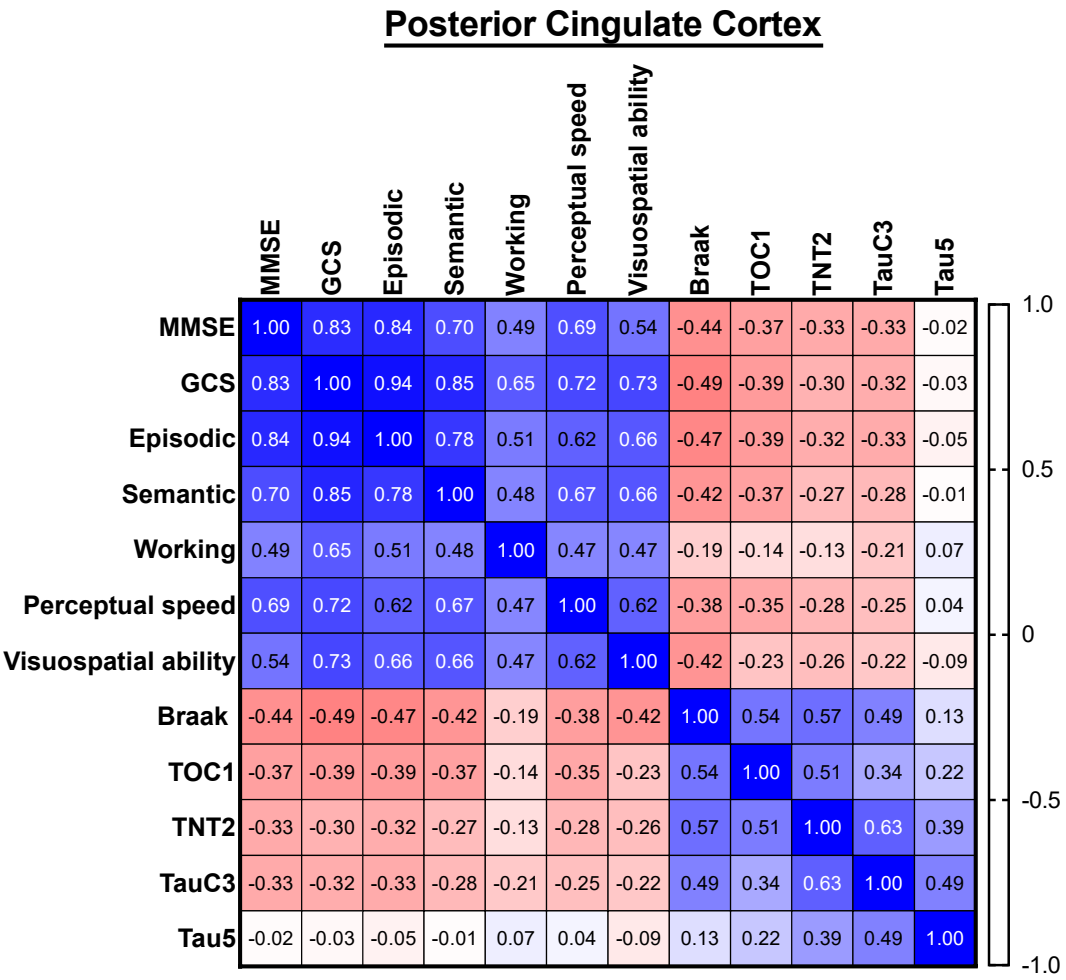

Figure 3. 3 (cont'd)

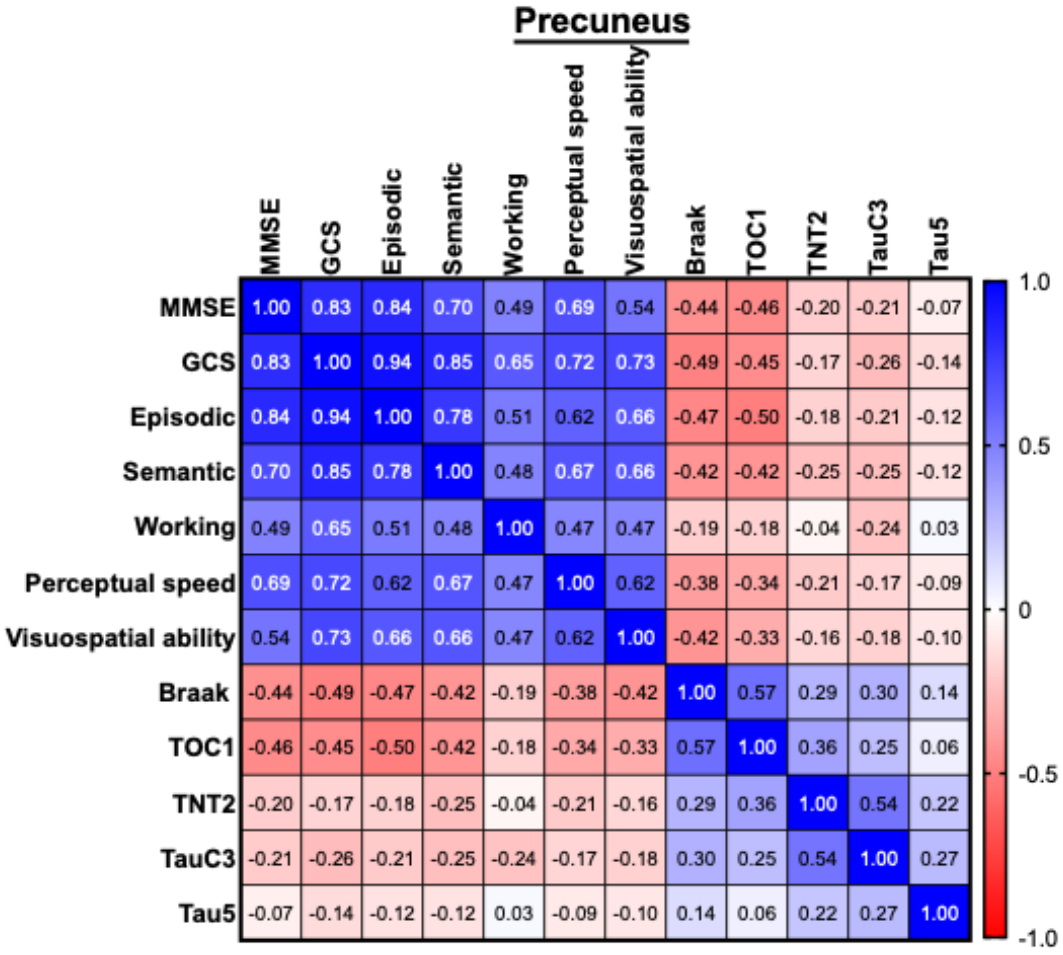

Spearman coefficients between the pre-tangle tau levels and cognitive variables in the fontal cortex, posterior cingulate cortex, and precuneus are shown. Heat map reflects the strength of correlation.

FC												
	MMSE	**GCS**	**Episodic**	**Semantic**	**Working**	**Perceptu**	**Visuospa**	**Braak**	**TOC1**	**TNT2**	**TauC3**	**Tau5**
MMSE		3E-25	3E-27	2E-15	4E-07	8E-15	9E-09	8E-06	0.1338	0.0527	0.0301	0.4612
GCS	**3E-25**		3E-46	1E-28	4E-13	1E-16	3E-17	2E-07	0.0223	0.031	0.0219	0.3918
Episodic	**3E-27**	**3E-46**		2E-21	6E-08	1E-11	2E-13	9E-07	0.0779	0.0466	0.0838	0.3168
Semantic	**2E-15**	**1E-28**	**2E-21**		5E-07	7E-14	1E-13	2E-05	0.0092	0.0599	0.1835	0.5377
Working	**4E-07**	**4E-13**	**6E-08**	**5E-07**		9E-07	8E-07	0.0616	0.1464	0.1038	0.3873	0.6462
Perceptual speed	**8E-15**	**1E-16**	**1E-11**	**7E-14**	**9E-07**		1E-11	1E-04	0.0225	0.082	0.0244	0.8455
Visuospatial ability	**9E-09**	**3E-17**	**2E-13**	**1E-13**	**8E-07**	**1E-11**		2E-05	0.0508	0.1359	0.0514	0.6941
Braak	**8E-06**	**2E-07**	**9E-07**	**2E-05**	0.0616	**1E-04**	**2E-05**		0.0003	7E-05	3E-05	0.327
TOC1	0.1338	**0.0223**	0.0779	**0.0092**	0.1464	**0.0225**	0.0508	**0.0003**		3E-06	3E-07	0.0163
TNT2	0.0527	**0.031**	**0.0466**	0.0599	0.1038	0.082	0.1359	**7E-05**	**3E-06**		2E-06	0.0776
TauC3	**0.0301**	**0.0219**	0.0838	0.1835	0.3873	**0.0244**	0.0514	**3E-05**	**3E-07**	**2E-06**		0.0111
Tau5	0.4612	0.3918	0.3168	0.5377	0.6462	0.8455	0.6941	0.327	**0.0163**	0.0776	**0.0111**	
PCC												
	MMSE	**GCS**	**Episodic**	**Semantic**	**Working**	**Perceptu**	**Visuospa**	**Braak**	**TOC1**	**TNT2**	**TauC3**	**Tau5**
MMSE		3E-25	3E-27	2E-15	4E-07	8E-15	9E-09	8E-06	0.0002	0.0008	0.0008	0.87
GCS	**3E-25**		3E-46	1E-28	4E-13	1E-16	3E-17	2E-07	6E-05	0.0024	0.0011	0.7819
Episodic	**3E-27**	**3E-46**		2E-21	6E-08	1E-11	2E-13	9E-07	6E-05	0.0012	0.0009	0.5979
Semantic	**2E-15**	**1E-28**	**2E-21**		5E-07	7E-14	1E-13	2E-05	0.0002	0.0083	0.006	0.8959
Working	**4E-07**	**4E-13**	**6E-08**	**5E-07**		9E-07	8E-07	0.0616	0.1715	0.1986	0.0357	0.5212
Perceptual speed	**8E-15**	**1E-16**	**1E-11**	**7E-14**	**9E-07**		1E-11	1E-04	0.0005	0.0046	0.012	0.6917
Visuospatial ability	**9E-09**	**3E-17**	**2E-13**	**1E-13**	**8E-07**	**1E-11**		2E-05	0.0212	0.0105	0.0306	0.3802
Braak	**8E-06**	**2E-07**	**9E-07**	**2E-05**	0.0616	**1E-04**	**2E-05**		1E-08	1E-09	2E-07	0.2162
TOC1	**0.0002**	**6E-05**	**6E-05**	**0.0002**	0.1715	**0.0005**	**0.0212**	**1E-08**		8E-08	0.0007	0.0317
TNT2	**0.0008**	**0.0024**	**0.0012**	**0.0083**	0.1986	**0.0046**	**0.0105**	**1E-09**	**8E-08**		6E-12	7E-05
TauC3	**0.0008**	**0.0011**	**0.0009**	**0.006**	**0.0357**	**0.012**	**0.0306**	**2E-07**	**0.0007**	**6E-12**		3E-07
Tau5	0.87	0.7819	0.5979	0.8959	0.5212	0.6917	0.3802	0.2162	0.0317	**7E-05**	**3E-07**	
PreC												
	MMSE	**GCS**	**Episodic**	**Semantic**	**Working**	**:eptual sp**	**ospatial a**	**Braak**	**TOC1**	**TNT2**	**TauC3**	**Tau5**
MMSE		3E-25	3E-27	2E-15	4E-07	8E-15	9E-09	8E-06	2E-06	0.0527	0.0424	0.5175
GCS	**3E-25**		3E-46	1E-28	4E-13	1E-16	3E-17	2E-07	3E-06	0.0934	0.0084	0.1699
Episodic	**3E-27**	**3E-46**		2E-21	6E-08	1E-11	2E-13	9E-07	1E-07	0.077	0.0396	0.256
Semantic	**2E-15**	**1E-28**	**2E-21**		5E-07	7E-14	1E-13	2E-05	2E-05	0.012	0.0116	0.2588
Working	**4E-07**	**4E-13**	**6E-08**	**5E-07**		9E-07	8E-07	0.0616	0.0743	0.6918	0.0197	0.8026
Perceptual speed	**8E-15**	**1E-16**	**1E-11**	**7E-14**	**9E-07**		1E-11	1E-04	0.0007	0.0384	0.1019	0.4038
Visuospatial ability	**9E-09**	**3E-17**	**2E-13**	**1E-13**	**8E-07**	**1E-11**		2E-05	0.001	0.1155	0.0726	0.352
Braak	**8E-06**	**2E-07**	**9E-07**	**2E-05**	0.0616	**1E-04**	**2E-05**		1E-09	0.0033	0.0025	0.1846
TOC1	**2E-06**	**3E-06**	**1E-07**	**2E-05**	0.0743	**0.0007**	**0.001**	**1E-09**		0.0003	0.0118	0.5564
TNT2	0.0527	0.0934	0.077	**0.012**	0.6918	**0.0384**	0.1155	**0.0033**	**0.0003**		7E-09	0.0265
TauC3	**0.0424**	**0.0084**	**0.0396**	**0.0116**	**0.0197**	0.1019	0.0726	**0.0025**	**0.0118**	**7E-09**		0.0077
Tau5	0.5175	0.1699	0.256	0.2588	0.8026	0.4038	0.352	0.1846	0.5564	**0.0265**	**0.0077**	

Table 3. 2 p-values for Spearman rank correlations with cognitive scores in the soluble fractions

Significant p-values are bolded.

Correlations Between DMN Pre-Tangle Tau Markers and Postmortem Neuropathology

Quantitative IHC and ELISA measurements of pre-tangle tau markers and oligomeric amyloid within each region of the DMN (Chapter 2) were correlated with

postmortem neuropathological assessments of neuritic plaque density and number, diffuse plaque density and number, NFT density and number, cerebral amyloid angiopathy (CAA), and TDP-43, as well as diagnostic scores based on CERAD, Braak, and NIA-Reagan criteria. Pre-tangle tau marker levels derived from DMN IHC demonstrated that all the tau markers, in addition to the MOAB-2, the oligomeric Aβ marker, strongly correlated with the neuritic plaque density and number in all three hubs (Figure 3.4, Table 3.3). Interestingly, only pS422 levels were correlated with diffuse plaque density. On the other hand, increasing levels of all four pre-tangle markers were positively associated with increasing NFT density, number, and Braak stage. Strong correlations of tau marker levels with CAA and TDP-43 scores were also noted, especially in the PCC.

Increasing pS422, TNT2, and TauC3 levels were all significantly associated with CERAD and NIA-Reagan scores in the DMN hubs, although these associations were generally weaker for TauC3. TOC1 levels followed a similar pattern in PCC and FC but did not correlate with these diagnostic scores in PreC. Levels of the more advanced NFT marker PHF1 were highly significantly associated with postmortem diagnosis in PCC, the hub where it was measured. Interestingly, MOAB-2 levels were significantly associated with CERAD and NIA-Reagan scores in the DMN hubs but not with Braak stage in FC and PreC.

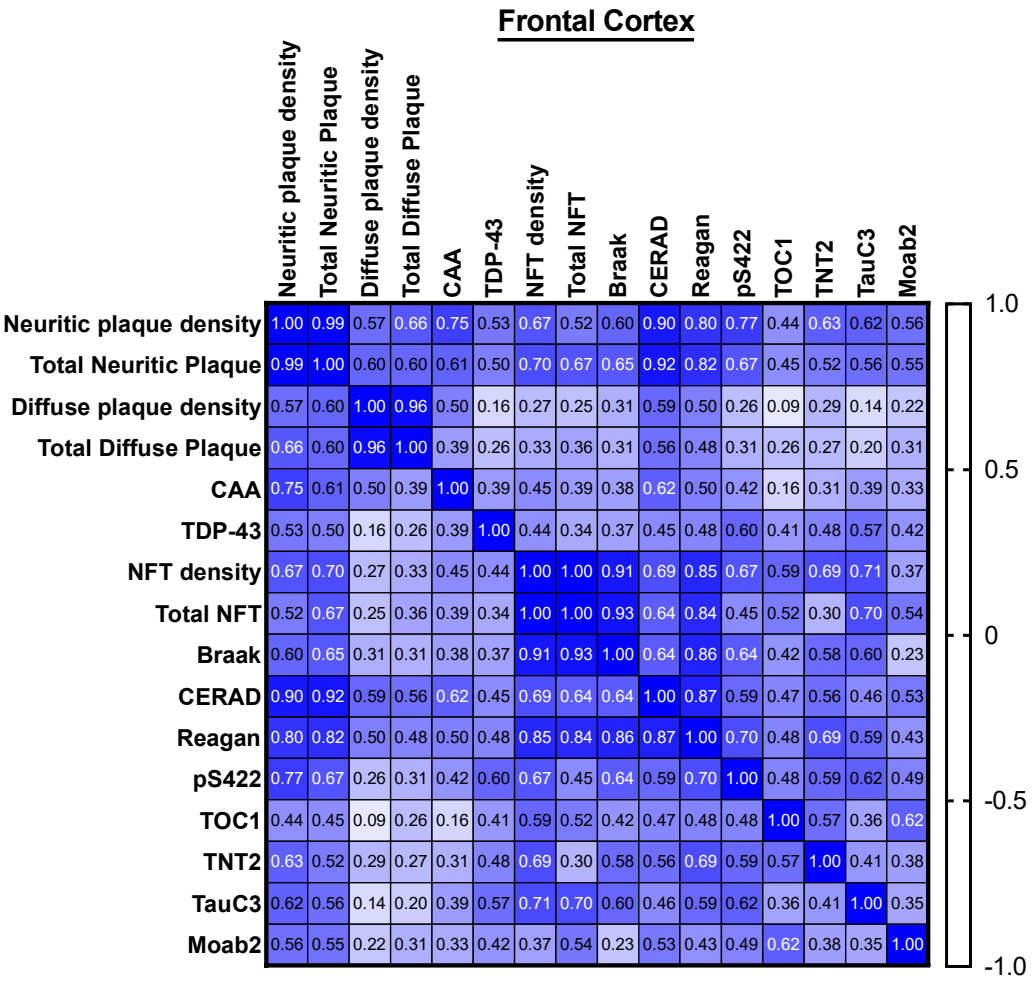

Figure 3. 4 Correlation matrices show relationships between IHC-measured pre-tangle DMN tau levels and neuropathological diagnostic scores in the RROS cohort

Figure 3. 4 (cont'd)

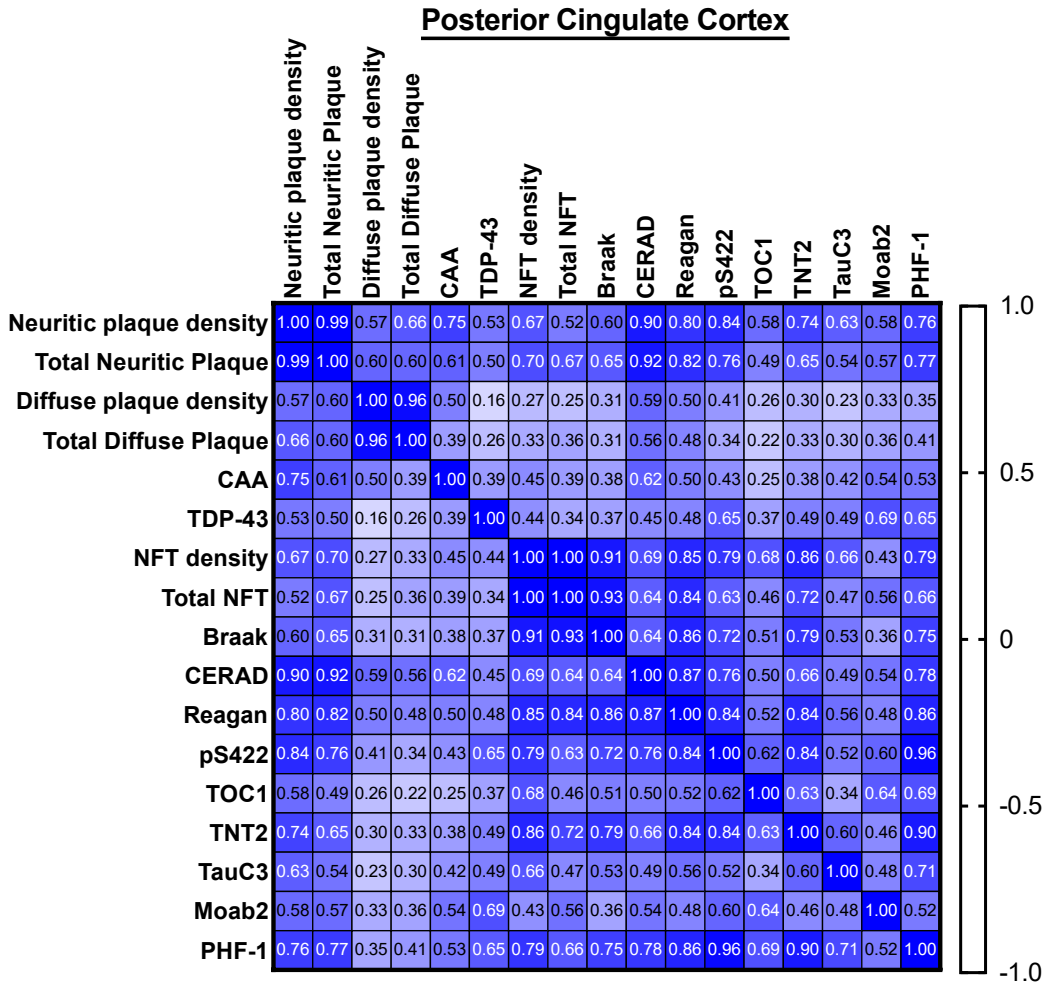

Figure 3. 4 (cont'd)

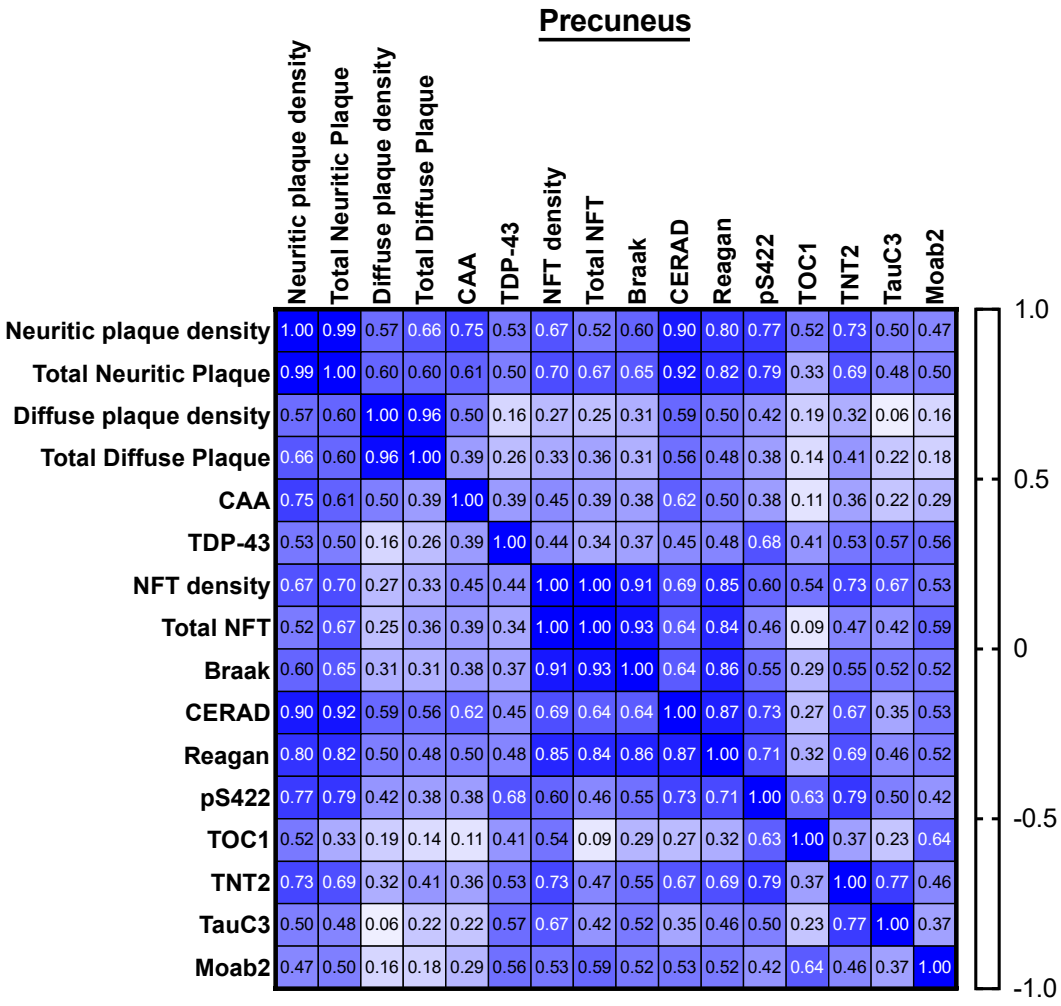

Spearman coefficients between the pre-tangle tau levels and pathological scores in the fontal cortex, posterior cingulate cortex, and precuneus are shown. Heat map reflects the strength of correlation.

FC																
	Neuritic p	Total Neu	Diffuse pl	Total Diff	CAA	TDP-43	NFT dens	Total NFT	Braak	CERAD	Reagan	pS422	TOC1	TNT2	TauC3	Moab2
Neuritic plaque densit	9.7E-27	0.00099	0.00011	1.5E-06	0.00281	4.4E-05	0.07283	0.00045	6.7E-12	1.3E-07	7.8E-07	0.01543	0.00022	0.00037	0.0013	
Total Neurit	9.7E-27		0.00053	1.6E-05	3.5E-06	0.00031	2.3E-05	2.3E-05	4.5E-07	1.8E-20	6.9E-13	4.5E-07	0.00209	0.00029	7.2E-05	0.00203
Diffuse plac	**0.00099**	**0.00053**		3E-16	0.00498	0.40209	0.14878	0.40846	0.09343	0.00062	0.00458	0.16504	0.62879	0.12309	0.45918	0.23442
Total Diffus	**0.00011**	**1.6E-05**	**3E-16**		0.00901	0.09017	0.07954	0.05642	0.04046	6.2E-05	0.00088	0.04839	0.09375	0.0827	0.21326	0.09814
CAA	**1.5E-06**	**3.5E-06**	**0.00498**	**0.00901**		0.00507	0.01233	0.02404	0.00653	1E-06	0.00019	0.00309	0.27397	0.03283	0.0074	0.07265
TDP-43	**0.00281**	**0.00031**	0.40209	0.09017	**0.00507**		0.01597	0.05218	0.00857	0.00093	0.00046	8.6E-06	0.00456	0.00061	3.8E-05	0.02059
NFT density	**4.4E-05**	**2.3E-05**	0.14878	0.07954	**0.01233**	**0.01597**		6.4E-10	5.7E-12	2.2E-05	2.7E-09	4.6E-05	0.00053	2E-05	1.8E-05	0.04419
Total NFT	0.07283	**2.3E-05**	0.40846	0.05642	**0.02404**	0.05218	**6.4E-10**		1.2E-15	5.5E-05	4.2E-10	0.0103	0.00302	0.10653	1.2E-05	0.06152
Braak	**0.00045**	**4.5E-07**	0.09343	**0.04046**	**0.00653**	**0.00857**	**5.7E-12**	**1.2E-15**		3.6E-07	3.3E-16	7.8E-07	0.0031	1.8E-05	1E-05	0.21948
CERAD	**6.7E-12**	**1.8E-20**	**0.00062**	**6.2E-05**	**1E-06**	**0.00093**	**2.2E-05**	**5.5E-05**	**3.6E-07**		6.2E-17	1.1E-05	0.00066	3.2E-05	0.00119	0.00285
Reagan	**1.3E-07**	**6.9E-13**	**0.00458**	**0.00088**	**0.00019**	**0.00046**	**2.7E-09**	**4.2E-10**	**3.3E-16**	**6.2E-17**		3.3E-08	0.00055	4.4E-08	1.4E-05	0.01716
pS422	**7.8E-07**	**4.5E-07**	0.16504	**0.04839**	**0.00309**	**8.6E-06**	**4.6E-05**	**0.0103**	**7.8E-07**	**1.1E-05**	**3.3E-08**		0.00063	1.4E-05	4.3E-06	0.00629
TOC1	**0.01543**	**0.00209**	0.62879	0.09375	0.27397	**0.00456**	**0.00053**	**0.00302**	**0.0031**	**0.00066**	**0.00055**	**0.00063**		2.6E-05	0.01213	0.00023
TNT2	**0.00022**	**0.00029**	0.12309	0.0827	**0.03283**	**0.00061**	**2E-05**	**0.10653**	**1.8E-05**	**3.2E-05**	**4.4E-08**	**1.4E-05**	**2.6E-05**		0.00431	0.03896
TauC3	**0.00037**	**7.2E-05**	0.45918	0.21326	**0.0074**	**3.8E-05**	**1.8E-05**	**1.2E-05**	**1E-05**	**0.00119**	**1.4E-05**	**4.3E-06**	**0.01213**	**0.00431**		0.06212
Moab2	**0.0013**	**0.00203**	0.23442	0.09814	0.07265	**0.02059**	**0.04419**	0.06152	0.21948	**0.00285**	**0.01716**	**0.00629**	**0.00023**	**0.03896**	0.06212	

PCC																	
	Neuritic p	Total Neu	Diffuse pl	Total Diff	CAA	TDP-43	NFT dens	Total NFT	Braak	CERAD	Reagan	pS422	TOC1	TNT2	TauC3	Moab2	PHF-1
Neuritic plaque densit	9.7E-27	0.00099	0.00011	1.5E-06	0.00281	4.4E-05	0.07283	0.00045	6.7E-12	1.3E-07	9.2E-09	0.00087	3.2E-06	0.00017	0.00071	3E-06	
Total Neurit	**9.7E-27**		0.00053	1.6E-05	3.5E-06	0.00031	2.3E-05	2.3E-05	4.5E-07	1.8E-20	6.9E-13	2.5E-09	0.00086	3.8E-06	0.00017	0.00113	2.5E-06
Diffuse plac	**0.00099**	**0.00053**		3E-16	0.00498	0.40209	0.14878	0.40846	0.09343	0.00062	0.00458	0.02529	0.17305	0.10643	0.23062	0.0759	0.07143
Total Diffus	**0.00011**	**1.6E-05**	**3E-16**		0.00901	0.09017	0.07954	0.05642	0.04046	6.2E-05	0.00088	0.03298	0.17611	0.04307	0.05877	0.05704	0.03483
CAA	**1.5E-06**	**3.5E-06**	**0.00498**	**0.00901**		0.00507	0.01233	0.02404	0.00653	1E-06	0.00019	0.00274	0.08788	0.00969	0.00345	0.00198	0.00377
TDP-43	**0.00281**	**0.00031**	0.40209	0.09017	**0.00507**		0.01597	0.05218	0.00857	0.00093	0.00046	9.3E-07	0.01243	0.00056	0.00048	2.6E-05	0.00018
NFT density	**4.4E-05**	**2.3E-05**	0.14878	0.07954	**0.01233**	**0.01597**		6.4E-10	5.7E-12	2.2E-05	2.7E-09	1.6E-07	3.7E-05	1.7E-09	7E-05	0.01656	5E-07
Total NFT	0.07283	**2.3E-05**	0.40846	0.05642	**0.02404**	0.05218	**6.4E-10**		1.2E-15	5.5E-05	4.2E-10	0.00024	0.01162	1.4E-05	0.01094	0.05142	0.02291
Braak	**0.00045**	**4.5E-07**	0.09343	0.04046	**0.00653**	**0.00857**	**5.7E-12**	**1.2E-15**		3.6E-07	3.3E-16	1.3E-08	0.00032	1E-10	0.00016	0.0523	4E-06
CERAD	**6.7E-12**	**1.8E-20**	**0.00062**	6.2E-05	**1E-06**	**0.00093**	**2.2E-05**	**5.5E-05**	**3.6E-07**		6.2E-17	1.3E-09	0.00039	7.1E-07	0.00049	0.0022	8.2E-07
Reagan	**1.3E-07**	**6.9E-13**	**0.00458**	0.00088	**0.00019**	**0.00046**	**2.7E-09**	**4.2E-10**	**3.3E-16**	**6.2E-17**		2.3E-13	0.00019	6.2E-13	4.6E-05	0.00727	6.5E-09
pS422	**9.2E-09**	**2.5E-09**	**0.02529**	0.03298	**0.00274**	**9.3E-07**	**1.6E-07**	**0.00024**	**1.3E-08**	**1.3E-09**	**2.3E-13**		5.1E-06	6.8E-13	0.00021	0.00044	3.3E-16
TOC1	**0.00087**	**0.00086**	0.17305	0.17611	0.08788	**0.01243**	**3.7E-05**	**0.01162**	**0.00032**	**0.00039**	**0.00019**	**5.1E-06**		3.5E-06	0.01978	0.00012	5.7E-05
TNT2	**3.2E-06**	**3.8E-06**	0.10643	**0.04307**	**0.00969**	**0.00056**	**1.7E-09**	**1.4E-05**	**1E-10**	**7.1E-07**	**6.2E-13**	**6.8E-13**	**3.5E-06**		1.2E-05	0.01109	7.3E-11
TauC3	**0.00017**	**0.00017**	0.23062	0.05877	**0.00345**	**0.00048**	**7E-05**	**0.01094**	**0.00016**	**0.00049**	**4.6E-05**	**0.00021**	**0.01978**	**1.2E-05**		0.00754	2.3E-05
Moab2	**0.00071**	**0.00113**	0.0759	0.05704	**0.00198**	**2.6E-05**	**0.01656**	0.05142	0.0523	**0.0022**	**0.00727**	**0.00044**	**0.00012**	**0.01109**	**0.00754**		0.00472
PHF-1	**3E-06**	**2.5E-06**	0.07143	**0.03483**	**0.00377**	**0.00018**	**5E-07**	**0.02291**	**4E-06**	**8.2E-07**	**6.5E-09**	**3.3E-16**	**5.7E-05**	**7.3E-11**	**2.3E-05**	**0.00472**	

PreC																
	Neuritic p	Total Neu	Diffuse pl	Total Diff	CAA	TDP-43	NFT dens	Total NFT	Braak	CERAD	Reagan	pS422	TOC1	TNT2	TauC3	Moab2
Neuritic plaque densit	9.7E-27	0.00099	0.00011	1.5E-06	0.00281	4.4E-05	0.07283	0.00045	6.7E-12	1.3E-07	5.8E-07	0.00306	5.6E-06	0.00581	0.01224	
Total Neurit	**9.7E-27**		0.00053	1.6E-05	3.5E-06	0.00031	2.3E-05	2.3E-05	4.5E-07	1.8E-20	6.9E-13	3.5E-09	0.02403	1.4E-07	0.00249	0.00802
Diffuse plac	**0.00099**	**0.00053**		3E-16	0.00498	0.40209	0.14878	0.40846	0.09343	0.00062	0.00458	0.02237	0.30832	0.08722	0.76039	0.41754
Total Diffus	**0.00011**	**1.6E-05**	**3E-16**		0.00901	0.09017	0.07954	0.05642	0.04046	6.2E-05	0.00088	0.02212	0.37317	0.00645	0.20576	0.37377
CAA	**1.5E-06**	**3.5E-06**	**0.00498**	**0.00901**		0.00507	0.01233	0.02404	0.00653	1E-06	0.00019	0.01466	0.46402	0.01149	0.16995	0.14109
TDP-43	**0.00281**	**0.00031**	0.40209	0.09017	**0.00507**		0.01597	0.05218	0.00857	0.00093	0.00046	2.2E-06	0.00341	0.00011	0.00019	0.002
NFT density	**4.4E-05**	**2.3E-05**	0.14878	0.07954	**0.01233**	**0.01597**		6.4E-10	5.7E-12	2.2E-05	2.7E-09	0.00047	0.00201	4.9E-06	8.2E-05	0.00357
Total NFT	0.07283	**2.3E-05**	0.40846	0.05642	**0.02404**	0.05218	**6.4E-10**		1.2E-15	5.5E-05	4.2E-10	0.02589	0.61354	0.00749	0.04786	0.04748
Braak	**0.00045**	**4.5E-07**	0.09343	**0.04046**	**0.00653**	**0.00857**	**5.7E-12**	**1.2E-15**		3.6E-07	3.3E-16	0.00021	0.04421	4.5E-05	0.00073	0.00475
CERAD	**6.7E-12**	**1.8E-20**	**0.00062**	**6.2E-05**	**1E-06**	**0.00093**	**2.2E-05**	**5.5E-05**	**3.6E-07**		6.2E-17	7.1E-08	0.06477	2E-07	0.0305	0.0038
Reagan	**1.3E-07**	**6.9E-13**	**0.00458**	**0.00088**	**0.00019**	**0.00046**	**2.7E-09**	**4.2E-10**	**3.3E-16**	**6.2E-17**		2.4E-07	0.02517	5.8E-08	0.00325	0.00454
pS422	**5.8E-07**	**3.5E-09**	**0.02237**	**0.02212**	**0.01466**	**2.2E-06**	**0.00047**	**0.02589**	**0.00021**	**7.1E-08**	**2.4E-07**		1.4E-05	1.7E-09	0.00203	0.02658
TOC1	**0.00306**	**0.02403**	0.30832	0.37317	0.46402	**0.00341**	**0.00201**	0.61354	**0.04421**	0.06477	**0.02517**	**1.4E-05**		0.00974	0.16554	0.00025
TNT2	**5.6E-06**	**1.4E-07**	0.08722	**0.00645**	**0.01149**	**0.00011**	**4.9E-06**	**0.00749**	**4.5E-05**	**2E-07**	**5.8E-08**	**1.7E-09**	**0.00974**		1.2E-08	0.01272
TauC3	**0.00581**	**0.00249**	0.76039	0.20576	0.16995	**0.00019**	**8.2E-05**	**0.04786**	**0.00073**	**0.0305**	**0.00325**	**0.00203**	0.16554	**1.2E-08**		0.05885
Moab2	**0.01224**	**0.00802**	0.41754	0.37377	0.14109	**0.002**	**0.00357**	**0.04748**	**0.00475**	**0.0038**	**0.00454**	**0.02658**	**0.00025**	**0.01272**	0.05885	

Table 3. 3 p-values from the Spearman rank correlations for postmortem variables in the fixed tissue samples

Significant p-values are bolded.

In line with these results, pre-tangle tau in the soluble tissue fraction also revealed strong correlations with pathology. Notably, TOC1+ oligomer levels were significantly correlated with plaque and NFT variables as well as Braak stage, CERAD, and NIA-Reagan scores in all regions and with TDP-43 only in the PCC (Figure 3.5, Table 3.4). TNT2 also correlated with majority of the pathology scores except for the diffuse plaque

measure and the TDP-43 in the FC and PreC. Showing its highest correlations in the FC, TauC3 correlated with all the scores except for the diffuse plaque measures. In contrast, levels of Tau5, the total tau marker, were only correlated with NFT density and TDP-43, highlighting the distinction between pathological vs physiological tau.

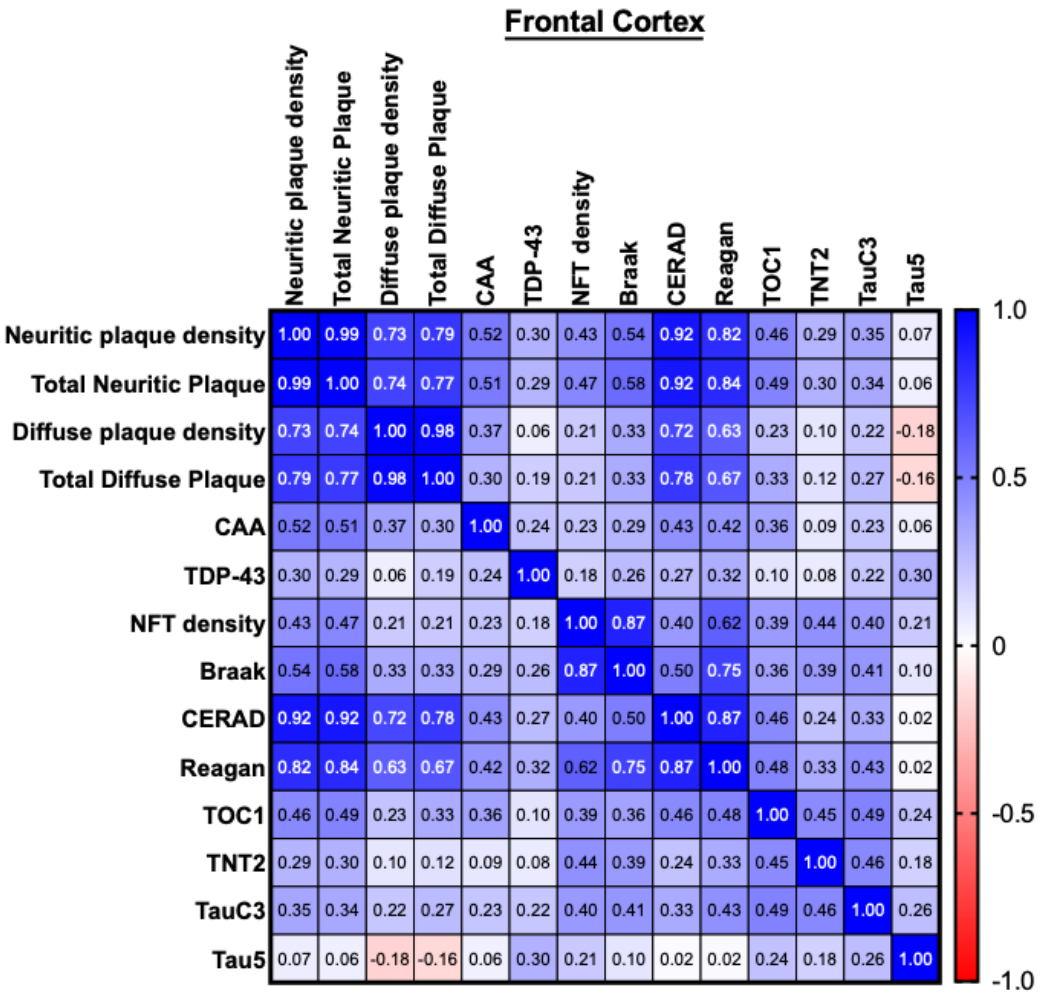

Figure 3. 5 Correlation matrices for the soluble pre-tangle DMN tau and neuropathological diagnostic scores in the RROS cohort

Figure 3. 5 (cont'd)

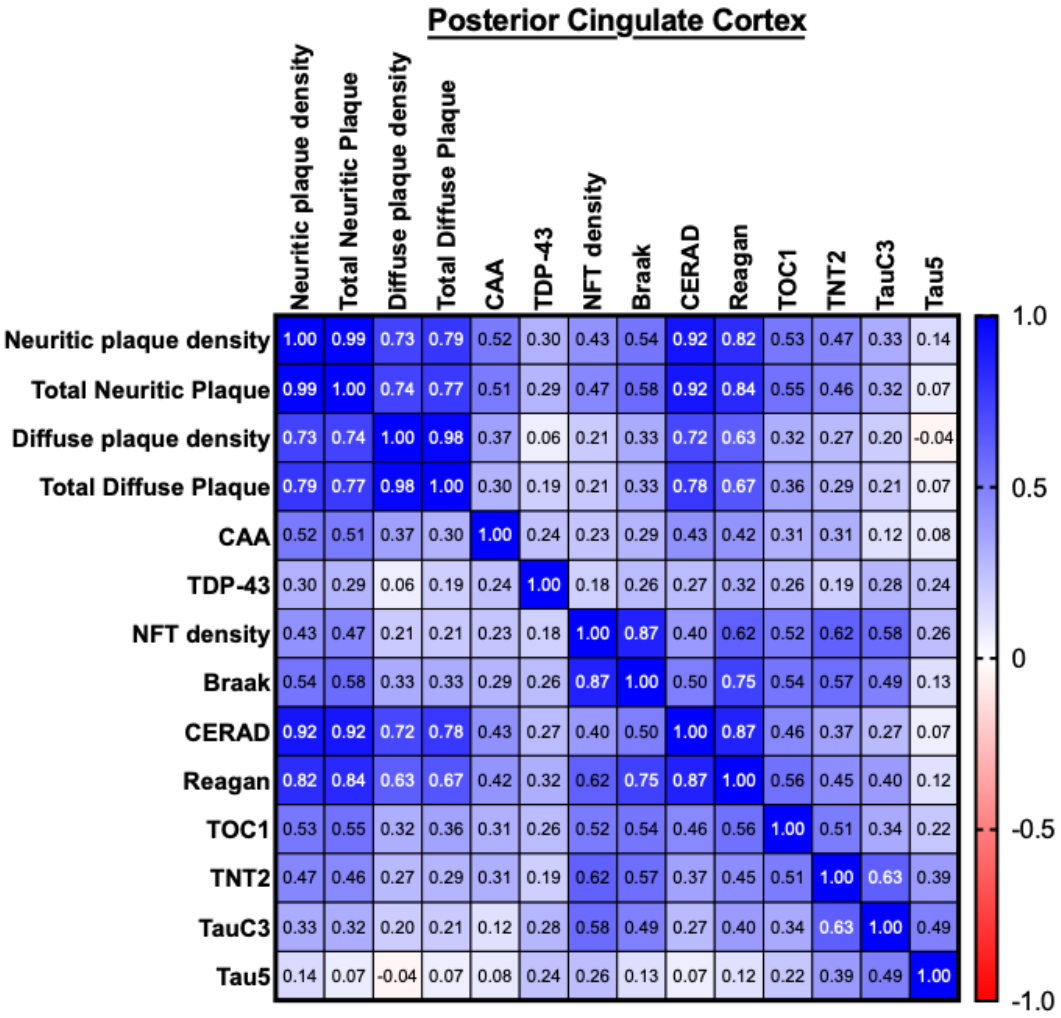

Figure 3. 5 (cont'd)

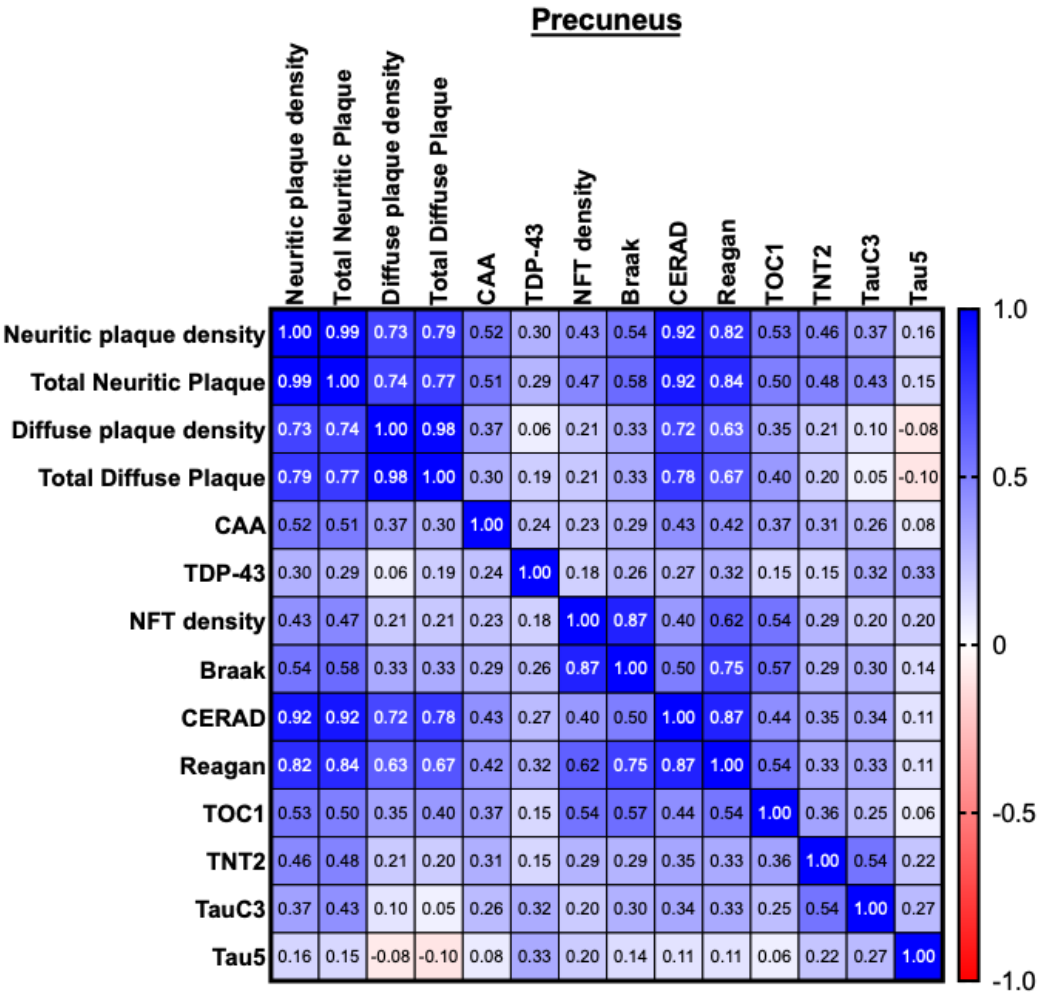

Spearman coefficients between the pre-tangle tau levels and pathological scores in the fontal cortex, posterior cingulate cortex, and precuneus are shown. Heat map reflects the strength of correlation.

FC														
	Neuritic plaque d	Neuritic Pe	plaque d	Diffuse Pl	CAA	TDP-43	IFT densit	Braak	CERAD	Reagan	TOC1	TNT2	TauC3	Tau5
Neuritic plaque density		4.7E-74	1.9E-16	2.1E-15	1.6E-07	0.00353	2.5E-05	4.7E-08	3.2E-37	2.1E-23	5.1E-06	0.00538	0.0008	0.51403
Total Neuriti	**4.7E-74**		2.2E-16	1.3E-14	7.2E-08	0.00424	3.5E-06	6.4E-10	1.6E-39	3.1E-27	4.5E-07	0.00243	0.00063	0.56361
Diffuse plaq	**1.9E-16**	**2.2E-16**		6.4E-50	0.00032	0.5464	0.0497	0.00152	1.3E-15	3E-11	0.02785	0.35841	0.03951	0.09784
Total Diffuse	**2.1E-15**	**1.3E-14**	**6.4E-50**		0.01269	0.11885	0.07989	0.00655	3.9E-15	5.5E-10	0.00652	0.33973	0.02813	0.20418
CAA	**1.6E-07**	**7.2E-08**	**0.00032**	**0.01269**		0.01755	0.02828	0.0036	7.7E-06	2E-05	0.00024	0.37138	0.02487	0.58552
TDP-43	**0.00353**	**0.00424**	0.5464	0.11885	**0.01755**		0.08701	0.00859	0.00817	0.0015	0.31342	0.44725	0.02998	0.00246
NFT density	**2.5E-05**	**3.5E-06**	**0.0497**	0.07989	**0.02828**	0.08701		1.4E-28	9.9E-05	6.8E-11	0.00015	1.8E-05	9.9E-05	0.04883
Braak	**4.7E-08**	**6.4E-10**	**0.00152**	**0.00655**	**0.0036**	**0.00859**	**1.4E-28**		1.2E-07	1E-18	0.00027	7.2E-05	2.6E-05	0.32698
CERAD	**3.2E-37**	**1.6E-39**	**1.3E-15**	**3.9E-15**	**7.7E-06**	**0.00817**	**9.9E-05**	**1.2E-07**		8.8E-31	2.1E-06	0.01797	0.00092	0.87567
Reagan	**2.1E-23**	**3.1E-27**	**3E-11**	**5.5E-10**	**2E-05**	**0.0015**	**6.8E-11**	**1E-18**	**8.8E-31**		5.8E-07	0.00102	8.3E-06	0.82776
TOC1	**5.1E-06**	**4.5E-07**	**0.02785**	**0.00652**	**0.00024**	0.31342	**0.00015**	**0.00027**	**2.1E-06**	**5.8E-07**		2.6E-06	3.1E-07	0.01625
TNT2	**0.00538**	**0.00243**	0.35841	0.33973	0.37138	0.44725	**1.8E-05**	**7.2E-05**	**0.01797**	**0.00102**	**2.6E-06**		1.5E-06	0.07761
TauC3	**0.0008**	**0.00063**	**0.03951**	**0.02813**	**0.02487**	**0.02998**	**9.9E-05**	**2.6E-05**	**0.00092**	**8.3E-06**	**3.1E-07**	**1.5E-06**		0.01112
Tau5	0.51403	0.56361	0.09784	0.20418	0.58552	**0.00246**	**0.04883**	0.32698	0.87567	0.82776	**0.01625**	0.07761	**0.01112**	

PCC														
	Neuritic plaque d	Neuritic Pe	plaque d	Diffuse Pl	CAA	TDP-43	IFT densit	Braak	CERAD	Reagan	TOC1	TNT2	TauC3	Tau5
Neuritic plaque density		4.7E-74	1.9E-16	2.1E-15	1.6E-07	0.00353	2.5E-05	4.7E-08	3.2E-37	2.1E-23	1E-07	2.7E-06	0.00153	0.18394
Total Neuriti	**4.7E-74**		2.2E-16	1.3E-14	7.2E-08	0.00424	3.5E-06	6.4E-10	1.6E-39	3.1E-27	4.8E-09	1.9E-06	0.0014	0.48494
Diffuse plaq	**1.9E-16**	**2.2E-16**		6.4E-50	0.00032	0.5464	0.0497	0.00152	1.3E-15	3E-11	0.00238	0.00897	0.06128	0.69698
Total Diffuse	**2.1E-15**	**1.3E-14**	**6.4E-50**		0.01269	0.11885	0.07989	0.00655	3.9E-15	5.5E-10	0.0025	0.01761	0.08951	0.59055
CAA	**1.6E-07**	**7.2E-08**	**0.00032**	**0.01269**		0.01755	0.02828	0.0036	7.7E-06	2E-05	0.00196	0.00175	0.24596	0.4233
TDP-43	**0.00353**	**0.00424**	0.5464	0.11885	**0.01755**		0.08701	0.00859	0.00817	0.0015	0.0087	0.05953	0.00463	0.01959
NFT density	**2.5E-05**	**3.5E-06**	**0.0497**	0.07989	**0.02828**	0.08701		1.4E-28	9.9E-05	6.8E-11	2E-07	8.1E-11	2.2E-09	0.01385
Braak	**4.7E-08**	**6.4E-10**	**0.00152**	**0.00655**	**0.0036**	**0.00859**	**1.4E-28**		1.2E-07	1E-18	1.1E-08	1.1E-09	2.5E-07	0.21622
CERAD	**3.2E-37**	**1.6E-39**	**1.3E-15**	**3.9E-15**	**7.7E-06**	**0.00817**	**9.9E-05**	**1.2E-07**		8.8E-31	1.6E-06	0.0002	0.00719	0.51473
Reagan	**2.1E-23**	**3.1E-27**	**3E-11**	**5.5E-10**	**2E-05**	**0.0015**	**6.8E-11**	**1E-18**	**8.8E-31**		2.7E-09	4.2E-06	5.7E-05	0.24343
TOC1	**1E-07**	**4.8E-09**	**0.00238**	**0.0025**	**0.00196**	**0.0087**	**2E-07**	**1.1E-08**	**1.6E-06**	**2.7E-09**		7.9E-08	0.00074	0.03167
TNT2	**2.7E-06**	**1.9E-06**	**0.00897**	**0.01761**	**0.00175**	0.05953	**8.1E-11**	**1.1E-09**	**0.0002**	**4.2E-06**	**7.9E-08**		5.9E-12	7.2E-05
TauC3	**0.00153**	**0.0014**	0.06128	0.08951	0.24596	**0.00463**	**2.2E-09**	**2.5E-07**	**0.00719**	**5.7E-05**	**0.00074**	**5.9E-12**		2.6E-07
Tau5	0.18394	0.48494	0.69698	0.59055	0.4233	**0.01959**	**0.01385**	0.21622	0.51473	0.24343	**0.03167**	**7.2E-05**	**2.6E-07**	

PreC														
	Neuritic plaque d	Neuritic Pe	plaque d	Diffuse Pl	CAA	TDP-43	IFT densit	Braak	CERAD	Reagan	TOC1	TNT2	TauC3	Tau5
Neuritic plaque density		4.7E-74	1.9E-16	2.1E-15	1.6E-07	0.00353	2.5E-05	4.7E-08	3.2E-37	2.1E-23	1.1E-07	4.4E-06	0.00035	0.12775
Total Neuriti	**4.7E-74**		2.2E-16	1.3E-14	7.2E-08	0.00424	3.5E-06	6.4E-10	1.6E-39	3.1E-27	1.8E-07	5.1E-07	9.9E-06	0.13776
Diffuse plaq	**1.9E-16**	**2.2E-16**		6.4E-50	0.00032	0.5464	0.0497	0.00152	1.3E-15	3E-11	0.00061	0.04978	0.32757	0.42976
Total Diffuse	**2.1E-15**	**1.3E-14**	**6.4E-50**		0.01269	0.11885	0.07989	0.00655	3.9E-15	5.5E-10	0.00078	0.10546	0.65669	0.40661
CAA	**1.6E-07**	**7.2E-08**	**0.00032**	**0.01269**		0.01755	0.02828	0.0036	7.7E-06	2E-05	0.00022	0.00171	0.0088	0.44972
TDP-43	**0.00353**	**0.00424**	0.5464	0.11885	**0.01755**		0.08701	0.00859	0.00817	0.0015	0.1416	0.13187	0.00117	0.0009
NFT density	**2.5E-05**	**3.5E-06**	**0.0497**	0.07989	**0.02828**	0.08701		1.4E-28	9.9E-05	6.8E-11	3.6E-08	0.00543	0.05642	0.06072
Braak	**4.7E-08**	**6.4E-10**	**0.00152**	**0.00655**	**0.0036**	**0.00859**	**1.4E-28**		1.2E-07	1E-18	1.1E-09	0.00333	0.00248	0.18461
CERAD	**3.2E-37**	**1.6E-39**	**1.3E-15**	**3.9E-15**	**7.7E-06**	**0.00817**	**9.9E-05**	**1.2E-07**		8.8E-31	6E-06	0.00044	0.00063	0.28475
Reagan	**2.1E-23**	**3.1E-27**	**3E-11**	**5.5E-10**	**2E-05**	**0.0015**	**6.8E-11**	**1E-18**	**8.8E-31**		1.2E-08	0.0009	0.00088	0.28406
TOC1	**1.1E-07**	**1.8E-07**	**0.00061**	**0.00078**	**0.00022**	0.1416	**3.6E-08**	**1.1E-09**	**6E-06**	**1.2E-08**		0.00028	0.01179	0.55643
TNT2	**4.4E-06**	**5.1E-07**	**0.04978**	0.10546	**0.00171**	0.13187	**0.00543**	**0.00333**	**0.00044**	**0.0009**	**0.00028**		7E-09	0.02649
TauC3	**0.00035**	**9.9E-06**	0.32757	0.65669	**0.0088**	**0.00117**	0.05642	**0.00248**	**0.00063**	**0.00088**	**0.01179**	**7E-09**		0.00775
Tau5	0.12775	0.13776	0.42976	0.40661	0.44972	**0.0009**	0.06072	0.18461	0.28475	0.28406	0.55643	**0.02649**	**0.00775**	

Table 3. 4 p-values from the Spearman rank correlations for postmortem variables in the soluble tissue samples

Significant p-values are bolded.

Possible regional differences in pre-tangle tau pathology burden in DMN hubs: relationships with Braak stage and global cognition

In the previous chapter, regional differences for each marker were shown (Chapter 2, Figure 2.8), with PCC bearing greater levels of pre-tangle pathology (higher

pS422, TOC1, and TNT2) in successive Braak stages and PreC lagging in the extent of tau marker accrual. This was a thought-provoking observation that two adjacent brain regions that synchronize in their activity by default showed different pathological tau loads, which raised the question of whether there would be any differences in the correlations between the pre-tangle DMN tau and postmortem NFT pathology scores as well as global cognitive measures in PCC vs PreC. To address this question, we conducted comparisons between the correlation coefficients of each marker for NFT density, Total NFT, Braak score, MMSE, and GCS in PCC vs PreC (Diedenhofen, 2015).

PCC vs PreC (p value)	**NFT density**	**Total NFT**	**Braak**	**MMSE**	**GCS**
pS422	0.1507	0.3779	0.1761	0.8727	0.5986
TOC1	0.4171	0.1392	0.2222	0.8527	0.46
sTOC1	0.8142	N/A	0.7656	0.4802	0.6297
TNT2	0.1973	0.1425	**0.0358**	0.3688	0.8339
sTNT2	**0.0052**	N/A	**0.0185**	0.3111	0.333
TauC3	0.9764	0.8389	0.9466	0.3452	0.6571
sTauc3	0.0026	N/A	0.1154	0.8366	0.8848

Table 3. 5 Comparing correlation coefficients between the markers and postmortem NFT scores as well as antemortem global cognitive measures in PCC vs PreC

Cocor analysis, an R package, was used to compare correlation coefficients (Diedenhofen, 2015).

TNT2 was the only marker better correlated with NFT density (p=0.0052) and Braak stage (TNT2 p=0.358, sTNT2 p=00185) in PCC when compared to PreC. However, there were no differences in strength of correlation between TNT2 levels and MMSE (p=0.311) or GCS (p=0.333) in PCC vs. PreC.

Validation studies

To validate the correlations between the DMN soluble pre-tangle tau and MMSE scores, we utilized the related data from the Michigan Alzheimer's Disease Center (MADC) cohort (Chapter 2- Table 2.3) from our previous studies. Pearson correlation analyses revealed strong and statistically significant inverse correlations between soluble TOC1 and TNT2 levels and antemortem MMSE scores across all three DMN regions (Figure 3.6). In contrast, TauC3 levels correlated with the MMSE scores only in PreC (Table 3.6).

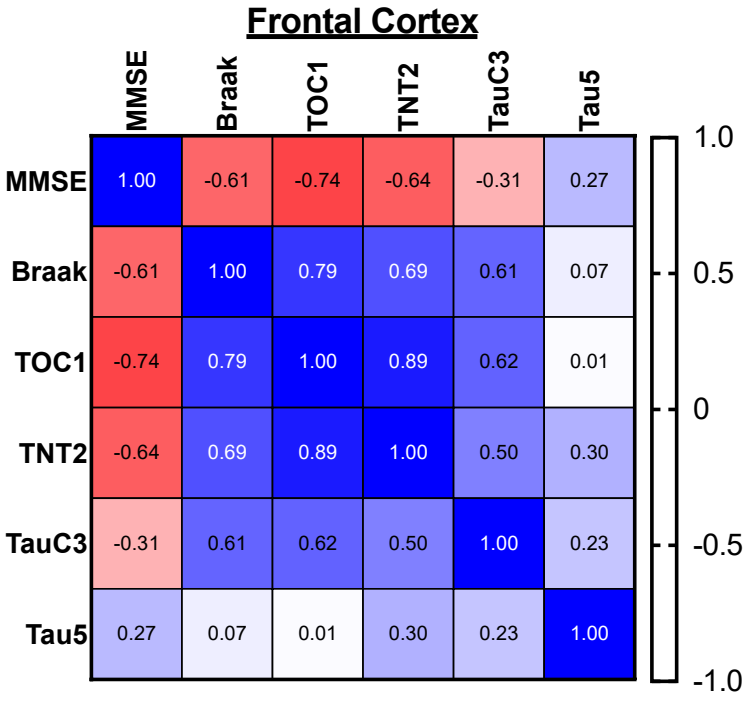

Figure 3. 6 Correlation matrices for the soluble pre-tangle DMN tau and MMSE scores in the MADC cohort

Figure 3. 6 (cont'd)

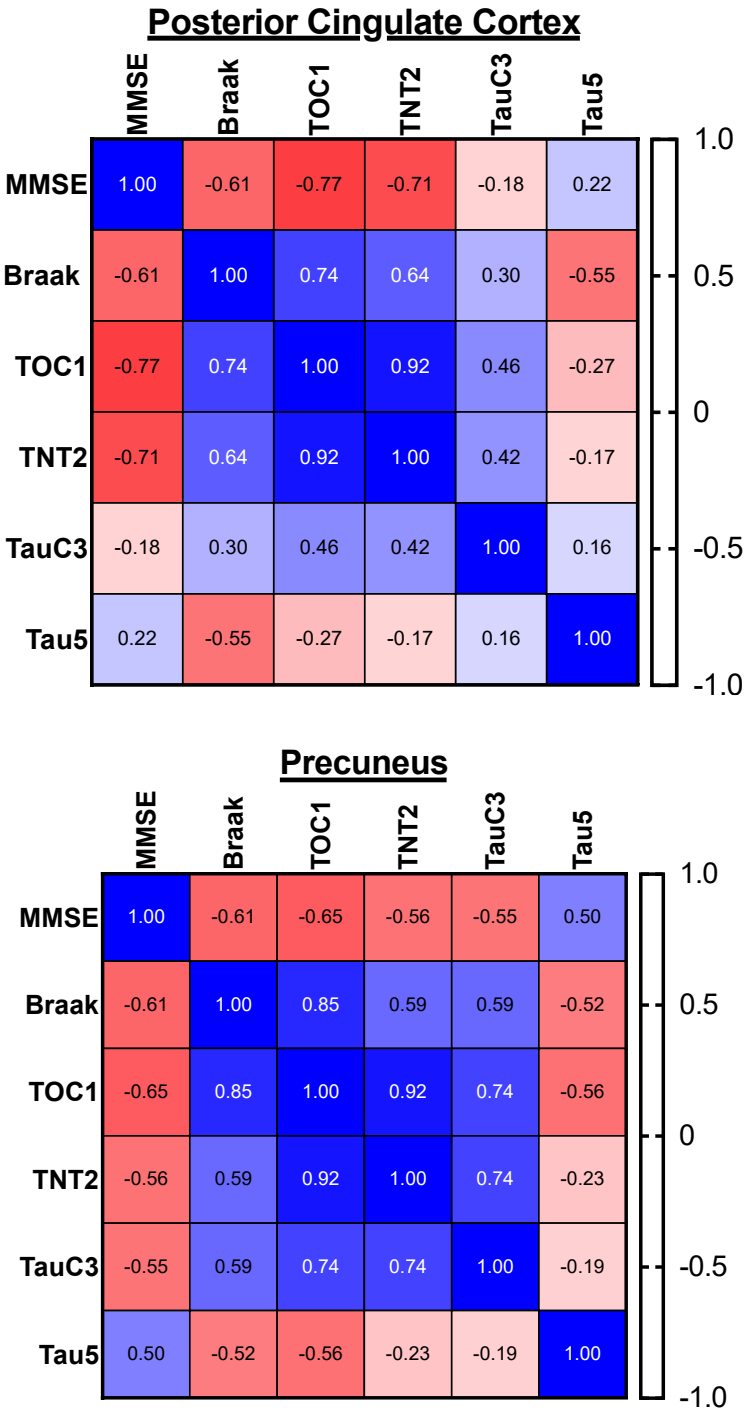

Spearman coefficients between the pre-tangle tau levels and pathological scores in the fontal cortex, posterior cingulate cortex, and precuneus are shown. Heat map reflects the strength of correlation.

	FC						
FC		**MMSE**	**Braak**	**TOC1**	**TNT2**	**TauC3**	**Tau5**
	MMSE		0.00356	0.000426	0.00404	0.218354	0.282166
	Braak	**0.00356**		0.000112	0.001701	0.007714	0.796167
	TOC1	**0.000426**	**0.000112**		5.47E-07	0.006531	0.961083
	TNT2	**0.00404**	**0.001701**	**5.47E-07**		0.035586	0.222379
	TauC3	0.218354	**0.007714**	**0.006531**	**0.035586**		0.36616
	Tau5	0.282166	0.796167	0.961083	0.222379	0.36616	
	PCC						
PCC		**MMSE**	**Braak**	**TOC1**	**TNT2**	**TauC3**	**Tau5**
	MMSE		0.00356	8.41E-05	0.00031	0.445202	0.326843
	Braak	**0.00356**		0.000181	0.001966	0.18065	0.009498
	TOC1	**8.41E-05**	**0.000181**		7.8E-09	0.041954	0.251131
	TNT2	**0.00031**	**0.001966**	**7.8E-09**		0.055823	0.460943
	TauC3	0.445202	0.18065	**0.041954**	0.055823		0.496334
	Tau5	0.326843	0.009498	0.251131	0.460943	0.496334	
	PreC						
Prec		**MMSE**	**Braak**	**TOC1**	**TNT2**	**TauC3**	**Tau5**
	MMSE		0.00356	0.003565	0.008733	0.009835	0.029671
	Braak	**0.00356**		9.95E-06	0.005213	0.004904	0.022862
	TOC1	**0.003565**	**9.95E-06**		5.62E-08	0.000473	0.020939
	TNT2	**0.008733**	**0.005213**	**5.62E-08**		0.000135	0.336357
	TauC3	**0.009835**	**0.004904**	**0.000473**	**0.000135**		0.437215
	Tau5	**0.029671**	**0.022862**	**0.020939**	0.336357	0.437215	

Table 3. 6 p-values for Spearman rank correlations with MADC pathology and MMSE in soluble fractions

Significant p-values are bolded.

Distribution of the Cognitive Scores Based on the Braak Stage

Finally, as an indicator of the overall cognitive status of the RROS cohort, the MMSE and GCS scores were distributed based on the Braak stage (Figure 3.7). Very interestingly, the graphs mimicked the DMN pre-tangle tau marker graphs and pair-wise comparisons as a significant decline by Braak stage 5 with an exacerbating decline in Braak 6 (Figures 2.4 & 2.6). When the data reorganized based on the clinical groups

(Figures 2.5 & 2.7), there was no significant changes between the NCI and MCI in this cohort versus a significant drop in both MMSE and GCS scores in the AD cases. Altogether, these findings emphasize the close relationship between the presence of significant pre-tangle tau and the initiation of the cognitive deterioration.

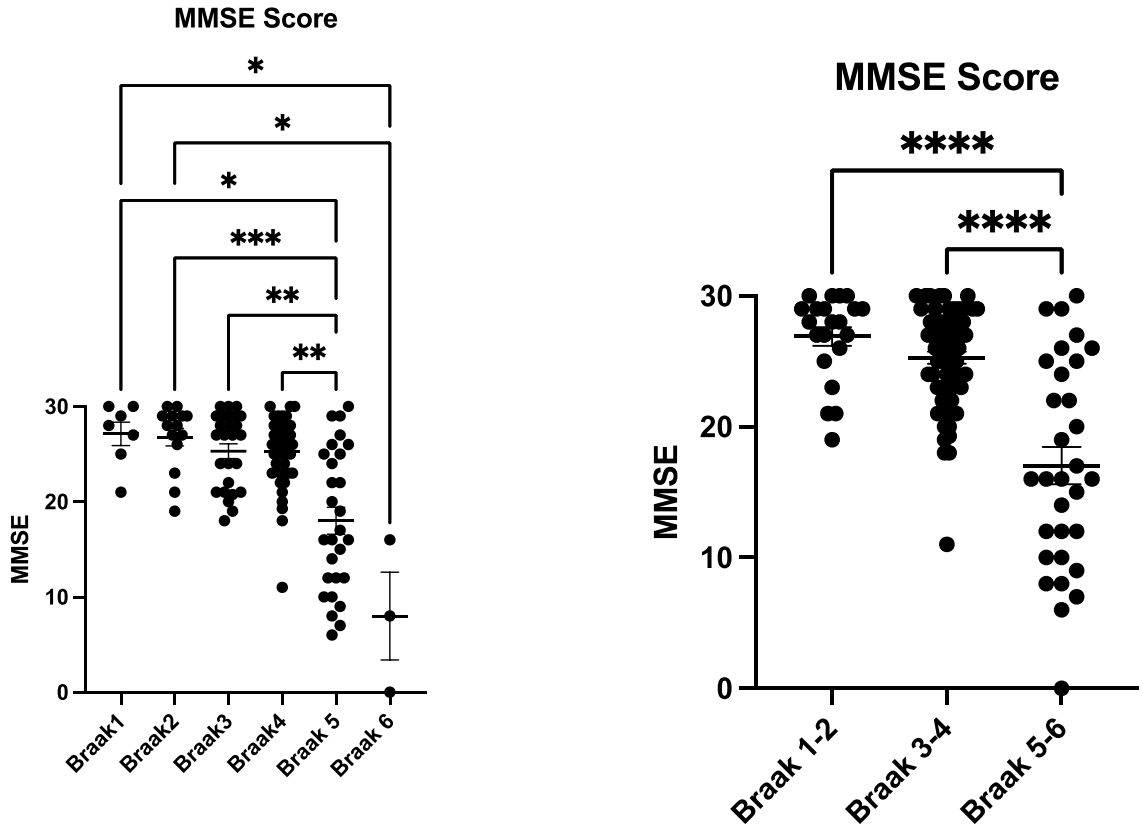

Figure 3. 7 The distribution of the global cognitive measures based on the Braak score

Figure 3. 7 (cont'd)

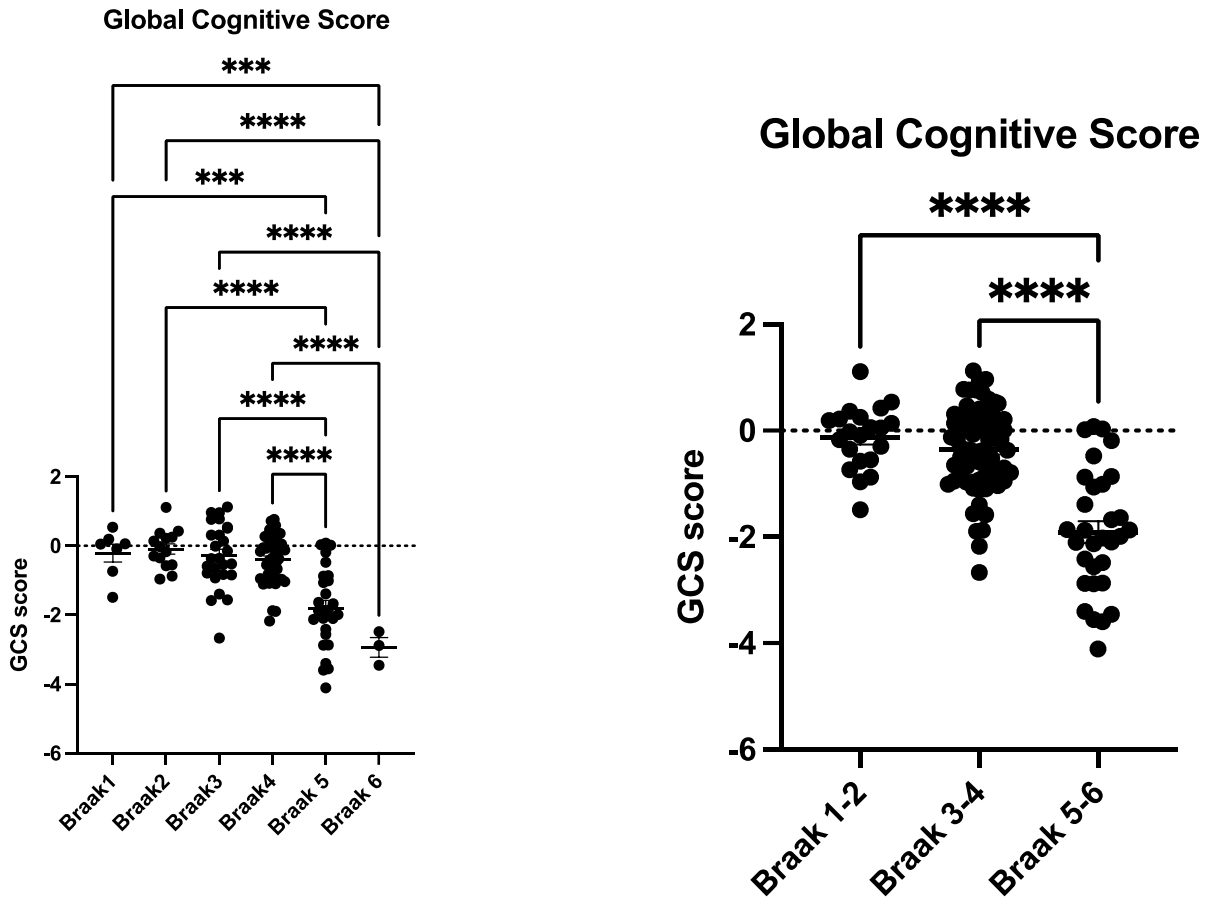

*Statistical analyses were conducted using the Kruskal-Wallis test, followed by Dunn's multiple comparisons for pairwise analysis for (A) MMSE scores and the One-Way ANOVA combined with the Tukey's multiple comparison test for the (B) GCS. Significance levels were indicated as follows: *p < 0.05, **p < 0.01, ***p < 0.001, and ****p < 0.0001.*

DISCUSSION

Both antemortem Tau-PET imaging and postmortem analysis have shown that NFT burden correlates tightly with cognitive decline in AD. However, the impact of more toxic pre-tangle tau on human cognition is a recently growing field. In Chapter 2, we

showed that pre-tangle tau begins to accumulate within the DMN hubs as early as Braak stage IV-V. In the present study, we built upon these observations to demonstrate that this accrual of DMN pre-tangle tau is associated with poorer performance on cognitive measures targeting memory, visuospatial abilities, and perceptual speed.

DMN Tau Correlates with Episodic and Semantic Memory and Other Cognitive Markers

Correlations between pS422 in cholinergic basal forebrain neurons and GCS & MMSE scores have been reported before (Vana, 2011). Consistent with these findings, data from both our IHC and ELISA studies showed strong inverse correlations between increasing pS422 (IHC only), TOC1, TNT2 and even TauC3 levels in all three DMN hubs and worsening antemortem GCS and MMSE scores (Figures 3.2, 3.3; Tables 3.1, 3.2). Additionally, these markers correlated with individual memory components included in the study, especially episodic and semantic memory (see Introduction for descriptions of these domains). Remarkably, data from both our IHC and ELISA studies showed strong inverse correlations between increasing pS422 (IHC only), TOC1, TNT2 and even TauC3 levels in all three DMN hubs and poorer performance on composite test scores for both episodic and semantic memory domains (Figures 3.2, 3.3; Tables 3.1, 3.2). In general, our ELISA results of S1 fractions showed that the strengths of correlation for soluble levels of these tau markers with MMSE, GCS, episodic memory, and semantic memory were weaker, and there were a few instances of nonsignificant associations (e.g., FC levels of TOC1 and MMSE, PreC levels of TNT2 and GCS). Such a finding is reminiscent of studies showing that cognitive deterioration begins to accelerate once appreciable NFTs appear in higher association cortical regions (Nelson, 2007), suggesting that soluble toxic tau has accumulated to a critical threshold to drive

neurodegeneration and frank NFT deposition. Since DMN function plays a role in both episodic and semantic memory function (Menon, 2023), these data suggest a potential relationship between tangle evolution in the DMN and cognitive deterioration. Hence, soluble tau pathology initiates degenerative processes in these regions, which is driven by the accumulating development of soluble and insoluble tau aggregates, as detected by IHC. In support of this hypothesis, with a few exceptions, tau pre-tangle markers levels in the DMN hubs were not associated with measures of working memory, a cognitive domain that is not associated with DMN function.

Two additional key cognitive domains that were tested were visuospatial ability and perceptual speed. Visuospatial ability refers to the skills to relate visual sensory information to the space, such as conceptualizing distances, volumes, or navigation (Kimchi, 2016). Although the damage to the occipital lobe occurs later in typical AD (Braak, 1989), visuospatial abilities include not only visual cues but spatial awareness as well. Therefore, impaired visual abilities, such as difficulty parking a car, misplacing items, or simply getting lost were reported in early AD (Bublak, 2011; Hamilton, 2009). On the other hand, perceptual speed is a measure of how quickly and accurately information can be processed. Perceptual speed may decline with aging, diabetes, depression, higher BMI, or alcohol consumption (Jaarsma, 2024). It has been shown that in MCI cases, the perceptual speed baseline was 40% lower compared to the cognitively normal controls (Bennett, 2002). Another study reported that perceptual speed can improve the accuracy of the clinical diagnosis of AD (Martorelli, 2020). Overall, our combined IHC and ELISA data revealed significant inverse correlations between increasing pS422 (IHC only), TOC1, TNT2 and TauC3 levels in all three DMN

hubs and poorer performance on composite test scores for both visuospatial ability and perceptual speed (Figures 3.2, 3.3; Tables 3.1, 3.2). There were a few notable exceptions, such as no significant associations between these cognitive measures and TOC1 and TauC3 levels in PCC and PreC. Moreover, performance on composite test scores for both visuospatial ability and perceptual speed generally correlated significantly with those of episodic and semantic memory in the RROS subjects (Figures 3.2, 3.3; Tables 3.1, 3.2). Given the additional roles of the DMN in mediating visuospatial ability (Gonzalez Alam, 2025) and perceptual speed (Staffaroni, 2018), our data suggest a relationship between the accumulation of tau pre-tangle markers in the DMN and deteriorating function in multiple cognitive domains. These data highlight the potential of the DMN as a model paradigm for studying mechanistic clinical pathology relationships in the context of a vulnerable connectome in AD.

Oligomeric Aβ Correlations with Cognitive Scores

Interestingly, MOAB-2 levels were strongly associated with pS422, TOC1, being the most correlated, and TNT2 levels in all three DMN regions, but they did not correlate with any of the cognitive scores or MMSE in FC or PreC (Figures 3.2, 3.3; Tables 3.1, 3.2). In contrast, MOAB-2 levels in PCC were significantly associated with episodic and semantic memory scores and performance on the MMSE. Together, these findings support the prevailing concept that tau pathology more strongly impacts cognitive decline than amyloid pathology, with new insights from a key resting state network. Further studies are needed to validate these results and explore the complex interplay between these co-pathologies.

Correlations between DMN pre-tangle tau markers and pathological scores

All three postmortem pathological scores (Braak, CERAD, and NIA-Reagan), which are used for diagnostic purposes to confirm or modify clinical diagnosis, highly correlated with the pS422, TNT2, and soluble TOC1 levels in the DMN hubs (Figures 3.4, 3.5, Tables 3.3, 3.4). All marker levels were correlated strongly with NFT burden especially in the IHC datasets, which is unsurprising. On the other hand, the tau markers correlated significantly with neuritic plaques (which have dense Aβ cores accompanied by dystrophic NFT+ neurites and surrounding NTs) but generally did not correlate with diffuse plaques (comprised of loosely accumulated fibrillar Aβ). It is worth mentioning that these pathological measures were taken from five different brain regions: Entorhinal cortex, hippocampus, angular gyrus, temporal and mid-frontal cortices. Although there is evidence for DMN connectivity with entorhinal cortex and hippocampus (Menon, 2023), only the mid-frontal cortex overlaps with the DMN regions examined in this study. However, our results suggest that DMN tau levels track well with global NFT and neuritic plaque burden and underscore the potential role of this brain connectome in driving tau-associated pathological progression in vulnerable cognitive brain regions.

CONCLUSION

In this postmortem study, we observed that pre-tangle tau was present at low Braak stages and significantly elevated as early as Braak stages IV to V in MADC and RROS cohorts, respectively (see Chapter 2), and closely correlated with cognitive decline, particularly in episodic and semantic memory. These findings are mirrored by the distribution of the global cognitive and neuropathological measures. Considering the

trend for higher pathology in the PCC in general compared to the PreC, in addition to the significantly higher correlation with the NFT measure and Braak stage with TNT2 positive tau, the possibility of differential vulnerability to pathological tau between the posterior DMN hubs will be explored in the next chapter using TNT2 pathology as our focal point.

REFERENCES

Ahn, S., Mathiason, M. A., Lindquist, R., & Yu, F. (2021). Factors predicting episodic memory changes in older adults with subjective cognitive decline: A longitudinal observational study. *Geriatr Nurs, 42*(1), 268-275. doi:10.1016/j.gerinurse.2020.08.016

Amieva, H., Le Goff, M., Millet, X., Orgogozo, J. M., Peres, K., Barberger-Gateau, P., . . . Dartigues, J. F. (2008). Prodromal Alzheimer's disease: successive emergence of the clinical symptoms. *Ann Neurol, 64*(5), 492-498. doi:10.1002/ana.21509

Backman, L., Small, B. J., & Fratiglioni, L. (2001). Stability of the preclinical episodic memory deficit in Alzheimer's disease. *Brain, 124*(Pt 1), 96-102. doi:10.1093/brain/124.1.96

Bateman, R. J., Xiong, C., Benzinger, T. L., Fagan, A. M., Goate, A., Fox, N. C., . . . Dominantly Inherited Alzheimer, N. (2012). Clinical and biomarker changes in dominantly inherited Alzheimer's disease. *N Engl J Med, 367*(9), 795-804. doi:10.1056/NEJMoa1202753

Bennett, D. A., Buchman, A. S., Boyle, P. A., Barnes, L. L., Wilson, R. S., & Schneider, J. A. (2018). Religious Orders Study and Rush Memory and Aging Project. *J Alzheimers Dis, 64*(s1), S161-S189. doi:10.3233/JAD-179939

Bennett, D. A., Wilson, R. S., Schneider, J. A., Evans, D. A., Beckett, L. A., Aggarwal, N. T., . . . Bach, J. (2002). Natural history of mild cognitive impairment in older persons. *Neurology, 59*(2), 198-205. doi:10.1212/wnl.59.2.198

Biel, D., Luan, Y., Brendel, M., Hager, P., Dewenter, A., Moscoso, A., . . . Alzheimer's Disease Neuroimaging, I. (2022). Combining tau-PET and fMRI meta-analyses for patient-centered prediction of cognitive decline in Alzheimer's disease. *Alzheimers Res Ther, 14*(1), 166. doi:10.1186/s13195-022-01105-5

Binder, J. R., & Desai, R. H. (2011). The neurobiology of semantic memory. *Trends Cogn Sci, 15*(11), 527-536. doi:10.1016/j.tics.2011.10.001

Bird, C. M., Keidel, J. L., Ing, L. P., Horner, A. J., & Burgess, N. (2015). Consolidation of Complex Events via Reinstatement in Posterior Cingulate Cortex. *J Neurosci, 35*(43), 14426-14434. doi:10.1523/JNEUROSCI.1774-15.2015

Borkowski, K., Taha, A. Y., Pedersen, T. L., De Jager, P. L., Bennett, D. A., Arnold, M., . . . Newman, J. W. (2021). Serum metabolomic biomarkers of perceptual speed in cognitively normal and mildly impaired subjects with fasting state stratification. *Sci Rep, 11*(1), 18964. doi:10.1038/s41598-021-98640-2

Braak, H., Braak, E., & Kalus, P. (1989). Alzheimer's disease: areal and laminar pathology in the occipital isocortex. *Acta Neuropathol, 77*(5), 494-506. doi:10.1007/BF00687251

Brandt, J., Aretouli, E., Neijstrom, E., Samek, J., Manning, K., Albert, M. S., & Bandeen-Roche, K. (2009). Selectivity of executive function deficits in mild cognitive impairment. *Neuropsychology, 23*(5), 607-618. doi:10.1037/a0015851

Brunoni, A. R., & Vanderhasselt, M. A. (2014). Working memory improvement with non-invasive brain stimulation of the dorsolateral prefrontal cortex: a systematic review and meta-analysis. *Brain Cogn, 86*, 1-9. doi:10.1016/j.bandc.2014.01.008

Bublak, P., Redel, P., Sorg, C., Kurz, A., Forstl, H., Muller, H. J., . . . Finke, K. (2011). Staged decline of visual processing capacity in mild cognitive impairment and Alzheimer's disease. *Neurobiol Aging, 32*(7), 1219-1230. doi:10.1016/j.neurobiolaging.2009.07.012

Bucci, M., Chiotis, K., Nordberg, A., & Alzheimer's Disease Neuroimaging, I. (2021). Alzheimer's disease profiled by fluid and imaging markers: tau PET best predicts cognitive decline. *Mol Psychiatry, 26*(10), 5888-5898. doi:10.1038/s41380-021-01263-2

Burke, S. N., & Barnes, C. A. (2006). Neural plasticity in the ageing brain. *Nat Rev Neurosci, 7*(1), 30-40. doi:10.1038/nrn1809

Camina, E., & Guell, F. (2017). The Neuroanatomical, Neurophysiological and Psychological Basis of Memory: Current Models and Their Origins. *Front Pharmacol, 8*, 438. doi:10.3389/fphar.2017.00438

Carretti, B., Borella, E., Fostinelli, S., & Zavagnin, M. (2013). Benefits of training working memory in amnestic mild cognitive impairment: specific and transfer effects. *Int Psychogeriatr, 25*(4), 617-626. doi:10.1017/S1041610212002177

Cassel, J. C., Cassel, D., & Manning, L. (2013). From Augustine of Hippo's Memory Systems to Our Modern Taxonomy in Cognitive Psychology and Neuroscience of Memory: A 16-Century Nap of Intuition before Light of Evidence. *Behav Sci (Basel), 3*(1), 21-41. doi:10.3390/bs3010021

Chatzikostopoulos, A., Moraitou, D., Tsolaki, M., Masoura, E., Papantoniou, G., Sofologi, M., . . . Papatzikis, E. (2022). Episodic Memory in Amnestic Mild Cognitive Impairment (aMCI) and Alzheimer's Disease Dementia (ADD): Using the "Doors and People" Tool to Differentiate between Early aMCI-Late aMCI-Mild ADD Diagnostic Groups. *Diagnostics (Basel), 12*(7). doi:10.3390/diagnostics12071768

Counts, S. E., Nadeem, M., Lad, S. P., Wuu, J., & Mufson, E. J. (2006). Differential expression of synaptic proteins in the frontal and temporal cortex of elderly

subjects with mild cognitive impairment. *J Neuropathol Exp Neurol, 65*(6), 592-601. doi:10.1097/00005072-200606000-00007

Cowan, N. (2008). What are the differences between long-term, short-term, and working memory? *Prog Brain Res, 169*, 323-338. doi:10.1016/S0079-6123(07)00020-9

Daselaar, S. M., Prince, S. E., Dennis, N. A., Hayes, S. M., Kim, H., & Cabeza, R. (2009). Posterior midline and ventral parietal activity is associated with retrieval success and encoding failure. *Front Hum Neurosci, 3*, 13. doi:10.3389/neuro.09.013.2009

Diedenhofen, B., & Musch, J. (2015). cocor: a comprehensive solution for the statistical comparison of correlations. *PLoS One, 10*(3), e0121945. doi:10.1371/journal.pone.0121945

Ekman, U., Eriksson, J., Forsgren, L., Mo, S. J., Riklund, K., & Nyberg, L. (2012). Functional brain activity and presynaptic dopamine uptake in patients with Parkinson's disease and mild cognitive impairment: a cross-sectional study. *Lancet Neurol, 11*(8), 679-687. doi:10.1016/S1474-4422(12)70138-2

Eriksson, J., Vogel, E. K., Lansner, A., Bergstrom, F., & Nyberg, L. (2015). Neurocognitive Architecture of Working Memory. *Neuron, 88*(1), 33-46. doi:10.1016/j.neuron.2015.09.020

Foudil, S. A., & Macaluso, E. (2024). The influence of the precuneus on the medial temporal cortex determines the subjective quality of memory during the retrieval of naturalistic episodes. *Sci Rep, 14*(1), 7943. doi:10.1038/s41598-024-58298-y

Gonzalez Alam, T. R. J., Krieger-Redwood, K., Varga, D., Gao, Z., Horner, A. J., Hartley, T., . . . Jefferies, E. (2025). A double dissociation between semantic and spatial cognition in visual to default network pathways. *Elife, 13*. doi:10.7554/eLife.94902

Haitas, N., Amiri, M., Wilson, M., Joanette, Y., & Steffener, J. (2021). Age-preserved semantic memory and the CRUNCH effect manifested as differential semantic control networks: An fMRI study. *PLoS One, 16*(6), e0249948. doi:10.1371/journal.pone.0249948

Hamilton, L., Fay, S., & Rockwood, K. (2009). Misplacing objects in mild to moderate Alzheimer's disease: a descriptive analysis from the VISTA clinical trial. *J Neurol Neurosurg Psychiatry, 80*(9), 960-965. doi:10.1136/jnnp.2008.166801

Hantke, N., Nielson, K. A., Woodard, J. L., Breting, L. M., Butts, A., Seidenberg, M., . . . Rao, S. M. (2013). Comparison of semantic and episodic memory BOLD fMRI activation in predicting cognitive decline in older adults. *J Int Neuropsychol Soc, 19*(1), 11-21. doi:10.1017/S1355617712000951

Hodges, J. R., & Patterson, K. (1995). Is semantic memory consistently impaired early in the course of Alzheimer's disease? Neuroanatomical and diagnostic implications. *Neuropsychologia, 33*(4), 441-459. doi:10.1016/0028-3932(94)00127-b

Hojjati, S. H., Feiz, F., Ozoria, S., Razlighi, Q. R., & Alzheimer's Disease Neuroimaging, I. (2021). Topographical Overlapping of the Amyloid-beta and Tau Pathologies in the Default Mode Network Predicts Alzheimer's Disease with Higher Specificity. *J Alzheimers Dis, 83*(1), 407-421. doi:10.3233/JAD-210419

Jaarsma, E., Nooyens, A., Kok, A. A. L., Kohler, S., van Boxtel, M., Verschuren, W. M. M., & Huisman, M. (2024). Modifiable Risk Factors for Accelerated Decline in Processing Speed: Results from Three Dutch Population Cohorts. *J Prev Alzheimers Dis, 11*(1), 108-116. doi:10.14283/jpad.2023.64

Kave, G., Samuel-Enoch, K., & Adiv, S. (2009). The association between age and the frequency of nouns selected for production. *Psychol Aging, 24*(1), 17-27. doi:10.1037/a0014579

Kimchi, R., Yeshurun, Y., Spehar, B., & Pirkner, Y. (2016). Perceptual organization, visual attention, and objecthood. *Vision Res, 126*, 34-51. doi:10.1016/j.visres.2015.07.008

Kirova, A. M., Bays, R. B., & Lagalwar, S. (2015). Working memory and executive function decline across normal aging, mild cognitive impairment, and Alzheimer's disease. *Biomed Res Int, 2015*, 748212. doi:10.1155/2015/748212

Krause, B. J., Schmidt, D., Mottaghy, F. M., Taylor, J., Halsband, U., Herzog, H., . . . Muller-Gartner, H. W. (1999). Episodic retrieval activates the precuneus irrespective of the imagery content of word pair associates. A PET study. *Brain, 122 (Pt 2)*, 255-263. doi:10.1093/brain/122.2.255

Krieger-Redwood, K., Jefferies, E., Karapanagiotidis, T., Seymour, R., Nunes, A., Ang, J. W. A., . . . Smallwood, J. (2016). Down but not out in posterior cingulate cortex: Deactivation yet functional coupling with prefrontal cortex during demanding semantic cognition. *Neuroimage, 141*, 366-377. doi:10.1016/j.neuroimage.2016.07.060

Lalla, A., Tarder-Stoll, H., Hasher, L., & Duncan, K. (2022). Aging shifts the relative contributions of episodic and semantic memory to decision-making. *Psychol Aging, 37*(6), 667-680. doi:10.1037/pag0000700

Lega, B., Germi, J., & Rugg, M. (2017). Modulation of Oscillatory Power and Connectivity in the Human Posterior Cingulate Cortex Supports the Encoding and Retrieval of Episodic Memories. *J Cogn Neurosci, 29*(8), 1415-1432. doi:10.1162/jocn_a_01133

Li, Y., Yao, Z., Yu, Y., Zou, Y., Fu, Y., Hu, B., & Alzheimer's Disease Neuroimaging, I. (2019). Brain network alterations in individuals with and without mild cognitive impairment: parallel independent component analysis of AV1451 and AV45 positron emission tomography. *BMC Psychiatry, 19*(1), 165. doi:10.1186/s12888-019-2149-9

Martorelli, M., Hartle, L., Coutinho, G., Mograbi, D. C., Chaves, D., Silberman, C., & Charchat-Fichman, H. (2020). Diagnostic accuracy of early cognitive indicators in mild cognitive impairment. *Dement Neuropsychol, 14*(4), 358-365. doi:10.1590/1980-57642020dn14-040005

McNab, F., & Klingberg, T. (2008). Prefrontal cortex and basal ganglia control access to working memory. *Nat Neurosci, 11*(1), 103-107. doi:10.1038/nn2024

Menon, V. (2023). 20 years of the default mode network: A review and synthesis. *Neuron, 111*(16), 2469-2487. doi:10.1016/j.neuron.2023.04.023

Moscovitch, M., Cabeza, R., Winocur, G., & Nadel, L. (2016). Episodic Memory and Beyond: The Hippocampus and Neocortex in Transformation. *Annu Rev Psychol, 67*, 105-134. doi:10.1146/annurev-psych-113011-143733

Moussavi, Z. (2022). Repetitive TMS applied to the precuneus stabilizes cognitive status in Alzheimer's disease. *Brain, 145*(11), 3730-3732. doi:10.1093/brain/awac322

Natu, V. S., Lin, J. J., Burks, A., Arora, A., Rugg, M. D., & Lega, B. (2019). Stimulation of the Posterior Cingulate Cortex Impairs Episodic Memory Encoding. *J Neurosci, 39*(36), 7173-7182. doi:10.1523/JNEUROSCI.0698-19.2019

Nelson, P. T., Jicha, G. A., Schmitt, F. A., Liu, H., Davis, D. G., Mendiondo, M. S., . . . Markesbery, W. R. (2007). Clinicopathologic correlations in a large Alzheimer disease center autopsy cohort: neuritic plaques and neurofibrillary tangles "do count" when staging disease severity. *J Neuropathol Exp Neurol, 66*(12), 1136-1146. doi:10.1097/nen.0b013e31815c5efb

Noroozian, M. (2016). Alzheimer's Disease: Prototype of Cognitive Deterioration, Valuable Lessons to Understand Human Cognition. *Neurol Clin, 34*(1), 69-131. doi:10.1016/j.ncl.2015.08.005

Nyberg, L. (2017). Functional brain imaging of episodic memory decline in ageing. *J Intern Med, 281*(1), 65-74. doi:10.1111/joim.12533

Renoult, L., Irish, M., Moscovitch, M., & Rugg, M. D. (2019). From Knowing to Remembering: The Semantic-Episodic Distinction. *Trends Cogn Sci, 23*(12), 1041-1057. doi:10.1016/j.tics.2019.09.008

Rogers, S. L., & Friedman, R. B. (2008). The underlying mechanisms of semantic memory loss in Alzheimer's disease and semantic dementia. *Neuropsychologia, 46*(1), 12-21. doi:10.1016/j.neuropsychologia.2007.08.010

Salimi, S., Irish, M., Foxe, D., Hodges, J. R., Piguet, O., & Burrell, J. R. (2018). Can visuospatial measures improve the diagnosis of Alzheimer's disease? *Alzheimers Dement (Amst), 10*, 66-74. doi:10.1016/j.dadm.2017.10.004

Salimi, S., Irish, M., Foxe, D., Hodges, J. R., Piguet, O., & Burrell, J. R. (2019). Visuospatial dysfunction in Alzheimer's disease and behavioural variant frontotemporal dementia. *J Neurol Sci, 402*, 74-80. doi:10.1016/j.jns.2019.04.019

Saunders, N. L., & Summers, M. J. (2011). Longitudinal deficits to attention, executive, and working memory in subtypes of mild cognitive impairment. *Neuropsychology, 25*(2), 237-248. doi:10.1037/a0021134

Scholl, M., Lockhart, S. N., Schonhaut, D. R., O'Neil, J. P., Janabi, M., Ossenkoppele, R., . . . Jagust, W. J. (2016). PET Imaging of Tau Deposition in the Aging Human Brain. *Neuron, 89*(5), 971-982. doi:10.1016/j.neuron.2016.01.028

Staffaroni, A. M., Brown, J. A., Casaletto, K. B., Elahi, F. M., Deng, J., Neuhaus, J., . . . Kramer, J. H. (2018). The Longitudinal Trajectory of Default Mode Network Connectivity in Healthy Older Adults Varies As a Function of Age and Is Associated with Changes in Episodic Memory and Processing Speed. *J Neurosci, 38*(11), 2809-2817. doi:10.1523/JNEUROSCI.3067-17.2018

Stopford, C. L., Thompson, J. C., Neary, D., Richardson, A. M., & Snowden, J. S. (2012). Working memory, attention, and executive function in Alzheimer's disease and frontotemporal dementia. *Cortex, 48*(4), 429-446. doi:10.1016/j.cortex.2010.12.002

Tchakoute, C. T., Sainani, K. L., Henderson, V. W., & Raloxifene in Alzheimer's Disease, I. (2017). Semantic Memory in the Clinical Progression of Alzheimer Disease. *Cogn Behav Neurol, 30*(3), 81-89. doi:10.1097/WNN.0000000000000131

Tromp, D., Dufour, A., Lithfous, S., Pebayle, T., & Despres, O. (2015). Episodic memory in normal aging and Alzheimer disease: Insights from imaging and behavioral studies. *Ageing Res Rev, 24*(Pt B), 232-262. doi:10.1016/j.arr.2015.08.006

Vana, L., Kanaan, N. M., Ugwu, I. C., Wuu, J., Mufson, E. J., & Binder, L. I. (2011). Progression of tau pathology in cholinergic Basal forebrain neurons in mild cognitive impairment and Alzheimer's disease. *Am J Pathol, 179*(5), 2533-2550. doi:10.1016/j.ajpath.2011.07.044

Vatansever, D., Smallwood, J., & Jefferies, E. (2021). Varying demands for cognitive control reveals shared neural processes supporting semantic and episodic memory retrieval. *Nat Commun, 12*(1), 2134. doi:10.1038/s41467-021-22443-2

Walker, M. P., & Stickgold, R. (2006). Sleep, memory, and plasticity. *Annu Rev Psychol, 57*, 139-166. doi:10.1146/annurev.psych.56.091103.070307

APPENDIX

Cognitive domain	Cognitive test
Episodic memory	Word list
	Word list recall
	Word list recognition
	East Boston immediate recall
	East Boston delayed recall
	Logical memory I (immediate recall)
	Logical memory II (delayed recall)
Semantic memory	Boston naming (15 items)
	Category fluency (animals-fruits/vegetables)
	Reading test (10 items)
Working memory	Digits forward
	Digits backward
	Digit ordering
	Symbol digit modalities test (oral)
Perceptual speed	Number comparison
	Stroop color naming
	Stroop word reading
Visuospatial ability	Line orientation
	Progressive matrices (16 items)
Global	MMSE
	Global Cognitive Score (GCS, a composite z score of the 19 tests)

Supplementary Table 3. 1 Cognitive tests that were used to evaluade the five memory components in the RROS cohort participants

CHAPTER 4: DIFFERENTIAL PROTEIN INTERACTION NETWORKS OF PRE-TANGLE TAU IN THE POSTERIOR DMN

INTRODUCTION

Proteins do not function as a single entity but as interacting players (protein-protein interactions) or as members of a whole team (protein complexes). Hence, to elucidate the etiology of diseases, we need to understand how disease-associated proteins mechanistically work in concert with their binding partners both in health and disease. As mentioned in the first chapter, tau is an intrinsically disordered/unfolded protein (IDP). In contrast to folded proteins, which have well-defined structures and need to fold into a certain conformation to function, IDPs or IDP regions do not need to be folded to bind to their partners (Uversky, 2018; Uversky, 2013). Instead, they can simultaneously fold while binding or fold afterward, which gives them an incredible amount of flexibility to interact with so many partners without requiring conformational pockets to bind, which makes them advantageous for interaction and for regulating a diverse array of cellular pathways (Dyson, 2016; Mueller, 2021). They are even referred to as “interaction specialists” due to their ability to adapt and change functional conformations upon binding (Uversky, 2018).

There are multiple techniques that can be leveraged to study protein-protein interactions such as co-immunoprecipitation, pull-down assays, proximity-based tagging systems, yeast-two hybrid systems, mass spectrometry, affinity chromatography, X-ray crystallography, NMR spectroscopy, as well as in silico tools (Hayes, 2016; Slater, 2020; Elhabashy, 2022; Soleymani, 2022). Although each method has strengths and weaknesses (Miura, 2018), co-immunoprecipitation coupled with mass spectrometry is preferred by many due to the high specificity provided by specific antibodies precisely targeting the protein of interests.

The tau interactome has been studied in the context of health and disease (Davies, 2024; Gunawardana, 2015; Betters, 2023; Tracy, 2022), emphasizing axonal, synaptic and mitochondrial interactions (Tracy, 2022) in addition to its RNA binding partners, among others (Kavanagh, 2022). In the context of AD, the tau interactome has been investigated mostly through co-immunoprecipitation in the frontal or temporal cortices using total tau antibodies (mostly Tau5 and Tau13) (Younas, 2024; Maziuk, 2018) and found several binding partners that are involved in such diverse processes as trafficking, mitochondrial function, apoptosis, ubiquitination, microglia activation, aberrant stress granules, and endoplasmic reticulum function, all of which have been implicated in neurodegeneration (Younas, 2024; Younas, 2023; Wei, 2022; Zhang, 2024; Meier, 2015; Abreha, 2021).

As previously mentioned in Chapter 1, AD-related tau has been investigated predominantly in the temporal and frontal lobes of the brain due to either tau trajectory or the vulnerability of those higher-order brain areas that control memory and critical thinking & executive function, respectively (Friedman, 2022; Simons, 2003). With the discovery of the large-scale brain networks and the formation of the Network Degeneration Hypothesis (NDH), which proposes that AD pathology and the consequent neurodegeneration proceed along with functionally connected brain regions (Tahmasian, 2016), we need a more comprehensive approach to study how pathological tau behaves in those regions at the cellular and connectome level. Consistent with the overarching hypothesis of this thesis work, we posit that the default mode network (DMN) is an excellent candidate for investigating this paradigm. From a technical perspective, it is expected that DMN functional connectivity (fc) would be the

subject of imaging-based studies in the clinic. However, there is now an urgent need to conduct more basic research on the mechanistic players mediating putative links between tau pre-tangle pathology and cognitive decline.

Most human tissue-based AD mechanistic studies have been focused on gene expression changes during AD progression by conducting bulk microarray or RNA sequencing in regions vulnerable to tau pathology, including the dorsolateral prefrontal cortex (DLPFC) and posterior cingulate cortex (PCC) of the DMN (Guennewig, 2021; O'Neill, 2024; Sobue, 2021). There are also groups that use laser capture microdissection to target distinct cell types or perform single-cell RNA seq from bulk tissue to investigate cell type-specific and regional-specific vulnerability (Wang, 2016). A major cellular mechanism shown to be impacted in the DMN during AD is related to inflammation. Sekar et al. detected mitochondrial DEGs in PCC astrocytes, possibly contributing to the energy metabolism failure in AD (Sekar, 2015). They also found associations between those DEGs and amyloid clearance. Winfree et al. did a bulk RNA seq in the DLFPC and PCC to investigate expression profiles of TREM2, an AD risk gene, in a large RROS cohort (which is described and used in Chapters 2 & 3). Similar TREM2 levels in the NCI and MCI cases while the expression was significantly elevated in the AD cases (2249). Another study found a decrease in the homeostatic microglial genes in the precuneus (PreC) (Sobue, 2021).

The second commonly altered cellular pathway in DMN samples during AD is cytoskeleton rearrangements related to structural integrity. RNA seq in the laser-captured neurons (Liang, 2008) and microarray analysis (Ray, 2010) from PCC in AD samples from two studies commonly found expression changes in the genes that are

involved in actin cytoskeleton changes. Similar results were shown later in a larger study by Wang et al. They performed a comprehensive assessment of selective vulnerability to AD by looking at DEGs in 19 brain regions (including the medial frontal cortex (mFC), PCC, and PreC) from a large spectrum of AD samples (Wang, 2016). Their results showed that two cytoskeleton-related pathways were among the top-ranked gene set modules associated with the DEGs, although temporal regions demonstrated the most significant gene changes, possibly due to more advanced pathology in these regions.

Interestingly, posterior DMN regions, PCC and PreC, have gained attention due to their potential role in resilience and/or resistance to AD pathology. We and others previously have shown differential micro-RNA profiles in the PCC in resilient cases (Kelley, 2024; Kelley, 2022; Perez, 2015). PreC has also been shown to preserve neurotrophic signaling despite the presence of amyloid plaques in prodromal AD cases (Perez, 2015).

These gene expression data are extremely important to exploring mechanistic changes at the transcriptomic level within the DMN, some of which may be related to tau pathology. However, they lack the aspect of possible functional interactions and communication at the proteomics level. This study is the first in this regard to investigate early pathological tau interactome in the posterior DMN. Our first goal was to define the binding partners of the pre-tangle marker TNT2 in the posterior DMN hubs from MCI and AD cases. Our second goal is to investigate potential regional differences between the PCC and PreC, as PCC demonstrated higher pre-tangle tau pathology levels in these hubs, whereas PreC pathology lagged suggesting potential

resistance. PCC and PreC also differed in their strength of correlation with Brak stage (Chapter 3, Table 3.5). Hence, we hypothesized that differential protein-protein interaction profiles of pre-tangle tau in PCC and PreC may differentiate tau pathways related to regional vulnerability. To test this hypothesis, we performed co-immunoprecipitation (IP) experiments in soluble PCC and PreC fractions using the TNT2 antibody followed by a mass spec analysis.

Our rationale for selecting TNT2 as our representative pre-tangle marker for IP was three-fold:

- Among the pre-tangle tau markers, pS422 and TNT2 showed the highest correlations with the MMSE and GCS scores with immunohistochemical quantification (Chapter 3, Figure 3.3). Although TOC1 better correlated with the cognitive scores in the soluble fraction, its correlations were considerably weaker in the immunohistochemical quantification.
- TNT2 more significantly correlated with Braak stage and neuritic plaque density in the PCC than the other markers (Chapter 3, Table 3.2).
- Technical/practical issues: The concentration of the commercial pS422 antibody was too dilute for IP. TOC1 as another alternative was also challenging due to the pentameric structures of IgM antibodies that do not bind Protein A or Protein G beads well. Therefore, TNT2 was the best candidate to further investigate protein binding partners of early pathological DMN tau and, importantly, our pilot studies demonstrated the feasibility of using this antibody (see below).

MATERIALS AND METHODS

Case Selection

Frozen PCC and PreC tissue blocks from the low-Braak/control (Braak stages I-II, n=6), mid-Braak (Braak stages III-IV, n=7), and high-Braak (Braak stages V-VI, n=5) MADC clinical cohort subjects (McKay, 2019) as described in Chapters 2 and 3. The subjects underwent routine antemortem Mini-Mental State Examination (MMSE) evaluations and postmortem neuropathological diagnostic analysis, including Braak staging (McKay, 2019).

Tissue homogenization and Immunoprecipitation (IP) with TNT2

300ug frozen tissue from each region and each case was collected into buffer A (20mM Tris base, 150mM NaCl, 1mM EDTA, 1mM EGTA, 5mM sodium pyrophosphate, 1x protein inhibitor cocktail (Thermo Fisher Scientific, #1861281)) and homogenized with a Tissue Tearor rotor-stator on ice. The homogenate was then centrifuged at 18,000 x *g* for 10 minutes to obtain the post-nuclear supernatant (PNS). For pre-clearing, PNS was transferred to a clean tube to be incubated with prewashed magnetic beads (Thermo Fisher Scientific, #88803) on a rotator at 4C for 3h followed by BCA (Thermo Fisher Scientific, A53226) protein quantification. 2mg of PNS from each sample was then incubated with either 2ug of TNT2 antibody (provided by Dr. Nicholas Kanaan, Michigan State University) or buffer A as the beads-only controls overnight on the rotator at 4C. The following day 40ul beads were added to the samples to pull down TNT2 bound tau and its binding partners. The remaining PNS flowthrough was saved for western blot validations for IP. 10ul of the immunoprecipitated material was also used for western blot

analysis, and the remaining 30ul was saved for enzyme digestion and subsequent mass spectrometry analysis.

Western blotting

Pre-cleared samples, IP beads with tau, and post-IP flowthrough samples were added into Laemmli sample buffer and boiled for 10min for protein reduction and elution of beads- bound tau. The samples were run on a 4–20% Criterion TGX Precast Midi Protein Gel (#5671095) and transferred to a nitrocellulose membrane. After total proteins were visualized with Ponceau stain, the membrane was blocked with 2%milk in TBS for one hour prior to the overnight primary incubation with a total tau antibody (R1, 1:200,000, provided by the Kanaan Laboratory, Michigan State University). The next day, IRDye 680LT conjugated anti-rabbit IgG secondary (1:5,000, LI-COR, #926-68021) was added to the membrane for one hour on the shaker, and the membrane was imaged with a LI-COR imager.

Enzyme Digestion and Mass Spec Analysis

The beads were washed three times in 25 mM ammonium bicarbonate (pH 8) (AMBIC) and then resuspended in 100µl of 25 mM AMBIC/50% acetonitrile (ACN). On-bead protein digestion was performed by adding 500 ng of rLys-C (Promega, #V1671) and incubating for 90 minutes at 37°C, then adding 1 µg trypsin (Promega, #V5280) and incubating for 16-18 hours at 37°C. The tubes were placed on a magnetic separation stand, and the supernatant was collected. Samples were dried to completion in a speed vacuum centrifuge at 30 °C before resuspending in 50 µl of 2% ACN, 0.1% formic acid (FA).

NanoLC-MS/MS separations were performed with a Thermo Scientific Ultimate 3000 RSLCnano System. Peptides were desalted in-line using a 3 μm diameter bead C18 column (75 μm × 20 mm) with 2% ACN, 0.1% FA for 8.75 min with a flow rate of 2 μl/min at 40°C. The trap column was then brought in-line with a 2 μm diameter bead, C18 EASY-Spray column (75 μm × 250 mm) for analytical separation over 127.5 min with a flow rate of 350 nl/min at 40°C. The mobile phase consisted of 0.1% FA (buffer A) and 0.1% FA in ACN (buffer B). The separation gradient was as follows: 8.75 min desalting, 98.75 min 4–40% B, 2 min 40–65% B, 3 min 65–95% B, 11 min 95% B, 1 min 95–4% B, 3 min 4% B. 5 μl of each sample were injected.

Top 20 data-dependent mass spectrometric analysis was performed with a Q Exactive HF-X Hybrid Quadrupole-Orbitrap Mass Spectrometer. MS1 resolution was 60K at 200 m/z with a maximum injection time of 45 ms, AGC target of 3e6, and scan range of 300–1500 m/z. MS2 resolution was 30K at 200 m/z, with a maximum injection time of 54 ms, AGC target of 1e5, and isolation range of 1.3 m/z. HCD normalized collision energy was 28. Only ions with charge states from +2 to +6 were selected for fragmentation, and dynamic exclusion was set to 30 s. The electrospray voltage was 1.9 kV at a 2.0 mm tip to inlet distance. The ion capillary temperature was 280°C and the RF level was 55.0. All other parameters were set as default.

Protein identification was conducted by Proteome Discoverer Software version 2.5.0.400. Spectra were searched with Sequest against the combined reviewed Homo sapiens Uniprot protein database (UP000005460), including contaminant sequences, trypsin (Acc: P00761), and LysC (Acc:Q02SZ7). Enzyme specificity was set to trypsin, allowing up to 2 missed cleavages with an MS1 tolerance of 10 ppm and a fragment

tolerance of 0.02 Da. Oxidation (M), biotinylation (K), acetylation (protein N-term), methionine loss (protein N-term) as dynamic modifications. Peptide and protein false discovery rates (FDR) were 1% with threshold determined via the Percolator node. At least two peptide identifications were required per protein identification. Peptide confidence was set to “High”. Label free quantitative values were determined using the Precursor Ion Quantifier node with normalization via Total Peptide Amount. The protein abundance ratio was calculated using pairwise ratios (excluding modified peptides). All other parameters were set as default.

Data curation was performed based on the criteria below:

- Proteins detected in each clinical group was compared to a respective beads-only control; and anything having Abundance ratio [sample/beads only] <1 was excluded from further analysis.
- Proteins identified in less than half of the experimental replicates of one clinical group were excluded from further analysis, as were all keratins, digestion enzymes, and common contaminants.
- Proteins from mid-Braak (n=7) and high-Braak (n=5) samples were compared to the low-Braak samples (=6) to calculate abundance ratios and adjusted p-values, which were set to 0.05. For differential binding partner between the regions, PCC and PreC protein lists were compared each other within each clinical group.

RESULTS

MADC Cohort Demographics

Demographics for this subset of cases from the main MADC cohort (Chapter 2&3) are summarized in Table 4.1. The subjects did not differ in age, sex, or PMI across the

low-Braak, mid-Braak, and high-Braak groups. Although there was a trend for lower MMSE in the high-Braak group, it did not reach significance (p=0.0676) (Table 4.1).

	Clinical diagnosis				Comparison by diagnosis group
	Low-Braak (n=6)	Mid-Braak (n=7)	High-Braak (n=5)	Total (n=18)	(*P* value)
Age at death (years)					
Mean ± SD	75.8 ± 7.7	83 ±8.7	76.4 ± 5.8	78.8 ± 8.0	0.2105
(Range)	(65-87)	(68-95)	(69-83)	(65-95)	
No. (%) Males	4 (66.7%)	3 (57.1%)	2 (40%)	9 (50%)	0.6036‡
Postmortem Interval (hours)					
Mean ± SD	11.3 ± 8.5	8.6 ± 5.3	9.6 ± 5.5	10.5 ± 6.4	0.7495
(Range)	(4-26)	(4-17)	(7-21)	(4-26)	
MMSE					
Mean ± SD	27 ± 2	17.3 ±11.2	8.1 ± 6.9	12.4 ± 6.2	0.0676
(Range)	(24-28)	(4-29)	(3-18)	(3-29)	
Braak Scores					
I-II	6	0	0	6	<0.0001****
III-IV	0	7	0	7	
V-VI	0	0	5	5	

*Table 4. 1 Demographic, Clinical, and Pathological Profile of the MADC cohort Pairwise comparisons showed no difference between the groups for age, sex, PMI, or MMSE. Braak scores were decreased across the groups. MMSE: Mini-Mental State Examination, SD: Standard deviation; ‡ Chi-Square test; p<0.0001*****

Pilot TNT2 Immunoprecipitation

TNT2+ positive tau and associated proteins were pulled down with magnetic beads as described in the methods section, with one low-Braak and one high-Braak pilot study from frontal cortex (FC) samples. Beads-precleared input,

immunoprecipitated proteins beads pellet that was resuspended in AMBIC and post IP flowthrough were boiled with Laemmli sample buffer and ran on an SDS gel and probed with R1, a total tau antibody. As shown in Figure 4.1A, some TNT2 tau around 75kDa was pulled down in the control cases, and the green bands were in the second well from the left. In high-Braak cases, higher molecular bands appeared in the IP well, third well from the right. Since this was a TNT2-specific immunoprecipitation, the total tau bands in the PostIP wells were expected. The red signal shows the TNT2 antibody (mouse IgG1) itself, which was digested into its heavy and light chains through reduction with boiling in Laemmli buffer. The final well contains just TNT2 antibody in the buffer and was included as a control. After the successful IP was shown, another pilot experiment was set for another low- and high-Braak pair in the PCC samples (Figure 4.1B). The same steps were repeated, and similar blots were generated.

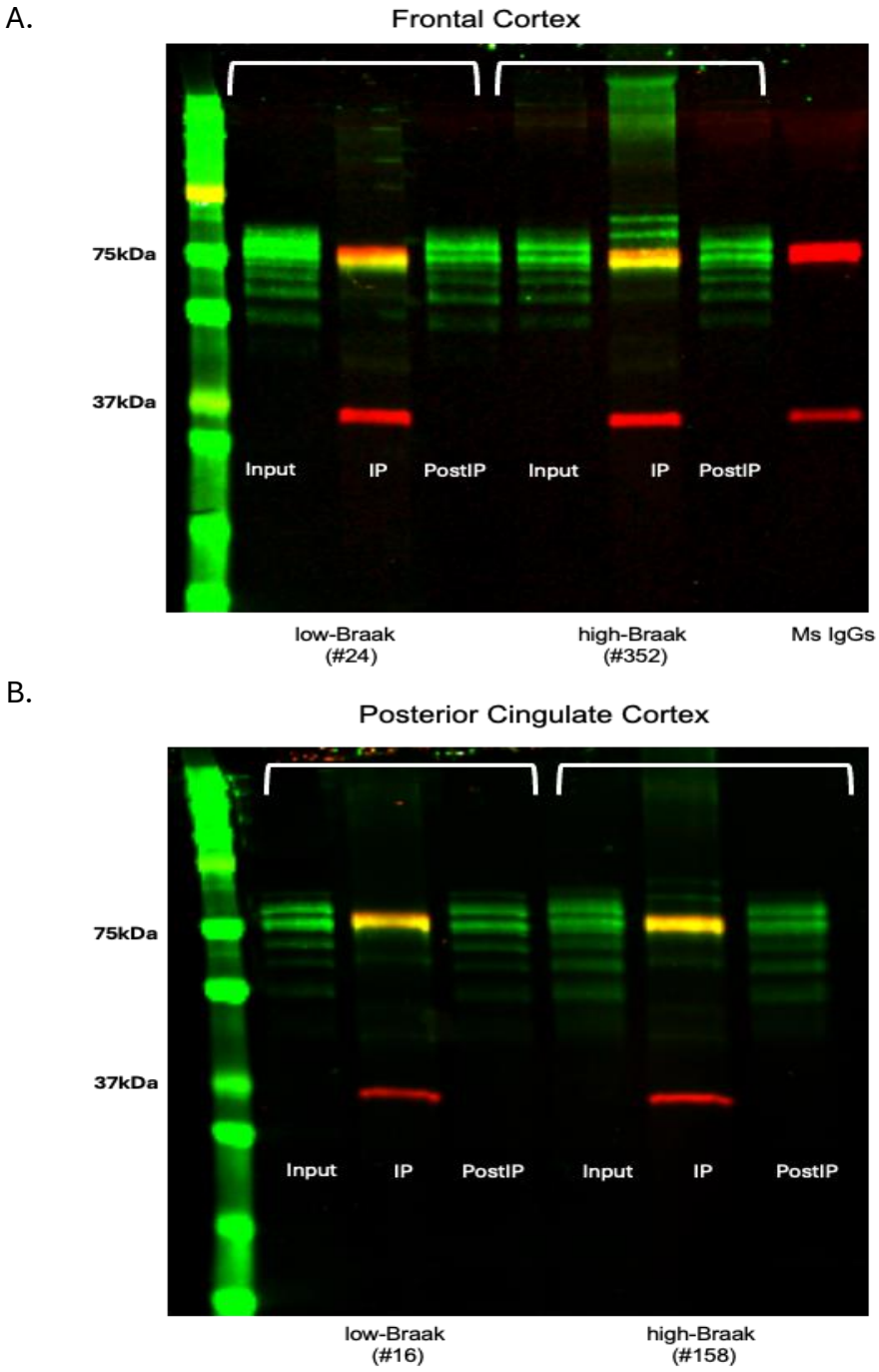

Figure 4. 1 Pilot IPs in the FC and PCC

TNT2 positive tau was pulled down and probed for a total tau antibody (R1, 1:200,000). Green channel shows IRDye 680LT conjugated anti-rabbit secondary (1:20,000) that

Figure 4. 1 (cont'd)

recognizes R1, and red channel shows IRDye800CW conjugated anti mouse secondary (1:20,000).

Validation of TNT2 Immunoprecipitation Prior to Mass Spec

After confirming a successful pull-down of TNT2 positive tau in the FC and PCC, the actual samples were processed, used for IP, and subsequent western blotting on two membranes in the same way described before (Figure 4.2A, 4.2B). Similar to the pilot studies, higher molecular tau bands started to appear gradually in low to high-Braak cases.

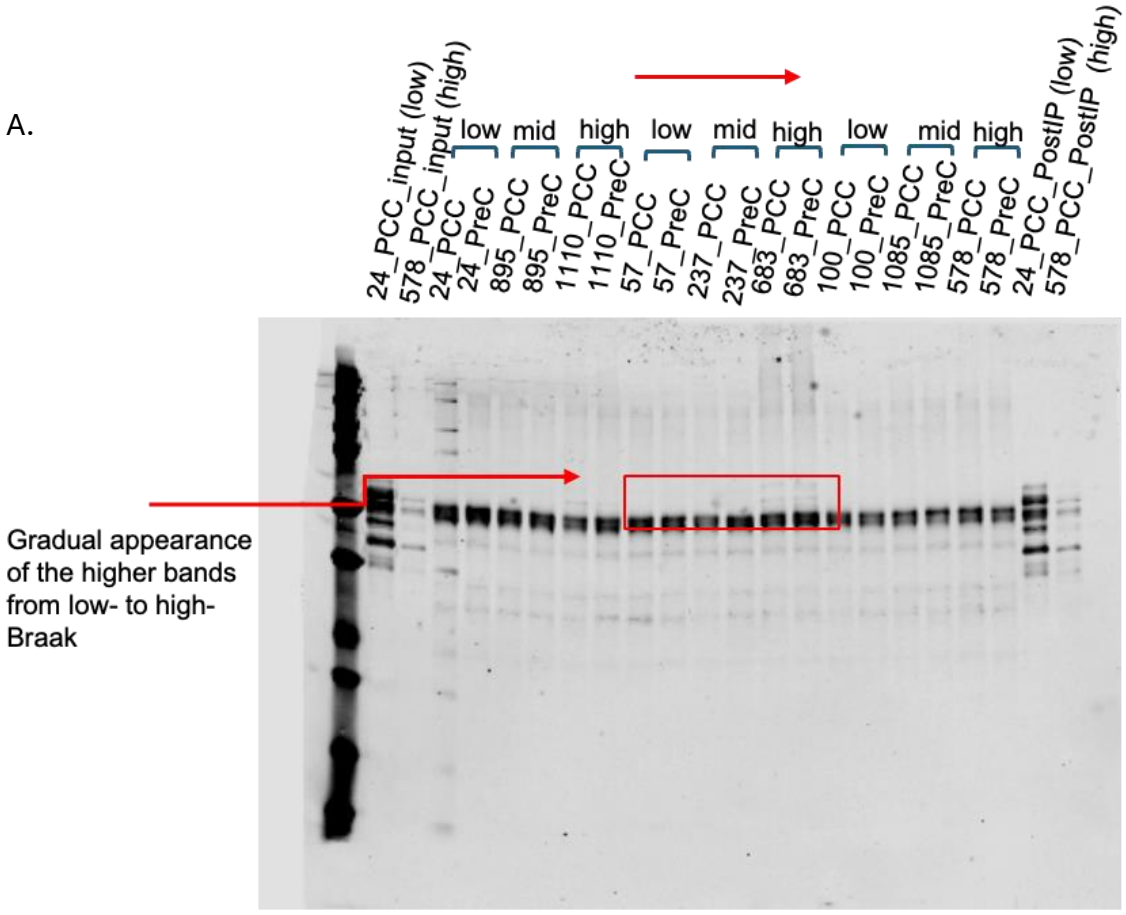

Figure 4. 2 Western blot validation of the IP in (A) sampel set1 and (B) sample set2 before proceeding to the mass spec analysis

Figure 4. 2 (cont'd)

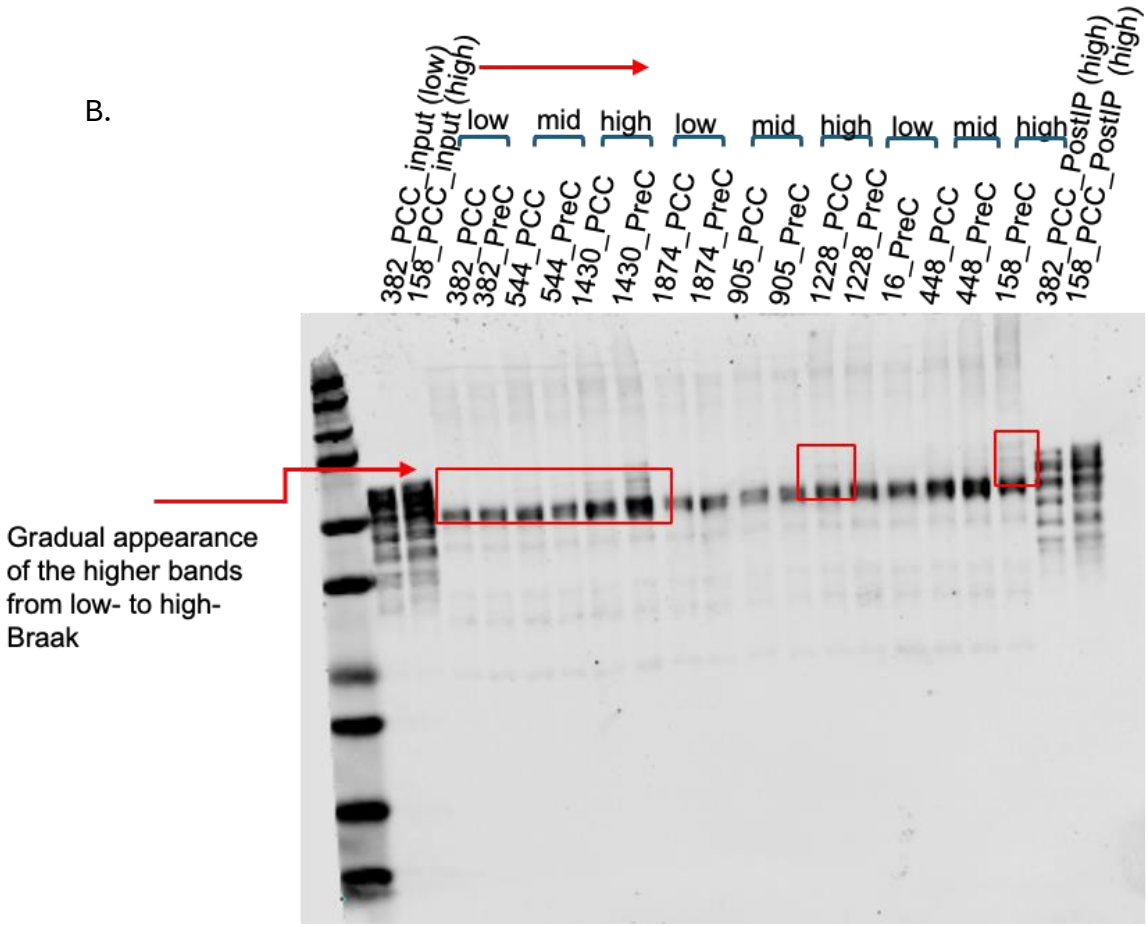

The samples were run on an SDS-gel and developed on a nitrocellulose membrane to be probed with R1 antibody and an IRDye 680LT conjugated anti-rabbit secondary. The signal was then visualized as black & white for better visibility.

Mass Spec Analysis

Based on the inclusion/exclusion criteria described in the Methods section, 569 total proteins (28 significant) in PCC and 511 total proteins (17 significant) in PreC were detected in the mid-Braak samples (Table 4.2). The proteins in red font indicate the detection only in the mid-Braak samples, as opposed to no detection in the low-Braak/control samples. The nuance is that, as mentioned in detail in the Introduction,

tau is an intrinsically disordered protein and potentially has various physiological binding partners (Brandt, 2020). Some of those interactions are expected to be seen in various stages of pathological tau formation. Since TNT2 recognizes an aberrant post-translational modification (PTM, PAD domain exposure, Chapters 1 & 2), this epitope is likely in low abundance in the DMN of control cases. Hence, the proteins detected only in the mid- and high-Braak groups may potentially be pathological binding partners. However, this requires further functional investigation.

Also, three MAPT isoforms were detected in the mid-Braak samples and four were in the high-Braak samples in both regions. Notably, the 2N4R isoform (P10636-8), which is often used to refer to mutations in tau according to the UniPort Consortium (UniProt, 2025), was not detected in any of the control cases except for one PCC sample.

mid-Braak							
Accession	Gene symbol **PCC**	Adj p-value	Abundance (mid>low-braak)	Accession	Gene symbol **PreC**	Adj p-value	Abundance (mid>low-braak)
P10636-8	MAPT	3.11061E-16	10.218	O00571	DDX3X	4.13737E-16	100
P09455	RBP1	3.11061E-16	100	Q9BW62	KATNAL1	4.13737E-16	100
Q9NT62	ATG3	3.11061E-16	100	P08754	GNAI3	4.13737E-16	100
P48444	ARCN1	3.11061E-16	100	Q5JT25	RAB41	4.13737E-16	100
Q7L266	ASRGL1	7.08238E-09	6.116	P10636-8	MAPT	4.13737E-16	100
Q8N4C8	MINK1	2.02771E-07	0.249	O75155	CAND2	4.13737E-16	100
P62979	RPS27A	2.66914E-05	3.136	P29508	SERPINB3	1.54879E-11	6.727
P46782	RPS5	8.79971E-05	2.981	P19338	NCL	1.59184E-05	3.718
P62249	RPS16	0.000505601	2.731	O00562	PITPNM1	0.000277063	3.168
Q13428	TCOF1	0.000947028	0.483	O43295	SRGAP3	0.001077489	2.9
O00116	AGPS	0.001589025	0.25	Q13630	GFUS	0.001346933	2.854
P62913	RPL11	0.004569454	2.677	P08962	CD63	0.006001061	2.575
P23396	RPS3	0.00501414	2.415	P10606	COX5B	0.007759517	0.368
Q5HYI7	MTX3	0.005242059	2.522	P62979	RPS27A	0.011588685	2.442
Q6IQ20	NAPEPLD	0.006213561	0.389	Q16720	ATP2B3	0.028124182	0.409
P18428	LBP	0.007349018	0.361	Q16777	H2AC20	0.032054125	2.239
O00499-2	BIN1	0.008622541	2.715	O43866	CD5L	0.043971574	2.172
Q9UHQ9	CYB5R1	0.010176072	3.591				
P62701	RPS4X	0.010514548	2.299				
Q8N1F7	NUP93	0.012476204	2.275				
P11166	SLC2A1	0.014143955	0.445				
Q9UKF7	PITPNC1	0.014911521	0.354				
O14910	LIN7A	0.015343857	0.393				
P29508	SERPINB3	0.018985964	0.544				
O14576	DYNC1I1	0.019724071	0.335				
Q9NTG7	SIRT3	0.035120165	3.121				
P01008	SERPINC1	0.037314762	3.122				
Q9HCM2	PLXNA4	0.03989587	2.18				

Table 4. 2 Significantly pulled-down proteins in mid-Braak stage cases compared to the controls in posterior DMN regions

The proteins in red font were not detected in control samples.

To investigate the possible interactions between the significantly detected proteins based on the previously known interaction patterns from numerous databases (KEGG, Gene Ontology, Reactome Pathway, etc.), we utilized the STRING database to create the interaction map shown in Figure 4.3.

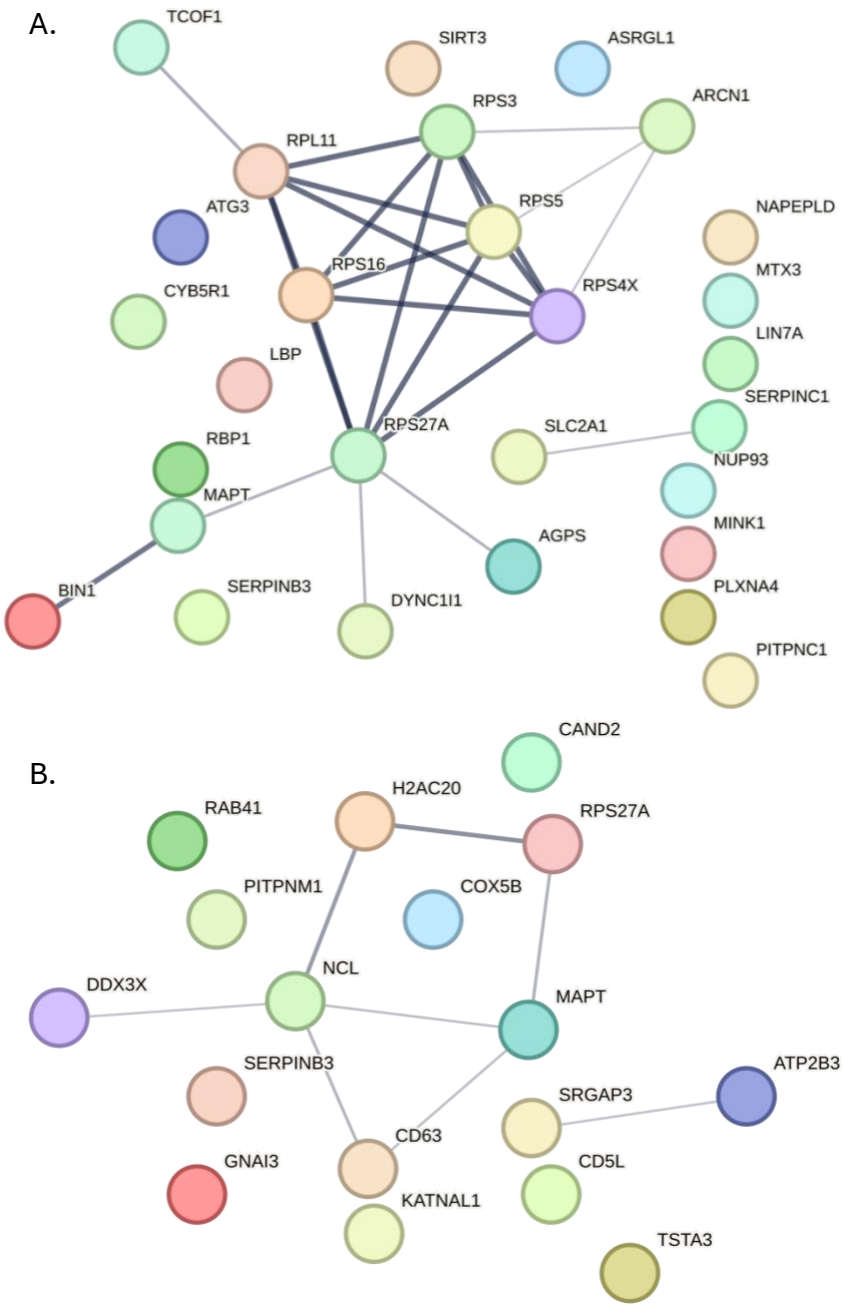

Figure 4. 3 STRING interaction map of TNT2 binding partners detected in mid-Braak stages

A. Proteins detected in PCC. B. Proteins detected in PreC. The line thickness of the edges indicates the strength of data support. The minimum required interaction score was set to medium confidence (0.400).

In high-Braak cases, 422 total proteins (31 significant) in PCC and 578 total proteins (15 significant) in PreC were detected (Table 4.3). Similar to the previous table, proteins that were detected only in the high-Braak cases are shown in red font. There were a few overlapping proteins detected in both regions, such as RPS27A, SPATS2L, NAP1L5, and H2BC18, compared to the two overlapping proteins, RPS27A and SERPINB3, between the PCC and PreC samples in the mid-Braak cases. Interestingly, RPS27A, a multifunctional ribosomal protein, (Luo, 2023) was the only protein detected in both regions in both groups. It also appeared to be a hub protein in the interaction maps (Figure 4.3 & 4.4).

high-Braak							
Accession	Gene symbol **PCC**	Adj p-value	Abundance (high>low-braak)	Accession	Gene symbol **PreC**	Adj p-value	Abundance (high>low-braak)
P62979	RPS27A	1.61389E-16	9.903	O75155	CAND2	1.85434E-16	100
P10636-6	MAPT	1.61389E-16	18.775	Q9BW62	KATNAL1	1.85434E-16	100
Q5QNW6	H2BC18	1.61389E-16	19.005	Q5JT25	RAB41	1.85434E-16	100
O95865	DDAH2	1.61389E-16	45.192	Q9NUQ6	SPATS2L	1.85434E-16	100
P13762	HLA-DRB4	1.61389E-16	100	P10636-8	MAPT	1.85434E-16	100
O15427	SLC16A3	1.61389E-16	100	P62979	RPS27A	1.79937E-12	18.975
Q9NUQ6	SPATS2L	1.61389E-16	100	Q5QNW6	H2BC18	3.14778E-05	6.238
P00488	F13A1	1.61389E-16	100	Q8TBF8	FAM81A	5.65817E-05	5.931
Q96MF6	COQ10A	2.15798E-09	5.68	P29508	SERPINB3	0.000425087	4.933
P47929	LGALS7	8.75617E-08	4.776	P26599	PTBP1	0.000658521	0.156
Q9Y2Z9	COQ6	5.54029E-05	0.193	P19338	NCL	0.000893747	4.585
P61225	RAP2B	0.000481728	4.706	Q96NT1	NAP1L5	0.002598809	4.116
Q02246	CNTN2	0.000562045	3.156	P07476	IVL	0.020195325	3.235
Q9Y5X3	SNX5	0.002450757	0.259	P53618	COPB1	0.025518479	3.141
Q9HD42	CHMP1A	0.003226669	4.086	Q9BUF5	TUBB6	0.040742533	0.25
P10599	TXN	0.005429169	2.767				
Q00839	HNRNPU	0.006655616	3.762				
Q7L266	ASRGL1	0.007158696	2.725				
P17980	PSMC3	0.007215745	3.064				
P14136	GFAP	0.008467572	2.351				
P02788	LTF	0.010272337	0.332				
Q8N4C8	MINK1	0.011160823	0.316				
P62328	TMSB4X	0.011843515	2.961				
Q92817	EVPL	0.017971842	2.196				
P15927	RPA2	0.020910395	0.324				
P35754	GLRX	0.021539012	0.261				
Q6NVY1	HIBCH	0.021539012	2.265				
P0CG47	UBB	0.02249283	2.982				
P08670	VIM	0.022714354	2.139				
Q96NT1	NAP1L5	0.024314744	2.256				
Q92982	NINJ1	0.04816227	2.924				

Table 4. 3 Significantly pulled-down proteins in high-Braak stage cases compared to the controls in posterior DMN regions

The proteins written with red ink indicate detection only in the high-Braak cases within the inclusion criteria used for data curation.

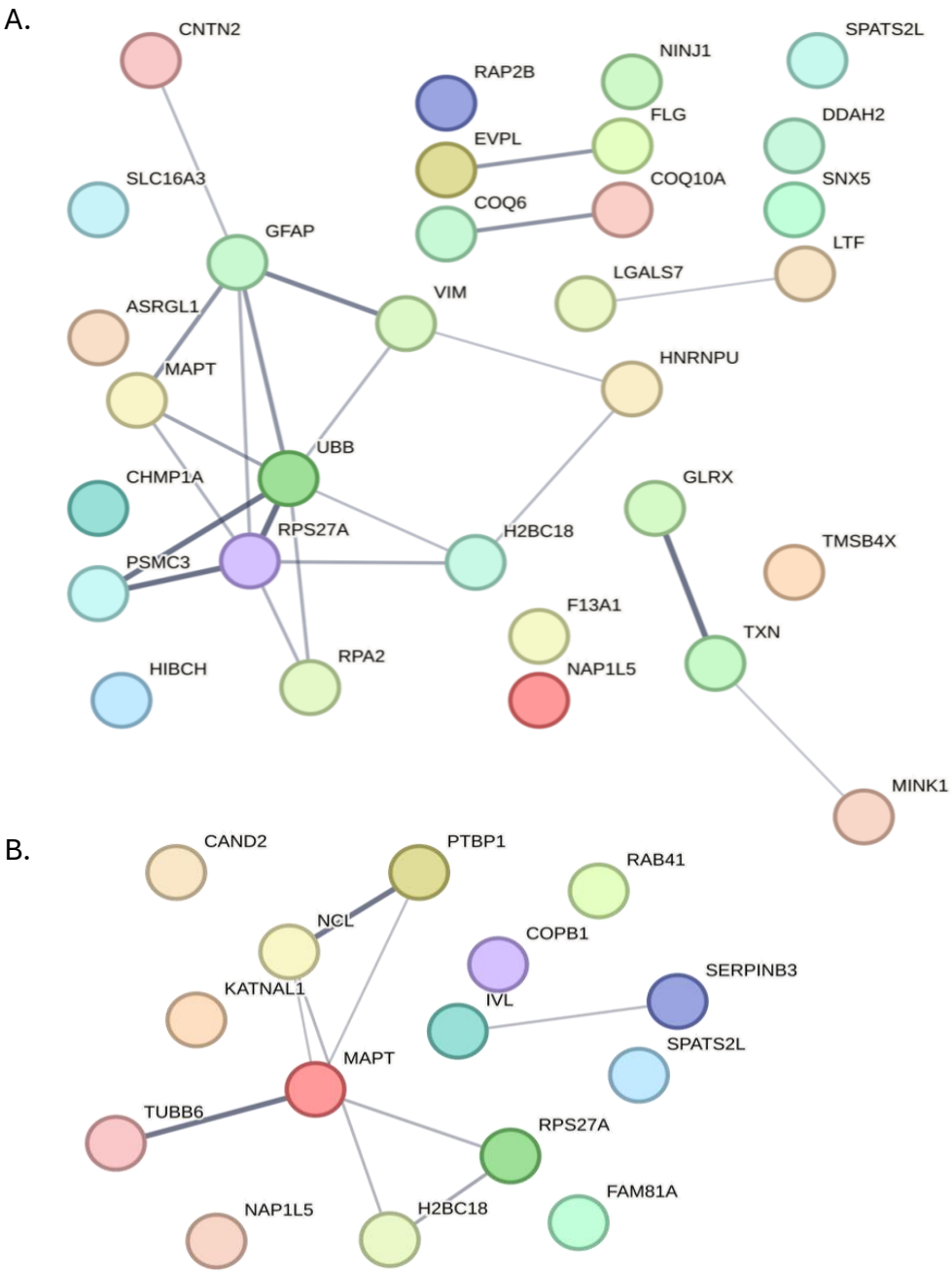

Figure 4. 4 STRING interaction map of TNT2 binding partners detected in high-Braak stages

A. Proteins detected in PCC. B. Proteins detected in PreC. The line thickness of the edges indicates the strength of data support. The minimum required interaction score was set to medium confidence (0.400).

As an overall pattern, more protein showing increased TNT2 binding were detected in the PCC with a differential expression compared to the PreC in both groups compared to controls, which may form a basis for regional differences, as PCC profiling more deviant protein levels or protein-protein interactions compared to the controls. Due to the low number of significant proteins, the STRING database could define biological pathways that those proteins collectively involve.

Early vs Late Changes in the Reactome Pathways

Besides studying PCC vs PreC protein partners of tau, we were also interested in understanding the functional pathways associated with activities of TNT2 tau-binding partners as the disease progresses. Therefore, we combined the protein lists from both regions in either mid-Braak or high-Braak case to perform a pathway enrichment analysis in STRING website to investigate the biological pathways that may be impacted from mid-stage of AD to the advanced stages.

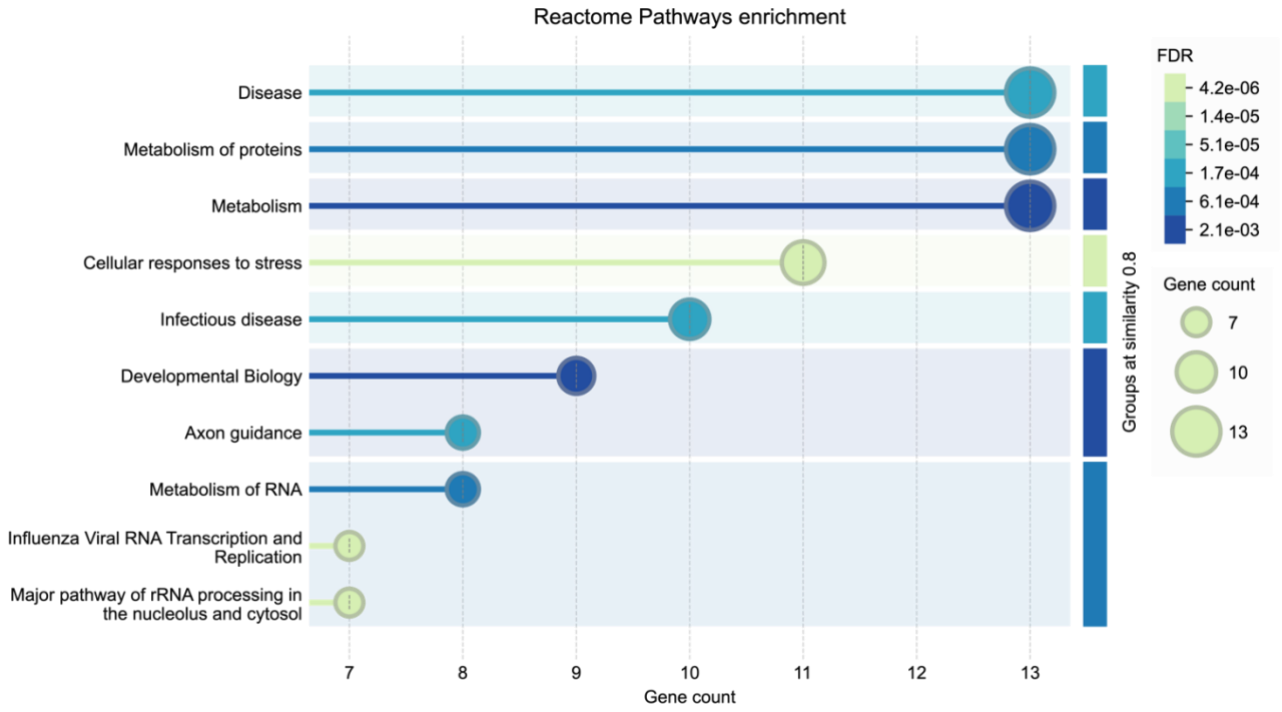

Figure 4. 5 Reactome Pathway Enrichment of the Binding Partners of TNT2+tau in Braak stages III-IV

False discovery rate (FDR) was set to 0.05. The minimum count in the network was 2. Group similarity was 0.8. Number of terms shown was 10.

We see most of the tau related changes in the metabolism in mid-Braak stage cases (Figure 4.5). There were multiple proteins detected that involve energy metabolism, especially ribosomal proteins (RPs), such as RPS27A, RPS4X, RPS3, as well as SLC2A1 (glucose transporter), AGPS (fatty acid metabolism), and COXB5 (mitochondrial electron transport). Stress response (with the involvement of the similar RPs in addition to MINK1, DYNC1I1, and NUP93) was another pathway that was highlighted (Figure 4.5) followed by axonal guidance (RPs, PLXNA4, SRGAP3) and RNA metabolism (RPs and NUP93).

Intriguingly, as the disease progressed in higher Braak stage cases, when we see significant increases in TNT2 and other pre-tangle markers in the posterior DN hubs, other pathways emerged such as activation of the immune system (SERPINB3, F13A1, TUBB6, GFAP), membrane trafficking (SNX5, COPB1, RAB41), autophagy (RPS27A, UBB, TUBB6), and apoptosis (PSMC3), in addition to the persisted metabolic alterations and cellular stress response (Figure 4.6). Some of the other pathways that were not shown were amyloid fiber formation (Reactome ID: HSA-977225), cell cycle-related pathways (HSA-69206, HSA-69481), and ER-Phagosome pathway (HSA-1236974).

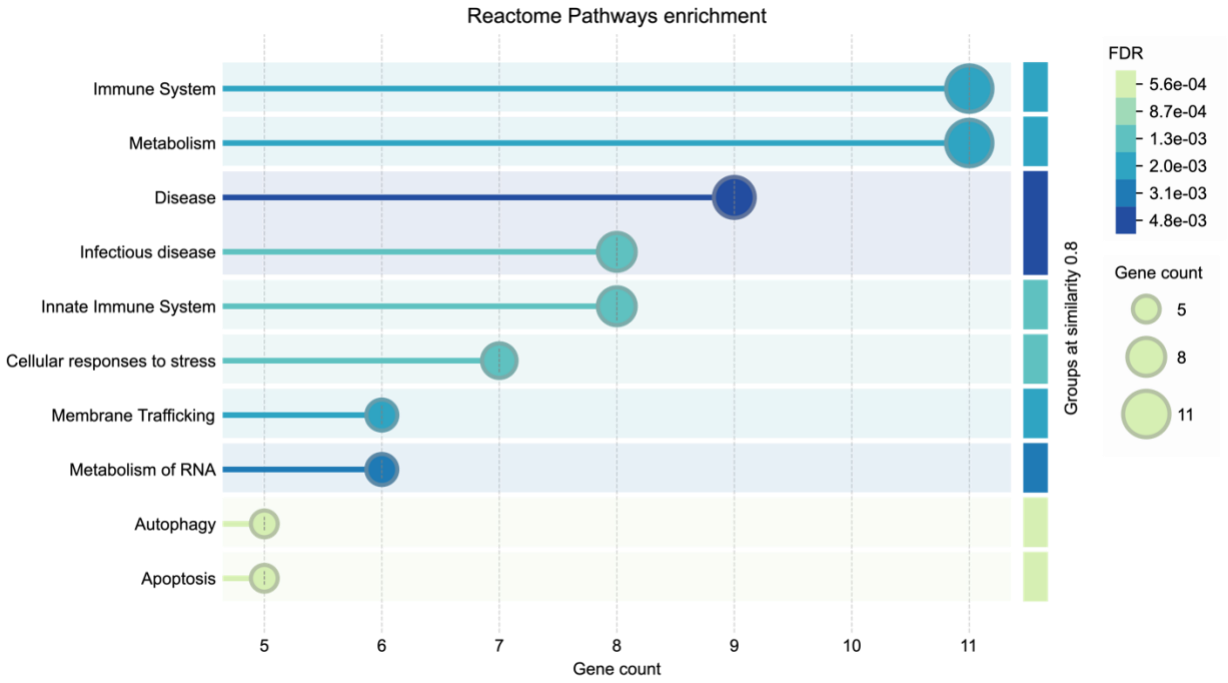

Figure 4. 6 Reactome Pathway Enrichment of the Binding Partners of TNT2+tau in Braak stages V-VI

False discovery rate (FDR) was set to 0.05. The minimum count in the network was 2. Group similarity was 0.8. Number of terms shown was 10.

DISCUSSION

Mechanisms of soluble pre-tangle tau toxicity has been a growing interest in the AD field, as multiple In vitro and in vivo studies have shown that recombinant pre-tangle tau can cause ionic imbalances, mitochondrial abnormalities, disrupted axonal transport and axonal degeneration, and diminished LTP and consequent memory impairment (Younas, 2024). Soluble AD brain-derived tau has been found to be even more toxic. When it was either added to neuronal cultures or injected into mice, AD brain-derived tau caused greater toxicity and showed higher seeding activity (Lasagna-Reeves, 2012 #2353). The basis for this greater toxicity is unclear, but it might be due to the different binding partners of tau in humans contributing to shaping its conformation or electrical charge distribution, together impacting tau function and self-aggregation. In this study, we investigated the protein interaction network of pre-tangle pathological tau by co-immunoprecipitation followed by a mass spec analysis in posterior DMN hubs.

Our findings indicated that PCC and PreC differ in their protein interaction network. In mid-Braak stages, the most predominant protein group was ribosomal proteins (RPs). The six significantly different proteins out of 28 were RP (RPS27A, RPS5, RPS16, RPL11, RPS3, RPS4X). Increased ribosomal activity, in general, indicates a high demand for the production of proteins. However, protein synthesis is a well-controlled mechanism and requires multiple layers of regulation. In tumor cells, due to the increased energy demand and need for more proteins for cellular growth, RP expression was reported to be increased (Zhou, 2015; Ebright, 2020). Similarly, in AD, ribosomal dysfunction and disrupted homeostasis were reported as an early change in MCI (Ding, 2005). A recent study named four RPs as an AD blood biomarker, two overlapping with our findings

(RPS27A, RPS4X) (Wang, 2023). Interestingly, they found a decreased level of those RPs in the blood. We, on the other hand, found RPS27A and RPS4X levels elevated. Especially for RPS27A, elevated levels were consistent between the regions.

Another set of proteins detected in the PCC in mid-Braak stage cases was lipid biosynthesis (NAPEPLD, CYB5R1, PITPNC1, AGPS). While CYB5R1 expression tripled compared to the controls, the other three protein levels decreased 3-4-fold (Table 4.2). In PreC, there were a few proteins related to energy production, such as elevated GFUS (mannose metabolism, (Feichtinger, 2021) and CD5L (lipid metabolism and immune response, (Wang, 2015) and decreased COX5B (a subunit of the mitochondrial respiratory chain, (Chu, 2020). CD63 (regulates cholesterol and endosomal vesicle, (Palmulli, 2024) levels were also elevated in the PreC. Dysregulation of lipid metabolism has been repeatedly reported in AD (Yin, 2023). Besides the indirect effects of abnormal lipids on brain vasculature and insulin resistance (Tong, 2024) on pathology development in AD, tau has been shown to interact with lipids in intracellular liquid-phase droplets with a functional impact on neuron-astrocyte crosstalk (Oliveras, 2023). Increased tau levels were also found to correlate with increased production of lipid droplets in microglia (Olesova, 2024).

The bridging integrator 1 (BIN1) and Misshapen Like Kinase 1 (MINK1) were also among the TNT2-binding proteins detected in PCC in mid-Braak cases; both have been shown to confer AD risk in GWAS studies (Voskobiynyk, 2020; Lawingco, 2021). BIN1 plays a role in regulating membrane remodeling, cellular trafficking, and inflammation (Sudwarts, 2022; Giraud, 2024). In AD, BIN1 was found to be increased (Chapuis, 2013). We also detected a 2.7-fold increase in BIN1 in PCC. Compared to BIN1, the role of

MINK1 in AD pathology is relatively new, but it is reported to be involved in APP catabolism or tau binding (Lawingco, 2021). In a proteomics study, increased phosphorylation at Ser82 on HSP27, a heat shock protein that interacts with tau to alleviate abnormal tau aggregation (Zhang, 2022), was strongly correlated with MINK1 level (Dammer, 2015). In parallel, we found decreased MINK1 levels in the PCC.

Decreased MINK1 and increased RPS27A persisted in the PCC in the high-Braak cases. In addition, Asparaginase-like protein 1 (ASRGL1) was also detected as a TNT2 binding partner in the PCC in both mid and high-Braak stages. This is an enzyme that catalyzes the production of aspartic acid and ammonia (Wang, 2023). Interestingly, a whole genome sequencing study among Caribbean Hispanic families demonstrated a missense mutation in ASRGL1 that segregated with late onset AD (Vardarajan, 2018). The same study also reported rare variants in BIN1. Notably, ASRGL was not detected in the PreC regardless of Braak stage in our study.

Another protein that showed a clear regional difference in abundance was Serpin Family B Member 3 (SERPINB3). The serpin family is a large protein family and is mostly known for their roles as serine protease inhibitors (Bouton, 2023). Some serpins were shown to be involved in AD (Zattoni, 2022). In our previous microarray study, we found increased expression of SERPINI1 in the frontal cortex of AD cases (Beck, 2022). In the present study, we observed an interesting directionality in the SERPINB3 abundance; in both the mid- and high-Braak stage groups, it was highly elevated in the PreC yet decreased in the PCC (Tables 4.3 & 4.4).

Finally, a few more proteins with regional differences in TNT2 binding are worth mentioning. Ras-Related Protein Rab-41 (RAB41) was found only in the PreC. Rab

proteins regulate membrane and vesicular transport, such as vesicle formation and docking in concert with SNAREs (Zerial, 2001), and they have been shown to alter in postmortem tissue from AD patients (Zhang, 2019). A colleague of ours performed laser capture microdissection of vulnerable layer III cathepsin-D positive pyramidal neurons in PreC combined with microarray and found an increased expression of RAB11A in AD cases (He, 2020). Similarly, our data showed an increased level of RAB41 in the mid and high-Braak cases, but only in PreC, without revealing much about whether it functions in favor of the pathology development or not. However, two proteins indicated microtubule breakdown in the PreC. Katanin Catalytic Subunit A1 Like (KATNAL1) is a subunit of the catalytic enzyme Katanin that severs microtubules (Lynn, 2021). Tau was suggested to be protective of microtubule degradation, and in the absence of tau, microtubules become more prone to katanin degradation, and KATNAL1 expression increases (Lynn, 2021). KATNAL1 was also increased in our PreC samples, which may be due to the increased detachment of tau from the microtubules as a consequence of the tangle formation process. Tubulin Beta-6 Chain (TUBB6) which is a beta tubulin isotype level was also decreased in the PreC.

Regarding APP processing, there were two proteins known to regulate APP cleavage through the BACE1 enzyme were detected: Nucleosome Assembly Protein 1 Like 5 (NAP1L5) and Heterogeneous Nuclear Ribonucleoprotein U (HNRNPU). A profiling study found decreased NAP1L5 expression in the temporal cortex of AD cases (Tan, 2010). However, we found an increase in PCC and PreC samples in high-Braak cases (Table 4.4). HNRNPU was also reported to regulate APP metabolism by stabilizing and

promoting BACE-1 activity (Qu, 2021). We found increased HNRNPU levels in the PCC of high-Braak cases.

Finally, the inflammation-related proteins were detected in the high-Braak cases such as Serpin Family B Member 3 (SERPINB3), Glial Fibrillary Acidic Protein (GFAP), Lactotransferrin (LTP), and Major Histocompatibility Complex, Class II, DR Beta 4 (HLA-DRB4). Immune activation as an enriched pathway was also demonstrated in the Reactome Pathway enrichment that we performed as well (Figure 4.6).

Future Directions

We have started working on the protein validation of mass spec analysis within select MADC and RROS cases (Chapter 2). We are planning on using TNT2 co-IP/western blot analysis and fluorescence immunohistochemistry/confocal microscopy analysis to demonstrate the interaction and colocalization of TNT2+ tau and the validation candidates.

CONCLUSION

In the present study, we showed different protein interaction partners of TNT2+ pre-tangle tau in the PCC and PreC regions of the DMN, with potential mechanistic involvement in functional pathways including (lipid metabolism, membrane remodeling, abnormal ribosomal activity, and inflammation). We also detected more TNT2 binding partners in the PCC compared to PreC in the Braak III-VI cases compared to control Braak I-II cases. Future exploration of these differential TNT2 interactome proteins and their functional interactions may provide novel insights into the potential differential vulnerability of these regions and the role of DMN pre-tangle tau accrual in cognitive decline during the progression of AD.

REFERENCES

Abreha, M. H., Ojelade, S., Dammer, E. B., McEachin, Z. T., Duong, D. M., Gearing, M., . . . Seyfried, N. T. (2021). TBK1 interacts with tau and enhances neurodegeneration in tauopathy. *J Biol Chem, 296*, 100760. doi:10.1016/j.jbc.2021.100760

Beck, J. S., Madaj, Z., Cheema, C. T., Kara, B., Bennett, D. A., Schneider, J. A., . . . Counts, S. E. (2022). Co-expression network analysis of frontal cortex during the progression of Alzheimer's disease. *Cereb Cortex, 32*(22), 5108-5120. doi:10.1093/cercor/bhac001

Betters, R. K., Luhmann, E., Gottschalk, A. C., Xu, Z., Shin, M. R., Ptak, C. P., . . . Hefti, M. M. (2023). Characterization of the Tau Interactome in Human Brain Reveals Isoform-Dependent Interaction with 14-3-3 Family Proteins. *eNeuro, 10*(3). doi:10.1523/ENEURO.0503-22.2023

Bouton, M. C., Geiger, M., Sheffield, W. P., Irving, J. A., Lomas, D. A., Song, S., . . . Lucas, A. R. (2023). The under-appreciated world of the serpin family of serine proteinase inhibitors. *EMBO Mol Med, 15*(6), e17144. doi:10.15252/emmm.202217144

Brandt, R., Trushina, N. I., & Bakota, L. (2020). Much More Than a Cytoskeletal Protein: Physiological and Pathological Functions of the Non-microtubule Binding Region of Tau. *Front Neurol, 11*, 590059. doi:10.3389/fneur.2020.590059

Chapuis, J., Hansmannel, F., Gistelinck, M., Mounier, A., Van Cauwenberghe, C., Kolen, K. V., . . . consortium, G. (2013). Increased expression of BIN1 mediates Alzheimer genetic risk by modulating tau pathology. *Mol Psychiatry, 18*(11), 1225-1234. doi:10.1038/mp.2013.1

Chu, Y. D., Lin, W. R., Lin, Y. H., Kuo, W. H., Tseng, C. J., Lim, S. N., . . . Yeh, C. T. (2020). COX5B-Mediated Bioenergetic Alteration Regulates Tumor Growth and Migration by Modulating AMPK-UHMK1-ERK Cascade in Hepatoma. *Cancers (Basel), 12*(6). doi:10.3390/cancers12061646

Dammer, E. B., Lee, A. K., Duong, D. M., Gearing, M., Lah, J. J., Levey, A. I., & Seyfried, N. T. (2015). Quantitative phosphoproteomics of Alzheimer's disease reveals cross-talk between kinases and small heat shock proteins. *Proteomics, 15*(2-3), 508-519. doi:10.1002/pmic.201400189

Davies, D. S., Arthur, A. T., Aitken, H. L., Crossett, B., & Goldsbury, C. S. (2024). Protein complexes from mouse and chick brain that interact with phospho-KXGS motif tau/microtubule associated protein antibody. *Biol Open, 13*(2). doi:10.1242/bio.060067

Ding, Q., Markesbery, W. R., Chen, Q., Li, F., & Keller, J. N. (2005). Ribosome dysfunction is an early event in Alzheimer's disease. *J Neurosci, 25*(40), 9171-9175. doi:10.1523/JNEUROSCI.3040-05.2005

Dyson, H. J. (2016). Making Sense of Intrinsically Disordered Proteins. *Biophys J, 110*(5), 1013-1016. doi:10.1016/j.bpj.2016.01.030

Ebright, R. Y., Lee, S., Wittner, B. S., Niederhoffer, K. L., Nicholson, B. T., Bardia, A., . . . Micalizzi, D. S. (2020). Deregulation of ribosomal protein expression and translation promotes breast cancer metastasis. *Science, 367*(6485), 1468-1473. doi:10.1126/science.aay0939

Elhabashy, H., Merino, F., Alva, V., Kohlbacher, O., & Lupas, A. N. (2022). Exploring protein-protein interactions at the proteome level. *Structure, 30*(4), 462-475. doi:10.1016/j.str.2022.02.004

Feichtinger, R. G., Hullen, A., Koller, A., Kotzot, D., Grote, V., Rapp, E., . . . Wortmann, S. B. (2021). A spoonful of L-fucose-an efficient therapy for GFUS-CDG, a new glycosylation disorder. *EMBO Mol Med, 13*(9), e14332. doi:10.15252/emmm.202114332

Friedman, N. P., & Robbins, T. W. (2022). The role of prefrontal cortex in cognitive control and executive function. *Neuropsychopharmacology, 47*(1), 72-89. doi:10.1038/s41386-021-01132-0

Giraud, Q., & Laporte, J. (2024). Amphiphysin-2 (BIN1) functions and defects in cardiac and skeletal muscle. *Trends Mol Med, 30*(6), 579-591. doi:10.1016/j.molmed.2024.02.005

Guennewig, B., Lim, J., Marshall, L., McCorkindale, A. N., Paasila, P. J., Patrick, E., . . . Sutherland, G. T. (2021). Defining early changes in Alzheimer's disease from RNA sequencing of brain regions differentially affected by pathology. *Sci Rep, 11*(1), 4865. doi:10.1038/s41598-021-83872-z

Gunawardana, C. G., Mehrabian, M., Wang, X., Mueller, I., Lubambo, I. B., Jonkman, J. E., . . . Schmitt-Ulms, G. (2015). The Human Tau Interactome: Binding to the Ribonucleoproteome, and Impaired Binding of the Proline-to-Leucine Mutant at Position 301 (P301L) to Chaperones and the Proteasome. *Mol Cell Proteomics, 14*(11), 3000-3014. doi:10.1074/mcp.M115.050724

Hayes, S., Malacrida, B., Kiely, M., & Kiely, P. A. (2016). Studying protein-protein interactions: progress, pitfalls and solutions. *Biochem Soc Trans, 44*(4), 994-1004. doi:10.1042/BST20160092

He, B., Perez, S. E., Lee, S. H., Ginsberg, S. D., Malek-Ahmadi, M., & Mufson, E. J. (2020). Expression profiling of precuneus layer III cathepsin D-immunopositive

pyramidal neurons in mild cognitive impairment and Alzheimer's disease: Evidence for neuronal signaling vulnerability. *J Comp Neurol, 528*(16), 2748-2766. doi:10.1002/cne.24929

Kavanagh, T., Halder, A., & Drummond, E. (2022). Tau interactome and RNA binding proteins in neurodegenerative diseases. *Mol Neurodegener, 17*(1), 66. doi:10.1186/s13024-022-00572-6

Kelley, C. M., Ginsberg, S. D., Liang, W. S., Counts, S. E., & Mufson, E. J. (2022). Posterior cingulate cortex reveals an expression profile of resilience in cognitively intact elders. *Brain Commun, 4*(4), fcac162. doi:10.1093/braincomms/fcac162

Kelley, C. M., Maloney, B., Beck, J. S., Ginsberg, S. D., Liang, W., Lahiri, D. K., . . . Counts, S. E. (2024). Micro-RNA profiles of pathology and resilience in posterior cingulate cortex of cognitively intact elders. *Brain Commun, 6*(2), fcae082. doi:10.1093/braincomms/fcae082

Lasagna-Reeves, C. A., Castillo-Carranza, D. L., Sengupta, U., Guerrero-Munoz, M. J., Kiritoshi, T., Neugebauer, V., . . . Kayed, R. (2012). Alzheimer brain-derived tau oligomers propagate pathology from endogenous tau. *Sci Rep, 2*, 700. doi:10.1038/srep00700

Lawingco, T., Chaudhury, S., Brookes, K. J., Guetta-Baranes, T., Guerreiro, R., Bras, J., . . . Morgan, K. (2021). Genetic variants in glutamate-, Abeta-, and tau-related pathways determine polygenic risk for Alzheimer's disease. *Neurobiol Aging, 101*, 299 e213-299 e221. doi:10.1016/j.neurobiolaging.2020.11.009

Liang, W. S., Dunckley, T., Beach, T. G., Grover, A., Mastroeni, D., Ramsey, K., . . . Stephan, D. A. (2008). Altered neuronal gene expression in brain regions differentially affected by Alzheimer's disease: a reference data set. *Physiol Genomics, 33*(2), 240-256. doi:10.1152/physiolgenomics.00242.2007

Luo, J., Zhao, H., Chen, L., & Liu, M. (2023). Multifaceted functions of RPS27a: An unconventional ribosomal protein. *J Cell Physiol, 238*(3), 485-497. doi:10.1002/jcp.30941

Lynn, N. A., Martinez, E., Nguyen, H., & Torres, J. Z. (2021). The Mammalian Family of Katanin Microtubule-Severing Enzymes. *Front Cell Dev Biol, 9*, 692040. doi:10.3389/fcell.2021.692040

Maziuk, B. F., Apicco, D. J., Cruz, A. L., Jiang, L., Ash, P. E. A., da Rocha, E. L., . . . Wolozin, B. (2018). RNA binding proteins co-localize with small tau inclusions in tauopathy. *Acta Neuropathol Commun, 6*(1), 71. doi:10.1186/s40478-018-0574-5

McKay, E. C., Beck, J. S., Khoo, S. K., Dykema, K. J., Cottingham, S. L., Winn, M. E., . . . Counts, S. E. (2019). Peri-Infarct Upregulation of the Oxytocin Receptor in

Vascular Dementia. *J Neuropathol Exp Neurol, 78*(5), 436-452. doi:10.1093/jnen/nlz023

Meier, S., Bell, M., Lyons, D. N., Ingram, A., Chen, J., Gensel, J. C., . . . Abisambra, J. F. (2015). Identification of Novel Tau Interactions with Endoplasmic Reticulum Proteins in Alzheimer's Disease Brain. *J Alzheimers Dis, 48*(3), 687-702. doi:10.3233/JAD-150298

Miura, K. (2018). An Overview of Current Methods to Confirm Protein-Protein Interactions. *Protein Pept Lett, 25*(8), 728-733. doi:10.2174/0929866525666180821122240

Mueller, R. L., Combs, B., Alhadidy, M. M., Brady, S. T., Morfini, G. A., & Kanaan, N. M. (2021). Tau: A Signaling Hub Protein. *Front Mol Neurosci, 14*, 647054. doi:10.3389/fnmol.2021.647054

O'Neill, N., Stein, T. D., Olayinka, O. A., Empawi, J. A., Hu, J., Tong, T., . . . Farrer, L. A. (2024). Cognitive resilience to Alzheimer's disease characterized by cell-type abundance. *Alzheimers Dement, 20*(10), 6910-6921. doi:10.1002/alz.14187

Olesova, D., Dobesova, D., Majerova, P., Brumarova, R., Kvasnicka, A., Kouril, S., . . . Kovac, A. (2024). Changes in lipid metabolism track with the progression of neurofibrillary pathology in tauopathies. *J Neuroinflammation, 21*(1), 78. doi:10.1186/s12974-024-03060-4

Oliveras, A. (2023). Tau and lipid coalescence drives early lipid dysregulation in Alzheimer’s disease. Alzheimer’s & Dementia, 19(S24). https://doi.org/10.1002/alz.083100

Palmulli, R., Couty, M., Piontek, M. C., Ponnaiah, M., Dingli, F., Verweij, F. J., . . . van Niel, G. (2024). CD63 sorts cholesterol into endosomes for storage and distribution via exosomes. *Nat Cell Biol, 26*(7), 1093-1109. doi:10.1038/s41556-024-01432-9

Perez, S. E., He, B., Nadeem, M., Wuu, J., Scheff, S. W., Abrahamson, E. E., . . . Mufson, E. J. (2015). Resilience of precuneus neurotrophic signaling pathways despite amyloid pathology in prodromal Alzheimer's disease. *Biol Psychiatry, 77*(8), 693-703. doi:10.1016/j.biopsych.2013.12.016

Qu, J., Xiong, X., Hujie, G., Ren, J., Yan, L., & Ma, L. (2021). MicroRNA-132-3p alleviates neuron apoptosis and impairments of learning and memory abilities in Alzheimer's disease by downregulation of HNRNPU stabilized BACE1. *Cell Cycle, 20*(21), 2309-2320. doi:10.1080/15384101.2021.1982507

Ray, M., & Zhang, W. (2010). Analysis of Alzheimer's disease severity across brain regions by topological analysis of gene co-expression networks. *BMC Syst Biol, 4*, 136. doi:10.1186/1752-0509-4-136

Sekar, S., McDonald, J., Cuyugan, L., Aldrich, J., Kurdoglu, A., Adkins, J., . . . Liang, W. S. (2015). Alzheimer's disease is associated with altered expression of genes involved in immune response and mitochondrial processes in astrocytes. *Neurobiol Aging, 36*(2), 583-591. doi:10.1016/j.neurobiolaging.2014.09.027

Simons, J. S., & Spiers, H. J. (2003). Prefrontal and medial temporal lobe interactions in long-term memory. *Nat Rev Neurosci, 4*(8), 637-648. doi:10.1038/nrn1178

Slater, O., Miller, B., & Kontoyianni, M. (2020). Decoding Protein-protein Interactions: An Overview. *Curr Top Med Chem, 20*(10), 855-882. doi:10.2174/1568026620666200226105312

Sobue, A., Komine, O., Hara, Y., Endo, F., Mizoguchi, H., Watanabe, S., . . . Yamanaka, K. (2021). Microglial gene signature reveals loss of homeostatic microglia associated with neurodegeneration of Alzheimer's disease. *Acta Neuropathol Commun, 9*(1), 1. doi:10.1186/s40478-020-01099-x

Soleymani, F., Paquet, E., Viktor, H., Michalowski, W., & Spinello, D. (2022). Protein-protein interaction prediction with deep learning: A comprehensive review. *Comput Struct Biotechnol J, 20*, 5316-5341. doi:10.1016/j.csbj.2022.08.070

Sudwarts, A., Ramesha, S., Gao, T., Ponnusamy, M., Wang, S., Hansen, M., . . . Rangaraju, S. (2022). BIN1 is a key regulator of proinflammatory and neurodegeneration-related activation in microglia. *Mol Neurodegener, 17*(1), 33. doi:10.1186/s13024-022-00535-x

Tahmasian, M., Shao, J., Meng, C., Grimmer, T., Diehl-Schmid, J., Yousefi, B. H., . . . Sorg, C. (2016). Based on the Network Degeneration Hypothesis: Separating Individual Patients with Different Neurodegenerative Syndromes in a Preliminary Hybrid PET/MR Study. *J Nucl Med, 57*(3), 410-415. doi:10.2967/jnumed.115.165464

Tan, M. G., Chua, W. T., Esiri, M. M., Smith, A. D., Vinters, H. V., & Lai, M. K. (2010). Genome wide profiling of altered gene expression in the neocortex of Alzheimer's disease. *J Neurosci Res, 88*(6), 1157-1169. doi:10.1002/jnr.22290

Tong, B., Ba, Y., Li, Z., Yang, C., Su, K., Qi, H., . . . Yu, P. (2024). Targeting dysregulated lipid metabolism for the treatment of Alzheimer's disease and Parkinson's disease: Current advancements and future prospects. *Neurobiol Dis, 196*, 106505. doi:10.1016/j.nbd.2024.106505

Tracy, T. E., Madero-Perez, J., Swaney, D. L., Chang, T. S., Moritz, M., Konrad, C., . . . Gan, L. (2022). Tau interactome maps synaptic and mitochondrial processes associated with neurodegeneration. *Cell, 185*(4), 712-728 e714. doi:10.1016/j.cell.2021.12.041

UniProt, C. (2025). UniProt: the Universal Protein Knowledgebase in 2025. *Nucleic Acids Res, 53*(D1), D609-D617. doi:10.1093/nar/gkae1010

Uversky, V. N. (2013). A decade and a half of protein intrinsic disorder: biology still waits for physics. *Protein Sci, 22*(6), 693-724. doi:10.1002/pro.2261

Uversky, V. N. (2018). Intrinsic Disorder, Protein-Protein Interactions, and Disease. *Adv Protein Chem Struct Biol, 110*, 85-121. doi:10.1016/bs.apcsb.2017.06.005

Vardarajan, B. N., Barral, S., Jaworski, J., Beecham, G. W., Blue, E., Tosto, G., . . . Wang, L. S. (2018). Whole genome sequencing of Caribbean Hispanic families with late-onset Alzheimer's disease. *Ann Clin Transl Neurol, 5*(4), 406-417. doi:10.1002/acn3.537

Voskobiynyk, Y., Roth, J. R., Cochran, J. N., Rush, T., Carullo, N. V., Mesina, J. S., . . . Roberson, E. D. (2020). Alzheimer's disease risk gene BIN1 induces Tau-dependent network hyperexcitability. *Elife, 9*. doi:10.7554/eLife.57354

Wang, C., Yosef, N., Gaublomme, J., Wu, C., Lee, Y., Clish, C. B., . . . Kuchroo, V. K. (2015). CD5L/AIM Regulates Lipid Biosynthesis and Restrains Th17 Cell Pathogenicity. *Cell, 163*(6), 1413-1427. doi:10.1016/j.cell.2015.10.068

Wang, M., Roussos, P., McKenzie, A., Zhou, X., Kajiwara, Y., Brennand, K. J., . . . Zhang, B. (2016). Integrative network analysis of nineteen brain regions identifies molecular signatures and networks underlying selective regional vulnerability to Alzheimer's disease. *Genome Med, 8*(1), 104. doi:10.1186/s13073-016-0355-3

Wang, X., Wang, Y., Yang, L., Yuan, J., Shen, W., Zhang, W., . . . Tao, K. (2023). ASRGL1 downregulation suppresses hepatocellular carcinoma tumorigenesis in a CDK1-dependent manner. *Dig Liver Dis, 55*(7), 955-966. doi:10.1016/j.dld.2022.12.003

Wang, Y., Zhan, D., & Wang, L. (2023). Ribosomal proteins are blood biomarkers and associated with CD4+ T cell activation in Alzheimer's disease: a study based on machine learning strategies and scRNA-Seq data validation. *Am J Transl Res, 15*(4), 2498-2514. Retrieved from https://www.ncbi.nlm.nih.gov/pubmed/37193138

Wei, Z., Zeng, K., Hu, J., Li, X., Huang, F., Zhang, B., . . . Wang, X. (2022). USP10 deubiquitinates Tau, mediating its aggregation. *Cell Death Dis, 13*(8), 726. doi:10.1038/s41419-022-05170-4

Winfree, R. L., Seto, M., Dumitrescu, L., Menon, V., De Jager, P., Wang, Y., . . . Hohman, T. J. (2023). TREM2 gene expression associations with Alzheimer's disease neuropathology are region-specific: implications for cortical versus subcortical microglia. *Acta Neuropathol, 145*(6), 733-747. doi:10.1007/s00401-023-02564-2

Yin, F. (2023). Lipid metabolism and Alzheimer's disease: clinical evidence, mechanistic link and therapeutic promise. *Febs j, 290*(6), 1420-1453. doi:10.1111/febs.16344

Younas, A., Younas, N., Iqbal, M. J., Ferrer, I., & Zerr, I. (2024). Comparative interactome mapping of Tau-protein in classical and rapidly progressive Alzheimer's disease identifies subtype-specific pathways. *Neuropathol Appl Neurobiol, 50*(1), e12964. doi:10.1111/nan.12964

Younas, N., Zafar, S., Saleem, T., Fernandez Flores, L. C., Younas, A., Schmitz, M., & Zerr, I. (2023). Differential interactome mapping of aggregation prone/prion-like proteins under stress: novel links to stress granule biology. *Cell Biosci, 13*(1), 221. doi:10.1186/s13578-023-01164-7

Zattoni, M., Mearelli, M., Vanni, S., Colini Baldeschi, A., Tran, T. H., Ferracin, C., . . . Legname, G. (2022). Serpin Signatures in Prion and Alzheimer's Diseases. *Mol Neurobiol, 59*(6), 3778-3799. doi:10.1007/s12035-022-02817-3

Zerial, M., & McBride, H. (2001). Rab proteins as membrane organizers. *Nat Rev Mol Cell Biol, 2*(2), 107-117. doi:10.1038/35052055

Zhang, L., Gai, Y., Liu, Y., Meng, D., Zeng, Y., Luo, Y., . . . Liu, R. (2024). Tau induces inflammasome activation and microgliosis through acetylating NLRP3. *Clin Transl Med, 14*(3), e1623. doi:10.1002/ctm2.1623

Zhang, S., Zhu, Y., Lu, J., Liu, Z., Lobato, A. G., Zeng, W., . . . Li, D. (2022). Specific binding of Hsp27 and phosphorylated Tau mitigates abnormal Tau aggregation-induced pathology. *Elife, 11*. doi:10.7554/eLife.79898

Zhang, X., Huang, T. Y., Yancey, J., Luo, H., & Zhang, Y. W. (2019). Role of Rab GTPases in Alzheimer's Disease. *ACS Chem Neurosci, 10*(2), 828-838. doi:10.1021/acschemneuro.8b00387

Zhang, X., Wang, J., Zhang, Z., & Ye, K. (2024). Tau in neurodegenerative diseases: molecular mechanisms, biomarkers, and therapeutic strategies. *Transl Neurodegener, 13*(1), 40. doi:10.1186/s40035-024-00429-6

Zhou, X., Liao, W. J., Liao, J. M., Liao, P., & Lu, H. (2015). Ribosomal proteins: functions beyond the ribosome. *J Mol Cell Biol, 7*(2), 92-104. doi:10.1093/jmcb/mjv014

CHAPTER 5: OVERALL DISCUSSION

“I have lost myself” -Auguste Deter, the first patient diagnosed with Alzheimer’s disease

Sooner or later, things go back to where they started. She was not the first human to get Alzheimer’s disease (AD), but clearly the one who was mentioned the most. I started my thesis with her story and would like to bring everything back to her and other patients who suffer the most. Because without understanding what AD means to them, the facts would sound just like numbers.

AD is the fifth-leading cause of death nationwide among those age 65 and older (Alzheimer's disease facts and figures, 2024) and cost about $360 billion dollars for health care only in 2024. Besides the financial burden, AD is physically and psychologically devastating for both the patients and the caregivers. Current clinically approved drugs mostly address the symptoms, such as cholinesterase inhibitors, which help to maintain the physiological level of acetylcholine or Memantine, which helps prevent toxicity by blocking the extrasynaptic NMDA receptors (Matsunaga, 2014), rather than the overall cognitive impairment, partially due to not knowing the exact properties of pathological amyloid beta and tau and their spatiotemporal distribution in the brain throughout the disease as well as the other protein partners that may facilitate the propagation. This study aimed first to help quantify early toxic tau in the frontal cortex (FC), posterior cingulate cortex (PCC), and precuneus (PreC), which are functionally connected regions and together comprise a resting-state brain network called default mode network (DMN), by using postmortem control, mild cognitive impairment (MCI), and AD samples.

Brain Regions that Project to the DMN

We showed that selected pathological pre-tangle markers, especially pS422 and TNT2, significantly increased in the DMN by Braak stage V onwards (Chapter 2). Confirmatory measures of the same markers with ELISA in the soluble fractions from the same cases revealed similar results, however, emphasizing more significant TOC1 levels compared to TNT2 and TauC3 (Chapter 2). Regarding the location of the markers, pre-tangle tau was both in the cell soma and the neuropil threads (NTs), which are neuronal processes, many without a marker-positive cell body in close proximity. Although it is quite challenging to determine the origin of those NTs, if transsynaptic or prion-like tau propagation hypotheses are accurate (Chapter 1), we can speculate that distal projections from other brain regions may facilitate the tau spread. From that perspective, it is important to consider the major brain regions that project into the DMN. That would also help to interpret our results for the temporal establishment of pre-tangle pathology in the DMN.

First and foremost, it is the hippocampus that projections to the posterior DMN hubs through the entorhinal cortex (Rolls, 2019; Cavanna, 2006; Ghaem, 1997). Precuneus communicates with the hippocampus back as well as the medial prefrontal cortex during visuospatial imagery, episodic memory retrieval, and self-relevant information processing (Cavanna, 2006; Cunningham, 2017). The hippocampus also sends direct projections to the frontal cortex from the CA1 regions and the subiculum (Godsil, 2013). Therefore, all three DMN hubs receive projections from the hippocampus and send information to it in addition to the strong structural and functional connectivity among each other (Alves, 2019).

In typical AD, NFT pathology initiates from the transentorhinal cortex, entorhinal cortex, and the CA1 subregion of the hippocampus (Hyman, 1984). While the large pyramidal neurons of layer II of the transentorhinal cortex get largely present NFT accumulation, layers III and V are mostly unaffected initially. While the spread progresses (Braak stage I-II), the entorhinal cortex and the other layers of CA1 start accumulating NFTs. By the Braak stage III-IV, NFT pathology in the CA1 and the subiculum is established (Figure 5.1) (Mrdjen, 2019). The primary projection sites of the hippocampus to the posterior cingulate and retrosplenial cortex are parasubiculum and postsubiculum (Bubb, 2017), which postsubiculum was reported not to show aberrant cellular architecture with Nissl staining, unlike adjacent pyramidal CA1 neurons (Hyman, 1984). In light of those anatomical findings, it would not be surprising to see NFT accumulation in later stages (Braak stage V-VI) for the DMN hubs. While it is tempting to expect the pre-tangle tau moieties in the DMN earlier, 1) there might be a certain threshold to be surpassed for the pre-tangle tau to be biologically detected with the techniques that were used in this study 2) simply more samples might be needed for statistical significance for the pre-tangle tau presence to be detected in this study.

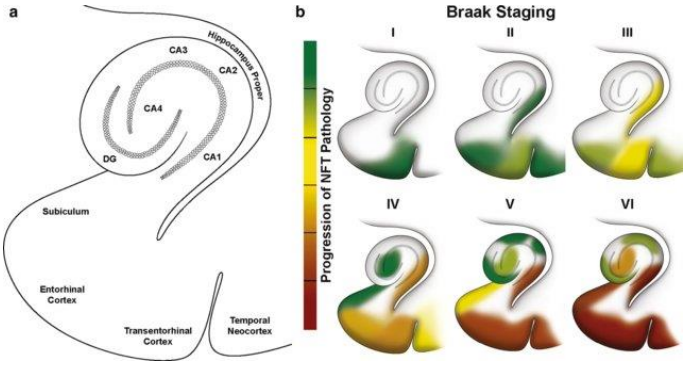

Figure 5. 1 NFT accumulation in the transentorhinal and entorhinal cortex and hippocampal regions during AD progression (Mrdjen et al., 2019)

To better interpret our data, it is worth mentioning another two important brain regions, noradrenergic locus coeruleus (LC) and cholinergic basal forebrain (CBF), that project not only to all three DMN hubs but also the transentorhinal cortex. LC is a noradrenergic nucleus located on the pons, and it releases the majority of the norepinephrine (NE) in the brain, innervating the entire neocortex, including the prefrontal cortex and the posterior DMN hubs (Sara, 2012; Kelly, 2019; Chandler, 2014). NE is a strong neuromodulator, and DMN regions are shown to have NE receptors (van den Brink, 2019), highlighting LC's role in DMN activity. As shown by Oyarzabal et al., chemogenetic stimulation of LC strengthened the DMN fc, especially the connectivity of the frontal hubs by reducing the posterior input from the retrosplenial cortex (RSC) and the hippocampus (Oyarzabal, 2022).

Regarding the tau pathology trajectory in AD, LC is one of the earliest regions that show tau tangles (Braak, 2011a; Andres-Benito, 2017). Braak et al. have shown subcortical AT8 (an early pathological marker that recognizes phosphorylation on the epitope serine 199 & 202 and threonine 205, (Biernat, 1992; Goedert, 1995) positive tau predominantly in the LC while showing no abnormal cortical tau, including the transethornial cortex (Braak, 2011b). The same group also examined brains from ages under 30 for AT8 positivity and found that 19 of 22 cases were indeed positive for AT8 in the subcortical LC (Braak, 2011). In another relevant study, Andres-Benito et al. analyzed the LC and its projections to the hippocampus in the asymptomatic Braak I-IV cases with AT8, pS422, PHF-1, TauC3, and a few other markers (Andres-Benito, 2017). The results indicated that the percentage of AT8 positive LC neurons was significantly increased by the Braak stage III and IV. Dual labeling indicated a largely overlapping

AT8 signal with pS422 and PHF-1. However, only a minority of AT8 positive neurons were stained with TauC3, parallel to the staining pattern that we observed in the DMN regions in this dissertation study. They also found that p-tau markers colocalized with several kinases, decreased mitochondrial protein, and increased oxidative stress markers were detected in TauC3-bearing LC neurons (Andres-Benito, 2017). Finally, assessments of several glial markers revealed that there was only a moderate increase in the microglial Iba-1 and no increase in the astrocytic GFAP markers, which also aligns with our proteomics assessments in Chapter 4 that we found significant GFAP increase only in the AD group (mostly Braak stage V-VI).

The second subcortical nuclei that project to DMN and hippocampus is the cholinergic basal forebrain (CBF). Similar to the LC, CBF innervates and provides acetylcholine to the entire neocortex as well as the hippocampus and amygdala (Mesulam, 1983). Those neurons often have an extremely large axonal arbor (total axon length might reach ~100 meters), which its maintenance would naturally require higher energy and sustained axonal trafficking (Wu, 2014), possibly making the CBF neurons more susceptible to tau pathology. In particular, our group and others have shown that CBF neurons within the nucleus basalis Mynert (NBM) began to display a rapid accumulation of pathological oligomeric tau in the initiation phase of the disease from no cognitive impairment (NCI) to mild cognitive impairment (MCI). The cholinergic neuron number also correlates with the worsening global cognitive function and increasing Braak stage (Tiernan, 2018).

Recently, the role of CBF in DMN modulation has started to be explored. In a rodent study, Nair et al. found that CBF showed a modulatory effect on gamma

oscillations of a DMN hub (Nair, 2018). However, it is important to be mindful of the fact that although it is similar, rodent DMN would not fully represent the human DMN (Lu, 2012). fMRI studies supported those findings showing that NBM can modulate switching between the brain networks, including the DMN (Aguilar, 2022). Serotonergic the raphe nuclei and dopaminergic the substantia nigra pars compacta (SNpc) and the ventral tegmental area (VTA) are also the subcortical nuclei that have DMN projections (van den Brink, 2019). Those regions are also known to be vulnerable to tau pathology and are shown to contribute to AD pathophysiology (Martorana, 2014; Kandimalla, 2017).

Since our DMN pre-tangle tau assessment indicated a significant increase in pre-tangle tau markers from Braak stage IV to V, it is tempting to speculate our results would temporally follow the significant tau accumulation in the LC, CBF, and hippocampus by lagging one or two Braak stages depending on the hub. This might be explained by a couple of reasons:

- Synaptic tau propagation: As was introduced in the first chapter, there are multiple theories for tau propagation in the brain. Synaptic tau spread claims that tau gets released in the synaptic cleft from the presynaptic neuron to be picked up by the post-synaptic dendrites, which would cause the pathological tau to propagate further in the brain in an activity-dependent manner (Ismael, 2021). If this applies to the tau propagation in the DMN or afferently to the DMN hubs from the projection sites, one expects a delayed tau accumulation in the DMN. Yet, as reported in Andres-Benito's study, even in the LC neurons, the AT8 level reached significance in Braak stage III (Andres-Benito, 2017), which might support our findings temporally.

- Our quantification method for immunolabeling: Our semiautomated HALO quantification method was less sensitive compared to stereology or a similar total number quantification method due to using % tissue area as the outcome measure, which may cause underestimation of the pre-tangle tau.
- Biological variability and resistant cases: RROS participants, consisting of priests and nuns, were largely cognitively healthy despite their elevated Braak stage (III-IV). This might be due to their profession, lifestyle, diet, or sleep patterns. More and more studies are coming from indigenous cohorts, such as South American Tsimane or Tibetan monks, regarding lower incidence of dementia. A recent NIH study found that Tsimane tribe has a lifestyle similar to the preindustrial times that they practice farming, hunting, gathering, fishing, having high physically activity in general. They also have a diet rich in fiber and omega fatty acids and low in saturated fat. Despite having higher inflammation markers due to various infectious diseases, they have the lowest prevalence of coronary atherosclerosis of any studied population and a significantly slower decrease in brain volume for both sexes compared to the United States and Europe (Irimia, 2021). Another study emphasized the lifestyle factor in dementia in Tibetan monks. The prevalence of dementia among the religious groups was reported to be lower (Prince, 2013). A cross-sectional study with over 4,000 participants over the age of 60 demonstrated that the prevalence of AD among the participants was 1.33% (Huang, 2016) compared to 10.9% for Americans over the age of 65 (Alzheimer's disease facts and figures, 2024). This might be due to their regular body-mind awareness practice or simply living at higher altitudes. Those examples might provide

an alternative explanation for our findings in pre-tangle DMN significant elevation not until later Braak stages in the RROS cohort.

Regional Differences in Pre-tangle Tau Load in Individual DMN Hubs

Unique contributions of the DMN hubs to particular cognitive tasks, also known as functional parcellation, have been shown before (Wang, 2020). Wang et al. looked at the coactivation patterns of FC, PCC, and temporal parietal junction (TPJ), they did not include PreC during several tasks, and they found that besides the general coactivation of those regions, they demonstrated different connectivity strengths among each other (Kobayashi, 2003). For instance, the PCC and TPJ activity was better coupled with the hippocampal activation compared to the FC, and FC activity was better coupled with the amygdala and the ventral striatum for emotional processing and decision making (Wang, 2020). Another study found that by changing the vividness of a future imagination task, it is possible to modulate dorsal and ventral DMN separately (Lee, 2021). Even within the individual hubs, subregions were shown to have distinct functional connectivity with the rest of the brain (Margulies, 2009). To explain those differences in fc, a very recent study combined postmortem immunolabeling (65-year-old male, n=1) with resting fMRI data from young healthy adults (n=1,000) to create a cytoarchitectural map for different DMN regions, including the PFC and PreC, as overlapping regions with our study (Paquola, 2025). Their study revealed cytoarchitectural heterogeneity among the hubs measured by the proportion of the cortical types, cell-body intensity over intercortical depth, and topographical maps. They also found subregional differences in the fc, for instance, the anterior precuneus

showing more efficient connectivity with the rest of the cortex, claiming it might be due to the cytoarchitectural heterogeneity (Paquola, 2025).

In the context of tau deposition, three DMN hubs may vary as well. Yokoi et al. looked at the distribution of NFT with 18F-THK5351 tau PET in the resting state networks in amyloid-positive early AD patients. Their principal component analysis revealed that PCC and PreC were by far the most prominent areas in the analysis to differentiate AD from the controls, followed by the dorsolateral prefrontal cortex (DLPFC), in correlation with cognitive scores (Yokoi, 2018). Additionally, they did confirmatory immunolabeling in the PCC in Braak stage II and V patients with AT8 (Figure 5.2) to find a similar labeling pattern to ours for pre-tangle tau markers from Chapter 2 (Figure 2.2). They also found astrocytic activation in those regions. As a side note, the 18F-THK5351 ligand has been shown off target-binding to monoamine oxidase (MAO) enzyme expressed in neuronal and non-neuronal cells (Ng, 2017), so the interpretation requires caution. However, they also showed that the astrocytic GFAP marker was increased in that Braak stage V case. This study might support the anterior vs posterior DMN differential role (Rami, 2012) in the overall connectivity as well as tau deposition.

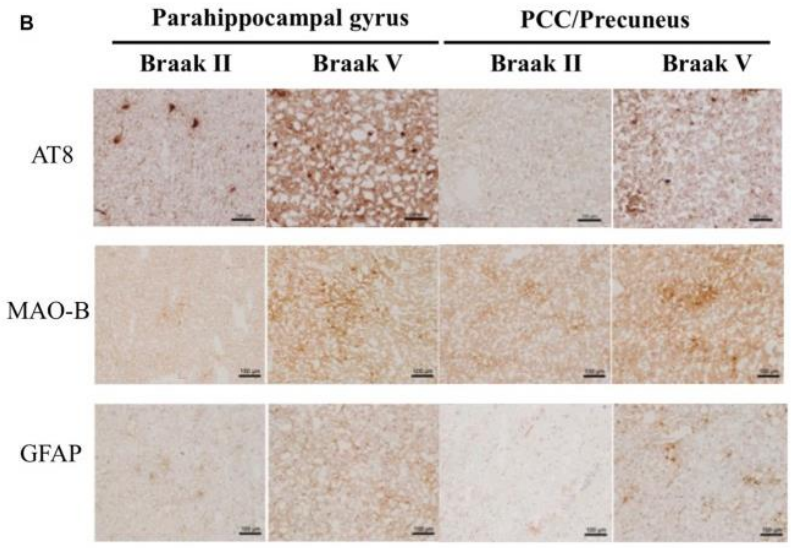

Figure 5. 2 AT8 positive tau quantification in PPP/PreC by Yokoi et al. mirrors our pre-tangle tau labeling in DMN (Yokoi et al., 2018)

A second study relevant to our findings was conducted by Maarouf and colleagues. They investigated how proteins are involved in neurodegeneration change in the PCC and PreC by healthy aging (Maarouf, 2014). Although most of the markers did not change between the young adults, middle-agers, and super-agers, there were two markers that changed: BACE1 and GFAP, both relevant to our proteomics results. As mentioned in Chapter 1, BACE1 is an enzyme that cleaves APP. Maarouf et al. reported a higher expression in the PCC compared to PreC; the level among the groups did not change. The HNRNPU protein, an RNA binding protein that regulates the mRNA stability of BACE-1 (Qu, 2021), was co-immunoprecipitated with TNT2 in our study (Chapter 4). While the HNRNPU level was higher in the PreC in NCI, the expression increased as the disease progressed, especially in the PCC, making the PCC>PreC abundance (2.395) significantly higher in AD (p=0.0421) (Chapter 4). The other marker they reported to increase expression with age was GAFP. Similarly, in our proteomics

study, we also found GFAP was elevated in the AD in both regions but reached significance only in the PCC (0.0383) despite the moderate increase in the abundance ratio PCC>PreC (1.617).

Potential Mechanisms that May Underlie the Regional Differences

As previously mentioned, literature consensually suggests that there might be regional differences among the DMN hubs functionally, cytoarchitecturally, or metabolically. For instance, PCC is metabolically very active (Leech, 2014), and during healthy aging, protein expression of tau, APP, or several inflammation markers in the PCC do not change (Maarouf, 2014). However, in early AD, its metabolic activity decreases (Leech, 2014). Similarly, the functional connectivity between the PCC and the dorsal DMN hubs also decreases as an indicator of tau accumulation in AD (Luo, 2019; Strom, 2022), which suggests that PCC is a key hub in the DMN with high susceptibility to tau pathology. Hence, the exact mechanisms underlie its vulnerability are still vastly unexplored. Our proteomics sub study was aiming for that gap.

Our co-immunoprecipitation of early pathological tau that was combined with mass spec analysis revealed that pathological tau shared numerous binding partners with the low-Braak stages. However, the abundances were mostly increased (up to 45-fold). Although they were not the same proteins standout between the mid-Braak vs high-Braak cases within each region, they showed a similar activation pattern for certain biological pathways, such as immune response, ribosomal activation, and lipid biosynthesis in the PCC. PreC, however, showed fewer proteins changing their abundance when they interacted with pathological tau. Interestingly, ribosomal activity was unanimously increased, possibly as a sign of neurons trying to tolerate the

pathology insult potentially differently in PCC vs PreC. Hence, we speculate that this may explain the higher pathology that we observed in the PCC. Due to the ongoing validation process, risky extrapolation will be avoided for those findings.

Pathology Relates to the Cognitive Changes

Our first research question in this study was how the pre-tangle tau distributes in the DMN temporally. So far, we have discussed how our findings parallel the numerous imaging and postmortem tissue analyses. Then, our second question was whether this pathology manifests clinically as cognitive decline. Although correlation does not mean causation, our results indicated a strong correlation between the GCS & MMSE and the sP422, TNT2, and soluble TOC1 measures (Chapter 3). We also found strong inverse correlations between the early markers and episodic and semantic memory scores. Those memory types were shown extensively before to get impacted in AD (Tromp, 2015; Hodges, 1995), however to our knowledge, their relation to the pre-tangle tau in the DMN had not been explored before.

Recently, Pezzoli and collogues investigated the interplay between the structural atrophy of the brain and AD pathology in the context of healthy cognitive aging (Pezzoli, 2025). They assessed cognitively intact adults who were 70+ years old with sMRI, tau, and amyloid PET, as well as the cognitive tests. They concluded that cognitive aging, measured as the cognitive age gap, was related to the midcingulate cortex (MCC) atrophy, episodic memory decline, and multi-domain cognition. They also found that lower entorhinal cortex tau was associated with a slower decline in episodic memory. The same group did another study, which they longitudinally collected tau and amyloid PET images as well as cognitive test scores from cognitively intact older individuals

(Chen, 2025). They concluded that Aβ pathology in the frontal/ parietal regions was associated with decreased executive function, whereas tau pathology, especially in left entorhinal/parahippocampal regions, was associated with faster memory decline, not the vice versa, emphasizing the domain-specific decline to track the disease progression. The findings go well with our correlation assessments; however we did find significant correlations between the pre-tangle tau in the FC with memory decline, which may be due to the difference between the tau species that were quantified, NFT with PET in their study vs pre-tangle tau with histological and biochemical analyses in our study.

Finally, regarding the timeline of the significant pathology accumulation and the start of cognitive deterioration we found that once pre-tangle tau significantly elevated in the DMN, in Braak stage V in the RROS, it inversely and tightly correlated with the global cognitive measures, as well as the episodic and semantic memory scores. The phenomenon was shown in Chapter 3 where the GCS and MMSE scores were graphed based on either regular (6 stages) or minimal (combined into 3 stages) Braak stages. Similar to our results, another group used tissue samples from the Rush Religious Order Study (RROS) to investigate the TREM2 gene expression in the PCC samples and showed that the expression in the MCI cases was similar to the NCI cases (Winfree, 2023). However, the expression was significantly increased in the AD samples, triggering an immune response which supports our findings once again that elevated pathological tau in the DMN closely correlates with cognitive decline and possible biological processes that results the cognitive impairment, such as immune activation.

Study limitations

- There are a few limitations in this study in addition to 1) Using % tissue area as the outcome measure that may overlook some of the low NTs pathology 2) Absence of fMRI, sMRI, or amyloid/tau-PET images that would give more information about the disease progression rather than the postmortem snapshot assessments of the samples:
- Comorbidities along with tau and Aβ: RROS cohort is very well characterized for postmortem assessments, including TDP-43, CAA, stroke, and arteriolosclerosis in addition to the detailed plaque and tangle quantification in five brain regions. We have included the TDP-43 and CAA scores in our correlation assessments in Chapter 3. TDP-43 correlated with histological quantification of the select markers in all regions (Chapter 3, Table 3.3) and with soluble markers only in the PCC. Interestingly, TDP-43 correlated with the total tau (Tau-5) in all DMN regions (Chapter 3, Table 3.4). Although the exact mechanism is yet to be discovered, TDP-43 has been shown to interact with tau and facilitate pathology seeding (Tome, 2023). Therefore, it requires careful interpretation of the findings. CAA also correlated with the select tau markers and MOAB-2, though not as strong as TDP-43. CAA and tau interplay is suggested to promote AD pathology progression (Schoemaker, 2021; Rabin, 2022). TDP-43 and CAA also correlated with the cognitive scores (data not shown here).
- Sample collection may have caused heterogeneous subregional distribution: As mentioned in the arguments about the regional differences, all DMN hubs have functionally and structurally different subregions (i.e., FC vs DLPFC, or dorsal vs ventral PreC) with distinct cellular architectures and projections patterns (Kobayashi,

2003; Paquola, 2025). Unfortunately, our samples are lacking that level of detailed information regarding the sampling. That may introduce variability in the results on top of the biological differences among the cases.

Future Directions

- The validation process for the mass spec analysis of the TNT2 coimmunoprecipitated proteins is in progress. We tested five binding partners (RAB41, VAPA, DCKL2, HNRNPU, GFAP) so far with dual immunofluorescent labeling. The next steps will be repeating the TNT2 immunoprecipitation in 6 samples from the RROS cohort (2NCI/2MCI/2AD) and running the pulled down on an SDS gel for western blot quantification of those five proteins.
- We may reanalyze the histological slides for tau markers with stereology for a more sensitive quantification.
- We may further investigate the cohort differences in overall tau pathology. MADC Braak IV cases showed elevated pathology, although it lacked significance. By including more Braak stage III and IV cases and more demographical information, such as diabetes and years of education for that cohort, we may further investigate the matter. We have already received fixed samples from a partially overlapping cohort, which will be cut and analyzed with histology.
- To investigate the role of subcortical nuclei, particularly LC and CBF, we will perform colocalization studies with DBH (norepinephrine) and ChAT (acetylcholine) with tau markers, which may give us insight into the origin of the NT formations.

Highlights of the Study

- Pre-tangle tau significantly increases from Braak stage IV to V in the DMN.

- Total and soluble DMN pre-tangle measures correlated with all the cognitive measures except for the working memory.
- Postmortem pathology scores were collected from different brain regions, except for the FC, yet still tightly correlated with the DMN pre-tangle tau in all three regions.
- Although it is correlated with pS422, TOC1, and TNT2 in all three hubs, MOAB2 did not correlate with the cognitive measures in the FC or PreC. It also showed correlation in with the MMSE, GCS, episodic, and semantic memory in the PCC.
- TNT2-pulled down tau revealed differential protein-protein interactions in the PCC vs PreC.

Final Remarks

Despite the limitations in our study, we believed that we offered important new insights into the spatiotemporal distribution of pre-tangle tau, with several markers targeting different PTMs, in the DMN across all six Braak stages in a considerably large cohort. The results may inform the development of more effective treatment strategies for each patient in the absence of pre-tangle tau PET ligands. Once we understand the pathophysiology of AD, and which tau species accumulate when and where in the brain, we may be able to create better therapeutic interventions to slow down the disease to prevent excessive neuronal loss and subsequent cognitive deterioration.

REFERENCES

2024 Alzheimer's disease facts and figures. (2024). *Alzheimers Dement, 20*(5), 3708-3821. doi:10.1002/alz.13809

Aguilar, D. D., & McNally, J. M. (2022). Subcortical control of the default mode network: Role of the basal forebrain and implications for neuropsychiatric disorders. *Brain Res Bull, 185*, 129-139. doi:10.1016/j.brainresbull.2022.05.005

Alves, P. N., Foulon, C., Karolis, V., Bzdok, D., Margulies, D. S., Volle, E., & Thiebaut de Schotten, M. (2019). An improved neuroanatomical model of the default-mode network reconciles previous neuroimaging and neuropathological findings. *Commun Biol, 2*, 370. doi:10.1038/s42003-019-0611-3

Andres-Benito, P., Fernandez-Duenas, V., Carmona, M., Escobar, L. A., Torrejon-Escribano, B., Aso, E., . . . Ferrer, I. (2017). Locus coeruleus at asymptomatic early and middle Braak stages of neurofibrillary tangle pathology. *Neuropathol Appl Neurobiol, 43*(5), 373-392. doi:10.1111/nan.12386

Biernat, J., Mandelkow, E. M., Schroter, C., Lichtenberg-Kraag, B., Steiner, B., Berling, B., . . . Mandelkow, E. (1992). The switch of tau protein to an Alzheimer-like state includes the phosphorylation of two serine-proline motifs upstream of the microtubule binding region. Embo j, 11(4), 1593-1597. doi:10.1002/j.1460-2075.1992.tb05204.x

Braak, H., & Del Tredici, K. (2011b). The pathological process underlying Alzheimer's disease in individuals under thirty. *Acta Neuropathol, 121*(2), 171-181. doi:10.1007/s00401-010-0789-4

Braak, H., Thal, D. R., Ghebremedhin, E., & Del Tredici, K. (2011a). Stages of the pathologic process in Alzheimer disease: age categories from 1 to 100 years. *J Neuropathol Exp Neurol, 70*(11), 960-969. doi:10.1097/NEN.0b013e318232a379

Bubb, E. J., Kinnavane, L., & Aggleton, J. P. (2017). Hippocampal - diencephalic - cingulate networks for memory and emotion: An anatomical guide. *Brain Neurosci Adv, 1*(1). doi:10.1177/2398212817723443

Cavanna, A. E., & Trimble, M. R. (2006). The precuneus: a review of its functional anatomy and behavioural correlates. *Brain, 129*(Pt 3), 564-583. doi:10.1093/brain/awl004

Chandler, D. J., Gao, W. J., & Waterhouse, B. D. (2014). Heterogeneous organization of the locus coeruleus projections to prefrontal and motor cortices. *Proc Natl Acad Sci U S A, 111*(18), 6816-6821. doi:10.1073/pnas.1320827111

Chen, X., Juarez, A., Mason, S., Kobayashi, S., Baker, S. L., Harrison, T. M., . . . Jagust, W. J. (2025). Longitudinal relationships between Abeta and tau to executive function and memory in cognitively normal older adults. *Neurobiol Aging, 145*, 32-41. doi:10.1016/j.neurobiolaging.2024.10.004

Cunningham, S. I., Tomasi, D., & Volkow, N. D. (2017). Structural and functional connectivity of the precuneus and thalamus to the default mode network. *Hum Brain Mapp, 38*(2), 938-956. doi:10.1002/hbm.23429

Ghaem, O., Mellet, E., Crivello, F., Tzourio, N., Mazoyer, B., Berthoz, A., & Denis, M. (1997). Mental navigation along memorized routes activates the hippocampus, precuneus, and insula. *Neuroreport, 8*(3), 739-744. doi:10.1097/00001756-199702100-00032

Godsil, B. P., Kiss, J. P., Spedding, M., & Jay, T. M. (2013). The hippocampal-prefrontal pathway: the weak link in psychiatric disorders? *Eur Neuropsychopharmacol, 23*(10), 1165-1181. doi:10.1016/j.euroneuro.2012.10.018

Goedert, M., Jakes, R., & Vanmechelen, E. (1995). Monoclonal antibody AT8 recognises tau protein phosphorylated at both serine 202 and threonine 205. *Neurosci Lett, 189*(3), 167-169. doi:10.1016/0304-3940(95)11484-e

Hodges, J. R., & Patterson, K. (1995). Is semantic memory consistently impaired early in the course of Alzheimer's disease? Neuroanatomical and diagnostic implications. *Neuropsychologia, 33*(4), 441-459. doi:10.1016/0028-3932(94)00127-b

Huang, F., Shang, Y., Luo, Y., Wu, P., Huang, X., Tan, X., . . . Hu, X. (2016). Lower Prevalence of Alzheimer's Disease among Tibetans: Association with Religious and Genetic Factors. *J Alzheimers Dis, 50*(3), 659-667. doi:10.3233/JAD-150697

Hyman, B. T., Van Hoesen, G. W., Damasio, A. R., & Barnes, C. L. (1984). Alzheimer's disease: cell-specific pathology isolates the hippocampal formation. *Science, 225*(4667), 1168-1170. doi:10.1126/science.6474172

Irimia, A., Chaudhari, N. N., Robles, D. J., Rostowsky, K. A., Maher, A. S., Chowdhury, N. F., . . . Kaplan, H. (2021). The Indigenous South American Tsimane Exhibit Relatively Modest Decrease in Brain Volume With Age Despite High Systemic Inflammation. *J Gerontol A Biol Sci Med Sci, 76*(12), 2147-2155. doi:10.1093/gerona/glab138

Ismael, S., Sindi, G., Colvin, R. A., & Lee, D. (2021). Activity-dependent release of phosphorylated human tau from Drosophila neurons in primary culture. *J Biol Chem, 297*(4), 101108. doi:10.1016/j.jbc.2021.101108

Kandimalla, R., & Reddy, P. H. (2017). Therapeutics of Neurotransmitters in Alzheimer's Disease. *J Alzheimers Dis, 57*(4), 1049-1069. doi:10.3233/JAD-161118

Kelly, S. C., McKay, E. C., Beck, J. S., Collier, T. J., Dorrance, A. M., & Counts, S. E. (2019). Locus Coeruleus Degeneration Induces Forebrain Vascular Pathology in a Transgenic Rat Model of Alzheimer's Disease. *J Alzheimers Dis, 70*(2), 371-388. doi:10.3233/JAD-190090

Kobayashi, Y., & Amaral, D. G. (2003). Macaque monkey retrosplenial cortex: II. Cortical afferents. *J Comp Neurol, 466*(1), 48-79. doi:10.1002/cne.10883

Lee, S., Parthasarathi, T., & Kable, J. W. (2021). The Ventral and Dorsal Default Mode Networks Are Dissociably Modulated by the Vividness and Valence of Imagined Events. *J Neurosci, 41*(24), 5243-5250. doi:10.1523/JNEUROSCI.1273-20.2021

Leech, R., & Sharp, D. J. (2014). The role of the posterior cingulate cortex in cognition and disease. *Brain, 137*(Pt 1), 12-32. doi:10.1093/brain/awt162

Lu, H., Zou, Q., Gu, H., Raichle, M. E., Stein, E. A., & Yang, Y. (2012). Rat brains also have a default mode network. *Proc Natl Acad Sci U S A, 109*(10), 3979-3984. doi:10.1073/pnas.1200506109

Luo, X., Li, K., Jia, Y. L., Zeng, Q., Jiaerken, Y., Qiu, T., . . . Alzheimer's Disease Neuroimaging, I. (2019). Altered effective connectivity anchored in the posterior cingulate cortex and the medial prefrontal cortex in cognitively intact elderly APOE epsilon4 carriers: a preliminary study. *Brain Imaging Behav, 13*(1), 270-282. doi:10.1007/s11682-018-9857-5

Maarouf, C. L., Kokjohn, T. A., Walker, D. G., Whiteside, C. M., Kalback, W. M., Whetzel, A., . . . Roher, A. E. (2014). Biochemical assessment of precuneus and posterior cingulate gyrus in the context of brain aging and Alzheimer's disease. *PLoS One, 9*(8), e105784. doi:10.1371/journal.pone.0105784

Margulies, D. S., Vincent, J. L., Kelly, C., Lohmann, G., Uddin, L. Q., Biswal, B. B., . . . Petrides, M. (2009). Precuneus shares intrinsic functional architecture in humans and monkeys. *Proc Natl Acad Sci U S A, 106*(47), 20069-20074. doi:10.1073/pnas.0905314106

Martorana, A., & Koch, G. (2014). "Is dopamine involved in Alzheimer's disease?". *Front Aging Neurosci, 6*, 252. doi:10.3389/fnagi.2014.00252

Matsunaga, S., Kishi, T., & Iwata, N. (2014). Combination therapy with cholinesterase inhibitors and memantine for Alzheimer's disease: a systematic review and meta-analysis. *Int J Neuropsychopharmacol, 18*(5). doi:10.1093/ijnp/pyu115

Mesulam, M. M., Mufson, E. J., Levey, A. I., & Wainer, B. H. (1983). Cholinergic innervation of cortex by the basal forebrain: cytochemistry and cortical connections of the septal area, diagonal band nuclei, nucleus basalis (substantia innominata), and hypothalamus in the rhesus monkey. *J Comp Neurol, 214*(2), 170-197. doi:10.1002/cne.902140206

Mrdjen, D., Fox, E. J., Bukhari, S. A., Montine, K. S., Bendall, S. C., & Montine, T. J. (2019). The basis of cellular and regional vulnerability in Alzheimer's disease. *Acta Neuropathol, 138*(5), 729-749. doi:10.1007/s00401-019-02054-4

Nair, J., Klaassen, A. L., Arato, J., Vyssotski, A. L., Harvey, M., & Rainer, G. (2018). Basal forebrain contributes to default mode network regulation. *Proc Natl Acad Sci U S A, 115*(6), 1352-1357. doi:10.1073/pnas.1712431115

Ng, K. P., Pascoal, T. A., Mathotaarachchi, S., Therriault, J., Kang, M. S., Shin, M., . . . Rosa-Neto, P. (2017). Monoamine oxidase B inhibitor, selegiline, reduces (18)F-THK5351 uptake in the human brain. *Alzheimers Res Ther, 9*(1), 25. doi:10.1186/s13195-017-0253-y

Oyarzabal, E. A., Hsu, L. M., Das, M., Chao, T. H., Zhou, J., Song, S., . . . Shih, Y. I. (2022). Chemogenetic stimulation of tonic locus coeruleus activity strengthens the default mode network. *Sci Adv, 8*(17), eabm9898. doi:10.1126/sciadv.abm9898

Paquola, C., Garber, M., Frassle, S., Royer, J., Zhou, Y., Tavakol, S., . . . Bernhardt, B. C. (2025). The architecture of the human default mode network explored through cytoarchitecture, wiring and signal flow. *Nat Neurosci*. doi:10.1038/s41593-024-01868-0

Pezzoli, S., Giorgio, J., Chen, X., Ward, T. J., Harrison, T. M., & Jagust, W. J. (2025). Cognitive aging outcomes are related to both tau pathology and maintenance of cingulate cortex structure. *Alzheimers Dement, 21*(2), e14515. doi:10.1002/alz.14515

Prince, M., Bryce, R., Albanese, E., Wimo, A., Ribeiro, W., & Ferri, C. P. (2013). The global prevalence of dementia: a systematic review and metaanalysis. *Alzheimers Dement, 9*(1), 63-75 e62. doi:10.1016/j.jalz.2012.11.007

Qu, J., Xiong, X., Hujie, G., Ren, J., Yan, L., & Ma, L. (2021). MicroRNA-132-3p alleviates neuron apoptosis and impairments of learning and memory abilities in Alzheimer's disease by downregulation of HNRNPU stabilized BACE1. *Cell Cycle, 20*(21), 2309-2320. doi:10.1080/15384101.2021.1982507

Rabin, J. S., Nichols, E., La Joie, R., Casaletto, K. B., Palta, P., Dams-O'Connor, K., . . . Brickman, A. M. (2022). Cerebral amyloid angiopathy interacts with neuritic amyloid plaques to promote tau and cognitive decline. *Brain, 145*(8), 2823-2833. doi:10.1093/brain/awac178

Rami, L., Sala-Llonch, R., Sole-Padulles, C., Fortea, J., Olives, J., Llado, A., . . . Molinuevo, J. L. (2012). Distinct functional activity of the precuneus and posterior cingulate cortex during encoding in the preclinical stage of Alzheimer's disease. *J Alzheimers Dis, 31*(3), 517-526. doi:10.3233/JAD-2012-120223

Rolls, E. T. (2019). The cingulate cortex and limbic systems for emotion, action, and memory. *Brain Struct Funct, 224*(9), 3001-3018. doi:10.1007/s00429-019-01945-2

Sara, S. J., & Bouret, S. (2012). Orienting and reorienting: the locus coeruleus mediates cognition through arousal. *Neuron, 76*(1), 130-141. doi:10.1016/j.neuron.2012.09.011

Schoemaker, D., Charidimou, A., Zanon Zotin, M. C., Raposo, N., Johnson, K. A., Sanchez, J. S., . . . Viswanathan, A. (2021). Association of Memory Impairment With Concomitant Tau Pathology in Patients With Cerebral Amyloid Angiopathy. *Neurology, 96*(15), e1975-e1986. doi:10.1212/WNL.0000000000011745

Strom, A., Iaccarino, L., Edwards, L., Lesman-Segev, O. H., Soleimani-Meigooni, D. N., Pham, J., . . . Alzheimer's Disease Neuroimaging, I. (2022). Cortical hypometabolism reflects local atrophy and tau pathology in symptomatic Alzheimer's disease. *Brain, 145*(2), 713-728. doi:10.1093/brain/awab294

Tiernan, C. T., Mufson, E. J., Kanaan, N. M., & Counts, S. E. (2018). Tau Oligomer Pathology in Nucleus Basalis Neurons During the Progression of Alzheimer Disease. *J Neuropathol Exp Neurol, 77*(3), 246-259. doi:10.1093/jnen/nlx120

Tome, S. O., Tsaka, G., Ronisz, A., Ospitalieri, S., Gawor, K., Gomes, L. A., . . . Thal, D. R. (2023). TDP-43 pathology is associated with increased tau burdens and seeding. *Mol Neurodegener, 18*(1), 71. doi:10.1186/s13024-023-00653-0

Tromp, D., Dufour, A., Lithfous, S., Pebayle, T., & Despres, O. (2015). Episodic memory in normal aging and Alzheimer disease: Insights from imaging and behavioral studies. *Ageing Res Rev, 24*(Pt B), 232-262. doi:10.1016/j.arr.2015.08.006

van den Brink, R. L., Pfeffer, T., & Donner, T. H. (2019). Brainstem Modulation of Large-Scale Intrinsic Cortical Activity Correlations. *Front Hum Neurosci, 13*, 340. doi:10.3389/fnhum.2019.00340

Wang, S., Tepfer, L. J., Taren, A. A., & Smith, D. V. (2020). Functional parcellation of the default mode network: a large-scale meta-analysis. *Sci Rep, 10*(1), 16096. doi:10.1038/s41598-020-72317-8

Winfree, R. L., Seto, M., Dumitrescu, L., Menon, V., De Jager, P., Wang, Y., . . . Hohman, T. J. (2023). TREM2 gene expression associations with Alzheimer's disease neuropathology are region-specific: implications for cortical versus

subcortical microglia. *Acta Neuropathol, 145*(6), 733-747. doi:10.1007/s00401-023-02564-2

Wu, H., Williams, J., & Nathans, J. (2014). Complete morphologies of basal forebrain cholinergic neurons in the mouse. *Elife, 3*, e02444. doi:10.7554/eLife.02444

Yokoi, T., Watanabe, H., Yamaguchi, H., Bagarinao, E., Masuda, M., Imai, K., . . . Sobue, G. (2018). Involvement of the Precuneus/Posterior Cingulate Cortex Is Significant for the Development of Alzheimer's Disease: A PET (THK5351, PiB) and Resting fMRI Study. *Front Aging Neurosci, 10*, 304. doi:10.3389/fnagi.2018.00304